ROYAUME DU MAROC
Université Mohammed V - RABAT - جامعة محمد الخامس - الرباط -
Faculté des sciences
كلية العلوم

CENTRE D'ETUDES DOCTORALES - SCIENCES ET TECHNOLOGIES

N° d'ordre : 3639

THESE

En vue de l'obtention du : ***DOCTORAT***

Structure de Recherche *: Equipe de science de la matière et du rayonnement*
Discipline *: Physique*
Spécialité *: Physique quantique*

Présentée et soutenue le 25 / 06 / 2022 par :

Chaibata SEIDA

Efficiency of the bidirectional quantum teleportation and proposal of new bidirectional teleportation protocols

JURY

Morad EL BAZ	PES, Université Mohammed V de Rabat, Faculté des Sciences.	Président-Rapporteur
Adil BELHAJ	PH, Université Mohammed V de Rabat, Faculté des Sciences.	Rapporteur-Examinateur
Oussama EL ABOUTI	PH, Université Abdelmalek Essaâdi de Tétouan, Faculté des Sciences et Techniques d'Al-Hoceima.	Rapporteur-Examinateur
Tarik MRABTI	PH, Université Abdelmalek Essaâdi de Tétouan, Faculté Polydisiplinaire de Larache.	Examinateur
Hicham AMELLAL	PA, Université Ibn Zohr Agadir, faculté des Sciences	Invité
Abderrahim EL ALLATI	PH, Université Abdelmalek Essaâdi de Tétouan, Faculté des Sciences et Techniques d'Al-Hoceima.	Codirecteur de thèse
Yassine HASSOUNI	PES, Université Mohammed V de Rabat, Faculté des Sciences.	Directeur de thèse

Année Universitaire : **2021/2022**

✉ Faculté des Sciences, avenue Ibn Battouta, BP. 1014 RP, Rabat –Maroc
☎ 00212 (05) 37 77 18 76 00212(05) 37 77 42 61; http://www. fsr.um5.ac.ma

“***What we observe is not nature itself, but nature exposed to our method of questioning.***”

– *Werner Heisenberg* (1901 – 1976), Physics and Philosophy: The Revolution in Modern Science –

Acknowledgements

First and foremost, I would like to thank God almighty for giving me the strength and the patience to achieve this dream. This doctoral thesis, in its current form, is jointly achieved in collaboration with **Equipe de Science de la Matière et du Rayonnement (ESMaR)**, at the faculty of sciences in Rabat and **the laboratory of R&D in Engineering Sciences**, faculty of sciences and techniques in Al-Hoceïma, thanks to the encouragement and advice from many persons. I would seize this opportunity to express my deepest thanks and gratitude to all the persons who have helped me to accomplish this study.

It's been an honor for me to work under the guidance of Mr. **Yassine HASSOUNI** professor at the faculty of sciences in Rabat. I would like to express my deep appreciation to him for accepting to supervise this work and for his cooperation and kindness.

I am very grateful to my co-supervisor Mr. **Abderrahim EL ALLATI** professor at the faculty of sciences and techniques in Al-Hoceïma, for his continuous support and his invaluable orientation in conducting this scientific research. I am very grateful that he has been always available to discuss the many problems and questions I bring him even on week-ends and holidays. I have always been impressed by his devotion and modesty. This thesis would not have been completed without his guidance and constant feedback. I am indebted to him forever.

I address all my deepest gratitude and appreciation to Mr. **Nasser METWALLY** professor at the college of science, university of Bahrain, for his invaluable suggestions about the topical issues covered in this thesis. I would also thank him for his motivation and constant feedback. His interest and wide knowledge in the different areas covered in this work was very beneficial for me.

I would like to express my thanks and appreciation to Mr. **Yahia TAYALATI**, professor at the faculty of sciences in Rabat, and the former *ESMaR* Head, for his cooperation and his kindness.

Very special thanks to Mr. **Adil BELHAJ** professor at the faculty of sciences in Rabat, and the *ESMaR* Head, for his support and encouragement.

I would like to express my deep thanks and appreciation to all the members of the jury. I am so thankful to Mr. **Morad EL BAZ** professor at the faculty of sciences in Rabat, for accepting to be the jury's president and a reviewer for my thesis. I would to express my special thanks to him for his encouragement and his kindness.

Also, I wish to convey my profuse thanks to Mr. **Tarik MRABTI** professor at the ploydisciplinary faculty of Larache, and to Mr. **Oussama EL ABOUTI** professor at the faculty of sciences and techniques in Al-Hoceïma, to accept being with the jury members and for their reviews and invaluable remarks that undoubtedly helped me to improve the quality of this thesis.

I thank my former supervisor in my master's thesis, Mr. **Hicham AMELLAL** professor at the faculty of sciences in Agadir, for accepting to be with the jury members in order to evaluate this work.

I would also like to express my sincere appreciation to my former and present colleagues at the *ESMaR* and the laboratory of *R&D* in Engineering Sciences, **Khadija EL ANOUZ**, **Mustapha ZIANE** and **Youssef KHLIFI** for their fruitful discussions and collaborations. Special thanks go to my childhood friend **Elwali TANAKHA** for his valuable discussion about different research topics even not related to quantum information theory.

My family has provided me with invaluable support throughout my entire life and education. My parents have always encouraged and supported me to pursue my higher education and earn my doctoral degree even far away from my hometown. Big thanks to my sisters, **Safia SEIDA** and **Leila SEIDA**, and to my brother **Mohammed SEIDA**, who have supported me during the inevitable ups and downs in a such experience. This work would have been impossible without the unlimited support of my soulmate, *Aichatou* who stuck with me during the hard times.

Finally I sincerely thank my colleagues in the office, and so many others who have left fingerprint in the successful making of this thesis.

Abstract

Significant development of new protocols for the processing and the control of individual quantum objects is a major step toward the second quantum revolution. In this thesis, we address the issue of bidirectional quantum teleportation, which is one of the most interesting subjects in quantum information science. In fact, the bidirectional quantum teleportation can not only be regarded as a reliable exchange of quantum information but it is also a building block for universal quantum information processing. The prime objective of this theoretical research is to investigate the bidirectional quantum teleportation of unknown quantum states and some relevant parameters. We consider that the quantum channel of the bidirectional teleportation protocol is subjected to environmental noise, which induces decoherence. We evaluate the negativity to quantify the amount of entanglement in the quantum channel of the bidirectional quantum teleportation protocol. Furthermore, we consider the average fidelities of teleportation and the quantum Fisher information as figures of merit to assess the bidirectional teleportation protocol. In order to overcome the decoherence effect and increase the BQT efficiency, we use the weak and reversed measurements method. We show that these measurements can only suppress the amplitude damping effect if, and only if, the average fidelities of the teleported states are greater than 0.5 and the quantum Fisher information is not null. Nonetheless, using noise classical correlations in the non-Markovian regime we could slightly improve the BQT. Besides, noise temporal correlations improve further the average fidelities of teleportation and the quantum Fisher information over a wide time range. In a further step, we extend the BQT protocol to a three-party scheme, where three partners can exchange their quantum states by means of a GHZ state. Then, we generalize the proposed scheme to a quantum network composed of N (with $N > 3$) partners. We also suggest a new bidirectional scheme for the non-local implementation of $CNOT$ operations. Based on this latter bidirectional scheme, we propose a bidirectional teleportation protocol for 2-qubit, 3-qubit and n-qubit states (with $n > 3$).

Keywords: Quantum Information Theory; Bidirectional quantum teleportation; Open Quantum Systems Theory; Fidelity; non-Markovianity; Quantum Correlation; Entanglement; Quantum Fisher Information.

Résumé

Le développement significatif de nouveaux protocoles pour le traitement et le contrôle des objets quantiques individuels constitue une étape majeure vers la deuxième révolution quantique. Dans cette thèse, nous abordons la téléportation quantique bidirectionnelle, l'un des sujet les plus intéressants dans le domaine de l'information quantique. En effet, la téléportation quantique bidirectionnelle peut, non seulement, être considérée comme un échange fiable de l'information quantique, mais elle est aussi un élément constitutif du réseau universel des informations quantiques. L'objectif principal de cette recherche théorique est d'étudier la téléportation quantique bidirectionnelle des états quantiques inconnus et de certains paramètres pertinents. Nous considérons que le canal quantique du protocole de téléportation bidirectionnelle est soumis au bruit ambiant, qui induit la décohérence quantique. Nous évaluons la négativité pour quantifier la quantité d'intrication dans le canal quantique du protocole de téléportation quantique bidirectionnel. En outre, nous considérons les fidélités moyennes de téléportation et l'information quantique de Fisher comme des figures de mérite pour évaluer le protocole de téléportation bidirectionnelle. Afin de surmonter l'effet de décohérence quantique et d'augmenter l'efficacité du protocole de téléportation, nous utilisons la méthode des mesures faibles et inversées (Weak and reversed measurements). Nous montrons que ces mesures ne peuvent supprimer l'effet de $l'amplitude\ damping$ que si, et seulement si, les fidélités moyennes des états téléportés sont supérieures à $0,5$ et que l'information quantique de Fisher n'est pas nulle. Néanmoins, l'utilisation de corrélations classiques dans le régime non-markovien pourrait améliorer légèrement la téléportation bidirectionnelle. En outre, les corrélations temporelles améliorent encore mieux les fidélités moyennes de téléportation et l'information de Fisher quantique. Dans une étape ultérieure, nous prolongeons le protocole de téléportation bidirectionnelle à un schéma composé de trois partenaires, ces trois partenaires peuvent échanger leurs états quantiques au moyen d'un état maximalement intriqués de type GHZ. Ensuite, nous généralisons le schéma proposé à un réseau quantique composé de N (avec $N > 3$) partenaires. Nous suggérons également un nouveau schéma pour l'implémentions non-locale de la porte quantique $CNOT$. En se basant sur le dernier schéma, nous proposons un protocole de téléportation bidirectionnel pour les états à 2-qubits, 3-qubits et n-qubits (avec $n > 3$).

Mots-clés: Théorie de l'information quantique; téléportation quantique bidirectionnelle; Théorie des systems quantique ouverts; Fidélité; non-Markovianity; Correlation quantique; intrication; Information de Fisher quantique.

Résumé étendu

La transmission sécurisée de l'information quantique d'un endroit à un autre est un objectif essentiel de la théorie de l'information quantique. En fait, l'information n'est pas une entité abstraite. En d'autres termes, nous pouvons certainement trouver l'information codée dans une entité physique, qu'il s'agisse d'un atome, d'un photon, d'un ion ou de toute autre particule quantique. Par conséquent, l'information est soumise aux lois de la physique quantique. La théorie de l'information quantique est apparue comme un nouveau domaine de recherche interdisciplinaire qui combine la théorie de l'information avec les lois de la physique quantique. En effet, l'information peut être codée sur un qubit, qui est le système quantique le plus simple. Un qubit peut être représenté par deux états différents : $|0\rangle$ et $|1\rangle$ ou dans une superposition arbitraire de ces états. La superposition quantique peut être interprétée comme une interférence des deux possibilités, $|0\rangle$ et $|1\rangle\rangle$. En fait, la superposition quantique est une caractéristique distinctive de la théorie quantique. De plus, elle a été démontrée dans de nombreuses particules comme l'électron, l'atome, le neutron. Il convient de noter qu'une superposition de N qubits donne lieu à 2N possibilités (pour $N > 1$). Pour cette raison, la prise en compte des qubits offre une capacité de stockage et de traitement de l'information plus puissante que le bit classique. En conséquence, l'exploitation du qubit comme support d'information, dans un ordinateur quantique, permet de simuler des situations assez complexes. Le qubit a été réalisé physiquement en utilisant la polarisation des photons, le spin de particules, la position d'un atome, etc. En outre, il est démontré que les corrélations quantiques sont une notion large dont l'intrication est un type particulier. Plus précisément, l'intrication quantique peut être identifiée comme des corrélations quantiques non-locales. Étant donné que l'intrication est le pilier central de l'exécution de tâches de traitement de l'information quantique avec hautes performances, son identification et sa quantification, dans différents systèmes, ont attiré l'attention des physiciens et restent un problème ouvert aux niveaux théorique et expérimental. L'intrication quantique, en effet, ne peut être créée ou augmentée par aucune opération locale. De plus, une mesure d'intrication devrait être nulle pour un état séparable et égal à "1" pour un état maximalement intriqué. Pourtant, l'intrication a été observée dans différents systèmes, comme les photons, les jonctions Josephson supraconductrices ainsi que dans les systèmes hybrides qui sont composés de qubits photoniques et de qubits de matière. Elle a également été démontrée pour deux électrons séparés par plus de 1 km.

En dépit de leur pertinence conceptuelle, l'exploitation de la superposition et de l'intrication quantique a conduit au développement de la science de l'information quantique et a ouvert la voie à des applications concrètes de l'informatique quantique. En 1993, Bennet et al. [34] ont proposé une idée révolutionnaire, selon Bennet et al.[34], il est possible de téléporter un état quantique inconnu en utilisant un état maximalement intriqué et un canal de communication classique. En outre, la téléportation quantique est d'une importance capitale pour l'établissement d'un réseau quantique à grande échelle. La téléportation quantique accélère, également, le développement de nouvelles applications technologiques telles que les répéteurs quantiques, l'internet quantique et le calcul quantique aveugle. La téléportation quantique a également été utile pour étudier d'autres domaines de recherche tels que l'évaporation des trous noirs. En outre, elle est utilisée pour les courbes fermées de type temporel. Présentement, la téleportation quantique est réalisé au moyen de différents substrats, tels que les qubits photoniques, les états solides, la résonance magnétique nucléaire (RMN), entre la lumière et la matière et entre la lumière et le mouvement. Quelques années plus tard, Huelga et. al. [211] a présenté une idée de téléportation quantique bidirectionnelle dans un contexte lié au contrôle quantique, où Alice téléporte un état quantique inconnu

à Bob. Après avoir reçu l'état, Bob applique une opération quantique à l'état quantique initial et le renvoie à Alice. Par la suite, divers protocoles de téléportation quantique bidirectionnelle et de téléportation quantique bidirectionnelle contrôlée (TQBC) ont été proposés en utilisant plusieurs canaux quantiques, tels que les états GHZ, les états composites GHZ-Bell et les états intriqués de n qubits (avec n >4). En effet, dans les protocoles TQBC, Alice et Bob ne peuvent pas échanger leurs états quantiques sans le contrôle d'une troisième partie, appelée Charlie, qui agit comme un superviseur du processus de téléportation bidirectionnelle. Étant donné que Charlie ne peut ni téléporter ni recevoir d'états quantiques dans le schéma de TQBC, nous posons la question : pouvons-nous étendre la téléportation quantique bidirectionnelle en incluant un tiers (Charlie) comme partenaire. Dans le même contexte, est-il possible d'étendre la téléportation bidirectionnelle d'états quantiques pour un réseau de N partenaire? En outre, pouvons-nous rendre la téléportation bidirectionnelle possible pour les états intriqués et les opérations quantiques ?

Le problème de la décohérence est le facteur le plus limitant pour la réalisation de protocoles de téléportation quantique et leur mise en œuvre avec une grande efficacité. Il est donc essentiel de préserver les ressources quantiques qui constituent l'essence de nombreux protocoles de calcul et d'information quantiques [75]. En effet, en présence de décohérence, la qualité de la reconstruction de l'état téléporté, d'Alice à Bob, est mesurée par la fidélité de téléportation (f). En effet, la fidélité f est une mesure de la similarité entre l'état initial (input state) d'Alice et l'état final (output state) de Bob $0 \leq f \leq 1$. Dans certains contextes, il est nécessaire de téléporter l'information codée dans un paramètre pertinent, comme le poids ou la phase d'un qubit, au lieu de l'état complet du système. Dans cet égard, l'information quantique de Fisher (IQF) est plus pratique pour quantifier la fiabilité de la téléportation de paramètres. La QFI quantifie la sensibilité d'un état quantique par rapport aux changements survenant sur le paramètre concerné. Elle a été largement étudiée dans différents domaines de recherche tels que l'estimation quantique, où elle donne la plus grande précision réalisable dans diverses tâches d'estimation de paramètres. En fait, l'IFQ joue un rôle important dans l'estimation d'un seul paramètre grâce à la borne de Cramer-Rao, alors qu'une plus grande précision est obtenue pour une grande valeur de QFI.

À cet égard, nous étudions la téléportation quantique bidirectionnelle dans une situation plus réaliste, où le bruit environnemental affecte le canal quantique du protocole du TQB. Le bruit environnemental a été modélisé par des canaux quantiques typiques, qui sont généralement utilisés dans la théorie de l'information quantique, tels que le bit-flip, le phase-flip, la dépolarisation et le canal d'amortissement d'amplitude. De plus, nous avons utilisé deux techniques pour supprimer l'effet du bruit sur du protocole du TQB, qui sont les mesures faibles et inversées (WRM), et les effets de mémoire non-markoviens. Notre objectif dans cette partie de notre étude est de savoir si ces méthodes sont efficaces pour tous les types de bruit considérés. Finalement, les résultats de cette étude ont été que le WRM pouvait juste atténuer le bruit d'amortissement d'amplitude si, et seulement si, les fidélités moyennes des états téléportés étaient supérieures à 0,5 et que l'information quantique de Fisher n'était pas nulle. Par ailleurs, dans le régime non-markovien, l'exploitation des corrélations classiques des canaux bruités pourrait améliorer, dans une certaine mesure, la téléportation bidirectionnelle de l'information. Alors qu'en prenant en compte les effets de mémoire dus aux corrélations temporelles, l'effet drastique de tous les types de bruit considérés sur la téléportation bidirectionnelle de l'information pourrait notamment être atténué pour une large gamme de temps.

En outre, nous avons étendu le protocole de TQB afin de permettre à trois partenaires, Alice, Bob et Charlie, d'échanger bilatéralement leurs états quantiques à l'aide d'un état GHZ. En outre, nous avons généralisé le schéma bidirectionnel tripartite proposé à un réseau quantique composé de N partenaires. Dans le schéma proposé, la tâche de téléportation ne peut être accomplie sans la contribution de tous les partenaires. Dans un autre contexte, afin de ne pas restreindre le BQT à la téléportation d'états quantiques inconnus seulement, nous avons proposé un nouveau schéma pour la téléportation bidirectionnelle de la porte CNOT. En se basant, sur ce dernier schéma, nous avons conçu un protocole BQT pour la téléportation de deux et trois qubits. Nous avons discuté de la possibilité de généraliser ce protocole aux états à n-qubits.

Contents

List of Figures

List of Tables

List of Abbreviations

QP	**Q**uantum **P**hysics.
BQT	**B**idirectional **Q**uantum **T**eleportation.
BCQT	**B**idirectional **C**ontrolled **Q**uantum **T**eleportation.
QM	**Q**uantum **M**easurement.
QT	**Q**uantum **T**eleportation.
NMR	**N**eclear **M**agnetic **R**esonance.
WRM	**W**eak and **R**eversal **M**easurements.
POVM	**P**ositive **O**perator **V**alue **M**easurement.
CNOT	**C**ontrolled **N**OT.
QN	**Q**uantum **N**etwork.
CPTP	**C**ompletely **P**ositive **T**race **P**reserving.
PP	**P**urification **P**rotocols.
DFS	**D**ecoherence **F**ree **S**ub-space.
QZE	**Q**uantum **Z**eno **E**ffect.
AD	**A**mplitude **D**amping.
QFI	**Q**uantum **F**isher **I**nformation.
QFIM	**Q**uantum **F**isher **I**nformation **M**atrix.
QIP	**Q**uantum **I**nformation **P**rocessing.

Introduction

Quantum physics (QP) is a discipline within theoretical physics that is interested in the study and description of matter and radiation at the atomic and subatomic scale. QP bridges the gap in our understanding of nature and it is at the heart of our current technological development. The origins of quantum theory can be traced back to the early nineteenth century, when physicists were confronted with new and unexpected problems that they were unable to solve using classical physics laws, such as the black body radiation and the photoelectric effect. In fact, quantum physics is a probabilistic [1] and counter-intuitive theory [2], which is often presented in a mathematical formalism that can be confusing. Thus, all the predictions given by quantum theory are of a probabilistic character and it is not totally compressible in the classical reasoning [3]. In fact, quantum physics has proven a clear description of the atom structure. Furthermore, it has proven compatible with the electromagnetic, weak and strong nuclear interactions, this compatibility leads to their unification on the standard model [3]. Despite its successful explanation of many problems and conformity to experiment expectations, there is no agreement on the physical interpretation of its concepts and ideas [4]. Among these concepts and ideas, the particle-wave duality, the measurement problem, and the physicality of information. To put it another way, can we consider information as a constituent of physical reality?

In fact, information is not an abstract entity, but it can only exist through a physical representation [5]. In other words, we can certainly find information encoded in a physical entity, whether it is an atom, photon, ion or any other quantum particle. Accordingly, information is subjected to the laws of quantum physics. The seminal works done by *Shannon* [6, 7], which is one of information theory's pioneers, is mainly focused on the rates of information transmission via noisy and noiseless classical communication channels. Furthermore, *Shannon* introduces the notion of the classical *bit*, which can be represented as a vector pointing in two different states 0 or 1, for example a switch that could be *up* or *down*, or a capacitor that can be full or discharged. Later on, physicists have been interested in the investigation of information transmission through systems that are governed by the laws of quantum physics. Consequently, quantum information theory has emerged as a new interdisciplinary research field that combines information theory with the laws of quantum physics.

Basically, information could be encoded on a qubit [8], which is the basic quantum system. A qubit can be represented in two different vector states: $|0\rangle$ and $|1\rangle$ or in an arbitrary superposition of these states [9]. The quantum superposition could be interpreted as an interference of the two possibilities, $|0\rangle$ and $|1\rangle$. In effect, the quantum superposition is a distinguishing feature of quantum theory. Moreover, it has been demonstrated in many particles such as electron [10], atom [11], neutron [12] and in multi-particle systems [13]. A superposition of N qubits results in 2^N possibilities ($N > 1$). For this reason, considering qubits offers more powerful capacity to store and process information than the classical bit [14]. Accordingly, exploiting the qubit as support of information, in a quantum computer, enables the simulation of complicated situations [15]. The qubit has been physically realized using the polarization of photons, spin of particles, position of an atom, electronic degree of freedom of an ion or atom [9]. On the other hand, the fact that quantum physics is a non-local theory was not accepted by *Einstein*, *Podolsky* and *Rosen* (EPR). In 1935, they tried to demonstrate that the quantum theory does not completely describe physical reality [16] by elaborating a thought experiment, known as the EPR paradox [16], to be the Achilles' heel of the quantum theory. Indeed, the EPR paradox has attracted the attention of *Bohr* who discussed it deeply with *Einstein*, but the EPR paradox had not been a matter of concern to the large scientific community until the publication of *Bell*'s paper in 1964 [17]. *Bell* presented a mathematical reformulation of the EPR paradox based on the local hidden variables [17]. Actually, *Bell* proposed a test for the existence of the hidden variables. Thus, he developed his famous inequality as the basis for such a test. Thereafter, many experiments have been conducted to test the Bell's inequality [18, 19]. Eventually, *Alain Aspect et al.* experiments have confirmed the violation of Bell's inequality [20], which relies on hidden variables and validates, with no doubt, the non-locality of the quantum theory [21] and the existence of entanglement.

In early studies, quantum correlations were considered as a synonym of the quantum entanglement. Nowadays, however, it is shown that quantum correlations are a wide notion in which entanglement is a special type of them. More precisely, entanglement can be identified as non-local quantum correlations [22]. Due to the fact that entanglement is the central pillar for performing quantum information processing tasks with high performance, its identification and quantification, in different systems, have attracted the attention of physicists, and it is still an open problem at the theoretical and experimental levels. During the last three decades, many efforts have been made to elaborate an efficient measurement of the entanglement amount in bipartite and multi-partite systems. Among these measures, we cite: the concurrence [23], the negativity of the partial transpose [24] and the residual tangle [25]. The entanglement, in fact, cannot be created or increased using any local operation. Moreover, an entanglement measure should be null for a separable state and equal "1" for a maximally entangled state. Yet, entanglement has been observed in different systems, such as photons [26], superconducting Josephson junctions [27] as well as in the hybrid systems [28] which are composed of photonic and matter qubits. Also, it was demonstrated for two electrons separated by more than $1Km$ [29]. Nowadays, entanglement has passed from being a spooky action at a distance [17] to be one of the main studied topics in the field of quantum information, which certainly leads to the second quantum revolution. Wherein the second quantum revolution, the rules that govern the physical world are used to boost the technological development. In the current time, different sources of entanglement are already exploited and commercialized [30, 31].

In spite of their conceptual relevance, the exploitation of the superposition and entanglement led to the development of quantum information science and paved the way to real-world applications for quantum communication and quantum computing. In the $1990s$, several incremental proposals have been done in the fields of quantum computation and communication, by exploiting the physical resources such as, superposition and entanglement, yielding to more powerful algorithms compared to their classical counterparts. *Shor* [32] proposed a quantum algorithm for factoring large numbers, which is a very though task to do without taking into consideration quantum resources. Moreover, *Grover* presented that quantum resources can speed up a range of search applications over unordered database [33]. In the meantime, numerous quantum communication protocols have been proposed, offering a reliable way of transmitting quantum states between distant communication parties [34].

The safe transmission of quantum states from one location to another is a primary objective for quantum information processing [30]. Unfortunately, the direct replication of one quantum state to another is forbidden [35], and measuring the quantum states can destroy their superposition [36]. Accordingly, *Bennet et al.* [34] came up with a revolutionary idea, in which it is possible to teleport an unknown quantum state of a qubit using a two-qubit maximally entangled state and classical communication. It is worthwhile to mention that this teleportation is rather only about transferring unknown quantum information, not at superluminal velocity, which agrees with the theory of relativity. Besides, quantum teleportation (QT) is of paramount importance for the establishment of a large-scale quantum network [37, 38]. It also accelerates the development of new technological applications such as quantum repeaters [39], the quantum internet [37] and quantum blind computing [40, 41]. Quantum teleportation has also been useful in investigating other areas of research such as black-hole evaporation [42]. In addition, it is used for closed time-like curves [43]. In light of its importance, QT has become a research hot-spot in the last two decades. It is achieved experimentally by means of different substrates, such as photonic qubits [44, 45, 46], solid-states [47, 48], time-bin [49, 50], using Nuclear Magnetic Resonance (NMR) [51], between light and matter [52] and between light and motion [53]. In principle, the solid-state is promising for short teleportation distance, which is less than $1km$. As for a few kilometers, it could be developed using optical modes. However, for long-distance quantum teleportation (beyond 100 km), the photonic qubits are the best carriers for information over long fibres or free-space [54]. Nevertheless, in 2012, quantum teleportation over 143 km was achieved between the Canary Islands "La Palma" and "Tenerife" [55]. In 2017, quantum teleportation was accomplished over a 1400 km distance from a ground observatory to a low-orbit satellite [56]. On the theoretical side, there are plenty of modified teleportation protocols, such as controlled teleportation [57], quantum gate teleportation [58] and cyclic teleportation [59]. QT was not limited to discrete variables but was extended to continuous-variables (CV) [60, 61], which are quantum systems with an infinite-dimensional Hilbert space [62]. In effect, all these teleportation protocols are unidirectional, meaning that the transmission of information can be assured only in one direction from a sender to a receiver, namely from Alice to Bob.

A significant step in the path towards a scalable quantum network is by making the quantum teleportation process possible in two opposite directions, from Alice to Bob and reversely from Bob to Alice. The issue of the bidirectional teleportation of quantum states is firstly raised by *Vaidman et al*. [63] as a thought experiment. In this work [63], *Vaidman et al*. aim at swapping the quantum states of two separated atoms, using two independent quantum channels. Afterwards, *Huelga et al*. [64, 65] presented an idea of bidirectional quantum teleportation in a context related to quantum control, where Alice teleports an unknown quantum state to Bob. After he (Bob) receives the state, Bob applies a quantum operation to the quantum state and returns it to Alice. Later on, various bidirectional quantum teleportation and bidirectional controlled quantum teleportation protocols ($BCQT$) have been suggested using several quantum channels, such as GHZ states [66], composite GHZ-Bell states [67], and n-entangled qubit states (with $n > 4$) [68, 69]. Indeed, in the $BCQT$ protocols, Alice and Bob cannot exchange their quantum states without the control of a third part, called *Charlie*, which acts like a supervisor of the bidirectional teleportation process. Because Charlie can neither teleport nor receive quantum states in the bidirectional controlled quantum teleportation scheme, we ask the question if we can extend the bidirectional quantum teleportation by including a third party (Charlie) as a partner. In the same regard, is it possible to extend the bidirectional teleportation of quantum states to the N party? Furthermore, can we unlimit the BQT from unknown quantum states only, and make it possible for entangled states and quantum operations?

As a matter of fact, bidirectional quantum teleportation protocols seldom take into account the problem of decoherence [70], which was the result of addressing the problem of the quantum-to-classical transition [71]. The issue is that the quantum system cannot be perfectly isolated from its surrounding environment and the complete control of the environment is not always possible [1]. In addition, when a quantum system interacts with its environment it will, in general, become entangled with the large number of environmental degrees of freedom. This entanglement of the open system with the environment dramatically influences the quantum resources, in particular the superposition and entanglement, of the system even when the impact of the environment is small. Many efforts have been devoted to investigate the decoherence through the master equation [1]. Moreover, it is possible to observe the drastic effect of decoherence in experiments using cavity QED [72], superconducting systems [73], and ion traps [74]. Thus, decoherence is the most limiting factor for the realization of quantum teleportation protocols and their implementation with high efficiency. So, it is essential to preserve the quantum resources which serve as the essence of many quantum information and computation protocols [75].

Indeed, any physical operation can be represented by a quantum channel [1], mapping an initial state to a final state [76]. For closed quantum systems, unitary evolution is sufficient to describe the dynamics. However, for open quantum systems, the interaction between the system and the environment leads to a non-unitary evolution (e.g., dissipation, dephasing). Generally, a physical[2] non-unitary evolution can be

[1]The term "quantum channel" typically refers to the actions of the noisy environment on the system of interest. It does not, however, coincide with the quantum channel of bidirectional quantum teleportation, which is an entangled state.

[2]An example of non-physical operation is the transposition (please see [77] page 369)

described by a quantum channel which must be a completely positive trace preserving $(CPTP)$ map [77]. Actually, $CPTP$ maps can be described by means of the *Kraus* operators [78], which encode the effect of the environmental noise on the open quantum system of interest. Well-defined quantum noisy channels are considered for the study and the description of the environment effects on quantum systems, such as the amplitude damping channel [77], which describes an open quantum system undergoing a spontaneous dissipation of energy, and the dephasing channel [79] describing the loss of information without loss of energy [74]. Moreover, the bit-flip, bit-phase flip and the depolarizing channel [77], describe a quantum system that is assumed to suffer from Pauli X (bit-flip) errors, Z (phase flip) errors, or Y (both), frequently used in the context of error correction and it can be efficiently simulated with a classical computer [74]. All the former noisy quantum channels are usually encountered in realistic implementations of quantum communication protocols [74]. In particular, we indicate memoryless or with memory noisy channels where multiple actions of the environmental noise are independent from each other or correlated, respectively. Nevertheless, it is recently shown that more noise leads to more efficiency. In other words, *Fortes et al*. [80] have shown that, in the case of unavoidable noise, it is better to subject the quantum system to different noise channels in order to increase the efficiency of the teleportation protocol. The main effect of noise is to turn pure states into mixed ones. It is shown that noise decreases the quantum entanglement and coherence [81, 82]. it may also cause the complete vanishing of entanglement in a finite time or what is known as entanglement sudden death (ESD) phenomenon [83].

In this regard, to mitigate the decoherence effect, several techniques have been suggested in the literature, such as the purification protocols (PP) which permit the distillation of highly entangled states from less entangled ones. However, if the states are fully separable, we cannot obtain an entangled state from separable states [84]. Another approach to mitigate the effect of the decoherence is the decoherence-free subspace (DFS). DFS requires a symmetry in the system-environment interaction which is not always applicable [85]. Also, the quantum Zeno effect (QZE) could be used to mitigate the effect of decoherence. QZE relies on the idea that the time evolution of a given quantum state slows down due to the frequent measurements of the system [86]. On the other hand, if the frequent measurements are not rapid enough, we could have a reverse effect which may accelerate the system evolution (quantum anti-zeno effect) [87]. Another method to overcome the effects of decoherence is the weak and reversed measurements[3] (WRM). The (WRM) allow us to extract little information about the quantum state by weakening the coupling strength sufficiently between the system of interest and the measurement device [89]. Due to the weak measurement, the system does not fully collapse toward an eigenstate [90]. Therefore, it is possible to recover the initial state with some operations [91]. Recently, it was shown that the weak and reversed measurements can preserve the qubit state from decoherence due to zero temperature relaxation [92]. Later on, this work [92] was extended to preserve the entanglement of two-qubit and three-qubit systems from decoherence [93, 94, 95]. Moreover, the weak and reversed measurements can preserve entanglement and improve the fidelity of GHZ and W states undergoing amplitude damping (AD) [96]. In the unidirectional quantum teleportation context, *Pramanik et al*. showed that the weak and the reversed measurements can increase the teleportation fidelity through noisy quantum channels [97]. Beside the weak and reversed measurements, another technique to overcome the problem of decoherence is based on the exploitation of the memory effects arising when the open quantum system interacts with its environment in the non-Markovian regime, inwhich the recent state of the quantum system depends on its previous states [98, 99]. In the non-Markovian regime, the system loses information to the surrounding environment and retrieves some of it [100]. In fact, there are two types of memory effects. The first one is due to the classical correlations between successive actions in the noisy environment [101], while the second one stems from the temporal correlations arising in the course of the time evolution of the system of interest [102]. The identification and quantification of the non-Markovian dynamics is an unsolved

[3] The weak and the reversed measurements discussed in our work are generalizations of von Neumann measurements and are associated with a positive operator-valued measure $(POVM)$, and should not be confused with the weak value elaborated by *Aharonov et al*. [88].

problem in open quantum system theory [103]. Many distinct criteria have been proposed to identify the non-Markovian memory effects. For a review on this subject, readers may look into references [104] and [105]. Numerous measures of non-Markovianity have been discussed, such as the trace distance [106], which is based on the distinguishability of quantum states, the fidelity [107], quantum Fisher information (QFI) [108] and quantum mutual information [109]. The relationship between the two types of memory effects is studied in Ref [110]. However, the combined effect of the two types of memory effects is shown for two-qubit coherence [111]. Although both techniques, the weak and the reversed measurements technique and the memory effects, have been widely explored in the literature as separate subjects, we do not know if these techniques are equivalent or not. In other words, we still do not know if these methods could mitigate the noise effects and enhance entanglement and bidirectional teleportation with the same efficiency.

Actually, in the presence of decoherence, the quality of the reconstruction of the teleported state, from Alice to Bob, is measured by means of its teleportation fidelity (f). Indeed, the fidelity f is a measure of the closeness between Alice's input state and Bob's output state [77], where $0 \leq f \leq 1$. The fidelity equals the unity $(f = 1)$, which is the maximal value of the fidelity, when the protocol works perfectly. Otherwise, it is less. Indeed, the fidelity was first studied by *Uhlmann* [112] and *Alberti* [113] who investigated the transition probability between quantum states. After that, it was studied by *Josza* [114], and by *Schaumacher* [115] in the field of quantum communication. The threshold of the fidelity $f = \frac{2}{3}$ is known as the fidelity of classical teleportation, inwhich Alice may directly measure her qubit state and sends the measurement outcome to Bob in order to prepare a similar qubit state. Therefore, a teleportation fidelity of qubit states which is greater than the classical threshold, namely $f > \frac{2}{3}$, is a clear evidence that the quantum resources are utilized to accomplish the teleportation process [54].

Apart from quantum state teleportation, in some contexts, one needs to teleport the information encoded in a relevant parameter, like the weight or the phase of a qubit, instead of the whole system state. In this regard, the quantum Fisher information (QFI) [116] is more practical to quantify the reliability of the parameter teleportation [117]. The notion of Fisher information is introduced thanks to the earlier studies of *Ronald Aylmer Fisher* in which he was interested in the concept of information in the frame of the estimation theory [118]. Due to the high interest devoted to Fisher information, this leads to the development of a quantum version of Fisher information, namely QFI, which is developed for quantum systems [119]. In particular, QFI quantifies the sensitivity of a quantum state with respect to the changes occurring on the relevant parameter [120]. It has been extensively investigated in different fields of research such in quantum Estimation, where it gives the highest achievable precision in various parameter estimation tasks [121]. Actually, QFI plays an important role in the estimation of a single parameter through the Cramer-Rao bound, whereas more precision is achieved for a large value of QFI [119, 122, 123]. In addition, the measurement of different quantities of interest in quantum information theory cannot be directly done such as the purity of a quantum state or quantum correlations. In such a situation, the problem becomes a parameter estimation problem and one must turn to estimate the quantity of interest by means local quantum estimation tools [122]. In fact, estimation problems involve assigning appropriate values to the quantities that are unknown because they are not fully accessible by observation. The objective of an estimation procedure is to find the best strategy for inferring the value of an unknown parameter with the highest possible accuracy [122]. This is done by performing indirect measurements on the quantum system, i.e. by deducing the value of the parameter by processing the set of measurement results of another observable. The Cramer-Rao bound gives the ultimate limit of the precision withwhich the parameter of a physical system can be estimated [119, 122, 123], where the variance of the parameter is small for a large value of QFI. However, the issue of simultaneous multi-parameter estimation is required in many scenarios [124]. Thus, the quantum Fisher information matrix $(QFIM)$ [125] provides a tool to determine the estimation precision of any multi-parametric protocol. Beside the quantum estimation theory, QFI and $QFIM$ are crucial concepts in quantum metrology [126, 127], quantum sensing [128]. QFI and $QFIM$ also connect to other aspects of quantum physics, such as quantum phase transition [129, 130], entanglement detection [131]. QFI measures the phase sensitivity of the systems [132]. Moreover, QFI in non-inertial frames has been investigated for different systems, such as the behavior of the teleported QFI under the Unruh-acceleration effect is investigated by *Metwally* [133, 134]. QFI is used to predict decoherence in the preparation of cat states [135]. It is also used as a quantifier of the degree of estimation of two interacting qubits under decoherence [136].Furthermore, it has been shown that QFI can be considered as a widely used and a successful tool to measure the credibility of transmitting the information encoded in a quantum paramrter through the process of quantum teleportation [117, 137]. Accordingly, the link between QFI, entanglement and teleportation is an open area of research until now.

Certainly, the fidelity and the quantum Fisher information are two figures of merit to assess the bidirectional teleportation protocol. Both quantities are related to the *Bruse* distance [138], which is a geometrical measure for distinguishing quantum states. It was shown that, in the case of pure states and full-rank density operators, the fidelity susceptibility is proportional to the quantum Fisher information [139, 140]. Furthermore, *Liu et al*. [141] have proven that the proportionality of the fidelity susceptibility and the quantum Fisher information remains even in the case of non-full rank matrices. Besides, it was shown that the fidelity and the quantum Fisher information are very sensitive to the environmental noise [142, 143]. To the best of our knowledge, teleportation fidelity and quantum Fisher information have not yet been studied in relation to each other, particularly in light of bidirectional quantum teleportation. Moreover, a rigorous study on the effects of the WRM and the memory effects on the teleportation fidelities and on the quantum Fisher information, where the bidirectional teleportation protocol is affected by different noise types; such as: the bit flip, the phase flip, the depolarizing and the amplitude damping, is still missing.

Nowadays, improving the efficiency of quantum teleportation and its extension to scalable quantum network is a primordial step in the path toward a global quantum network. In fact, the aim of our research through this thesis is to investigate bidirectional quantum teleportation and suppress the effect of the noise, which drastically reduces the average fidelities of teleportation and the quantum Fisher information. In addition, we evaluate bidirectional quantum teleportation through typical noisy quantum channels, such as bit-flipping, phase-flipping, depolarizing, and amplitude-damping. We compare the impact of the WRM technique and the memory effects technique on the efficiency of bidirectional quantum teleportation. In this work, we take into account the challenge of extending the bidirectional quantum teleportation protocol to a large-scale quantum network and not restricting the bidirectional quantum teleportation only to unknown quantum states and relevant parameters but also make it possible for the quantum gate and entangled states.

.0.1 Outline of the thesis

This thesis is outlined according to the following plan:

In the first chapter:

We present some preliminary tools and concepts of quantum information that are useful for a good comprehension and more flowing reading. We will review the notion of qubit, quantum measurement, quantum gates and circuits, and noisy channels. Moreover, we will present entanglement and quantum teleportation quantifiers, such as the negativity of the partial transpose, fidelity average, quantum Fisher information and quantum Fisher information matrix.

In the second chapter:

We deal with the bidirectional quantum teleportation protocol by means of a perfect quantum channel, i.e., without noise. We demonstrate the connection between the teleportation fidelities and the quantum Fisher information. Then, the individual teleportation against the simultaneous parameter teleportation is studied.

In the third chapter:

We investigate the bidirectional quantum teleportation in the presence of typical noisy channels such as bit flip, phase flip, bit-phase flip, depolarizing, and amplitude damping. The effect of weak and reversed measurements on the efficiency of the bidirectional teleportation protocol will also be investigated. Later on, we will concentrate on the impact of the correlations in the quantum channels on the teleportation of information. We will also explore the combined effect of the classical and temporal correlations in the noisy quantum channels on the entanglement of the quantum channel of the BQT and on the teleportation fidelities and quantum Fisher information.

In the last chapter:

We will extend the bidirectional teleportation so that three partners can exchange states bilaterally by using a GHZ state and three auxiliary qubits. Subsequently, we will extend the suggested scheme to N partners. We will suggest a BQT scheme for a bipartite and a tripartite entangled states based on another suggested scheme for the non-local implementation of $CNOT$ gate.

Finally, we shall recapitulate the main findings of this thesis and we will mention some future perspectives.

.0.2 Contributions

The main findings presented in this thesis have been reported in various contributions:

List of publications:

- *"Bidirectional teleportation using Fisher information", **C. Seida**, A. El Allati, N. Metwally and Y. Hassouni. Modern Physics Letters A, 35 (33), 2050272 (2020).*
- *"Bidirectional teleportation under correlated noise", **C. Seida**, A. El Allati, N. Metwally and Y. Hassouni. The European Physical Journal D, 75 (6), 1-12 (2021).*
- *"Multi-party bidirectional teleportation", **C. Seida**, A. El Allati, N. Metwally and Y. Hassouni. Optik, 247, 167784 (2021).*
- *"Efficiency increasing of the bidirectional teleportation protocol via weak and reversal measurements", **C. Seida**, A. El Allati, N. Metwally and Y. Hassouni. Physica Scripta (2022).*
- *"Simultaneous communication of relevant parameters", **C. Seida**, M. Ziane and A. El Allati, 2nd International Conference on Innovative Research in Applied Science, Engineering and Technology (IRASET) pp. 1-4 (2022).*

- *"Memory effects on bidirectional teleportation", **C. Seida**, S. Seddik, Y. Hassouni and A. El Allati. (submitted)*
- *"Bidirectional non-local implementation of CNOT gate", **C.Seida**, A. El Allati and Y. Hassouni. (submitted)*

List of conferences:

- *The international conference on emerging trends in pure and applied mathematics, Bahrain (2021).*
  Title of the talk: Bidirectional quantum teleportation using Fisher information.
- *The 2nd international conference on innovative research in applied science, engineering and technology, faculty of sciences Meknes Morocco (2022).*
  Title of the talk: Simultaneous communication of relevant parameters.
- *The international conference of physics students, Niels Bohr institute Copenhagen Denmark (2021).*
  Title of the talk: Quantum teleportation- ubiquitous, enigmatic and essential.
- *The 25th Annual conference on quantum information processing, California institute of technology (2022).*
  Title of the talk: Bidirectional quantum teleportation, Applications and obstacles.
- *International conference of physics students Niels Bohr institute, Copenhagen Denmark (2021).*
  Title of the poster: Bidirectional teleportation of relevant parameters.
- *10 éme Rencontre Nationale des Jeunes Chercheurs en Physique (RNJC′10), faculty of sciences Ben M'Sick Casablanca Morocco (2021).*
  Title of the poster: Noisy two-way quantum teleportation aided with Weak measurement.
- *La journée doctorale du réseau Marocain de l'information quantique, faculty of sciences in Kenitra Morocco (2021).*
  Title of the poster: Two-Way quantum teleportation.
- *The second African Conference of Fundamental and Applied Physics, Marrakesh Morocco (2022).*
  Title of the poster: Quantum Remote control: teleportation of quantum gates.

Chapter I

Preliminary to quantum information processing

In this chapter, we shall introduce some preliminary concepts and tools of quantum information processing (QIP) which are useful for a good comprehension of the present thesis. We start, in Sec I.1, by the notion of qubit which is the basic system of quantum information. We describe, in Sec I.2, the notions of projective, weak and reversed measurements. In Sec I.3, we recall some quantum gates which are the building blocks of quantum information processes such as quantum teleportation and quantum algorithm. Subsequently, in Sec I.4, we present the notion of quantum circuit. Moreover, in Sec I.5, we provide a short review on independent and correlated noisy quantum channels. In Sec I.6, we present some entanglement and teleportation quantifiers, namely the Negativity and the fidelity average. Furthermore, we introduce quantum Fisher information and quantum Fisher information matrix in Sec I.7.

I.1 Qubit

In quantum information theory, transmission, storage and processing of information are done by means of qubits [77]. A qubit is a two-level system with one characteristic property that can have two possible values [144]. Actually, a qubit is a physical entity governed by the laws of quantum physics. Simple examples of qubits are the polarization of photons or two-level atoms [145, 146, 147, 148]. Moreover, the qubit may be mathematically represented as a unit vector in a two-dimensional *Hilbert* space $\mathcal{H}$. $\mathcal{H}$ is a complex vector space with inner product, the quantum sate lives in the Hilbert space$|\psi\rangle \in \mathcal{H}^2$ as:

$$|\psi\rangle = \alpha|0\rangle + \beta|1\rangle, \tag{I.1}$$

Where α and β are probability amplitudes ($\alpha, \beta \in \mathbb{C}^2$) that satisfy the normalization constraint:

$$|\alpha|^2 + |\beta|^2 = 1 \tag{I.2}$$

And $\{|0\rangle, |1\rangle\}$ is a computational basis which forms an orthonormal basis for $\mathcal{H}^2$. A qubit is generically represented as a coherent superposition of the basis states $|0\rangle$ and $|1\rangle$ (Eq.I.1), and depending on the values of the coefficient α and β, one can prepare an infinite number of states $|\psi\rangle$. While the classical bit is definitely either 0 or 1, the qubit generalizes the calssical bit [144].

A general pure qubit state can be written as:

$$|\psi\rangle = \cos\left(\frac{\theta}{2}\right)|0\rangle + e^{i\phi}\sin\left(\frac{\theta}{2}\right)|1\rangle. \tag{I.3}$$

Where θ, and $\phi \in \mathbb{R}$. The state is parameterized by two angles $0 \leq \theta \leq \pi$ and $0 \leq \phi \leq 2\pi$. The angles θ and ϕ correspond to the polar and azimuthal angle of spherical coordinates.

In matrix representation [77], the single qubit state, Eq.(I.1) could be represented by means of the density operator $\hat{\varrho}$:

$$\hat{\varrho} = |\psi\rangle\langle\psi| = \begin{pmatrix} |\alpha|^2 & \alpha\beta^* \\ \alpha^*\beta & |\beta|^2 \end{pmatrix} \tag{I.4}$$

Whereas:

$$|0\rangle\langle 0| = \begin{pmatrix} 1 & 0 \\ 0 & 0 \end{pmatrix}, \qquad |1\rangle\langle 1| = \begin{pmatrix} 0 & 0 \\ 0 & 1 \end{pmatrix}. \tag{I.5}$$

Theorem.1 An operator $\hat{\varrho}$ is said to be a density operator associated to a set $\{p_i, |\psi\rangle\}$ if and only if the following statements are verified:

1. $\hat{\varrho}$ is Hermitian, $\hat{\varrho} = \hat{\varrho}^\dagger$.
2. $Tr(\hat{\varrho}) = 1$.
3. $\hat{\varrho}$ must be positive.
4. $Tr(\hat{\varrho}\hat{A}) = \sum_i^n p_i \langle\psi|\hat{A}|\psi_\rangle, \forall \hat{A} \in \mathcal{H}$.
5. $Tr(\hat{\varrho}^2) \leq 1$.

Proof.1

- The hermicity of ϱ means that the eigenvalues of the density matrix are real. The density operator ϱ could be decomposed into the form:

$$\hat{\varrho} = \sum_i p_i |\psi_i\rangle\langle\psi_i| \tag{I.6}$$

With p_i is the probability $0 \leq p_i \leq 1$.

$$\hat{\varrho}^\dagger = (\sum_i p_i |\psi_i\rangle\langle\psi_i|)^\dagger = \sum_i p_i |\psi_i\rangle\langle\psi_i| = \hat{\varrho} \tag{I.7}$$

- $Tr(\hat{\varrho}) = 1$ is the normalization condition where $\sum_n p_n$ must equal one.

$$\begin{aligned} Tr(\hat{\varrho}) &= \sum_i p_i Tr(|\psi_i\rangle\langle\psi_i|) \\ &= \sum_{ij} p_i \langle\psi_j|\psi_i\rangle\langle\psi_i|\psi_j\rangle \\ &= \sum_i p_i = 1 \end{aligned} \tag{I.8}$$

- Positively
Let us suppose that $|\Phi\rangle$ is any arbitrary state. Then:

$$\begin{aligned} \langle\Phi|\hat{\varrho}|\Phi\rangle &= \sum_i p_i \langle\Phi|\psi_i\rangle\langle\psi_i|\Phi\rangle \\ &= \sum_i p_i |\langle\Phi|\psi_i\rangle|^2 \geq 0 \end{aligned} \tag{I.9}$$

- The expectation value of an observable $\hat{A}$

$$
\begin{aligned}
Tr(\hat{\varrho}\hat{A}) &= \sum_j \langle\psi_j|\hat{\varrho}\hat{A}|\psi_j\rangle \\
&= \sum_j p_i \langle\psi_j|\psi_i\rangle\langle\psi_i|\hat{A}|\psi_j\rangle \qquad \text{(I.10)} \\
&= \sum_i p_i \langle\psi_i|\hat{A}|\psi_i\rangle \qquad \text{(I.11)}
\end{aligned}
$$

- The fourth statement: Let us assume the orthonormal states $|\Phi_i\rangle$ and $|\Phi_j\rangle$ in $\mathcal{H}$.

$$
\begin{aligned}
Tr(\hat{\varrho}^2) &= \sum_n \langle n| \sum_i \sum_j p_i p_j |\Phi_i\rangle\langle\Phi_i|\Phi_j\rangle\langle\Phi_j|n\rangle \\
&= \sum_i \sum_j p_i p_j \langle\Phi_i|\Phi_j\rangle\langle\Phi_j| \sum_n |n\rangle\langle n|\Phi_i\rangle \\
&= \sum_i \sum_j p_i p_j |\langle\Phi_i|\Phi_j\rangle|^2 \qquad \text{(I.12)} \\
&= \sum_i p_i^2. \qquad \text{(I.13)}
\end{aligned}
$$

Since $0 \le p_i \le 1$, it is obvious that $p_i^2 \le p_i$ and, therefore, $\sum_i p_i^2 \le (\sum_i p_i = 1)$. Thus, we can conclude that $Tr(\hat{\varrho}^2) \le 1$.

The state Eq. (I.3) could be given in terms of Bloch vectors as follows [77]:

$$
\begin{aligned}
\hat{\varrho} = |\psi\rangle\langle\psi| &= \frac{1}{2}\hat{I} + \frac{1}{2}\begin{pmatrix} \cos(\theta) & \sin(\theta)e^{-i\phi} \\ \sin(\theta)e^{i\phi} & -\cos(\theta) \end{pmatrix} \qquad \text{(I.14)} \\
&= \frac{1}{2}\begin{pmatrix} 1+h_z & h_x - ih_y \\ h_x + ih_y & 1-h_z \end{pmatrix} = \frac{1}{2}(\hat{I} + \vec{h}.\vec{\sigma})
\end{aligned}
$$

Where: $\hat{I}$ is 2×2 identity matrix and $\boldsymbol{\sigma} = (\sigma_x, \sigma_y, \sigma_z)^T$ are the Pauli matrices which are given as:

$$
\sigma_x = \hat{X} = \begin{pmatrix} 0 & 1 \\ 1 & 0 \end{pmatrix}; \qquad \sigma_y = \hat{Y} = \begin{pmatrix} 0 & -i \\ i & 0 \end{pmatrix}; \qquad \sigma_z = \hat{Z} = \begin{pmatrix} 1 & 0 \\ 0 & -1 \end{pmatrix} \qquad \text{(I.15)}
$$

and

$$
\vec{h} = (h_x, h_y, h_z) = (\sin(\theta)\cos(\phi), \sin(\theta)\sin(\phi), \cos(\theta)). \qquad \text{(I.16)}
$$

The Bloch vector $|\vec{h}| = 1$ represents a pure state while for mixed states $|\vec{h}| < 1$. A geometric interpretation of a single qubit state can be given using the Bloch sphere, which is a unit sphere represented in Fig.(I.1). Each point on the Bloch sphere corresponds to a different possible superposition of a single qubit. The top and the bottom of the sphere correspond to the two measurable states of the qubit, $|0\rangle$ and $|1\rangle$ correspond to $\theta = 0$ and $\theta = \pi$, respectively. Indeed, the Bloch sphere provides a facility to understand ideas about quantum information and quantum computation [77].

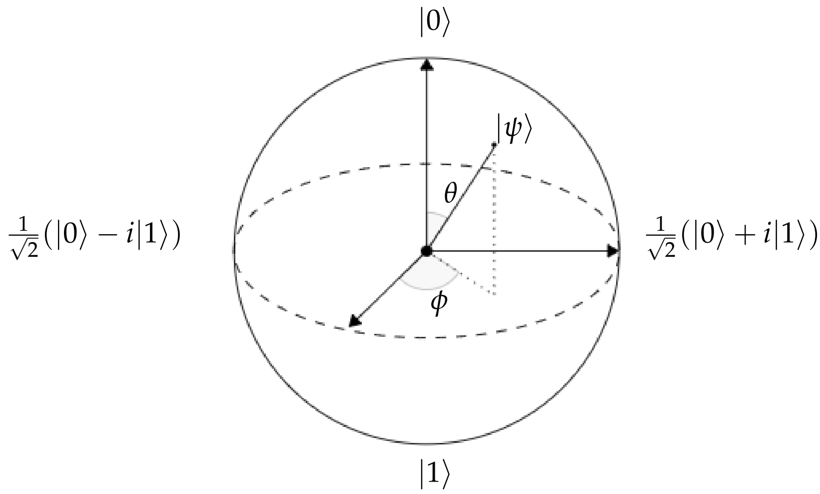

FIGURE I.1: Bloch sphere representation of a single qubit

The state of n composite qubit (with $n > 2$) is given by the tensor product state [79]:

$$|\psi\rangle^{\otimes n} = |\psi\rangle_1 \otimes \dots |\psi\rangle_n \tag{I.17}$$

$$|0\rangle^{\otimes n} = |0\rangle_1 \otimes \dots |0\rangle_n \tag{I.18}$$

$$|1\rangle^{\otimes n} = |1\rangle_1 \otimes \dots |1\rangle_n \tag{I.19}$$

The quantum information carried by a qubit could be extracted through quantum measurement; where the linear superposition of the qubit collapses into one of the basis states. In what follows, we define the notion of quantum measurement, we review the projection postulate which is one of the basic postulate of quantum mechanics.

I.2 Quantum measurement

The quantum measurement (QM) is one of the open problems in quantum physics. Due to the fact that it gives only the possibilities of getting different outcomes in an experiment and does not provide any mechanism by which these outcomes occur. Quantum measurement is a probabilistic process which provides the extraction of information about quantum states. It is an essential concept in quantum computation and quantum information fields [77]. Generally, quantum measurement can be classified to two types. The first one is quantum measurement that can be repeated on the same system without changing the result of measurement [149]. Otherwise, it is of the second type [150].

I.2.1 Projective measurement

The quantum measurement of the first type (also called projective or sharp measurement), which is introduced by *von Neumann* $(1903 - 1957)$, causes the complete demolition of the quantum state. In other words, the projective measurement leads to the total extraction of information encoded in the quantum state. As a price to pay, the system's state is totally collapsed to an eigenstate. The third postulate of quantum physics underlies the following

Measurement postulate: The only possible result of the measurement of a physical quantity $\mathcal{O}$ is one of the eigenvalues of the corresponding observable $\hat{\mathcal{O}}$.

To put it clearly, we consider the system's quantum state represented by $|\psi^{(s)}\rangle$. The quantum state $|\psi^{(s)}\rangle$ could be written as a decomposition into orthonoraml basis $|\mathcal{O}_n\rangle$ of the observable $\hat{O}$:

$$|\psi^{(s)}\rangle = \sum_n o_n |\mathcal{O}_n\rangle \tag{I.20}$$

The probability of measuring the eigenvalue a_n, where $\hat{O}|\mathcal{O}_n\rangle = a_n|\mathcal{O}_n\rangle$, is given as:

$$\mathcal{P}(a_n) = |\langle\psi^{(s)}|\mathcal{O}_n\rangle|^2 = \langle\psi^{(s)}|\mathbb{P}_n|\psi^{(s)}\rangle \tag{I.21}$$

Whereas: $\mathbb{P}_n$ is a projection operator defined as:

$$\mathbb{P}_n = |\mathcal{O}_n\rangle\langle\mathcal{O}_n| \tag{I.22}$$

The projector $\mathbb{P}$ verifies the statement:

$$\mathbb{P}_n^2 = \mathbb{P}_n \tag{I.23}$$

The sum probabilities must equal one,

$$\sum_n \mathcal{P}(a_n) = \sum_n \langle\psi^{(s)}|\mathbb{P}_n|\psi^{(s)}\rangle = 1 \tag{I.24}$$

Therefore, the operators $\mathbb{P}_n$ must satisfy the completeness relation: $\sum_n \mathbb{P}_n = \hat{I}$.

After performing the projective measurement and obtaining the outcome a_n, with the probability $\mathcal{P}(a_n)$. The quantum state of the system collapses to the eigenstate $|\mathcal{O}_n\rangle$.

The state of the system after the measurement is given as:

$$|\psi^{(s)}\rangle' = \frac{\mathbb{P}_n|\psi^{(s)}\rangle}{\sqrt{\langle\psi^{(s)}|\mathbb{P}_n|\psi^{(s)}\rangle}} \tag{I.25}$$

Using the density matrix formalism, we represent the state of the system by a convex combination, by means of the probabilities p_i and the vectors $|\psi_i^{(s)}\rangle$.

$$\hat{\varrho}^{(s)} = \sum_i p_i |\psi_i^{(s)}\rangle\langle\psi_i^{(s)}| \tag{I.26}$$

In this situation, the probability of measuring o_n is:

$$\mathcal{P}(a_n) = \sum_i p_i |\langle\psi_i^{(s)}|\mathcal{O}_n\rangle|^2 = \langle\mathcal{O}_n|\big(\sum_i p_i|\psi_i^{(s)}\rangle\langle\psi_i^{(s)}|\big)|\mathcal{O}_n\rangle = Tr\{\mathbb{P}\hat{\varrho}^{(s)}\} \tag{I.27}$$

Indeed, a projective measurement [151] is a irreversible process; the quantum state $|\psi^{(s)}\rangle$ after this measurement collapses irrevocably to one of the eigenstates of the measurement operator. Nevertheless, if the measurement is unsharp, the situation is different and it is possible to reverse the measurement [152].

I.2.2 Weak measurement

The weak measurement (WM) is a generalization of the projective measurement and is associated with a positive-operator-valued measure $(POVM)$, which was introduced by *S. Berberian* in 1966 [153]. Unlike the projective measures, the number of elements in $POVM$ can be larger than the dimension of the *Hilbert* space $\mathcal{H}$. Actually, $POVMs$ allow the extraction of information even if the operator inside the trace (Eq. I.27) is not a projector, but only a positive operator $\hat{\mathbb{A}}$ suffices: [154].

$$Tr\{\hat{\mathbb{A}}\hat{\varrho}^{(s)}\} = \sum_i p_i \langle\psi_i^{(s)}|\hat{\mathbb{A}}|\psi_i^{(s)}\rangle \tag{I.28}$$

Where:

$$\sum_n \hat{\mathbb{A}}_n = \hat{I} \tag{I.29}$$

Thus:

$$\sum_n P(a_n) = \sum_n Tr\{\hat{\mathbb{A}}\hat{\varrho}^{(s)}\} = Tr\{\sum_n \hat{\mathbb{A}}\hat{\varrho}^{(s)}\} = Tr\{\hat{I}\hat{\varrho}^{(s)}\} = 1 \tag{I.30}$$

Indeed, WM gives a handle to extract small amount of information about the quantum state without destroying it, by weakening the coupling between the measurement's apparatus and the quantum state, as much as possible [155]. The Weak measurement describes a non-unitary transformation of the quantum state; where the collapse of the quantum state is partial. It has been predicted that after such a weak measurement, the initial quantum state of the system can be recovered by reversing the effect of the measurement [156]. In other words, the weak measurement can be reversible and the probability of the successful reversal is related to the unsharpness of the measurement [152]. Recently, *Jordan et al*. [157] discussed how to restore a quantum state to its initial configuration after quantum measurement. *Sun et al*. [158] experimentally demonstrated that a non-unitary transformation of a photonic qubit, caused by a weak quantum measurement, can be reversed by applying an appropriately designed reversing operation.

To illustrate the concept of weak measurement, we consider a detector (please see Fig I.2) which measures the qubit state Eq. (I.1), where the detector functions as follows: the detector clicks with a probability p_{det} if the qubit is in the state $|1\rangle$ and never clicks if the qubit is in the state $|0\rangle$. The detector's output (clicks or does not click) can be used to guess the initial state [158].
If we consider that the detector clicks, the qubit state irrevocably collapses to the state $|1\rangle$. The measure-

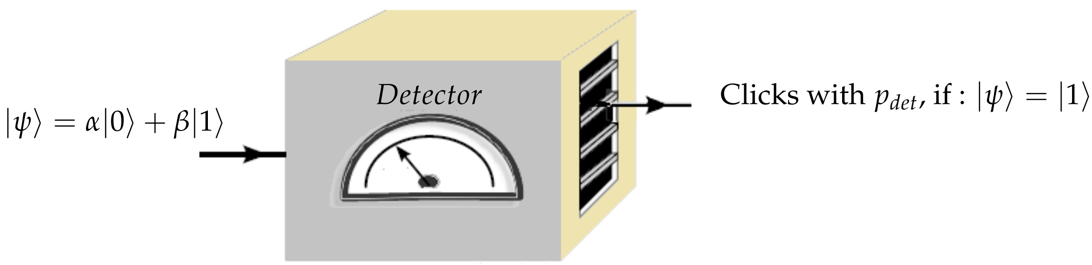

FIGURE I.2: Illustration of detector. The input state $|\psi\rangle$ in a superposition of $|0\rangle$ and $|1\rangle$, the detector clicks with probability p_{det} if $|\psi\rangle$ is in $|1\rangle$. Otherwise it does not click.

ment operator describing this situation is:

$$\mathcal{M}_1 = \sqrt{p_{det}}|1\rangle\langle 1| = \begin{pmatrix} 0 & 0 \\ 0 & \sqrt{p_{det}} \end{pmatrix} \tag{I.31}$$

$\mathcal{M}_1$ is irreversible, with no mathematical inverse. However, if the detector does not click, we consider the measurement operator to be $\mathcal{M}_0$. These operators satisfy the completeness relation:

$$\mathcal{M}_0^\dagger \mathcal{M}_0 + \mathcal{M}_1^\dagger \mathcal{M}_1 = \hat{I}. \tag{I.32}$$

Using the previous Eqs. (I.31, I.32), we can easily get the expression of $\mathcal{M}_0$:

$$\mathcal{M}_0 = |0\rangle\langle 0| + \sqrt{1-p_{det}}|1\rangle\langle 1| = \begin{pmatrix} 1 & 0 \\ 0 & \sqrt{1-p_{det}} \end{pmatrix} \tag{I.33}$$

$\mathcal{M}_0$ has a mathematical inverse. Thus, it is reversible.

I.2.3 Reversal measurement

The state of the qubit after the null outcome of the detector is given as;

$$|\psi'\rangle = \frac{\mathcal{M}_0|\psi\rangle}{\sqrt{\langle\psi|\mathcal{M}_0^\dagger\mathcal{M}_0|\psi\rangle}} = \alpha'|0\rangle + \beta'|1\rangle \tag{I.34}$$

Where

$$\alpha' = \frac{\alpha}{\sqrt{1-p_{det}|\beta|^2}} \quad , \qquad \beta' = \frac{\beta\sqrt{1-p_{det}}}{\sqrt{1-p_{det}|\beta|^2}}. \tag{I.35}$$

To reverse the effect of the weak measurement, by the same token, to recover the original state $|\psi\rangle$ from the $|\psi'\rangle$, we need to apply the inverse of $\mathcal{M}_0$ to $|\psi\rangle'$, namely $\mathcal{M}_0^{-1}$

$$\mathcal{M}_0^{-1} = \frac{1}{\sqrt{1-p_{det}}} \begin{pmatrix} \sqrt{1-p_{det}} & 0 \\ 0 & 1 \end{pmatrix} \tag{I.36}$$

The reversing operation $\mathcal{M}_0$ exists mathematically where p_{det} is defined as the weak measurement strength. In fact, the reversing operation erases the information gained via the weak measurement [159]. An experimental setup to implement the weak and reversal measurements for different substrates, such as photonic qubit [158], solid-state [160] and superconducting phase qubit [161], is suggested.

I.3 Quantum gates

A Quantum gate is a unitary operator that acts on one or more qubits [162]. they are the building blocks of quantum communication and computation processes such as quantum algorithm and quantum teleportation [77]. Moreover, a quantum gate is reversible; if we know the output state of the gate, we can conclude what the input state is [163]. Mathematically, a quantum gate could be described by a square matrix U, with the condition $UU^\dagger = \hat{I}$, where $\hat{I}$ is the unitary matrix. The former condition is essential to preserve the norm of vectors [77]. In what follows, we describe some universal quantum gates, for instance, the Pauli gates $\hat{X}$, $\hat{Z}$, Hadamard, $CNOT$ and $CCNOT$ gates.

I.3.1 X-gate

- The X-gate flips the state $|0\rangle$ to $|1\rangle$, and vice versa $|1\rangle$ to $|0\rangle$. In the matrix representation, we write;

$$\hat{X} = \hat{\sigma}_x = \begin{pmatrix} 0 & 1 \\ 1 & 0 \end{pmatrix}. \tag{I.37}$$

Where:

$$\hat{X}|0\rangle = |1\rangle; \qquad \hat{X}|1\rangle = |0\rangle \tag{I.38}$$

When $\hat{X}$ acts on a quantum state of the qubit (I.1), we, by consequence, get :

$$\hat{X}|\psi\rangle = \hat{X}(\alpha|0\rangle + \beta|1\rangle) = \alpha|1\rangle + \beta|0\rangle \tag{I.39}$$

The action of $\hat{X}$ on $|\psi\rangle$ represents interchanged probabilities of the state being in $|0\rangle$ or $|1\rangle$.

I.3.2 Z-gate

- Z-gate leaves $|0\rangle$ unchanged, and flips the sign of $|1\rangle$ to $-|1\rangle$:

$$\hat{Z}|0\rangle = |0\rangle; \qquad \hat{Z}|1\rangle = -|1\rangle \tag{I.40}$$

In matrix representation, the Z-gate is given as:

$$\hat{Z} = \hat{\sigma}_z = \begin{pmatrix} 1 & 0 \\ 0 & -1 \end{pmatrix}. \tag{I.41}$$

When $\hat{Z}$ acts on the quantum state $|\psi\rangle$. The initial state Eq.(I.1) transforms to the state:

$$\hat{Z}|\psi\rangle = \hat{Z}(\alpha|0\rangle + \beta|1\rangle) = \alpha|0\rangle - \beta|1\rangle \tag{I.42}$$

The flip phase gate changes the sign of the state $|1\rangle$, that is important when it acts on a superposed state. For exemple, the state $\frac{1}{\sqrt{2}}(|0\rangle + |1\rangle$ becomes the orthogonal state $\frac{1}{\sqrt{2}}(|0\rangle - |1\rangle)$.

I.3.3 Y-gate

- Y-gate or the bit-phase flip gate is given as follows:

$$\hat{Y}|0\rangle = i|1\rangle; \qquad \hat{Y}|1\rangle = -i|0\rangle \tag{I.43}$$

In matrix representation, the Y-gate is given as:

$$\hat{Y} = i\hat{X}\hat{Z} = \begin{pmatrix} 0 & -i \\ i & 0 \end{pmatrix}. \tag{I.44}$$

When $\hat{Y}$ acts on the quantum state $|\psi\rangle$. The initial state Eq.(I.1) transforms to the state:

$$\hat{Y}|\psi\rangle = \hat{Y}(\alpha|0\rangle + \beta|1\rangle) = i\alpha|1\rangle - i\beta|0\rangle \tag{I.45}$$

I.3.4 Hadamard gate

- Hadamard gate is one of the most frequently used quantum gates in the field of quantum information. The role of Hadamard is to create the superposition from states as follows:

$$\hat{H}|0\rangle = \frac{|0\rangle + |1\rangle}{\sqrt{2}}; \qquad \hat{H}|1\rangle = \frac{|0\rangle - |1\rangle}{\sqrt{2}} \tag{I.46}$$

Generally, its action on the state $|x\rangle$ can be given by,

$$\hat{H}|x\rangle = \frac{1}{\sqrt{2}} \sum_{y=0,1} (-1)^{xy}|y\rangle \tag{I.47}$$

In matrix representation, the Hadamard gate is presented as follows:

$$H = \frac{1}{\sqrt{2}} \begin{pmatrix} 1 & 1 \\ 1 & -1 \end{pmatrix} = \frac{1}{\sqrt{2}}(\hat{\sigma}_x + \hat{\sigma}_z) \tag{I.48}$$

I.3.5 CNOT gate

- The *CNOT* gate is a two-qubit operation, where the first qubit usually refers to the control qubit and the second qubit is considered as the target qubit. Indeed, the *CNOT* gate leaves the control qubit unchanged and performs the $\hat{X}-$Pauli gate on the target qubit if, and only if, the control qubit is in state $|1\rangle$, and leaves the target qubit unchanged when the control qubit is in state $|0\rangle$. We can write:

$$CNOT|ab\rangle = |a, a \oplus b\rangle. \tag{I.49}$$

Explicitly we write:

$$\begin{aligned} |0\rangle|0\rangle &\to |0\rangle|0\rangle; \quad |0\rangle|1\rangle \to |0\rangle|1\rangle; \\ |1\rangle|0\rangle &\to |1\rangle|1\rangle; \quad |1\rangle|1\rangle \to |1\rangle|0\rangle. \end{aligned} \tag{I.50}$$

However, it is more convenient to perform the *CNOT* operations using Pauli's operators. Yet, in the computational basis, the *CNOT* operation is defined as shown in Tab.(1).

	$\hat{I}^{(2)}$	$\hat{X}^{(2)}$	$\hat{Y}^{(2)}$	$\hat{Z}^{(2)}$
$\hat{I}^{(1)}$	1	$\hat{X}^{(1)}\hat{X}^{(2)}$	$\hat{Y}^{(1)}\hat{X}^{(2)}$	$\hat{Z}^{(1)}$
$\hat{X}^{(1)}$	$\hat{X}^{(2)}$	$\hat{X}^{(1)}$	$\hat{Y}^{(1)}$	$\hat{Z}^{(1)}\hat{X}^{(2)}$
$\hat{Y}^{(1)}$	$\hat{Z}^{(1)}\hat{Y}^{(2)}$	$\hat{Y}^{(1)}\hat{Z}^{(2)}$	$-\hat{X}^{(1)}\hat{Z}^{(2)}$	$\hat{Y}^{(2)}$
$\hat{Z}^{(1)}$	$\hat{Z}^{(1)}\hat{Z}^{(2)}$	$-\hat{Y}^{(1)}\hat{Y}^{(2)}$	$\hat{X}^{(1)}\hat{Y}^{(2)}$	$\hat{Z}^{(2)}$

TABLE I.1: Bilateral *CNOT* operation between two qubits which are defined by superscripts 1 and 2.

The interesting thing about *CNOT* gate is the universality of this gate for quantum computation, where any unitary operation may be approximated to arbitrary accuracy by *CNOT* and a set of quantum gates [163].

I.3.6 CCNOT gate

- The *CCNOT* gate, also called controlled-controlled-Not gate, which was introduced in 1980 by *Tommaso Toffoli* [164], is a three-qubit operation which applies $\hat{X}$ on the third qubit only if the first two qubits are in the state $|1\rangle$ [165]. The *CCNOT* gate is of great interest in numerous quantum computation tasks such as quantum error correction schemes [166], fault-tolerant quantum computing [167], and quantum algorithms [168]. It is used widely in the context of quantum purification [169] and in quantum error correction schemes [170, 171]. The *CCNOT* gate has been implemented in nuclear magnetic resonance [171], linear optics [172] and ion trap systems [173].
  In a generic form, one can write its effect as $CCNOT|abc\rangle = |ab, c \oplus a.b\rangle$, where the *CCNOT* gate may be defined by using the Pauli operators as:

$$\begin{aligned} CCNOT &= \frac{1}{4}\Big[(1+\hat{Z}^{(1)})(1+\hat{Z}^{(2)})\hat{X}^{(3)} + (1+\hat{Z}^{(1)})(1-\hat{Z}^{(2)}) \\ &\quad +(1-\hat{Z}^{(1)})(1+\hat{Z}^{(2)}) + (1-\hat{Z}^{(1)})(1-\hat{Z}^{(2)})\Big]. \end{aligned} \tag{I.51}$$

I.4 Quantum circuit

A quantum circuit (QC) [174] is a combination of wires and gates which carry classical and quantum information around and perform some computational tasks, respectively [77]. Quantum circuit could be thought of as a time sequence of events, where time flows from left to right. Every wire is a way of representing qubit states, while gates represent the processing of these qubits [175]. A quantum circuit is characterized by the following proprieties [175]:

- *QC* is performed for once: it is non-cyclic and never contains loops.
- Quantum wire indicates qubits moving from one location to another through space.
- Double wires indicate a classical communication channel.
- All the wires in *QC* cannot be left unconnected to a quantum gate.

- A quantum wire can generate any secondary quantum wires.

Indeed, in the circuit notation, every quantum gate has a specified symbol; The Pauli gates, namely $\hat{X}$ and $\hat{Z}$ gates are represented by the symbol in Figs (I.3, I.4), respectively.

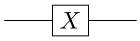

FIGURE I.3: Circuit symbol for the $\hat{\sigma}_x$ or $\hat{X}$ gate

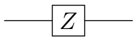

FIGURE I.4: Circuit symbol for the $\hat{\sigma}_z$ or $\hat{Z}$ gate

In addition, the *CNOT* gate is represented by the symbol in Fig I.5.

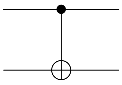

FIGURE I.5: Circuit symbol for the CNOT gate

The Hadamard (H) gate is represented by the symbol in Fig I.6.

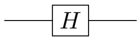

FIGURE I.6: Circuit symbol for the Hadamard or H gate

The *CCNOT* gate is represented by the symbol in Fig I.7.

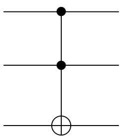

FIGURE I.7: Circuit symbol for the CCNOT gate

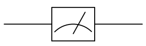

FIGURE I.8: Circuit symbol for Measurement gate

To extract quantum information after performing series of quantum gates on a quantum state, we need to measure the output state. We denote this process by the measurement gate, which is represented by the symbol in Fig (I.8). The measurement in the computational basis $\{|0\rangle, |1\rangle\}$ leads to obtaining the classical bits 0 or 1.

A simple example of the quantum circuit is quantum circuit to create Bell states displayed in Fig I.9.

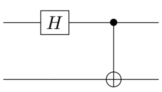

FIGURE I.9: Quantum circuit to create Bell states

This quantum circuit has a Hadamard gate followed by a $CNOT$ and transforms the four computational basis states according to the table given bellow:

Input	Output
$\|00\rangle$	$\frac{1}{\sqrt{2}}(\|00\rangle + \|11\rangle)$
$\|01\rangle$	$\frac{1}{\sqrt{2}}(\|01\rangle + \|10\rangle)$
$\|10\rangle$	$\frac{1}{\sqrt{2}}(\|00\rangle - \|11\rangle)$
$\|11\rangle$	$\frac{1}{\sqrt{2}}(\|01\rangle - \|10\rangle)$

TABLE I.2: Input-output table for quantum circuit to create Bell states.

The table above describes the input and the output states of the scheme shown if Fig (I.9). Indeed, the scheme shows the construction of bipartite entangled states. The Hadamard gate takes the input (let it $|01\rangle$) to $\frac{1}{\sqrt{2}}(|0\rangle + |1\rangle)|1\rangle$. Subsequently, by applying the $CNOT$ gate, we get the state $\frac{1}{\sqrt{2}}(|01\rangle + |10\rangle)$. The quantum circuit of the construction of three-partite entangled states is given easily by adding another $CNOT$ gate to the quantum circuit shown in the Fig. (I.9).

I.5 Quantum Noisy channels

Any physical process can be represented by a quantum channel [176]. The notion of quantum channel is widely used to describe the input-output qubit states relationship. Therefore, quantum channels can be used to describe the transfer information. Indeed, quantum teleportation can be viewed as a quantum channel [177] since it is a process of information transmission. Moreover, quantum channels describe the transmission of qubits, in-which these qubits interact with a noisy environment. Indeed, quantum channels can be memoryless, where the qubits of interest are supposed to undergo the action of noisy environment which affects them independently and identically. However, in realistic situations, spatial and temporal memory effects [176] must be taken into account. Generally, quantum channels with memory is a wide framework inwhich the memoryless quantum channels are a special case.

I.5.1 Quantum channel

Definition:
A quantum channel ϵ is a map taking density operators $\hat{\varrho} \in \mathcal{H}_n$ into density operators $\hat{\varrho}^{'} \in \mathcal{H}_m$:

$$\begin{aligned} \epsilon : \mathcal{H}_n &\rightarrow \mathcal{H}_m & \text{(I.52)} \\ \hat{\varrho} &\rightarrow \hat{\varrho}^{'} = \epsilon(\hat{\varrho}) & \text{(I.53)} \end{aligned}$$

A quantum channel ϵ satisfies three properties:

- ϵ is Linear
$$\epsilon(\lambda\hat{\varrho}_1 + (1-\lambda)\hat{\varrho}_2) = \lambda\epsilon(\hat{\varrho}_1) + (1-\lambda)\epsilon(\hat{\varrho}_2) \tag{I.54}$$
- ϵ is Trace preserving
$$Tr(\epsilon(\hat{\varrho})) = Tr(\hat{\varrho}); \qquad \hat{\varrho} \in \mathcal{H}_n. \tag{I.55}$$
- ϵ is completely positive:

  By assuming that a quantum system "A" is part of a larger composite system "A" and "B".
$$(\epsilon \otimes \mathcal{I})(\hat{\varrho}_{AB}) = (\hat{\varrho}_{AB})^{'} \geq 0 \tag{I.56}$$

  Thus, a quantum channel is a completely positive trace preserving $(CPTP)$ map.

I.5.2 Kraus representation

We consider a state of a quantum system A, $\hat{\varrho}_A$. Now, we suppose the system interacts with an environment (system B) in a state $\hat{\varrho}_B$ with a unitary transformation operator $\hat{U}_{AB}$. By tracing out the system B, this transformation on the state $\hat{\varrho}_A$ is described by [178]:

$$\begin{aligned} \hat{\varrho}_A \rightarrow \hat{\varrho}_A^{'} &= Tr_B[\hat{U}_{AB}(\hat{\varrho}_A \otimes \hat{\varrho}_B)\hat{U}_{AB}^{\dagger}] \\ &= \sum_k \langle k|\hat{U}_{AB}[\hat{\varrho}_A \otimes (\sum_l \hat{\varrho}_l |l\rangle_B \langle l|)]\hat{U}_{AB}^{\dagger}|k\rangle_B \\ &= \sum_{k,l} (\langle k|\sqrt{\hat{\varrho}_l}\hat{U}_{AB}|l\rangle_B)\hat{\varrho}_A(\langle l|\sqrt{\hat{\varrho}_l}\hat{U}_{AB}|k\rangle_B) \\ &= \sum_{k,l} \mathcal{K}_{k,l}\hat{\varrho}_A\mathcal{K}_{k,l}^{\dagger} = \epsilon(\hat{\varrho}_A) \end{aligned} \tag{I.57}$$

The last line of the equation (I.57) is an operator-sum representation of the quantum channel, and the operators $\{\mathcal{K}_{k,l}\}$ are called the Kraus operators or operation elements of the channel. The operator $\mathcal{K}_{k,l}$ is an operator in the Hilbert space of the system A. In the simple case, where the system B is in the state $\hat{\varrho}_B = |0\rangle_B\langle 0|$, we obtain the operator sum in Eq. (I.57) with $\mathcal{K}_{k,l} =_B \langle k|\hat{U}_{AB}|0\rangle_B$.

The trace preserving (TP) property is easily confirmed through the following:

$$\begin{aligned} Tr[\epsilon(\hat{\varrho})] &= Tr(\sum_k \mathcal{K}_k\hat{\varrho}\mathcal{K}_k^{\dagger}) = \sum_k Tr(\mathcal{K}_k^{\dagger}\mathcal{K}\hat{\varrho}) \\ &= Tr[(\sum_k \mathcal{K}_k^{\dagger}\mathcal{K}_k)\rho] = 1 \end{aligned} \tag{I.58}$$

Where: $\sum_k \mathcal{K}_k^{\dagger}\mathcal{K}_k = 1$ is necessary and sufficient for the trace preserving property [178], that means the trace over the system B gives a new normalized state for the system A. Furthermore, for the linear map

ϵ to be physical, it must satisfy the completely positive (CP) property, where $\epsilon(\hat{\varrho}) \geq 0$. However, there are some operations that satisfy this condition but are unphysical [178]. So, a stricter condition is that the channel must remain positive even when we consider it to be acting on just a part of a larger system $(\epsilon \otimes \mathcal{I})\hat{\varrho}_{AB} \geq 0$ [162].

I.5.3 Correlated Noisy channels

Generally, there are two types of quantum channels including memoryless and memory channels. The memoryless or uncorrelated quantum channels describe the scenario in which the environment acts identically and independently on each element of the N sequence of qubits that passes through the channel. In this situation, the consecutive actions of the channel are expressed as tensor product of CPTP maps ϵ that acts on each qubit :

$$\epsilon^{(N)}(\hat{\varrho}) = \epsilon^{\otimes N}(\hat{\varrho}) \tag{I.59}$$

with $\epsilon^{\otimes N} = \epsilon \otimes ... \otimes \epsilon$. Furthermore, the Kraus operators of the memoryless map ($\epsilon^{(N)}$) can be expressed as a tensor product $\mathcal{K}_{k1} \otimes ... \otimes \mathcal{K}_{kn}$ formed by independent and identically distributed sequences extracted from the Kraus set $\{\mathcal{K}_k\}_i$ associated with the quantum channel ϵ. However, In real physical quantum transmission channels, with-memory or correlated noise channels, it is common to have correlated noise acting on consecutive uses [179]. In such channels, when the correlations between consecutive uses of the channel act dependently to each other, the tensorial decomposition of Eq. (I.59) is not valid:

$$\epsilon^{(N)}(\hat{\varrho}) \neq \epsilon^{\otimes N}(\hat{\varrho}) \tag{I.60}$$

Macchiavelo and Palma [180] suggested a model to describe the channels where successive uses of the channel are correlated. In this model, the quantum channel is given as:

$$\epsilon(\hat{\varrho}) = (1-u)\sum_{i,j} \mathcal{K}^u_{i,j}\hat{\varrho}\mathcal{K}^{u\dagger}_{i,j} + u\sum_k \mathcal{K}^c_k\hat{\varrho}\mathcal{K}^{c\dagger}_k, \tag{I.61}$$

With $0 \leq u \leq 1$ and with the probability $(1-u)$, the noise is uncorrelated. In what follows, we give the Kraus operators that describe different typical noisy channels.

- **Bit flip**

  The bit flip channel changes the state of a qubit from $|0\rangle$ to $|1\rangle$ (and vice versa from $|1\rangle$ to $|0\rangle$) with the probability $\mathbf{p}_B$ [77]. The Kraus operators of the Bit flip are given as follows:

$$\begin{aligned} \mathcal{K}^u_{00} &= p_0\hat{I}\otimes\hat{I}; \quad \mathcal{K}^u_{01} = \sqrt{p_0p_1}\hat{I}\otimes\hat{X}; \quad \mathcal{K}^u_{10} = \sqrt{p_1p_0}\hat{X}\otimes\hat{I}; \\ \mathcal{K}^u_{11} &= p_1\hat{X}\otimes\hat{X}\mathcal{K}^c_{00} = \sqrt{p_0}\hat{I}\otimes\hat{I}; \quad \mathcal{K}^c_{11} = \sqrt{p_1}\hat{X}\otimes\hat{X} \end{aligned} \tag{I.62}$$

  Whereas, $p_0 = 1-\mathbf{p}_B$, $p_1 = \mathbf{p}_B$. $0 \leq \mathbf{p}_B \leq 1$ is the bit flip factor, and $\hat{I}, \hat{X}$ are the unitary and the X-Pauli operator, respectively.

- **Phase flip**

  The phase flip, or phase damping, operation describes the loss of information in a quantum state without energy loss [162]. The Kraus operators describing this process are given as follows:

$$\begin{aligned} \mathcal{K}^u_{00} &= p_0\hat{I}\otimes\hat{I}; \quad \mathcal{K}^u_{01} = \sqrt{p_0p_1}\hat{I}\otimes\hat{Z}; \quad \mathcal{K}^u_{10} = \sqrt{p_1p_0}\hat{Z}\otimes\hat{I} \\ \mathcal{K}^u_{11} &= p_1\hat{Z}\otimes\hat{Z}; \quad \mathcal{K}^c_{00} = \sqrt{p_0}\hat{I}\otimes\hat{I}; \quad \mathcal{K}^c_{11} = \sqrt{p_1}\hat{Z}\otimes\hat{Z} \end{aligned} \tag{I.63}$$

Whereas, $p_0 = 1 - \mathbf{p}_p$, $p_1 = \mathbf{p}_p$, $\mathbf{p}_p$ is the decoherence factor, $0 \leq \mathbf{p}_p \leq 1$.

- **Bit-Phase flip**

The bit-phase flip noise combines phase-flip and bit-flip [181]. The Kraus operators describing this process are given as follows:

$$\begin{aligned} \mathcal{K}^u_{00} &= p_0 \hat{I} \otimes \hat{I}; \quad \mathcal{K}^u_{01} = \sqrt{p_0 p_1} \hat{I} \otimes \hat{Y}; \quad \mathcal{K}^u_{10} = \sqrt{p_1 p_0} \hat{Y} \otimes \hat{I} \\ \mathcal{K}^u_{11} &= p_1 \hat{Y} \otimes \hat{Y}; \quad \mathcal{K}^c_{00} = \sqrt{p_0} \hat{I} \otimes \hat{I}; \quad \mathcal{K}^c_{11} = \sqrt{p_1} \hat{Y} \otimes \hat{Y} \end{aligned} \tag{I.64}$$

Whereas, $p_0 = 1 - \mathbf{p}_{bp}$, $p_1 = \mathbf{p}_{bp}$, $\mathbf{p}_{bp}$ is the bit-phase flip factor, $0 \leq \mathbf{p}_{bp} \leq 1$.

- **Depolarizing**

This type of noise brings any density matrix to the completely mixed state, $\frac{1}{2}\hat{I}$, with probability p_i (i=1,2,3). However, with probability p_0 the system's density matrix is left untouched [77]. Moreover, the noise is uncorrelated and specified by the Kraus operators:

$$\begin{aligned} \mathcal{K}^u_{00} &= p_0 \hat{I} \otimes \hat{I}; \quad \mathcal{K}^u_{01} = \sqrt{p_0 p_1} \hat{I} \otimes \hat{X}; \quad \mathcal{K}^u_{02} = \sqrt{p_0 p_2} \hat{I} \otimes \hat{Y}; \quad \mathcal{K}^u_{03} = \sqrt{p_0 p_3} \hat{I} \otimes \hat{Z}; \\ \mathcal{K}^u_{10} &= \sqrt{p_0 p_1} \hat{X} \otimes \hat{I}; \quad \mathcal{K}^u_{11} = p_1 \hat{X} \otimes \hat{X}; \quad \mathcal{K}^u_{12} = \sqrt{p_1 p_2} \hat{X} \otimes \hat{Y}; \quad \mathcal{K}^u_{13} = \sqrt{p_1 p_3} \hat{X} \otimes \hat{Z}; \\ \mathcal{K}^u_{20} &= \sqrt{p_0 p_2} \hat{Y} \otimes \hat{I}; \quad \mathcal{K}^u_{21} = \sqrt{p_1 p_2} \hat{Y} \otimes \hat{X}; \quad \mathcal{K}^u_{22} = p_2 \hat{Y} \otimes \hat{Y}; \quad \mathcal{K}^u_{23} = \sqrt{p_2 p_3} \hat{Y} \otimes \hat{Z}; \\ \mathcal{K}^u_{30} &= \sqrt{p_0 p_3} \hat{Z} \otimes \hat{I}; \mathcal{K}^u_{31} = \sqrt{p_1 p_3} \hat{Z} \otimes \hat{X}; \mathcal{K}^u_{32} = \sqrt{p_2 p_3} \hat{Z} \otimes \hat{Y}; \mathcal{K}^u_{33} = p_3 \hat{Z} \otimes \hat{Z}; \end{aligned} \tag{I.65}$$

While, with probability u, the noise is correlated and specified by:

$$\mathcal{K}^c_{00} = \sqrt{p_0} \hat{I} \otimes \hat{I}; \mathcal{K}^c_{11} = \sqrt{p_1} \hat{X} \otimes \hat{X}; \mathcal{K}^c_{22} = \sqrt{p_2} \hat{Y} \otimes \hat{Y}; \mathcal{K}^c_{33} = \sqrt{p_3} \hat{Z} \otimes \hat{Z}. \tag{I.66}$$

Where, $p_0 = 1 - \mathbf{p}_D$, and $p_i = \frac{\mathbf{p}_D}{3}$ $(i = 1, 2, 3)$. Furthermore, $\mathbf{p}_D \in [0, 1]$ is the depolarizing factor.

- **Amplitude damping**

The Amplitude damping channel (ADC) describes a general energy dissipation process between the qubit system and the environment [77]. ADC is a widely discussed model for various realistic physical evolution. The dissipative interaction between an open quantum system (S) and its surrounding environment (E) can be represented by the evolution U_{AD}:

$$U_{AD} = \begin{cases} |0\rangle_S |0\rangle_E \longrightarrow |0\rangle_S |0\rangle_E \\ \\ |1\rangle_S |0\rangle_E \longrightarrow \sqrt{p_0} |1\rangle_S |0\rangle_E + \sqrt{p_1} |0\rangle_S |1\rangle_E, \quad \text{with:} \end{cases} \tag{I.67}$$

Where: $p_0 = 1 - \mathbf{p}_A$ and $p_1 = \mathbf{p}_A$.

$\mathbf{p}_A \in [0, 1]$ is the strength of the amplitude damping; $|0\rangle_S$ and $|1\rangle_S$ are the ground and the excited state of the system; while $|0\rangle_E$ and $|1\rangle_E$ denote the vacuum state and the one excitation of the environment, respectively.

The Kraus operators that represent the correlated amplitude damping channel [182] are given by:

$$\mathcal{K}^{Ad}_{00} = |00\rangle\langle 00| + |01\rangle\langle 01| + |10\rangle\langle 10| + \sqrt{1 - \mathbf{p}_A} |11\rangle\langle 11|, \quad \mathcal{K}^{Ad}_{11} = \sqrt{\mathbf{p}_A} |00\rangle\langle 11| \tag{I.68}$$

$$\mathcal{K}_0^{Ad} = \begin{pmatrix} \sqrt{\mathbf{p}_A} & 0 & 0 & 0 \\ 0 & 1 & 0 & 0 \\ 0 & 0 & 1 & 0 \\ 0 & 0 & 0 & 1 \end{pmatrix}; \qquad \mathcal{K}_1^{Ad} = \begin{pmatrix} 0 & 0 & 0 & 0 \\ 0 & 0 & 0 & 0 \\ 0 & 0 & 0 & 0 \\ \sqrt{1-\mathbf{p}_A} & 0 & 0 & 0 \end{pmatrix} \tag{I.69}$$

It is worthy to note that the above discussed types of noise, namely the bit flip, phase flip (phase damping), bit-phase flip, depolarizing and amplitude damping, are usually encountered in real world implementations of quantum communication protocols such as the quantum teleportation [80].

I.6 Quantum teleportation and entanglement quantifiers

In this framework, we introduce the Negativity of the partial transpose, which is an entanglement measure. Moreover, we present the average fidelity and the quantum Fisher information which are important quantifiers for the teleportation of unknown quantum states and relevant parameters such as the weight or the phase of qubits.

I.6.1 Entanglement

Entanglement is a potential resource for quantum information processing, such as quantum Teleportation, quantum key distribution, and quantum algorithm [183]. It is considered as non-local quantum correlations which are the reason behind the violation of Bell inequalities [184] and which are the origin of quantum weirdness [185]. The investigation of entanglement leads to several criteria and entanglement measures. The criteria help in the detection of entanglement, while, the entanglement measure quantifies the amount of entanglement that remains in a quantum state.

A generic entanglement monotone $T(\hat{\varrho})$ must fulfill the bellow proprieties [77]:

- (i) $0 \leq T(\hat{\varrho}) \leq 1$; $\hat{\varrho}$ is separable if $T(\hat{\varrho}) = 0$, and $\hat{\varrho}$ is maximally entangled if $T(\hat{\varrho}) = 1$.
- (ii) $T(\hat{\varrho})$ is invariant under local unitary transformations: $T(\hat{\varrho}) = T(U_A \otimes U_B \hat{\varrho} U_A^\dagger \otimes U_B^\dagger)$.
- (iii) Entanglement cannot be created by local operations and classical communication $(LOCC)$. So, the amount of entanglement does not increase under a $LOCC$ map $\mathcal{A}^{LOCC}$: $T[\mathcal{A}^{LOCC}(\hat{\varrho})] \leq T(\hat{\varrho})$.

I.6.2 Negative partial transpose

The negativity of the partially transposed density operator (NPT) is a necessary and sufficient condition for entanglement of any bipartite qubit state [186]. A density matrix of a composite quantum system (AB) could be written as follows:

$$\hat{\varrho} = \sum_{i,j}^{N} \sum_{k,l}^{M} \hat{\varrho}_{ij,kl} |i\rangle\langle j| \otimes |k\rangle\langle l| \tag{I.70}$$

The partial transpose of the density matrix $\hat{\varrho}$ is given by transposing $\hat{\varrho}$ with respect to one of the two subsystems. For instance, the partial transpose of the density matrix $\hat{\varrho}$, with respect to the subsystem A, is given by:

$$\hat{\varrho}^{T_A} = \sum_{i,j}^{N}\sum_{k,l}^{M} \hat{\varrho}_{ij,kl}|j\rangle\langle i| \otimes |k\rangle\langle l| \tag{I.71}$$

Similarly, the partial transpose with respect to the subsystem B, namely $\hat{\varrho}^{T_B}$, is represented as:

$$\hat{\varrho}^{T_B} = \sum_{i,j}^{N}\sum_{k,l}^{M} \hat{\varrho}_{ij,kl}|i\rangle\langle j| \otimes |l\rangle\langle k| \tag{I.72}$$

The *positive partial transpose* (PPT) affirms that if $\hat{\varrho}$ is a bipartite separable state, $\hat{\varrho}$ is PPT. It is, therefore, positive semi-definite with no negative eigenvalues; $\hat{\varrho}^{T_i} \geq 0$; $i = A, B$. However, if $\hat{\varrho}^{T_i}$, for $i = A, B$, has at least one negative eigenvalue, the state is entangled [186, 187]. In order to quantify the amount of entanglement in a quantum state $\hat{\varrho}$, we consider the Negativity of the partially transposed density operator, namely NPT. The expression of the entanglement measure using NPT is given as [187]:

$$NPT = 2\sum_{i} \lambda_i^{-}, \tag{I.73}$$

Where, λ_i^{-} are the negative eigenvalues of the partially transposed of the density matrix $\hat{\varrho}^{T_i}$, with $i = A, B$.

I.6.3 No-Cloning theorem

Theorem: [188]
There is no quantum copy machine which can copy any quantum state.

To prove the no-cloning theorem, there are two versions. The first version is based on the linearity of quantum physics. However, the second version fallows the norm preserving property of the inner product.

Proof 1
Wotters and *Zurek* [188] considered an apparatus, represented by the initial state $|A\rangle$, that copies the basis states $\{|0\rangle, |1\rangle\}$:

$$\begin{aligned} |0\rangle|A\rangle &\rightarrow |0\rangle|0\rangle|A^{'}\rangle, \\ |1\rangle|A\rangle &\rightarrow |1\rangle|1\rangle|A^{''}\rangle \end{aligned} \tag{I.74}$$

By considering an input state in the superposition state $|\psi\rangle = \alpha|0\rangle + \beta|1\rangle$, we write:

$$|\psi\rangle|A\rangle \rightarrow \alpha|0\rangle|0\rangle|A^{'}\rangle + \beta|1\rangle|1\rangle|A^{''}\rangle \tag{I.75}$$

The desired output state is $|\psi\rangle|\psi\rangle$, whereas:

$$\begin{aligned} |\psi\rangle|A\rangle &\rightarrow |\psi\rangle|\psi\rangle = (\alpha|0\rangle + \beta|1\rangle)(\alpha|0\rangle + \beta|1\rangle) \\ &\rightarrow \alpha^2|00\rangle + \beta\alpha|10\rangle + \alpha\beta|01\rangle + \beta^2|11\rangle \end{aligned} \tag{I.76}$$

In fact, the state (Eq. I.75) is different from the desired state (Eq. I.76). Therefore, due to the linearity of the quantum theory, one cannot clone the state $|\psi\rangle$.

Proof 2
We consider a unitary operator U which preserves inner products. U copies the no-identical quantum

states $|\psi\rangle$ and $|\phi\rangle$;

$$|\psi\rangle|0\rangle \xrightarrow{U} |\psi\rangle|\psi\rangle,$$
$$|\phi\rangle|0\rangle \xrightarrow{U} |\phi\rangle|\phi\rangle\ . \tag{I.77}$$

$$\langle\phi|\psi\rangle = (\langle\phi|\otimes\langle 0|)(|\psi\rangle\otimes|0\rangle) = \langle\phi|\psi\rangle^2 \tag{I.78}$$

Thus, the above argument allows the cloning of orthogonal states (if $\langle\phi|\psi\rangle = \langle\phi|\psi\rangle^2 = 0$). This is because the orthogonal states are distinguishable. Since the non-orthogonal states are not reliably distinguishable, we cannot make a perfect copy of them.

I.6.4 Unidirectional quantum teleportation

Quantum teleportation (QT) is the reliable transfer of unknown quantum information using classical communication and pre-shared entanglement. In the pioneering work [34], a sender (Alice) is able to transfer the unknown quantum state $|\psi\rangle = \alpha|0\rangle + \beta|1\rangle$ to a receiver (Bob), which is located distantly using entanglement and a classical communication channel. Indeed, Alice does not know the state $|\psi\rangle$ to be teleported. To determine α and β of $|\psi\rangle$, she needs to measure the quantum state. However, this measurement would destroy the quantum state. Moreover, Alice cannot make copies of the quantum state due to the no-cloning theorem (theorem: I.6.3).

The process of quantum teleportation is shown in the quantum circuit in Fig (I.10), where the steps in QT process are given as follows:

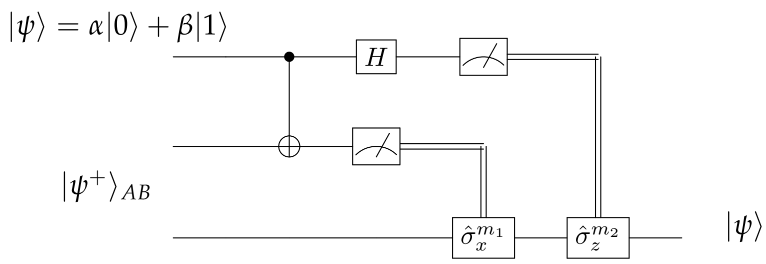

FIGURE I.10: Quantum circuit of unidirectional teleportation.

- Alice and Bob share an entangled pair of qubits in the state:

$$|\psi^+\rangle_{AB} = \frac{1}{\sqrt{2}}(|00\rangle + |11\rangle)_{AB} \tag{I.79}$$

  Where: A (B) denotes Alice (Bob), respectively.

- The state on Alice's side is given as:

$$\begin{aligned} |\psi\rangle_a \otimes |\psi^+\rangle_{AB} &= (\alpha|0\rangle + \beta|1\rangle)_a \otimes (\frac{|00\rangle + |11\rangle}{\sqrt{2}})_{AB} \\ &= \frac{1}{\sqrt{2}}(\alpha|000\rangle + \beta|100\rangle + \alpha|011\rangle + \beta|111\rangle)_{aAB} \end{aligned} \tag{I.80}$$

Alice performs a *CNOT* gate followed by a Hadamard gate. By a straightforward calculation, we write the state of the system as:

$$\frac{1}{\sqrt{2}}\left[|\phi^+\rangle_{aA}(\alpha|0\rangle_B+\beta|1\rangle_B)+|\phi^-\rangle_{aA}(\alpha|0\rangle_B-\beta|1\rangle_B)\right.$$
$$\left.+|\psi^+\rangle_{aA}(\alpha|1\rangle_B+\beta|0\rangle_B)+|\psi^-\rangle_{aA}(\alpha|1\rangle_B-\beta|0\rangle_B)\right] \tag{I.81}$$

Whereas the four Bell states are given as:

$$\begin{aligned}|\phi^+\rangle &= \frac{1}{\sqrt{2}}(|00\rangle+|11\rangle)\\ |\phi^-\rangle &= \frac{1}{\sqrt{2}}(|00\rangle-|11\rangle)\\ |\psi^+\rangle &= \frac{1}{\sqrt{2}}(|01\rangle+|10\rangle)\\ |\psi^-\rangle &= \frac{1}{\sqrt{2}}(|01\rangle-|10\rangle)\end{aligned} \tag{I.82}$$

- Alice makes a Bell measurement on the two qubits that she has (denoted by "aA"); one of them is the unknown qubit to be teleported to Bob and the other one is the entangled qubit from the state (Eq. I.79). The state collapses to one of the following four states with a uniform probability that equals $\frac{1}{4}$:

$$\begin{gathered}|\phi^+\rangle_{aA}|\psi\rangle_B;\\ |\phi^-\rangle_{aA}\hat{Z}|\psi\rangle_B;\\ |\psi^+\rangle_{aA}\hat{X}|\psi\rangle_B;\\ |\psi^-\rangle_{aA}\hat{Z}\hat{X}|\psi\rangle_B;\end{gathered} \tag{I.83}$$

- Alice sends two classical bits to Bob via classical channel. She indicates which measurement results she obtains.

Alice's measurement	Bits send to Bob	Operator
$\|\phi^+\rangle_{aA}$	00	$\hat{I}$
$\|\phi^-\rangle_{aA}$	01	$\hat{X}$
$\|\psi^+\rangle_{aA}$	10	$\hat{Z}$
$\|\psi^-\rangle_{aA}$	11	$\hat{Y}$

TABLE I.3: The four possible results of Bell measurement.

Table (I.3) displays the four possible results of Bell measurement performed by Alice. Depending on this measurement, Alice sends two classical bits to Bob. After receiving the classical bits, Bob performs Pauli operators ($\hat{X},\hat{Z},\hat{Y},\hat{I}$) in order to reconstruct the teleported state by Alice, $|\psi\rangle_a$.

As a matter of fact, quantum teleportation is not an instantaneous teleportation since there is no transfer of information before Bob receives the classical bits from Alice to reconstruct the teleported state on his side. For this reason, Alice and Bob would not be able to communicate faster than the speed of light. Hence, quantum teleportation agrees the theory of relativity [77, 163]. Actually, QT has plenty of applications in quantum communication as well as in quantum computation fields. It enables us to connect different quantum computers through a quantum network, where every device, in the quantum network, performs a part of the whole computation task. It is also of high importance for quantum repeaters [39]. Recently, there has been varied versions of QT [189, 190, 191, 192, 193] and they have been achieved experimentally using different substrates such as photonic qubits [44, 45, 46] and solid sates [47, 48]. Nevertheless, to quantify the accuracy of all teleportation protocols, we use the teleportation fidelity as a measure of the whole state teleportation of the quantum system. However, if we are only interested in the information about one parameter instead of the information about the whole state, it is more practical to evaluate the quantum Fisher information. In what follows, we introduce the teleportation fidelity and Fisher information.

I.6.5 Fidelity of teleportation

The accuracy of quantum teleportation process is measured by means of the teleportation fidelity. Indeed, The fidelity, f, measures the overlap between two states, $\hat{\varrho}_1$ and $\hat{\varrho}_2$. It has the following axioms [114]:

- $0 \leq f(\hat{\varrho}_1, \hat{\varrho}_2) \leq 1$; $f(\hat{\varrho}_1, \hat{\varrho}_2) = 1$ if and only if $\hat{\varrho}_1 = \hat{\varrho}_2$.
- Symmetry: $f(\hat{\varrho}_1, \hat{\varrho}_2) = f(\hat{\varrho}_2, \hat{\varrho}_1)$;
- f is preserved by unitary evolution: $f(U\hat{\varrho}_1, U\hat{\varrho}_2) = f(\hat{\varrho}_1, \hat{\varrho}_2)$; where U denotes a unitary transformation.
- Muliplicativity: $f(\hat{\varrho}_1 \otimes \hat{\varrho}_2, \hat{\varrho}'_1 \otimes \hat{\varrho}'_2) = f(\hat{\varrho}_1, \hat{\varrho}'_1) f(\hat{\varrho}_2, \hat{\varrho}'_2)$

Proof 2

The proof of the first, the second and the third axioms is given by the expression of the fidelity [114], where $f(\hat{\varrho}_1, \hat{\varrho}_2) = max|\langle\Phi|\Phi\rangle'|^2$ where $|\Phi\rangle$ and $|\Phi'\rangle$ are the purification of $\hat{\varrho}_1$ and $\hat{\varrho}_2$, respectively.

However, the fidelity expression of two mixed states is given as [114]:

$$f(\hat{\varrho}_1, \hat{\varrho}_2) = Tr(\hat{\varrho}_1 \hat{\varrho}_2) \tag{I.84}$$

With: $Tr(\mathcal{V} \otimes \mathcal{W})$= $Tr\mathcal{V}\ Tr\mathcal{W}$ and $(\mathcal{V} \otimes \mathcal{W})^{\frac{1}{2}}$=$\mathcal{V}^{\frac{1}{2}} \otimes \mathcal{W}^{\frac{1}{2}}$, the fourth multiplicativity axiom holds.

Besides, the expression of the fidelity f between a pure input state $|Q^{in}>$ and the mixed output state $\hat{\varrho}_{out}$, is written as [143, 194]:

$$f^{in\rightarrow out} =< Q^{in}|\hat{\varrho}_{out}|Q^{in} > \tag{I.85}$$

Since the teleported state is unknown, the averaged fidelity over all the input states may be described by [143]:

$$\mathcal{F}^{in\rightarrow out}_{avg} = \frac{1}{4\pi} \int_0^{\pi} d\theta_i \int_0^{2\pi} f^{in\rightarrow out}(\theta_i, \phi_i) \sin\theta_i d\phi_i \quad i = A, B \tag{I.86}$$

where, 4π is the solid angle.

I.7 Fisher information

Fisher information lies at the heart of the parameter estimation theory that was originally introduced by R. A. Fisher (1890–1962) [195], where it gives how members of a family of probability distributions can be distinguished [196]. It is a simple concept which does not require prior knowledge of statistics. Fisher information is a measure of the efficiency to estimate a parameter [123]. For example, we consider the basic problem of estimating a single parameter of a system from some measurements. Let the parameter have an unknown value θ, and let $\mathbf{y}$ the observation outcomes be done N times. In vector notation we write: $\mathbf{y} = y_1...y_N$.

The observations obey:

$$\mathbf{y} = \theta + \mathbf{x} \tag{I.87}$$

where $\mathbf{x} = x_1, x_2...x_N$ are added noise values. By considering $p(y|\theta)$ the conditional probability for the outcome result y. The expression of the classical Fisher information $\mathcal{I}$ is given as [197]:

$$\mathcal{I} = \int_y dy(\frac{\partial lnp}{\partial_\theta})^2 p \tag{I.88}$$

In the case of discrete probability, the integral becomes a sum, explicitly: $\mathcal{I} = \sum_y (\frac{\partial lnp}{\partial_\theta})^2 p$.

Fisher information is linked to the mean square error in such an estimation scenario [198]:

$$\mathcal{V}^2 \mathcal{I} \geq 1 \tag{I.89}$$

Where $\mathcal{V}^2$ is the mean square error and $\mathcal{I}$ is called the Fisher information. For unbiased estimator, the mean square error is identical to the variance of the parameter θ. The equation (I.89) could be written as:

$$Var(\theta)\mathcal{I} \geq 1 \tag{I.90}$$

The former equation (Eq. I.90) is called the Cramer-Rao inequality. It shows that the estimation quality increases ($Var(\theta)$ decreases) as $\mathcal{I}$ increases.

However, in case we have a multiparameter estimation scenario, where the parameters are assumed to be θ_i and θ_j, Fisher information matrix provides a tool to quantify the estimation degree of these parameters. Similarly, for a probability distribution $\{p(y|\theta)\}$ where $p(y|\theta)$ is the conditional probability for the outcome result y, an element of Fisher information matrix is given as:

$$\mathcal{I}_{ij} = \int_y \frac{\partial lnp}{\partial_{\theta_i}} \frac{\partial lnp}{\partial_{\theta_j}} p\, dy \tag{I.91}$$

For discrete outcome results, it becomes

$$\mathcal{I}_{ij} = \sum_y \frac{\partial lnp}{\partial_{\theta_i}} \frac{\partial lnp}{\partial_{\theta_j}} p \tag{I.92}$$

The diagonal entry of Fisher information matrix is referred to as Fisher information, namely $\mathcal{I}_{ii}$.

I.7.1 Quantum Fisher information

Quantum Fisher information is formally generalized from its classical version which is given in Eq (I.88). QFI of a parameter characterizes the sensitivity of the state with respect to the changes of the parameter.

Moreover, in the teleportation context, QFI quantifies the teleportation accuracy of the information that is carried by the weight parameter θ. The quantum Fisher information of one parameter θ, which is encoded in the density matrix $\hat{\varrho}$, is given as [199, 200]:

$$\mathcal{J}_\theta = Tr[\partial_\theta \hat{\varrho}]^2 + \frac{1}{det\hat{\varrho}} Tr[\hat{\varrho}\partial_\theta \hat{\varrho}]^2; \tag{I.93}$$

Where: $\partial_\theta = \frac{\partial}{\partial_\theta}$.

In the Bloch sphere representation, any single-qubit state is represented as:

$$\hat{\varrho} = \frac{1}{2}(\hat{I} + \overrightarrow{h}.\hat{\sigma}). \tag{I.94}$$

Whereas $\overrightarrow{h} = (h_x, h_y, h_z)$ describes the real Bloch vector and $\hat{\sigma} = (\hat{\sigma}_x, \hat{\sigma}_y, \hat{\sigma}_z)$ denotes the Pauli matrices.

A simple expression of QFI is given [200] by substituting Eq. (I.94) into Eq. (I.93) :

$$\mathcal{J}_\theta = \begin{cases} |\partial_\theta \overrightarrow{h}|^2 + \frac{(\overrightarrow{h}.\partial_\theta \overrightarrow{h})^2}{1-|\overrightarrow{h}|^2}, & \text{if } |\overrightarrow{h}| < 1 \\ |\partial_\theta \overrightarrow{h}|^2, & \text{if } |\overrightarrow{h}| = 1, \end{cases} \tag{I.95}$$

From Eq. (II.21), the quantum Fisher information of a pure state ($|\overrightarrow{h}| = 1$) is given by the expression $|\partial_\theta \overrightarrow{h}|^2$. While, for a mixed state ($|\overrightarrow{h}| < 1$), it is presented by $|\partial_\theta \overrightarrow{h}|^2 + \frac{(\overrightarrow{h}.\partial_\theta \overrightarrow{h})^2}{1-|\overrightarrow{h}|^2}$.
Another version of quantum Fisher information based on the symmetric logarithmic derivative (SLD) operator has also been widely used [119, 123]:

$$\mathcal{J}_\theta = Tr[\hat{\varrho}_\theta \mathcal{L}_\theta] = Tr[(\partial_\theta \hat{\varrho}_\theta)\mathcal{L}_\theta] \tag{I.96}$$

Where $\mathcal{L}_\theta$ represents the symmetric logarithmic derivation, which is determined by:

$$\partial_\theta \hat{\varrho}_\theta = \frac{(\mathcal{L}_\theta \hat{\varrho}_\theta + \hat{\varrho}_\theta \mathcal{L}_\theta)}{2}. \tag{I.97}$$

By using the spectrum decomposition of the density matrix $\hat{\varrho}_\theta = \sum_n \lambda_n |\phi_n\rangle\langle\phi_n|$, the quantum Fisher information is given as [201]

$$\mathcal{J}_\theta = \sum_n \frac{(\partial_\theta \lambda_n)^2}{\lambda_n} + \sum_n 4\lambda_n \langle \partial_\theta \lambda_n | \partial_\theta \lambda_n \rangle - \sum_{n \neq m} \frac{8\lambda_n \lambda_m}{\lambda_n + \lambda_m} |\langle \phi_n | \partial_\theta \phi_m \rangle|^2 \tag{I.98}$$

The first term which is called the classical term is equal to the classical Fisher information of Eq. (I.98), and the second terms are called the quantum terms.

The QFI plays a primordial role in the estimation of an unknown parameter through the Cramer-Rao bound [119, 122, 123]

$$Var(\theta) \geq \mathcal{J}_\theta^{-1} \tag{I.99}$$

With $Var(\theta)$ is the variance of the parameter θ, and $\mathcal{J}$ is the quantum Fisher information.

From the parameter estimation perspective, the larger QFI represents the higher estimation precision in general. Hence, improving the QFI becomes a key problem to be solved.

I.7.2 Quantum Fisher matrix

Definition

We consider a vector of parameters $\hat{\theta} = (\theta_0, \theta_1, ..., \theta_n, ...)^T$, with θ_n as the n-th parameter. An element of the quantum Fisher information matrix is determined by [119, 123]:

$$\mathcal{J}_{\theta_i\theta_j} = \frac{1}{2} Tr(\hat{\varrho}\{\mathcal{L}_{\theta_i}, \mathcal{L}_{\theta_j}\}), \tag{I.100}$$

Where θ is encoded in $\hat{\varrho}$. $\{.,.\}$ is the anti-commutation and $\mathcal{L}_i$ ($\mathcal{L}_j$) is the symmetric logarithmic derivative (SLD) for the parameter $\theta_i(\theta_j)$ which is defined as:

$$\partial_{\theta_i}\hat{\varrho} = \frac{1}{2}(\hat{\varrho}\mathcal{L}_{\theta_i} + \mathcal{L}_{\theta_j}\hat{\varrho}) \tag{I.101}$$

The expression of QFIM, $\mathcal{J}_{\theta_i\theta_j}$ is given by:

$$\mathcal{J}_{\theta_i\theta_j} = Tr(\mathcal{L}_{\theta_j}\partial_{\theta_i}\hat{\varrho}) \tag{I.102}$$

From the equation (I.100), the diagonal entries of QFIM represent the quantum Fisher information of parameter θ_i

$$\mathcal{J}_{\theta_i\theta_i} = Tr(\hat{\varrho}\mathcal{L}^2_{\theta_i}) \tag{I.103}$$

Proprieties of QFIM

The QFIM obeys some properties [202]:

- $\mathcal{J}$ is real symmetric. In other words, $\mathcal{J}_{\theta_i,\theta_j} = \mathcal{J}_{\theta_j,\theta_i} \in \mathbb{R}^2$.
- $\mathcal{J}$ is positive semi-definite, i.e., $\mathcal{J}_{\theta_i,\theta_j} \geq 0$.
- $\mathcal{J}(\hat{\varrho}) = \mathcal{J}(U\hat{\varrho}U^\dagger)$, with U is a θ-independent unitary operation.
- If $\hat{\varrho} = \otimes_i\hat{\varrho}_i(\theta)$, then $\mathcal{J}(\rho) = \sum_i \mathcal{J}(\hat{\varrho}_i)$.
- $\mathcal{J}$ is linear: $\mathcal{J}(\lambda\hat{\varrho}_1 + (1-\lambda)\hat{\varrho}_2) \leq \lambda\mathcal{J}(\hat{\varrho}_1) + (1-\lambda)\mathcal{J}(\hat{\varrho}_2)$.
- $\mathcal{J}$ is monotonic under completely positive and a trace preserving map ϵ: $\mathcal{J}(\epsilon(\hat{\varrho})) \leq \mathcal{J}(\hat{\varrho})$.

The quantum Fisher information matrix (QFIM) provides a tool to determine the precision in the multiparameter estimation, where the lower bound of the estimation is given by the Cramer Rao inequality [122] as:

$$Cov(\hat{\theta}) \geq \mathcal{J}^{-1}_{\theta_i,\theta_j} \tag{I.104}$$

With: $\hat{\theta} = \theta_1, \theta_2...$ it is a set of parameters which can be encoded in the density matrix $\hat{\varrho} = \hat{\varrho}(\hat{\theta})$ and $Cov(\hat{\theta})$ is the covariance of the parameters $\hat{\theta}$. $\mathcal{J}^{-1}_{\theta_i,\theta_j}$ is the inverse of the quantum Fisher information matrix. Indeed, the inverse of the QFIM gives the lower error limit of the estimation.

Calculation of QFIM

The traditional derivation of QFIM is usually based on the decomposition of $\hat{\varrho}$ into eigenvalues λ_m and eigenvectors $|\lambda_m\rangle$. As $\hat{\varrho} = \sum_{i=0}^{d-1} \lambda_m |\lambda_m\rangle\langle\lambda_m|$, an entry of QFIM can be calculated as [202]

$$\mathcal{J}_{\theta_i\theta_j} = \sum_{\lambda_m} \frac{(\partial_{\theta_i}\lambda_m)(\partial_{\theta_j}\lambda_m)}{\lambda_m} + \sum_{\lambda_m} 4\lambda_m Re(\langle\partial_{\theta_i}\lambda_m|\partial_{\theta_j}\lambda_m\rangle) - \sum_{\lambda_m,\lambda_n} \frac{8\lambda_m\lambda_n}{\lambda_m+\lambda_n} Re(\langle\partial_{\theta_i}\lambda_m|\lambda_n\rangle\langle\lambda_n|\partial_{\theta_j}\lambda_m\rangle) \quad (I.105)$$

The first term in equation (I.105) is the counterpart of the classical Fisher information as it only contains the derivatives of the eigenvalues which can be regarded as the counterpart of the probability distributions. Besides, The other terms are purely quantum. The expression of the QFIM [122] is given as follows:

$$\mathcal{J}_{\theta_i\theta_j} = Tr[\hat{\varrho}\frac{\mathcal{L}_{\theta_i}\mathcal{L}_{\theta_j} + \mathcal{L}_{\theta_j}\mathcal{L}_{\theta_i}}{2}] = Tr[\partial_{\theta_i}\hat{\varrho}\mathcal{L}_{\theta_i}] = Tr[\partial_{\theta_j}\hat{\varrho}\mathcal{L}_{\theta_j}] \quad (I.106)$$

$\mathcal{L}_{\theta_i}$ is the symmetric logarithmic derivative which corresponds to the parameter θ_i. It is determined by the equation:

$$\partial_{\theta_i}\hat{\varrho} = \frac{1}{2}(\mathcal{L}_{\theta_i}\hat{\varrho} + \hat{\varrho}\mathcal{L}_{\theta_i}), \quad (I.107)$$

An expression of the $QFIM$, based on the calculation of the exponential of $\hat{\varrho}$ and an integral, can be derived using the Eqs. (I.106) and (I.107). This expression is given as follows:

$$\mathcal{J}_{\theta_i\theta_j} = Tr[\partial_{\theta_i}\hat{\varrho}\mathcal{L}_{\theta_i}] = 2\int_0^\infty Tr[dte^{-\hat{\varrho}t}\partial_{\theta_i}\hat{\varrho}e^{-\hat{\varrho}t}\partial_{\theta_i}\hat{\varrho}]. \quad (I.108)$$

Moreover, A simple expression to calculate the $QFIM$ is given in [203] using the method of vectorization. In *Liouville* space [204], the density matrix is a vector containing all the entries of the density matrix in *Hilbert* space. For an invertible density matrix $\hat{\varrho}$, the QFIM can be analytically computed as:

$$\mathcal{J}_{\theta_i\theta_j} = 2Vec^\dagger[\partial_{\theta_i}\hat{\varrho}](\hat{\varrho}^T \otimes \hat{I} + \hat{I}\otimes\hat{\varrho})^{-1}Vec[\partial_{\theta_j}\hat{\varrho}], \quad (I.109)$$

$Vec(A)$ denotes the column vector of A in *Liouville* space and $Vec(A)^\dagger$ indicates the conjugate transpose of $Vec(A)$. $\hat{I}$ is the identity matrix and $\hat{\varrho}$ is the transpose of $\hat{\varrho}$. $Vec[\partial_{\theta_i}\hat{\varrho}]$ is the Vector column of the matrix $\partial_{\theta_i}\hat{\varrho}$. The SLD operator in Liouville space, denoted by $Vec(\mathcal{L}_{\theta_i})$, is given as:

$$Vec(\mathcal{L}_{\theta_i}) = 2(\hat{\varrho}\otimes\hat{I} + \hat{I}\otimes\hat{\varrho}^*), \quad (I.110)$$

This expression of $QFIM$ could be proven by using the proprieties [205, 206]:

$$(AB\hat{I}) = (A\otimes\hat{I})Vec(B) = (\hat{I}\otimes B^T)Vec(A) \quad (I.111)$$

Where: B^T is the transpose of B.

and

$$Tr(A^\dagger B) = Vec(A)^\dagger Vec(B) \quad (I.112)$$

A well-used version of $QFIM$, that uses Bloch representation, is frequently used in the context of quantum information. For a 2-dimensional density matrix $\hat{\varrho}$:

$$\hat{\varrho} = \frac{1}{2}(\hat{I} + \overrightarrow{h}.\overrightarrow{\sigma}) \quad (I.113)$$

Where $\overrightarrow{h} = (h_x, h_y, h_z)^T$ is the Bloch vector, and σ is the Pauli matrices $(\sigma_x, \sigma_y, \sigma_z)$. the QFIM in Bloch representation can be expressed by:

$$\mathcal{J}_{\theta_i,\theta_j} = \begin{cases} (\partial_{\theta_i}\overrightarrow{h})(\partial_{\theta_j}\overrightarrow{h}) + \frac{(\overrightarrow{h}.\partial_{\theta_i}\overrightarrow{h})(\overrightarrow{h}.\partial_{\theta_j}\overrightarrow{h})}{1-|\overrightarrow{h}|^2}, & \text{if } |\overrightarrow{h}| < 1 \\ (\partial_{\theta_i}\overrightarrow{h})(\partial_{\theta_j}\overrightarrow{h}), & \text{if } |\overrightarrow{h}| = 1. \end{cases} \tag{I.114}$$

For a single-qubit pure state, $\mathcal{J}_{\theta_i,\theta_j} = (\partial_{\theta_i}\overrightarrow{h})(\partial_{\theta_j}\overrightarrow{h})$. However, for a mixed state $\overrightarrow{h} \leq 1$ the QFIM is given as $\mathcal{J}_{\theta_i,\theta_j} = (\partial_{\theta_i}\overrightarrow{h})(\partial_{\theta_j}\overrightarrow{h}) + \frac{(\overrightarrow{h}.\partial_{\theta_i}\overrightarrow{h})(\overrightarrow{h}.\partial_{\theta_j}\overrightarrow{h})}{1-|\overrightarrow{h}|^2}$.

In matrix representation, one can write the quantum Fisher information matrix with respect to the two parameters θ_i and θ_j as:

$$\mathcal{J}_{\theta_i,\theta_j} = \begin{pmatrix} \mathcal{J}_{\theta_i,\theta_i} & \mathcal{J}_{\theta_j,\theta_i} \\ \mathcal{J}_{\theta_i,\theta_j} & \mathcal{J}_{\theta_j,\theta_j} \end{pmatrix}, \tag{I.115}$$

The diagonal entries of the matrix Eq. (I.115) are exactly the QFI of parameter θ_i and θ_j.

I.8 Conclusion

In this chapter we have presented the preliminary concepts of quantum information processing. We have reviewed the basic notions of quantum information such as qubit, sharp and unsharp quantum measurements and the concept of quantum noisy channels. We have briefly reviewed the negative partial transpose (NPT) as an entanglement monotone. Furthermore, we have recalled the notions of quantum gates and the quantum circuit. We have also reviewed the idea of unidirectional quantum teleportation and some teleportation quantifiers such as the average fidelity, quantum Fisher information and quantum Fisher information matrix. In the unidirectional quantum teleportation, the transmission of information is one-way, namely only Alice has the ability to teleport his state to Bob; which leads to asking the following question: is it possible to make a two-way teleportation? In the next chapter, we will tackle this issue and we will introduce the bidirectional quantum teleportation as a direct extension of the standard quantum teleportation.

Chapter II

Bidirectional quantum teleportation

In this chapter, we address the bidirectional transfer of unknown quantum states and relevant parameters from a sender usually called *Alice* to a distant receiver *Bob*, and vice versa. So we are faced with the issue of bidirectional quantum teleportation.

Bidirectional quantum teleportation (BQT) is become one of the main ingredients to develop the quantum information science. It is a vital element for the improvement of many quantum information tasks, such as quantum key distribution, quantum communication, and quantum networks [77, 79]. In fact, the entanglement with local operations and classical communication (LOCC) [207] are the pillars of all quantum teleportation processes. In 1993, *Bennet et al*. [34] presented the first teleportation scheme, which is a unidirectional teleportation, using a Bell state as a quantum channel. Since then, the quantum teleportation has attracted much interest in two directions, theoretically [208] and experimentally [209]. However, the two-way teleportation of atomic quantum states was presented as a thought experiment by *Vaidman* [210]. Subsequently, *Huelga et al*. [211] discussed the possibility of the bidirectional quantum teleportation (BQT) for a remote implementation of non-local unitary gates. After that, *Zhao et al*. [212] proposed a protocol for the remote implementation of a quantum operation. Actually, a large variety of bidirectional quantum teleportation (BQT) and bidirectional controlled quantum teleportation $(BCQT)$ schemes have been proposed in the last decade, based on different types of entangled states such as cluster states [213], composite GHZ-Bell state [214], n-entangled qubit [215, 216, 217], GHZ state [218, 219] and Bell state [193]. Indeed, these protocols are designed to transfer quantum states simultaneously between the two users. The $BCQT$ protocols necessitate the intervention from a supervisor (Charlie) to accomplish the task. However, from the perspective of the parameter estimation, it is the information carried by a relevant parameter, not the information of the whole system that needs to be teleported. The quantum Fisher information (QFI) provides a tool to quantify the parameter teleportation [220]. Nevertheless, QFI is directly related to the Cramer-Rao bound [119, 122, 123]. Furthermore, the quantum Fisher information matrix (QFIM), provides a tool to determine the precision in any multiparametric estimation protocol. Besides the quantum estimation, the QFI and the $QFIM$ are crucial concepts in quantum metrology [126, 127], quantum phase transition [130] and entanglement detection [131].

In this chapter, we provide a full description of bidirectional quantum teleportation protocol using the minimal quantum cost, i.e, 1 ebit i in Sec. II.1. This scheme could be implemented with now-days advanced technologies [193]. Later on, in Sec. II.2, we analyze the accuracy of the BQT protocol using the fidelities average and the quantum Fisher information. Both quantities are related to the Bruse distance, which is a closeness measure between the initial and the teleported states. Moreover, in Sec. II.3, we compare the suggested protocol with previous other protocols. In Sec II.4, we investigate the individual estimation degree against the simultaneous one . Finally, we summarize this chapter in II.5.

II.1 Perfect bidirectional teleportation

The idea of the standard one-qubit quantum teleportation protocol [34] is to transmit an unknown quantum state $|Q\rangle$ from one party to another distant party (Fig II.1a). Before the protocol starts, Alice and Bob may share the entangled state.:

$$|\psi^+_{AB}\rangle = \frac{1}{\sqrt{2}}(|00\rangle + |11\rangle)_{AB}. \tag{II.1}$$

The protocol consists of three steps (as described in chapter one):

- Alice performs a projective measurement on her state $|Q\rangle$ and the particle from the Bell state (Eq II.1) in the Bell basis $\{|\phi\rangle^+, |\phi\rangle^-, |\psi\rangle^+, |\psi\rangle^-\}$.
- Alice sends the index of the measurement outcome, as given in Table (I.3), to Bob via a classical communication channel.
- Bob performs the appropriate Pauli operation $(\hat{X}, \hat{Z}, \hat{Y}, \hat{I})$, on his particle from the Bell state (II.1) to recover the state $|Q\rangle$.

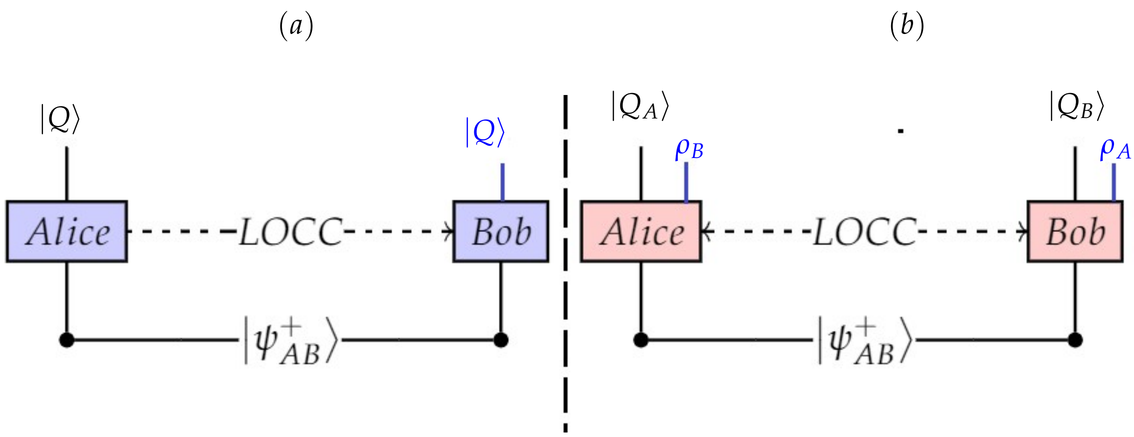

FIGURE II.1: Quantum teleportation protocol using Bell state $|\psi^+_{AB}\rangle$ with local operations and classical communication (LOCC). (a) Standard scheme of unidirectional quantum teleportation: the quantum state $|Q\rangle$ is perfectly teleported from Alice to Bob using the shared Bell state $|\psi^+_{AB}\rangle$. (b) Scheme of bidirectional quantum teleportation: Alice and Bob exchange their states $|Q_A\rangle$ and $|Q_B\rangle$ by means of the Bell state $|\psi^+_{AB}\rangle$.

In the one hand, it is worth to mention that Alice's measurement in the first step of the protocol breaks the initial entanglement of state (Eq. II.1), and her particle from the Bell state transforms to a maximally mixed state. On the other hand, Bob tries to minimize the interaction of his particle from the Bell state with an environment to avoid the decoherence effect. The previous points affirm that to make it possible to transfer information from Bob to Alice as well as from Alice to Bob, i.e., bidirectional teleportation, Alice should not perform a perfect projective measurement of her particles $|Q_A\rangle$ and $|\psi^+_A\rangle$. Actually, she should leave an amount of entanglement in the Bell state for the purpose of information transfer in the reverse direction. Meanwhile, Bob should do the same approach to get the quantum state from Alice and, at the same time, send his own one to Alice (Fig II.1b).

In this framework, a suggested scheme for bidirectional quantum teleportation (Fig: II.2) is suggested to transfer information from Bob to Alice as well as from Alice to Bob, i.e., bidirectional teleportation. This protocol is based on a single Bell state with classical communication in both directions. In addition, this scheme operates with 10 qubits which should be prepared locally for the two parties of the teleportation protocol.

II.1.1 Preparing the initial states

Firstly, the users share an entangled state of Bell type :

$$\left|\psi^{+}_{AB}\right\rangle = \frac{1}{\sqrt{2}}(|00\rangle + |11\rangle)_{AB} \tag{II.2}$$

where "A" and "B" refer to Alice and Bob respectively. However, since we are interested in estimating the teleported parameters by using quantum Fisher information, we have to describe the procedure of this protocol by means of the Bloch vectors. Therefore, we can write the initial Bell state as:

$$\hat{\varrho}_{AB} = \frac{1}{4}(\hat{I} + \hat{\sigma_x}^{(A)}\hat{\tau_x}^{(B)} - \hat{\sigma_y}^{(A)}\hat{\tau_y}^{(B)} + \hat{\sigma_z}^{(A)}\hat{\tau_z}^{(B)}), \tag{II.3}$$

where $\hat{\sigma_i}^{(A)}$ and $\hat{\tau_i}^{(B)}$ (for $i = x, y, z$) represent the Pauli operators of Alice's qubit and Bob's qubit, respectively [221]. Let us assume that Alice and Bob are given two different states, $|Q_A\rangle$ and $|Q_B\rangle$ to be bilaterally teleported, such as:

$$\begin{aligned} |Q_A\rangle &= \cos\left(\frac{\theta_A}{2}\right)|0_A\rangle + e^{i\phi_A}\sin\left(\frac{\theta_A}{2}\right)|1_A\rangle, \\ |Q_B\rangle &= \cos\left(\frac{\theta_B}{2}\right)|0_B\rangle + e^{i\phi_B}\sin\left(\frac{\theta_B}{2}\right)|1_B\rangle. \end{aligned} \tag{II.4}$$

Whereas: $\phi_i \in [0, 2\pi]$ is the qubits' phases and $\theta_i \in [0, \pi]$ is the qubits' weights (for $i = A, B$).

Similarly, these qubits can be represented by their Bloch vectors as:

$$\hat{\varrho}_q^{(A)} = \frac{1}{2}\Big(\hat{I} + \sum_{i=x,y,z} a_i\hat{\sigma_i}^{(A)}\Big), \quad \hat{\varrho}_q^{(B)} = \frac{1}{2}\Big(\hat{I} + \sum_{i=x,y,z} b_i\hat{\tau_i}^{(B)}\Big). \tag{II.5}$$

where a_i and b_i (for $i = x, y, z$) are the Bloch vectors of Alice's qubit and Bob's qubit, respectively. The users aim to exchange these states between them. Moreover, each user has two different types of qubits; the trigger qubits which they are defined initially as:

$$|T_A\rangle = \cos\Big(\frac{\tilde{\theta}_A}{2}\Big)|0_A\rangle + \sin\Big(\frac{\tilde{\theta}_A}{2}\Big)|1_A\rangle, \quad |T_B\rangle = \cos\Big(\frac{\tilde{\theta}_B}{2}\Big)|0_B\rangle + \sin\Big(\frac{\tilde{\theta}_B}{2}\Big)|1_B\rangle. \tag{II.6}$$

Whereas: $\tilde{\theta}_i \in [0, \pi]$ is the triggers' weights (for $i = A, B$). These states become in the Bloch vectors like:

$$\hat{\varrho}_{T_A} = \frac{1}{2}\Big(\hat{I} + \sum_{i=x,y,z} t_i^{(A)}\hat{\sigma_i}^{(A)}\Big), \quad \hat{\varrho}_{T_B} = \frac{1}{2}\Big(\hat{I} + \sum_{i=x,y,z} t_i^{(B)}\hat{\tau_i}^{(B)}\Big). \tag{II.7}$$

whereas $t_i^{(A)}$ ($t_i^{(B)}$) are the Bloch vectors of Alice's (Bob's) Trigger. Furthermore, Alice and Bob are supplied by four storage qubits; $\left|S_A^{(1)}\right\rangle, \left|S_A^{(2)}\right\rangle$ for Alice, and two for Bob $\left|S_B^{(1)}\right\rangle, \left|S_B^{(2)}\right\rangle$. It is assumed that these qubits are initially prepared in a vacuum state, i.e., $\left|S_j^{(i)}\right\rangle = |0\rangle, i = 1, 2$ and $j = A, B$. These states may be represented by Pauli operators as:

$$\hat{\varrho}_{s_A}^{(i)} = \frac{1}{2}(1 + \hat{\sigma_z}^{(A)}), \ \hat{\varrho}_{s_B}^{(i)} = \frac{1}{2}(1 + \hat{\tau_z}^{(B)}); \ with: \ \ i = 1, 2 \tag{II.8}$$

These types of qubits are used as a storage of the projective measurement outcomes. All these types of qubits are described clearly in the circuit (Fig $II.2$).

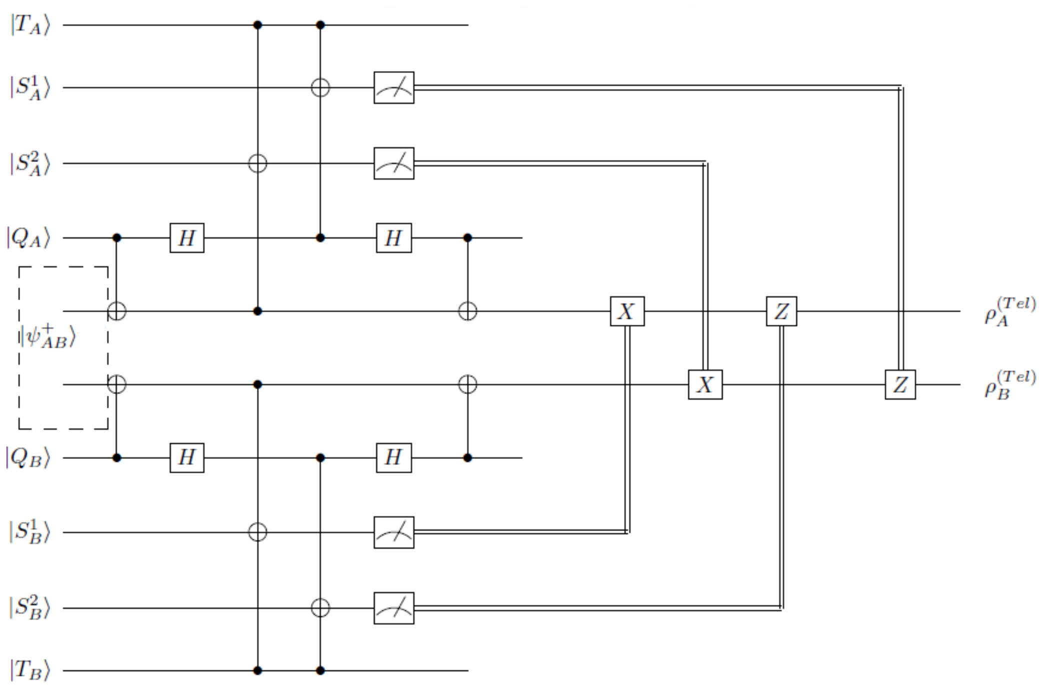

FIGURE II.2: Quantum circuits for bidirectional teleportation with the single Bell state $|\psi^+_{AB}\rangle$ (see Eq. (II.2)). Here $\hat{X}$, $\hat{Z}$ and H are Pauli and Hadamard gates respectively. Vertical lines represent *CNOT* and *CCNOT* gates, where control and target qubits are denoted by $\bullet$ and $\oplus$. All measurement outcome values (0 or 1) are transmitted via classical communication represented by double lines toward gates.

II.1.2 Performing the BQT Protocol

In the following, we describe the duty of the users to perform the suggested protocol step by step as shown in Figure (II.2).

- *From Alice to Bob*

  1. **Step one**:
     The users prepare their initial state, which consists of 10 qubits, by using the states in Eqs.(II.2-II.8). This state may be written as:

$$|\psi_s\rangle = |\psi^+_{AB}\rangle \left|Q_A S_A^{(1)} S_A^{(2)} T_A\right\rangle \left|Q_B S_B^{(1)} S_B^{(2)} T_B\right\rangle \tag{II.9}$$

  2. **Step two**:
     The users apply two *CNOT* gates where $|Q_{A,B}\rangle$ are control qubits and the Bell qubits $|\psi^+_{AB}\rangle$ are target qubits as,

$$CNOT\,|\psi_s\rangle = CNOT_2\big(|\psi^+_{AB}\rangle \left|Q_A S_A^{(1)} S_A^{(2)} T_A\right\rangle \left|Q_B S_B^{(1)} S_B^{(2)} T_B\right\rangle\big)$$

     followed by applying the Hadamard gates on the qubits $|Q_{A,B}\rangle$ in the previous output results

$$H\Big(CNOT\,|\psi_s\rangle\Big) = H_2\big(CNOT_2(|\psi^+_{AB}\rangle \left|Q_A S_A^{(1)} S_A^{(2)} T_A\right\rangle \left|Q_B S_B^{(1)} S_B^{(2)} T_B\right\rangle)\big) \tag{II.10}$$

  3. **Step three**:
     Alice and Bob perform two *CCNOT* gates. In the first one, the triggers $|T_{A,B}\rangle$ and the Bell pairs

$\left|\psi^{+}_{A,B}\right\rangle$ play the role of the control qubits and $\left|S^{(2)}_{A,B}\right\rangle$ are target qubits. While in the second $CCNOT$ gate, the triggers $|T_{A,B}\rangle$ and $|Q_{A,B}\rangle$ are control qubits and $\left|S^{(1)}_{A,B}\right\rangle$ are target qubits to get:

$$|\psi_s\rangle' = CCNOT_2\big(H_2(CNOT_2(|\psi^{+}_{AB}\rangle \left|Q_A S^{(1)}_A S^{(2)}_A T_A\right\rangle \left|Q_B S^{(1)}_B S^{(2)}_B T_B\right\rangle)))\tag{II.11}$$

4. **Step four**:
   The measurement's results are stored in the qubits $\left|S^{(1)}_{A}\right\rangle$ and $\left|S^{(2)}_{A}\right\rangle$. These results are sent by the classical communication channel to Bob. Based on Alice's measurements, Bob performs the adequate local operations $(\hat{X}, \hat{Z}, \hat{I})$, on his Bell state particle to recover the state $|Q_A\rangle$.

- *From Bob to Alice:*
  Bob may perform the same operation that Alice has done to teleport his state $|Q_B\rangle$ to Alice.

II.1.3 Implementation of the circuit

The final output of the circuit depends on the initial state of the triggers. However, we have the following possibilities:

1. The initial state of both triggers are initially prepared in the states, $\hat{\varrho}_{T_A} = \frac{1}{2}\left(\hat{I} + \hat{\sigma}_z{}^{(A)}\right)$ and $\hat{\varrho}_{T_B} = \frac{1}{2}\left(\hat{I} + \hat{\tau}_z{}^{(B)}\right)$. In this case, each partner obtains the completely mixed state: $\hat{\varrho}^{(A)}_q = \hat{\rho}^{(B)}_q = \hat{\varrho}_0$.

   Where

$$\hat{\varrho}_0 = \frac{1}{2}\begin{pmatrix} 1 & 0 \\ 0 & 1 \end{pmatrix}\tag{II.12}$$

2. Alice's and Bob's triggers are prepared in the states $\hat{\varrho}_{T_A} = \frac{1}{2}\left(\hat{I} - \hat{\sigma}_z{}^{(A)}\right)$ and $\hat{\varrho}_{T_B} = \frac{1}{2}\left(\hat{I} - \hat{\tau}_z{}^{(B)}\right)$. In this case, Alice and Bob perform a perfect projective measurement with the probabilities:

$$\mathcal{P}_i = tr\left\{\hat{\varrho}_{T_A}\hat{\varrho}^{(A)}_q\right\} = tr\left\{\hat{\varrho}_{T_B}\hat{\varrho}^{(B)}_q\right\} = \sin^2(\frac{\theta_i}{2}), \qquad i = A, B.\tag{II.13}$$

   The users will end up their protocol by two states, one of them at Alice's side:

$$\hat{\varrho}^{(A)}_{tel} = \mathcal{P}_B\bar{\mathcal{P}}_A\hat{\varrho}^{(B)}_q + (1 - \mathcal{P}_B\bar{\mathcal{P}}_A)\hat{\varrho}_0,\ \ \bar{\mathcal{P}}_A = 1 - \mathcal{P}_A\tag{II.14}$$

   and the other in Bob's side:

$$\hat{\varrho}^{(B)}_{tel} = \mathcal{P}_A\bar{\mathcal{P}}_B\hat{\varrho}^{(A)}_q + (1 - \mathcal{P}_A\bar{\mathcal{P}}_B)\hat{\varrho}_0,\ \ \bar{\mathcal{P}}_B = 1 - \mathcal{P}_B\tag{II.15}$$

3. If Alice's trigger qubit is prepared in the state $\hat{\varrho}_{T_A} = \frac{1}{2}\left(\hat{I} - \hat{\sigma}_z{}^{(A)}\right)$ and Bob's trigger qubit is prepared in the state $\hat{\varrho}_{T_B} = \frac{1}{2}\left(\hat{I} + \hat{\tau}_z{}^{(B)}\right)$, then only Alice has the ability to teleport her qubit to Bob. While, Alice gets the completely mixed state i.e., the final state at Alice's hand is $\hat{\varrho}^{(A)}_{tel} = \hat{\varrho}_0$ and at Bob's hand $\hat{\varrho}^{(B)}_{tel} = \hat{\varrho}^{(A)}_q$.

II.2 Quantifiers of bidirectional teleportation

Usually the credibility of teleportation is quantified by the fidelity, where information of the whole system is teleported. However, in some situations, there is no need to teleport the whole state of the system but only the information that is carried by a relevant parameter or parameters. If it is the case, the transfer of information is quantified by means of the quantum Fisher information. In what follows, we quantify the BQT using the fidelities of teleportation and the quantum Fisher information.

II.2.1 Fidelities of teleportation

The fidelity f of the teleported state. It measures the similarity between the input state $\varrho_q^{(A)}$ ($\varrho_q^{(B)}$) and the output state $\varrho_{tel}^{(B)}$ ($\varrho_{tel}^{(A)}$) respectively. The expression of the fidelity f is defined as [143, 194] :

$$f^{in\to out} =< Q^{in}|\varrho_{out}|Q^{in} >, \quad i = A, B \tag{II.16}$$

with $|Q^i >$ and ϱ_{out} are the input and the output states respectively. The essence of teleportation is that the state to be teleported is unknown. Therefore, it is more practical to evaluate the averaged fidelity over all the input states. The averaged fidelity may be described as [143]:

$$\mathcal{F}_{avg}^{in\to out} = \frac{1}{4\pi}\int_0^{\pi} d\theta_i \int_0^{2\pi} f^{in\to out}(\theta_i, \phi_i, \mathcal{P}_A, \mathcal{P}_B)\sin\theta_i d\phi_i\,, \quad i = A, B \tag{II.17}$$

where:

$$f^{in\to out}(\theta_i, \phi_i, \mathcal{P}_A, \mathcal{P}_B) = |c|_i^2\Big(A_2 + A_1|c|_t^2\Big) + A_1\Big(c_i^* s_i c_t s_t^* + s_i^* c_i s_t c_t^*\Big) + |s|_i^2\Big(A_1|s|_t^2 + A_2\Big), \tag{II.18}$$

with the different elements $c_i = \cos\left(\frac{\theta_i}{2}\right)$, $s_i = \sin\left(\frac{\theta_i}{2}\right)e^{i\phi_i}$, $c_t = \cos\left(\frac{\theta_t}{2}\right)$ and $s_t = \sin\left(\frac{\theta_t}{2}\right)e^{i\phi_t}$. Whereas, i and t indicate the initial and the teleported state respectively. The terms A_1 and A_2 depend on the direction of the teleportation, i.e, from Alice to Bob $A_1 = \mathcal{P}_A\bar{\mathcal{P}}_B$, $A_2 = \frac{1-\mathcal{P}_A\bar{\mathcal{P}}_B}{2}$. While, from Bob to Alice $A_1 = \mathcal{P}_B\bar{\mathcal{P}}_A$ and $A_2 = \frac{1-\mathcal{P}_B\bar{\mathcal{P}}_A}{2}$.

The fidelity of teleportation between the two users, $f^{A\to B}$ and $f^{B\to A}$ are given by:

$$f^{(A\to B)} = \frac{1}{2}(1 + \mathcal{P}_A\bar{\mathcal{P}}_B), \quad f^{(B\to A)} = \frac{1}{2}(1 + \mathcal{P}_B\bar{\mathcal{P}}_A), \tag{II.19}$$

where the probabilities may be written as:

$$\begin{aligned}
\mathcal{P}_A &= \frac{1}{2}\Big(1 + \cos(\tilde{\theta}_A)\cos(\theta_A) + \sin(\tilde{\theta}_A)\sin(\theta_A)\cos\phi_A + \sin(\tilde{\theta}_A)\sin(\theta_A)\sin\phi_A\Big),\\
\mathcal{P}_B &= \frac{1}{2}\Big(1 + \cos(\tilde{\theta}_B)\cos(\theta_B) + \sin(\tilde{\theta}_B)\sin(\theta_B)\cos\phi_B + \sin(\tilde{\theta}_B)\sin(\theta_B)\sin\phi_B\Big).
\end{aligned} \tag{II.20}$$

Now, by using Eqs. (II.19) and (II.20), one can obtain the Fidelity of the teleported state for both directions at an initial state setting.

Fig. (II.3) shows the behavior of the averaged Fidelity of the teleported state from both directions, namely $\mathcal{F}_{Avg}^{(A\to B)}$ and $\mathcal{F}_{Avg}^{(B\to A)}$; where it is assumed that the teleported state is initially prepared in the state $\hat{\varrho}_q^{(A)} = \frac{1}{2}(\hat{I} + \hat{\sigma}_z^{(A)})$ at Alice side, while Bob's teleported state is given by $\hat{\varrho}_q^{(B)} = \frac{1}{2}(\hat{I} + \hat{\tau}_z^{(B)})$, namely the users teleport only classical information, i.e. $\theta_A = \theta_B = 0$, while the triggers are prepared in an arbitrary

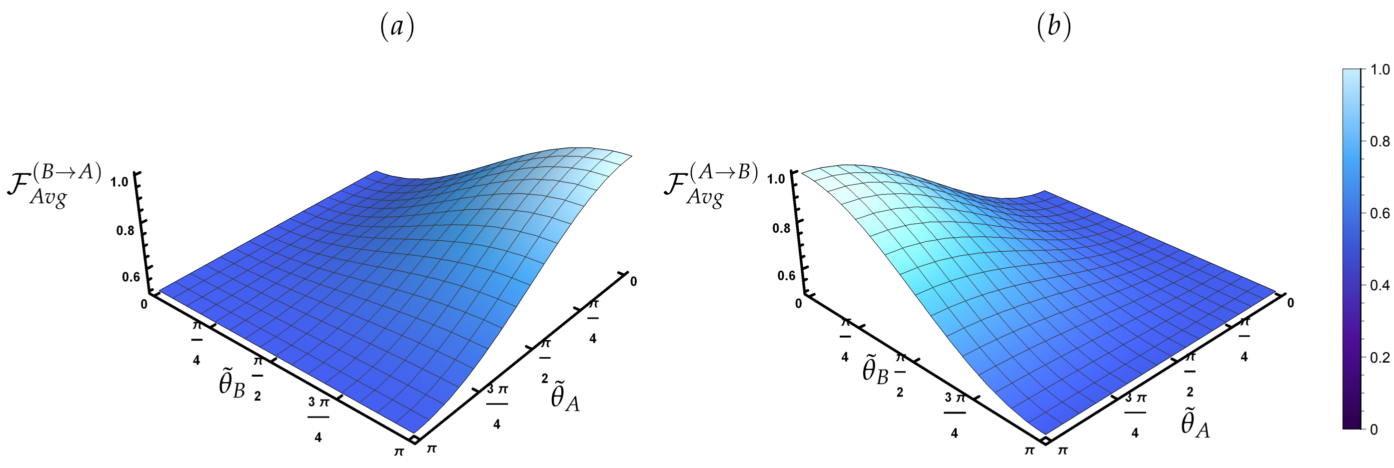

FIGURE II.3: Bidirectional teleportation averaged Fidelity, where the initial states are prepared such that $\theta_A = \theta_B = 0$ of the initial qubits $|Q_A\rangle$ and $|Q_B\rangle$. (a) The averaged fidelity of teleportation $\mathcal{F}_{Avg}^{(A\to B)}$ and (b) represents $\mathcal{F}_{Avg}^{(B\to A)}$.

state with $\phi = 0$. It is clear that, from Fig. (II.3a), which displays the behavior of the fidelity from Bob to Alice, namely $\mathcal{F}_{Avg}^{(B\to A)}$, where the teleported state is prepared in the state $\hat{\varrho}_q^{(B)} = \frac{1}{2}(\hat{I} + \hat{\tau}_z^{(B)})$, at any value of $\tilde{\theta}_B$, the Fidelity $\mathcal{F}_{Avg}^{(B\to A)}$ increases gradually as $\tilde{\theta}_B$ increases. The maximum Fidelity is reached at $\tilde{\theta}_B = \pi$, namely, Bob's trigger is prepared in the state $\hat{\varrho}_{T_B} = \frac{1}{2}(\hat{I} - \hat{\tau}_z^{(B)})$.
However, in Fig. (II.3b), the behavior of $\mathcal{F}_{Avg}^{(A\to B)}$ is similar to that predicted in Fig. (II.3a), where the increasing and decreasing of the teleportation fidelity average from Alice to Bob depends on the state of Alice's trigger, namely the maximum value is predicted at $\hat{\varrho}_{T_A} = \frac{1}{2}(\hat{I} - \hat{\sigma}_z^{(A)})$.

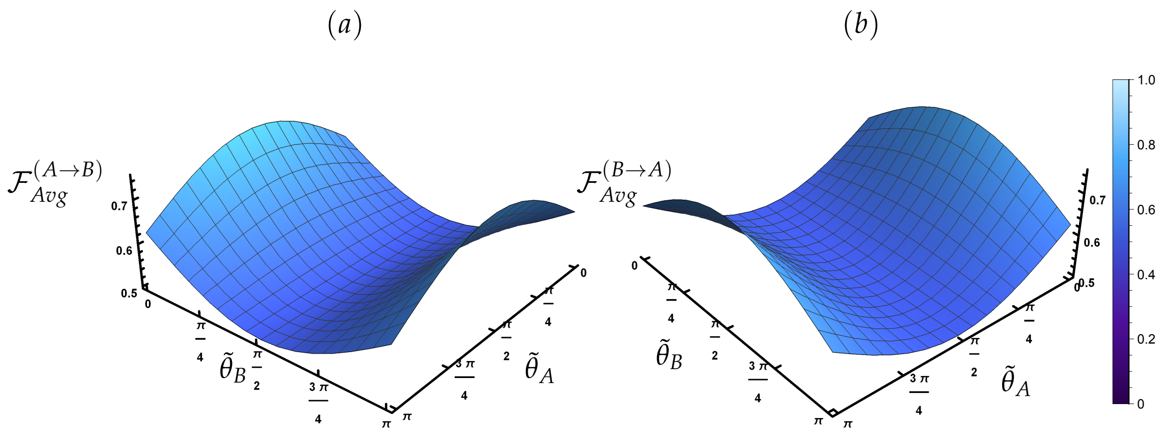

FIGURE II.4: The same as Fig.(2), but the initial teleported state is prepared in the state $|Q_A\rangle = |Q_B\rangle = \frac{1}{\sqrt{2}}(|0\rangle + |1\rangle)$, namely $\theta_A = \theta_B = \frac{\pi}{2}$.

The teleporting of quantum information via the bidirectional protocol is explored in Fig. (II.4), where it is assumed that Alice and Bob prepared their states as $|Q_A\rangle = |Q_B\rangle = \frac{1}{\sqrt{2}}(|0\rangle + |1\rangle)$, namely we set $\theta_A = \theta_B = \frac{\pi}{2}$. It is clear that the maximum values of $\mathcal{F}_{Avg}^{(A\to B)}$ and $\mathcal{F}_{Avg}^{(B\to A)}$ are smaller than those shown in Fig. (II.3). The behavior of both Fidelities is similar, where they decrease gradually as the weight of both triggers increases. The minimum values of $\mathcal{F}_{Avg}^{(A\to B)}$ are observed at $\tilde{\theta}_B = \frac{\pi}{2}$, while it is increased gradually when Bob's trigger angle $\tilde{\theta}_B$ increases. The state of both triggers have the same effect on the behavior of

$\mathcal{F}_{Avg}^{(B\to A)}$.

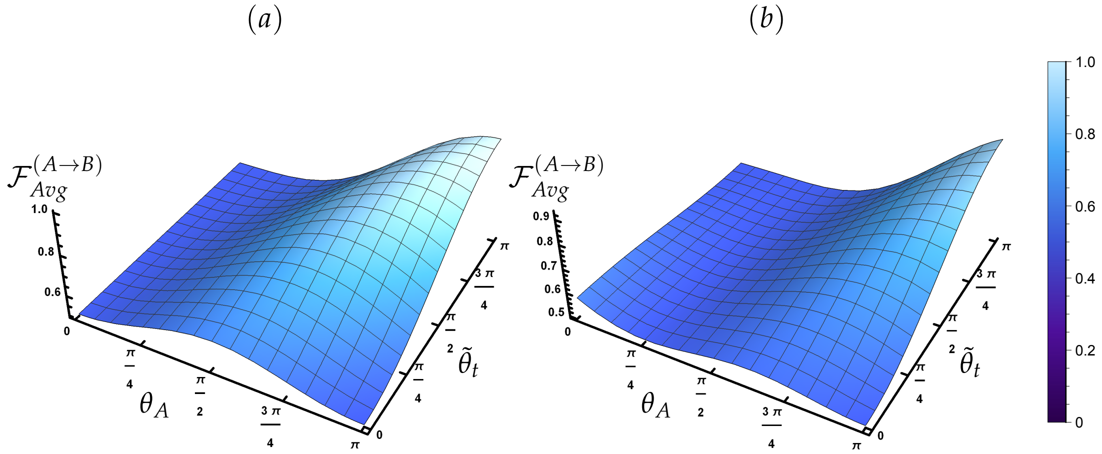

FIGURE II.5: The Fidelity, $\mathcal{F}_{Avg}^{(A\to B)}(\theta_A, \tilde{\theta}_t)$, (a): $\theta_B = 0$ and (b): $\theta_B = \frac{\pi}{4}$.

In the previous investigation, it is assumed that both initial qubits are prepared in the same state. In what follows, we discuss the possibility of bidirectional teleportation, when the partners have different initial states. For this aim, we consider the following figure, where it is assumed that Bob's qubit is initially prepared in the states $\hat{\varrho}_B = |0\rangle\langle 0|$, i.e., $\theta_B = 0$ and $\theta_B = \frac{\pi}{4}$, while Alice's qubit and her triggers are prepared in an arbitrary state with $\phi_A = \phi_B = 0$. Fig. (II.5.a) shows the behavior of the Fidelity $\mathcal{F}_{Avg}^{(A\to B)}(\theta_A, \tilde{\theta}_t)$, where the teleported Bob's qubit is prepared in the state $\hat{\varrho}_q^{(B)} = \frac{1}{2}(\hat{I} + \hat{\tau}_z^{(B)})$, i.e $\theta_B = 0$. Fidelity's behavior shows that $\mathcal{F}_{Avg}^{(A\to B)}$ increases as the weight angles of the teleported state and Alice's trigger increase. Therefore, the maximum Fidelity is predicted at $\theta_A = \tilde{\theta}_t = \pi$, namely $\hat{\varrho}_q^{(A)} = \frac{1}{2}(\hat{I} - \hat{\sigma}_z^{(A)})$. The effect of the initial state of the trigger shows that at any initial state settings of Alice's qubit, the $\mathcal{F}_{Avg}^{(A\to B)}$ increases to reach its maximum bounds. However, at further values of $\tilde{\theta}_t$, the Fidelity decreases gradually, where the minimum values are predicted at $\tilde{\theta}_t = 0$, i.e., the trigger is prepared in the state $\hat{\varrho}_{T_A} = \frac{1}{2}(\hat{I} + \hat{\sigma}_z^{(A)})$. In Fig.(II.5.b) we investigate the effect of a different initial state setting of Bob's state, where it is assumed that $\hat{\varrho}_q^{(B)}$ is prepared at $\theta_B = \frac{\pi}{4}$. The behavior is similar to that predicted in Fig.(II.5.a), but the maximum bounds are smaller than those displayed in Fig.(II.5.a). Moreover, the decay rate is larger compared with that displayed at $\theta_B = 0$. In this context, we would like to mention that, the same behavior is predicted for $\mathcal{F}_{Avg}^{(B\to A)}(\theta_B, \tilde{\theta}_t)$.

From Fig(II.5), one may conclude that the bidirectional Fidelity from Alice to Bob, and vice versa, depends on the initial state settings of all the three qubits. However, the maximum Fidelity is attended when all the qubits are polarized in the same direction. Moreover, the Fidelity of teleporting classical information is much better than teleporting quantum information.

II.2.2 Quantum Fisher information

Many quantum parameters cannot be measured directly, but quantum Fisher information may be used to estimate these parameters. Moreover, in the context of quantum teleportation process, it is shown that by teleporting the relevant parameters encoded in the teleported state, one could measure the credibility of the protocol by measuring QFI [222]. To calculate it, one can use the Bruse distance and the *Uhlmann* fidelity [141] or using the spectral decomposition of the state $\hat{\varrho}$. A simple expression is given in

[220] for any single qubit state $\hat{\varrho} = \frac{1}{2}(1 + \overrightarrow{h}.\hat{\sigma})$. Whereas $\overrightarrow{h} = (h_x, h_y, h_z)$ describes the real Bloch vector and $\hat{\sigma} = (\hat{\sigma}_x, \hat{\sigma}_y, \hat{\sigma}_z)$ denotes the Pauli matrices.

The amount Fisher information $\mathcal{J}_\theta$ with respect to the parameter θ is written as follows:

$$\mathcal{J}_\theta = \begin{cases} |\partial_\theta \overrightarrow{h}|^2 + \frac{(\overrightarrow{h}.\partial_\theta \overrightarrow{h})^2}{1-|\overrightarrow{h}|^2}, & \text{if } |\overrightarrow{h}| < 1 \\ |\partial_\theta \overrightarrow{h}|^2, & \text{if } |\overrightarrow{h}| = 1, \end{cases} \tag{II.21}$$

With $\partial_\theta = \partial/\partial_\theta$. From Eq.(II.21), the quantum Fisher information of a pure state ($|\overrightarrow{h}| = 1$) is given by the expression $|\partial_\theta \overrightarrow{h}|^2$. While for a mixed state ($|\overrightarrow{h}| < 1$), it is presented by the term: $|\partial_\theta \overrightarrow{h}|^2 + \frac{(\overrightarrow{h}.\partial_\theta \overrightarrow{h})^2}{1-|\overrightarrow{h}|^2}$.

According to Ref. [202], the QFI of a single qubit state $|\phi\rangle$ is defined as:

$$\mathcal{J}_\theta = 4(< \partial_\theta \phi | \partial_\theta \phi > - | < \partial_\theta \phi | \phi > |^2), \tag{II.22}$$

the expression of the quantum Fisher information in Eq.(II.22) can be obtained using only the term of the pure state $|\phi\rangle$. The QFI in the two previous equations (II.21) and (II.22) provides the estimation precision limit of only one parameter, through the $Cramer - Rao$ inequality ($Var(\hat{\theta}) \geq \mathcal{J}_{\hat{\theta}}^{-1}$) [122]; with $Var(\hat{\theta})$ is the variance of the parameter and $\mathcal{J}_{\hat{\theta}}$ is the quantum Fisher information; where the larger QFI represents the better estimation precision. However, the inverse of the QFI for one unknown parameter provides the lower error limit of the parameter estimation. Our main goal is to reach the smallest value of the paremeter's variance.

Now, let us assume that Alice and Bob have prepared their qubits in the states Eq. (II.5), while the trigger qubits are defined by Eq. (II.7). The users use the bidirectional protocol as described in (Sec.II.1), where the final teleported states between the two users are given by the states (II.14) and (II.15). In this context, the final teleported states depend on the initial states of all the used qubits. Therefore, our main aim of this section is to investigate the effect of these parameters on the initial weight angle of the teleported state from Alice to Bob or vice versa. However, by using the definition of the quantum Fisher information for a single qubit, Eq. (II.21) and Eq. (II.22), the Fisher information with respect to the weight angle of Alice and Bob qubits are given by $\mathcal{J}_{\theta_k} = 1, k = A(B)$. However, the quantum Fisher information for the phase parameter of both qubits is defined as $\mathcal{J}_{\phi_k} = \sin(\theta_k)^2$, $k = A(B)$. In Bloch representation form, the final state at Alice's and Bob's sides are described by the following Bloch vectors:

$$a_x^{(tel)} = \mathcal{P}_A \bar{\mathcal{P}}_B \cos\phi_A \sin\Big(\theta_A\Big), \quad a_y^{(tel)} = -\mathcal{P}_A \bar{\mathcal{P}}_B \sin\phi_A \sin\Big(\theta_A\Big), \quad a_z^{(tel)} = \mathcal{P}_A \bar{\mathcal{P}}_B \cos(\theta_A), \tag{II.23}$$

Alice received the state $(b_x^{(tel)}, b_y^{(tel)}, b_z^{(tel)})$ by replacing $\mathcal{P}_A \bar{\mathcal{P}}_B \leftrightarrow \mathcal{P}_B \bar{\mathcal{P}}_A$ and $\theta_A \leftrightarrow \theta_B$, $\phi_A \leftrightarrow \phi_B$ in Eq. (II.23):

$$b_x^{(tel)} = \mathcal{P}_B \bar{\mathcal{P}}_A \cos\phi_B \sin\Big(\theta_B\Big), \quad b_y^{(tel)} = -\mathcal{P}_B \bar{\mathcal{P}}_A \sin\phi_B \sin\Big(\theta_B\Big), \quad b_z^{(tel)} = \mathcal{P}_B \bar{\mathcal{P}}_A \cos(\theta_B), \tag{II.24}$$

In Fig. (II.6), we display the behavior of the teleported Fisher information with respect to the weight parameters (θ_A, θ_B), namely $\mathcal{J}_{\theta_A}$, $\mathcal{J}_{\theta_B}$, where we consider that the trigger qubits are polarized either on the state $\hat{\varrho}_T = \frac{1}{2}(\hat{I} + \hat{\sigma}_z)$, or $\hat{\varrho}_T = \frac{1}{2}(\hat{I} - \hat{\sigma}_z)$. This figure illustrates that the maximum bounds of the quantum Fisher information, $\mathcal{J}_{\theta_A}$ are predicted when both qubit and its trigger have the same polarization direction. As it is displayed from Fig. (II.6.a), the maximum values are predicted at $\theta_A = 0$, namely

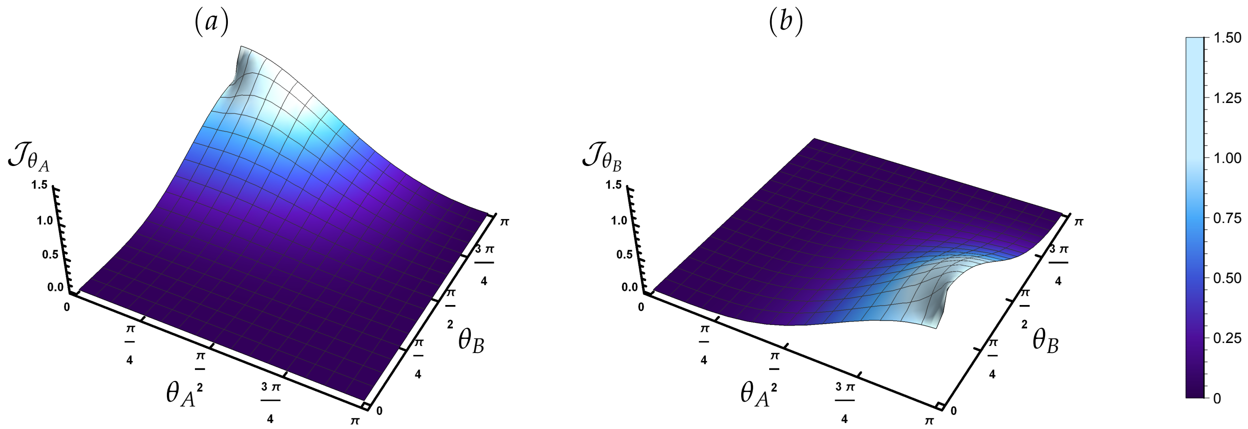

FIGURE II.6: Fisher information of θ_A, with arbitrary phase where (a): at $\tilde{\theta}_A = \tilde{\theta}_B = 0$ and (b): at $\tilde{\theta}_A = \tilde{\theta}_B = \pi$.

$\hat{\varrho}_q^{(A)} = \frac{1}{2}(\hat{I} + \hat{\sigma}_z^{(A)})$ and, $\mathcal{J}_{\theta_A}$ decreases gradually as θ_A increases. On the other hand, the initial state settings of Bob state play an important role in the assessment of maximum values of $\mathcal{J}_{\theta_A}$. However, if Bobs's qubit and Alice's trigger have the same polarization one may estimate the initial weight parameter of θ_A with high efficiency. The same behavior is displayed in Fig. (II.6.b), where it is assumed that Alice's and Bob's triggers are prepared in the state $\hat{\varrho}_T = \frac{1}{2}(\hat{I} - \hat{\tau}_z), T = A, B$. In this case, the $\mathcal{J}_{\theta_B}$ increases as θ_A increases while θ_B decreases, and the maximum bounds are reached if Alice's qubit and its trigger are prepared in the same state.

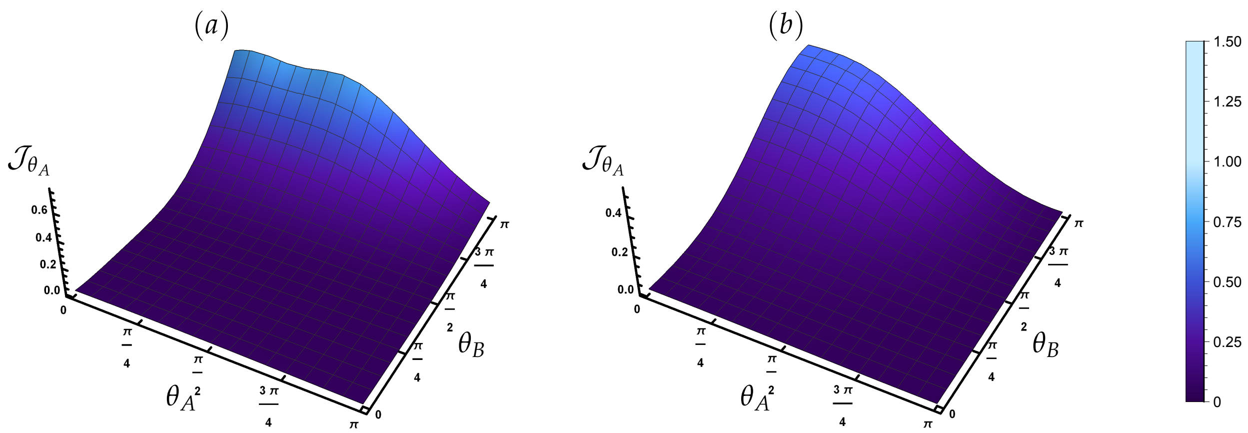

FIGURE II.7: Fisher information $\mathcal{F}_{\theta_A}$, with $\tilde{\theta}_A = \tilde{\theta}_B = \frac{\pi}{4}$ where we set (a): $\phi = 0$. (b): $\phi = \frac{\pi}{2}$

The effect of the phase on the estimation degree of the weight parameter angle θ_A is shown in Fig. (II.7), where two cases are considered of the phase, $\phi = 0, \frac{\pi}{2}$ in Figs.(II.7.a) and in (II.7.b), respectively, and it is assumed that the triggers are prepared at $\tilde{\theta}_A = \tilde{\theta}_B = \frac{\pi}{4}$. In general, the behavior of $\mathcal{J}_{\theta_A}$ is similar to that displayed in Fig. (II.6a). However, the maximum values that are predicted in Fig. (II.7) are much smaller than those displayed in Fig. (II.7.a). Also, from this figure one may explore that when the initial states of the triggers and the qubits are different, the possibility of estimating the weight parameter decreases. On the other hand, as θ_B increases, $\mathcal{J}_\theta$ increases, but the increasing rate is larger than that displayed in Fig. (II.6.a), where $\mathcal{J}_\theta$ increases gradually. Fig. (II.7.a), displays the effect of larger values of the phase, where we set $\phi = \frac{\pi}{2}$. The behavior of the quantum Fisher information is similar to that displayed in Fig. (II.7.a), but the upper bounds are smaller. Moreover, the increasing rate (as θ_B increases) and the decreasing rate as (θ_A increases) are smoothly compared with those shown in Fig. (II.7.a).

From Figs. (II.6) and (II.7), one may conclude that the possibility of maximizing the estimation degree, depends on the initial state of the triggers. The larger bounds are predicted when the qubits and their triggers are polarized in the same direction. The phase parameter plays the control parameter on the whole process, where the maximization of the quantum Fisher information is predicted at $\phi = 0, \pi$ and 2π. Otherwise, it is minimized. The minimum values are affected by the initial state preparation of Alice and Bob.

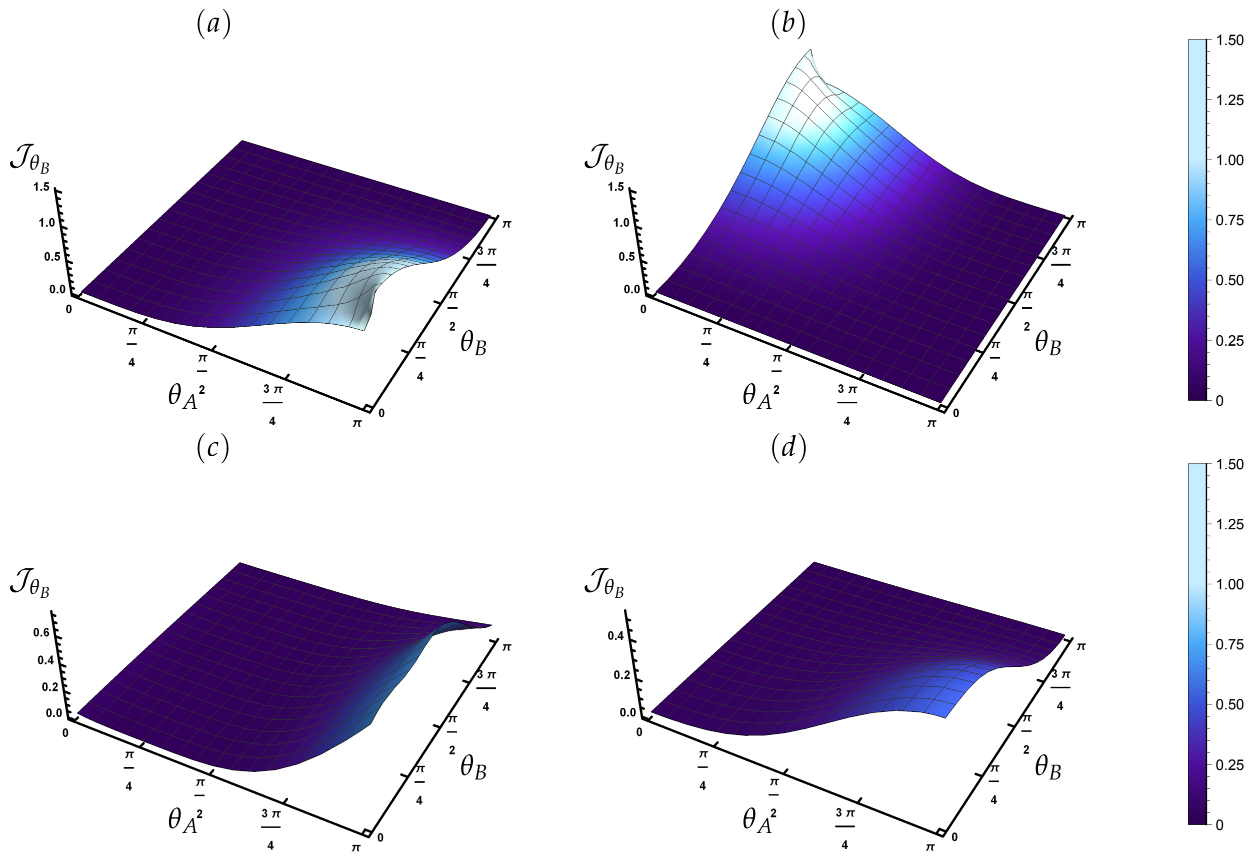

FIGURE II.8: Fisher information $\mathcal{J}_{\theta_B}$, where (a) and (b) are the same as Fig. (II.6), while (c) and (d) are the same as Fig.(II.7).

In Fig. (II.8), we summarize the effect of the initial state settings of Alice and Bob's qubit as well as the state of their triggers on the behavior of $\mathcal{J}_{\theta_B}$. In Fig. (II.8.a), we used to assume that the initial states of the trigger are prepared in the states $\frac{1}{2}(\hat{I} + \hat{\sigma}_z^{(A)})$ for Alice's trigger, while Bob's trigger is prepared in the state $\frac{1}{2}(\hat{I} + \hat{\tau}_z^{(B)})$, where the phase of all the qubits is arbitrary. The behavior is similar to that displayed in Fig. (II.6), but as the $\mathcal{J}_{\theta_A}$ increases, $\mathcal{J}_{\theta_B}$ decreases. This means that, as the information at Alice's hand starts to increases, the information at Bob's hand decreases. Therefore, the maximum bounds are predicted at different initial state settings. However, the states of the triggers play the same role as it is played in Fig. (II.6). As it is shown in Fig. (II.8.b), the maximum bound of $\mathcal{J}_{\theta_B}$ is shown at $\theta_B = \pi$, namely $\hat{\varrho}_q^{(B)} = \frac{1}{2}(\hat{I} - \hat{\tau}_z^{(B)})$. This means that the Bob state is prepared on its trigger's state, where $\hat{\varrho}_T^{(B)} = \frac{1}{2}(\hat{I} - \hat{\tau}_z^{(B)})$. On the other hand, the minimum values of the quantum Fisher information $\mathcal{J}_{\theta_B}$ are predicted at $\theta_B = 0$, namely $\hat{\varrho}_q^{(B)} = \frac{1}{2}(\hat{I} + \tau_z^{(B)})$ and $\hat{\varrho}_q^{(A)} = \frac{1}{2}(\hat{I} - \hat{\sigma}_z^{(B)})$.

Figs. (II.8.c) and (II.8.d) describe the effect of the phase on the estimation degree of $\mathcal{J}_{\theta_B}$, where we assume that the trigger states are prepared with a weight angle $\tilde{\theta}_A = \tilde{\theta}_B = \frac{\pi}{4}$. It is clear that the behavior of the quantum Fisher information is similar to that shown of $\mathcal{J}_{\theta_A}$ as displayed in Fig. (II.7). However, the maximum bound of $\mathcal{J}_{\theta_B}$ is displayed at $\theta_B = \frac{\pi}{4}$, namely when the weight angle $\theta_B = \tilde{\theta}_B = \frac{\pi}{4}$. Moreover, at $\phi_A = \phi_B = \phi = 0$, the losses in Fisher information are due to the difference between the initial state preparation of both qubits. In fact, an additional loss of the quantum Fisher information is due to the no null phase, where at $\phi = \frac{\pi}{2}$, the maximum bounds of $\mathcal{J}_{\theta_B}$ are smaller than those shown at $\phi = 0$.

II.2.3 Relation between fidelities and QFI

To show the link between the fidelities of teleportation and the quantum Fisher information with respect to θ_A and θ_B in this system, we use the expression of the fidelities of teleportation Eq. (II.19):

$$f^{(A\to B)} = \frac{1}{2}(1+\mathcal{P}_A\bar{\mathcal{P}}_B) \quad f^{(B\to A)} = \frac{1}{2}(1+\mathcal{P}_B\bar{\mathcal{P}}_A), \tag{II.25}$$

The quantum Fisher information with respect to the weights parameters θ_i, for $i = A, B$:

$$\begin{aligned} \mathcal{J}_{\theta_B} &= \frac{(\mathcal{P}_B\bar{\mathcal{P}}_A)^2(1-(\mathcal{P}_B\bar{\mathcal{P}}_A)^2)+(\bar{\mathcal{P}}_A\partial_{\theta_B}\mathcal{P}_B)^2}{1-(\mathcal{P}_B\bar{\mathcal{P}}_A)^2}, \\ \mathcal{J}_{\theta_A} &= \frac{(\mathcal{P}_A\bar{\mathcal{P}}_B)^2(1-(\mathcal{P}_A\bar{\mathcal{P}}_B)^2)+(\bar{\mathcal{P}}_B\partial_{\theta_A}\mathcal{P}_A)^2}{1-(\mathcal{P}_A\bar{\mathcal{P}}_B)^2}. \end{aligned} \tag{II.26}$$

We can write at Bob's side:

$$f^{(A\to B)} = \frac{1}{2}\Big(1+(\mathcal{J}_{\theta_A}-\frac{(\bar{\mathcal{P}}_B\partial_{\theta_A}\mathcal{P}_A)^2}{1-(\mathcal{P}_A\bar{\mathcal{P}}_B)^2})^{\frac{1}{2}}\Big) \tag{II.27}$$

Where at Alice's side:

$$f^{(B\to A)} = \frac{1}{2}\Big(1+(\mathcal{J}_{\theta_B}-\frac{(\bar{\mathcal{P}}_A\partial_{\theta_B}\mathcal{P}_B)^2}{1-(\mathcal{P}_B\bar{\mathcal{P}}_A)^2})^{\frac{1}{2}}\Big) \tag{II.28}$$

The maximum fidelity is corresponding to QFI

$$\mathcal{J}_{\theta_B} = 1+\frac{(\bar{\mathcal{P}}_A\partial_{\theta_B}\mathcal{P}_B)^2}{1-(\mathcal{P}_B\bar{\mathcal{P}}_A)^2}; \qquad \mathcal{J}_{\theta_A} = 1+\frac{(\bar{\mathcal{P}}_B\partial_{\theta_A}\mathcal{P}_A)^2}{1-(\mathcal{P}_A\bar{\mathcal{P}}_B)^2} \tag{II.29}$$

The minimum fidelity is corresponding to QFI

$$\mathcal{J}_{\theta_B} = \frac{(\bar{\mathcal{P}}_A\partial_{\theta_B}\mathcal{P}_B)^2}{1-(\mathcal{P}_B\bar{\mathcal{P}}_A)^2}; \qquad \mathcal{J}_{\theta_A} = \frac{(\bar{\mathcal{P}}_B\partial_{\theta_A}\mathcal{P}_A)^2}{1-(\mathcal{P}_A\bar{\mathcal{P}}_B)^2} \tag{II.30}$$

From the above equations, one can conclude that for a maximum fidelity of teleportation, we can teleport fisher information with a high accuracy, where the QFI can be bounded by the values 1 to 1.5.
However, if the fidelity is minimum, the quantum Fisher information cannot reach high values, namely, it is limited in the interval 0 to 0.5.

II.3 Efficiency of bidirectional quantum teleportation

The efficiency $\mathcal{E}$ [223] is a useful tool to judge the feasibility of bidirectional quantum teleportation (BQT) and to compare it with other BQT protocols, the expression of $\mathcal{E}$ is described as:

$$\mathcal{E} = \frac{N_t}{N_q + N_c + N_{Ax}} \tag{II.31}$$

where N_t indicates the number of qubits to be teleported, N_q is the number of the qubits used as the quantum channel, N_c represents the number of qubits used as the classical channel and N_{Ax} is the number of the auxiliary qubits used in the protocol. Indeed, the classical communication which links Alice and Bob in quantum teleportation is an obvious requirement to avoid the faster-than-light (FTL) signaling.

The effective efficiency can be written as:

$$\mathcal{E} = \frac{N_t}{N_q + N_{Ax}} \tag{II.32}$$

In what follows, we compare different bidirectional quantum teleportation protocols and bidirectional controlled quantum teleportation $(BCQT)$ protocols. In BCQT, an intervention from a third party is necessary to accomplish the task. However, in BQT, Alice and Bob could exchange their quantum states without any intervention from a supervisor.

This protocol is based on $CNOT$, $Toffoli$, $Hadamard$ operations, and a single qubit measurement. In Refs [215, 216, 217, 218, 219], the process of the teleportation needs at least five entangled qubits to teleport one single qubit, and at least six entangled qubits to teleport two qubits. Nevertheless, this protocol [193] needs a single Bell state to teleport a single qubit state. So, the proposed protocol requires less quantum cost. Additionally, In Ref [215, 216, 217, 218, 219], the partners apply two-qubit measurements which is less efficient than single-qubit measurement [218]. In Table(1), we introduce details of comparison between BQT and BCQT protocols.

Reference	Efficiency%	Teleported qubits	Quantum channel	Auxiliary qubits
Li et al. [215]	40	1	5-qubit	0
Li et al. [216]	44	2	9-qubits	0
Sun et al. [217]	33	1	6-qubits	0
$Hassanpour$ et al.[218]	66	$(2)EPR$	$(6qubits)GHZ_6$	0
$Yang$ et al.[219]	75	$(3)GHZ$	$(8qubits)GHZ_8$	0
$Kiktenko$ et al.[193]	50	1	Bell state	2

TABLE II.1: Comparison between different BQT protocols.

II.4 Simultaneous and individual estimation form

The quantum Fisher information matrix (QFIM) provides a tool to determine the precision in the multiparameter estimation. Where the lower bound of the estimation is given by the Cramer Rao inequality [122] as:

$$Cov(\hat{\theta}) \geq \mathcal{J}_{\hat{\theta}}^{-1}, \tag{II.33}$$

With $\hat{\theta} = \theta_1, \theta_2...$ is a set of parameters can be encoded in the density matrix $\varrho = \varrho(\hat{\theta})$ and $Cov(\hat{\theta})$ is the covariance of the parameters $\hat{\theta}$. $\mathcal{J}_{\hat{\theta}}^{-1}$ is the quantum Fisher information matrix. The inverse of the QFIM gives the lower error limit of the estimation. The matrix representation of the quantum Fisher information matrix with respect to the two parameters θ_A and θ_B as:

$$\mathcal{J}_{\theta_A,\theta_B} = \begin{pmatrix} \mathcal{J}_{\theta_A,\theta_A} & \mathcal{J}_{\theta_B,\theta_A} \\ \mathcal{J}_{\theta_A,\theta_B} & \mathcal{J}_{\theta_B,\theta_B} \end{pmatrix}, \tag{II.34}$$

Where,

$$\mathcal{J}_{\theta_i,\theta_j} = \begin{cases} (\partial_{\theta_i}\overrightarrow{h})(\partial_{\theta_j}\overrightarrow{h}) + \frac{(\overrightarrow{h}.\partial_{\theta_i}\overrightarrow{h})(\overrightarrow{h}.\partial_{\theta_j}\overrightarrow{h})}{1-|\overrightarrow{h}|^2}, & \text{if } |\overrightarrow{h}| < 1 \\ (\partial_{\theta_i}\overrightarrow{h})(\partial_{\theta_j}\overrightarrow{h}), & \text{if } |\overrightarrow{h}| = 1. \end{cases} \tag{II.35}$$

Explicitly on Alice's side, the QFIM is given by:

$$\mathcal{J}_{\theta_A,\theta_B}^{Alice} = \frac{1}{1-(\mathcal{P}_B\bar{\mathcal{P}}_A)^2} \begin{pmatrix} (\mathcal{P}_B\partial_{\theta_A}\bar{\mathcal{P}}_A)^2 & \mathcal{P}_B\bar{\mathcal{P}}_A\partial_{\theta_B}\mathcal{P}_B\partial_{\theta_A}\bar{\mathcal{P}}_A \\ \mathcal{P}_B\bar{\mathcal{P}}_A\partial_{\theta_B}\mathcal{P}_B\partial_{\theta_A}\bar{\mathcal{P}}_A & (\mathcal{P}_B\bar{\mathcal{P}}_A)^2(1-(\mathcal{P}_B\bar{\mathcal{P}}_A)^2) + (\bar{\mathcal{P}}_A\partial_{\theta_B}\mathcal{P}_B)^2 \end{pmatrix}. \tag{II.36}$$

A similar expression is obtained for QFIM at Bob's side, we just switched between the suffix A and B. However, the amount of Fisher information at the users Alice (Bob) that injected on the parameters $\theta_B(\theta_A)$ respectively is given by,

$$\begin{aligned} \mathcal{J}_{\theta_B} &= \frac{(\mathcal{P}_B\bar{\mathcal{P}}_A)^2(1-(\mathcal{P}_B\bar{\mathcal{P}}_A)^2) + (\bar{\mathcal{P}}_A\partial_{\theta_B}\mathcal{P}_B)^2}{1-(\mathcal{P}_B\bar{\mathcal{P}}_A)^2}, \\ \mathcal{J}_{\theta_A} &= \frac{(\mathcal{P}_A\bar{\mathcal{P}}_B)^2(1-(\mathcal{P}_A\bar{\mathcal{P}}_B)^2) + (\bar{\mathcal{P}}_B\partial_{\theta_A}\mathcal{P}_A)^2}{1-(\mathcal{P}_A\bar{\mathcal{P}}_B)^2}. \end{aligned} \tag{II.37}$$

By using the Cramer-Rao bound for one parameter estimation, one can estimate the single parameter by means of the variance as,

$$\begin{aligned} Var(\theta_A)^{Ind} &\geq \frac{1-(\mathcal{P}_A\bar{\mathcal{P}}_B)^2}{(\mathcal{P}_A\bar{\mathcal{P}}_B)^2(1-(\mathcal{P}_A\bar{\mathcal{P}}_B)^2) + (\bar{\mathcal{P}}_A\partial_{\theta_A}\mathcal{P}_A)^2} \\ Var(\theta_B)^{Ind} &\geq \frac{1-(\mathcal{P}_B\bar{\mathcal{P}}_A)^2}{(\mathcal{P}_B\bar{\mathcal{P}}_A)^2(1-(\mathcal{P}_B\bar{\mathcal{P}}_A)^2) + (\bar{\mathcal{P}}_A\partial_{\theta_B}\mathcal{P}_B)^2}, \end{aligned} \tag{II.38}$$

Where it is assumed that the estimation process of each parameter is independent. However, the variance estimation of the two parameters θ_A and θ_B is given simultaneously as [122],

$$Var(\theta_B)^{Sim} \geq \frac{(\mathcal{P}_B \partial_{\theta_B} \bar{\mathcal{P}}_A)^2}{\bar{\mathcal{P}}_A^2 \mathcal{P}_B^4 (\partial_{\theta_A} \bar{\mathcal{P}}_A)^2} \qquad ; Var(\theta_A)^{Sim} \geq \frac{(\mathcal{P}_A \partial_{\theta_B} \bar{\mathcal{P}}_B)^2}{\bar{\mathcal{P}}_B^2 \mathcal{P}_A^4 (\partial_{\theta_B} \bar{\mathcal{P}}_B)^2}. \tag{II.39}$$

The ratios of the minimum variances of the two parameters may be described by,

$$\Delta = \frac{Var^{Sim}(\theta_A)}{V^{Ind}(\theta_A)}, \qquad \delta = \frac{V^{Sim}(\theta_B)}{V^{Ind}(\theta_B)}. \tag{II.40}$$

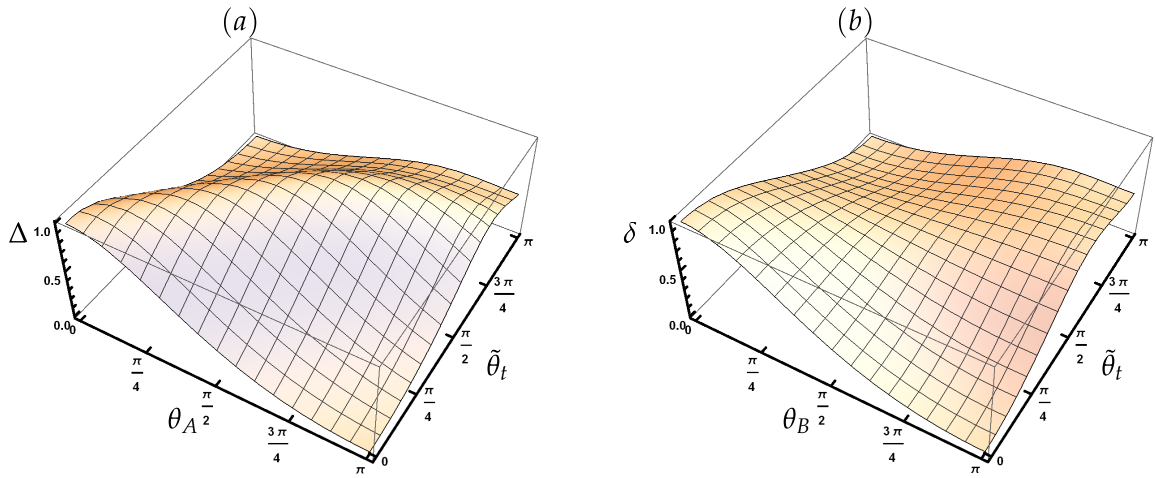

FIGURE II.9: Ratios of estimations Δ (for Alice) and δ (for Bob), with $\theta_A = \theta_B = \frac{\pi}{4}$. We set $\phi = 0$ for (a) and $\phi = \frac{\pi}{2}$ for (b).

In Fig.(II.9), we investigate the behavior of the ratio variances Δ and δ for different initial state settings. It is clear that the ratios $\Delta < 1$, and $\delta < 1$. Therefore, $V_S(\theta_i) < V_I(\theta_i)$ $i = A, B$. Consequently, those ratios satisfy the maximum/minimum probability of the quantum mechanics, where Δ and $\delta \in [0,\ 1]$. So, these ratios demonstrate the full classical/quantum systems at 0 and 1, respectively. Moreover, these ratios obey the uncertainty principle for $0 \leq \Delta(\delta) \leq 1$. On the other hand, for individual estimation, we can see that the quantum Fisher information $(\mathcal{J}_{\theta_A})(\mathcal{J}_{\theta_B}) > 1$, which is outside of the entangled systems range. Therefore, using the multi-parameter form is much better than the single parameter form. Fig.(II.9.a) describes the behavior of $\Delta(\theta_A, \tilde{\theta}_t)$ at a particular initial state of Bob's qubit, where we set $\theta_B = \frac{\pi}{4}$, with zero-phase for all the qubits. Also, the maximum/minimum bounds are depicted when the qubits and their triggers have the same polarization. As an example, the maximization is predicted at $\theta_A = \tilde{\theta}_t = 0$ or π, while the minimum values are predicted when θ_A and $\tilde{\theta}_t$ are different. The same behavior is predicted for the ratio δ, but the maximum and minimum are displayed at different angles.

II.5 Conclusion

In this chapter, we are interested in the bidirectional quantum teleportation between two users, Alice and Bob where the users' qubits and their trigger qubits are described by using the Bloch vectors. Moreover, the local operations of $CNOT$ and $CCNOT$ gates are represented by Pauli operators and the circuit which describes this protocol is introduced clearly. We have discussed the fidelities average of the bidirectional teleported states between the two users, where analytical forms of the fidelities are obtained. These fidelities depend on the initial states of the teleported qubit as well as on the states of the triggers.

The fidelity of the teleported state is maximized when the teleported qubit and its trigger are polarized in the same direction. However, the initial state settings of the qubits play an important role in maximizing/minimizing the fidelity of the teleported state, where the maximization is achieved if both qubits are initially prepared in the same direction. The minimization takes place at the non-zero phase angle or at different initial state settings. The fidelity of the classical information which is bidirectionally teleported via the quantum channel is much better than teleporting quantum information.

We have also investigated the possibility of estimating the weight parameters of the bidirectionally teleported states. This has been quantified by using quantum Fisher information. An analytical form based on the Bloch vectors is introduced. Similarly, the quantum Fisher information depends on the initial states of all the qubits. It is shown that the possibility of maximizing the estimation degree depends on the initial state of the triggers. The larger bounds are predicted when the qubits and their triggers are polarized in the same direction. The phase parameter plays the control parameter on the whole process, where the maximization of the quantum Fisher information is predicted at $\phi = 0, \pi, 2\pi$. Otherwise, it is minimum. The minimum values are affected by the initial state settings of Alice and Bob. In addition to estimating a single parameter, we quantify the weight parameters of the bidirectionally teleported states by means of the variances' ratios. It is shown that the multi-parameter estimation form is much better than the single parameter estimation, where the ratios running between "0" for fully classical systems and "1" for completely entangled system. Additionally, the uncertainty principle in this case is obeyed. Indeed, the maximum/minimum estimation of these parameters depends on the initial states of the triggers. Also, as the maximum estimation is predicted at Alice 's side and the minimum estimation is displayed at Bob's side since the initial states of Alice and Bob as well as the states of their trigger are similar. Therefore, the maximum/minimum values of the fidelity of the teleported states and the quantum Fisher information are the same for both directions. However, as soon as Alice gets the maximum information, Bob loses all the information and vice versa. Therefore, the maximum bounds of the fidelity and the quantum Fisher information are obtained at different weight angles.

By comparing this protocol to other ones, we notice that its efficiency is greater than other ones, where it uses the minimum quantum cost which is a single Bell state to teleport single qubit states bidirectionally. Indeed, since this protocol is in a noiseless channel, we will consider how to achieve our schemes in noisy channels in the next chapter.

Chapter III

Bidirectional Teleportation through Noisy Channels

Actually, real quantum systems can never be perfectly isolated from their surrounding environment [1]. Hence, the real implementation of the bidirectional quantum teleportation protocol makes us face the problem of the unavoidable coupling of the qubits with their environment. It is, therefore, important to understand the impact of the coupling in a noisy environment has on the performance of the BQT protocol. In particular, the investigation of this BQT protocol, through typical noise models, promises to give useful insights for the future design and improvement of bidirectional quantum teleportation protocols.

The share of a noiseless maximally entangled quantum channel between Alice and Bob is required to accomplish the teleportation process perfectly, i,e. with a fidelity equal to unity [34]. However, during the distribution of the qubits between Alice and Bob, we must take into account the interactions of the qubits with the external environment. Recently, there has been much interest in the study of the unidirectional teleportation fidelity via noisy channels [143, 224]. It is well known that noise is detrimental to the fidelity of teleportation. As a consequence of the unavoidable environmental coupling, the quantum system of interest becomes entangled with its environment. Therefore, its state is described by a density matrix, whose evolution is given in the Kraus representation [225]; which encodes the effect of the environment on the system of interest. Generally, a quantum operation that can be represented in the Kraus representation is guaranteed to be completely positive (CP) [226]. On the other hand, we can model the effect of the environment through well defined noise channels, such as the dephasing and amplitude damping channels [77]. However, many techniques are discussed in the literature to overcome the effect of noise on entanglement and teleportation [226]. For instance, the weak and reversed measurements (WRM), which is a technique used to extract as much information as possible without totally collapsing the system state [160]. Nevertheless, exploiting the memory effects could mitigate the effect of noise on different quantum features [227]. Generally, there are two types of memory effects, the first one is the non-Markovianity memory effects due to the temporal correlations arising is the noisy quantum channel, and the second one is due to the classical correlations [228]. In general, memory or memoryless channels refer to the situation in which multiple actions of the channel are correlated or independent from each other. To distinguish between these two different notions of memory, we shall use the term "correlated channels" to describe the classical correlations of the quantum channels with memory. On the other hand, the type of memory occurring due to the temporal correlations in the dynamics will be said to be non-Markovian memory effects.

The chapter is organized as follows: we first investigate the impact of applying the weak and reversed measurements on the bidirectional teleportation process in (Sec.III.1). In addition, we focus on how the weak and reversed measurements could improve the entanglement of the BQT quantum channel, which is distributed by different typical noise channels such as the bit-flip, phase-flip, bit-phase flip, depolarizing and amplitude damping noise channels. We consider the negativity of the partial transpose as an entanglement quantifier in order to quantify the amount of entanglement remaining in the quantum channel. However, we evaluate the teleportation fidelities average and the quantum Fisher information (QFI) to quantify the accuracy of BQT aided with the weak and reversed measurements. In Sec(III.4), we discuss the effect of the memory effects on the entanglement and the bidirectional teleportation. in Sec (III.5), we answer the following question: how could the combined effect of the correlated channel and the non-Markovianity memory effects be on the entanglement ond on the BQT?

III.1 Weak and reversed measurements effect on Entanglement

The weak and reversed measurements are reversible quantum measurements [158], which allow the extraction of information without totally projecting the system. The reversibility of weak quantum measurement was originally discussed in the context of quantum error correction [229] and was demonstrated for a single superconducting qubit and a single photonic qubit [158, 230]. Moreover, the decoherence phenomenon is caused by the unavoidable interaction of qubits with their surrounding environment, which leads to the loss of quantum coherence [231], and the degradation of entanglement. In certain cases, it leads to the phenomenon of entanglement sudden death (ESD) [232]. It is well known that entanglement is a vital resource for many quantum information applications including bidirectional quantum teleportation. Here, we investigate a scheme to protect the entanglement from decoherence and, consequently, enhance the bidirectional quantum teleportation of information. Generally, the unavoidable interaction between the qubits and their environment could be modeled by well known quantum noise channels, such as the bit-flip, phase-flip, bit-phase flip, depolarizing and amplitude damping channels. In the following, we investigate the effect of the weak and reversed measurements on the amount of entanglement in the quantum channel of BQT protocol.

Dephazing channel:

The dephazing channel is also known as the phase-flip channel. It is used to characterize the loss of quantum information that occurs without the loss of energy [79]. In other words, the relative phase between the energy eigenstates of the system is lost, which leads to the decay of the off-diagonal elements of the density matrix of the system.

We consider that the state (Eq. II.3) is prepared in the laboratory and distributed to Alice and Bob as displayed in the scheme (Fig. III.1). Before passing through the dephazing channel, it is assumed that we perform weak measurements on the qubits $''A''$ and $''B''$ with a strength of p_{w1}, p_{w2}, respectively. The weak measurements partially collapse the qubits towards their ground state $|00\rangle_{AB}$.

The Kraus operators representing the weak measurements are:

$$\hat{\mathcal{M}}_{w1} = \begin{pmatrix} 1 & 0 \\ 0 & \sqrt{1-p_{w1}} \end{pmatrix} \quad ; \quad \hat{\mathcal{M}}_{w2} = \begin{pmatrix} 1 & 0 \\ 0 & \sqrt{1-p_{w2}} \end{pmatrix}. \tag{III.1}$$

The output state after applying the weak measurements is given as:

$$\hat{\varrho}^{W}_{AB} = (\hat{\mathcal{M}}_{w1} \otimes \hat{\mathcal{M}}_{w2})\hat{\varrho}_{AB}(\hat{\mathcal{M}}_{w1} \otimes \hat{\mathcal{M}}_{w2})^{\dagger} \tag{III.2}$$

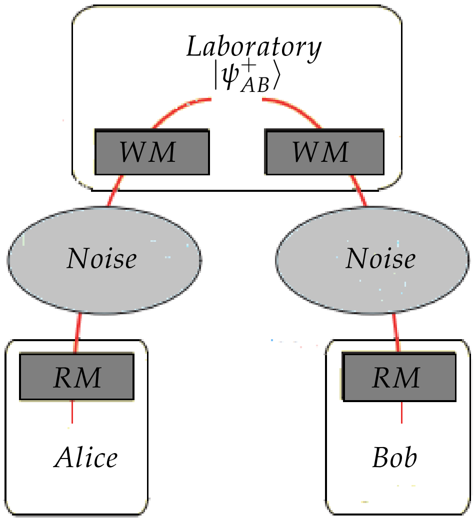

FIGURE III.1: Scheme for protecting entanglement of the quantum channel using weak and reversed measurements. We first perform a weak measurement (WM) on $|\psi^+_{AB}\rangle$ before distribution through noise. The reversed measurement (RM) is carried out by Alice and Bob.

with: $\hat{\varrho}_{AB} = |\psi^+_{AB}\rangle\langle\psi^+_{AB}|$. Now, if it is assumed that both qubits ("A" and "B") are forced to pass through the dephasing channel, where the Kraus operators describing the dephasing noise are:

$$\mathcal{K}_0 = \sqrt{1-\mathbf{p}}\begin{pmatrix} 1 & 0 \\ 0 & 1 \end{pmatrix} \quad ; \quad \mathcal{K}_1 = \sqrt{\mathbf{p}}\begin{pmatrix} 1 & 0 \\ 0 & -1 \end{pmatrix} \tag{III.3}$$

which satisfy the completeness relation,

$$\sum_{\nu=0}^{1} \mathcal{K}_\nu \mathcal{K}_\nu^\dagger = \hat{I}_{2\times 2}. \tag{III.4}$$

The dephasing channel acts on the state $\hat{\rho}_{AB}$ with probability $\mathbf{p}$ and it preserves the density operator with probability $1-\mathbf{p}$. The output state is given as:

$$\begin{aligned}\hat{\varrho}_{AB}^{W-DP} = {} & (\mathcal{K}_0\otimes\mathcal{K}_0)\hat{\varrho}_{AB}^{W}(\mathcal{K}_0\otimes\mathcal{K}_0)^\dagger + (\mathcal{K}_1\otimes\mathcal{K}_1)\hat{\varrho}_{AB}^{W}(\mathcal{K}_1\otimes\mathcal{K}_1)^\dagger + \\ & (\mathcal{K}_0\otimes\mathcal{K}_1)\hat{\varrho}_{AB}^{W}(\mathcal{K}_0\otimes\mathcal{K}_1)^\dagger + (\mathcal{K}_1\otimes\mathcal{K}_0)\hat{\varrho}_{AB}^{W}(\mathcal{K}_1\otimes\mathcal{K}_0)^\dagger.\end{aligned} \tag{III.5}$$

Later on, Alice and Bob perform the reversed measurements, by strength p_{r1} and p_{r2}, respectively, on their qubits. The reversed measurement operators are as follows:

$$\hat{\mathcal{R}}_{r1} = \begin{pmatrix} \sqrt{1-p_{r1}} & 0 \\ 0 & 1 \end{pmatrix} \quad ; \quad \hat{\mathcal{R}}_{r2} = \begin{pmatrix} \sqrt{1-p_{r2}} & 0 \\ 0 & 1 \end{pmatrix}. \tag{III.6}$$

The final state shared between Alice and Bob becomes :

$$\hat{\varrho}_{AB}^{W-DP-R} = (\hat{\mathcal{R}}_{r1} \otimes \hat{\mathcal{R}}_{r2})\hat{\varrho}_{AB}^{W-DP}(\hat{\mathcal{R}_{r1}} \otimes \hat{\mathcal{R}}_{r2})^{\dagger}. \tag{III.7}$$

For the sake of simplicity, we assume that the weak and reversed measurements are performed by Alice and Bob with equal strengths, namely $p_{w1} = p_{w2} = p_w$ and $p_{r1} = p_{r2} = p_r$. We present the state (Eq.III.7) in the computational basis $\{|00\rangle, |01\rangle, |10\rangle, |11\rangle\}$:

$$\hat{\varrho}_{AB}^{W-DP-R} = \frac{1}{2}\begin{pmatrix} 1 & 0 & 0 & \alpha\beta(1-4(\mathbf{p}+\mathbf{p}^2)) \\ 0 & 0 & 0 & 0 \\ 0 & 0 & 0 & 0 \\ \alpha\beta(1-4(\mathbf{p}+\mathbf{p}^2)) & 0 & 0 & 1 \end{pmatrix}, \tag{III.8}$$

where: $\alpha = 1 - p_w$ and $\beta = 1 - p_r$. A straightforward calculation gives the negativity of the partial transpose for the state (III.8):

$$\mathcal{N}_{Dph}^{PT} = \alpha\beta(1-4(\mathbf{p}+\mathbf{p}^2)). \tag{III.9}$$

When the quantum channel is distributed by the bit flip or bit-phase flip channel, the final state can be obtained in the same way. A further calculation reveals that the expressions for the negativity of the partial transpose for the bit-flip and bit-phase flip, $\mathcal{N}_{Dph}^{PT}$, are the same as those for the dephasing channel, so we do not list the corresponding expressions of $\hat{\varrho}_{AB}^{W-Bf-R}$ $\hat{\varrho}_{AB}^{W-BFf-R}$ here.Furthermore, when the quantum channel is distributed through a depolarizing channel, the expression of $\mathcal{N}_{Dpl}^{PT}$ is as follows:

$$\mathcal{N}_{Dpl}^{PT} = \alpha\beta^2(1 - \frac{8}{9}(3\mathbf{p} - 2\mathbf{p}^2)) - \frac{4\beta}{9}(1+\alpha^2)(3\mathbf{p} - 2\mathbf{p}^2)) \tag{III.10}$$

Fig. (III.2) shows the behavior of the negativity $\mathcal{N}^{(PT)}$ of the quantum channel for bidirectional telepor-

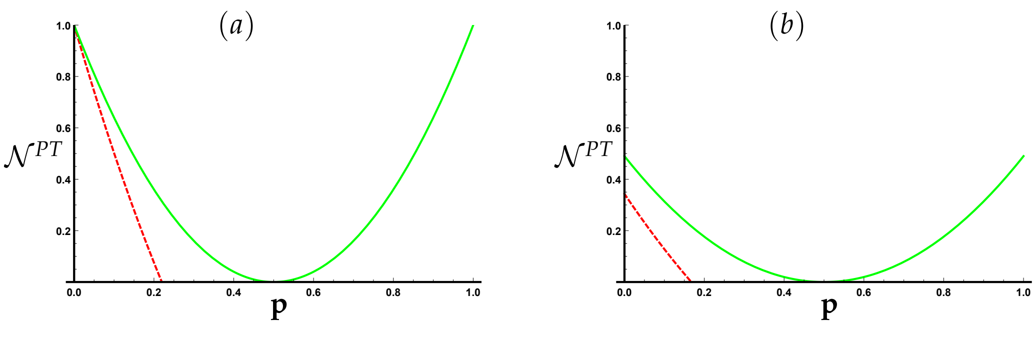

FIGURE III.2: $\mathcal{N}^{PT}$ vs **p** the noise strength, depolarizing channel (Red dashed). The dephasing, bit-flip and the bit-flip channels (Green solid), at (a) $p_w = 0$ and $p_r = 0$. (b) $p_w = 0,3$ and $p_r = 0,7$.

tation in the presence of four typical noise channels, which are the bit flip, phase flip, bit-phase flip and the depolarizing channels. The negativity of the partial transpose under the dephasing, the bit flip and the bit-phase flip channels have the same expression. So, the green-solid curve describes the behavior of $\mathcal{N}^{(PT)}$ under these three noise channels. While the red-dotted curve describes the negativity of the partial transpose under a depolarizing channel. The entanglement is greatest at $\mathbf{p} = 0$, as shown in Fig. (III.2a). However, due to the decoherence caused by noisy channels, the quantum channel of the bidirectional quantum teleportation loses its entanglement, where the negativity $\mathcal{N}^{(PT)}$ decreases as the channels' noise strengths increase. The decreasing rate depends on the type of the noisy channel, where the entanglement sudden death of entanglement is predicted for the depolarizing channel at $\mathbf{p} = 0.22$. Furthermore, the minimum value of the entanglement ($\mathcal{N}^{(PT)} = 0$) is depicted at $\mathbf{p} = 0.5$ for the dephasing, bit-flip, and bit-phase flip channels. As one increases the channel strength, the entanglement increases gradually to reach its maximum value at $\mathbf{p} = 1$. In this context, it is worth mentioning that the vanishing entanglement is displayed at different strengths of the used channel, where the dephasing, bit-flip and bit-phase flip channels are more robust than the depolarizing channel.

The effect of the weak and the reversed measurements on the noisy channel is described in Fig. (III.2b), where we set a non-zero value for the weak and the reversed measurements at $p_w = 0.3$ and $p_r = 0.7$. The amount of the entanglement is smaller at $\mathbf{p} = 0$, where $\mathcal{N}^{(PT)}$ decreases as the weak and the reversed measurements strengths increase. Moreover, the phenomenon of the entanglement sudden death appears at a small value of the depolarizing noise, namely at $\mathbf{p} = 0.19$. This result, shows that the weak and reversed measurements decrease the entanglement of the quantum channel of the BQT, where the maximum values of the negativity are always less than those shown in Fig. (III.2a).

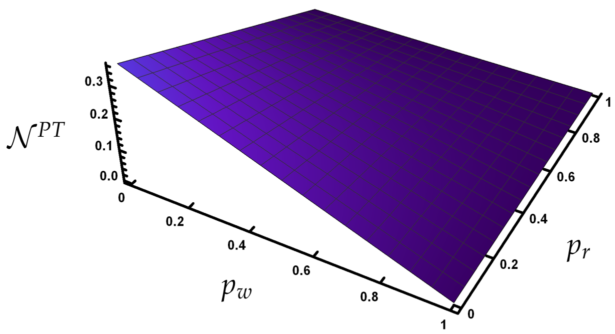

FIGURE III.3: $\mathcal{N}^{PT}$ vs (p_w, p_r) the weak-reversed measurements strengths.

The Fig. (III.3) shows that the weak and the reversal measurements cannot improve the Negativity of the partial transpose. On the contrary, by increasing the weak and the reversed strengths, $\mathcal{N}^{PT}$ decreases whatever the values of the strengths p_w and p_r are.

Amplitude damping channel:

The amplitude damping channel (ADC) is a schematic model that describes the dissipative interaction between a two level quantum system S and the environment E [162], which is represented as follows:

$$U_{AD} = \begin{cases} |0\rangle_S|0\rangle_E \longrightarrow |0\rangle_S|0\rangle_E \\ |1\rangle_S|0\rangle_E \longrightarrow \sqrt{1-\mathbf{p}}|1\rangle_S|0\rangle_E + \sqrt{\mathbf{p}}|0\rangle_S|1\rangle_E, \quad \text{with: } 1-\mathbf{p} = e^{-\gamma t/2}. \end{cases} \tag{III.11}$$

Where $|0\rangle_S$ and $|1\rangle_S$ represent the ground and excited states of the system S, respectively. $|0\rangle_E$ and $|1\rangle_E$ denote the vacuum state and one excitation of the environment.The amplitude damping channel's strength $\mathbf{p} \in [0, 1]$, i.e. the probability of decay from the excited level to the ground level with damping rate γ.The

Eq. (III.11) clearly shows that the qubit loses one excitation to the environment with a probability of $\mathbf{p}$.

In this case, we assume that during the distribution process from the laboratory to the users (as displayed in Fig. III.1), Alice's and Bob's qubits are forced to pass through the amplitude damping channel. Due to this process, the shared state between Alice and Bob becomes:

$$\begin{aligned}\tilde{\varrho}_{AB}^{W-AD} &= (\mathcal{K}_0\otimes\mathcal{K}_0)\hat{\varrho}_{AB}^{W}(\mathcal{K}_0\otimes\mathcal{K}_0)^{\dagger} + (\mathcal{K}_1\otimes\mathcal{K}_1)\hat{\varrho}_{AB}^{W}(\mathcal{K}_1\otimes\mathcal{K}_1)^{\dagger}\\ &+(\mathcal{K}_0\otimes\mathcal{K}_1)\hat{\varrho}_{AB}^{W}(\mathcal{K}_0\otimes\mathcal{K}_1)^{\dagger} + (\mathcal{K}_1\otimes\mathcal{K}_0)\hat{\varrho}_{AB}^{W}(\mathcal{K}_0\otimes\mathcal{K}_0)^{\dagger},\end{aligned} \tag{III.12}$$

where: $\hat{\varrho}_{AB}^{W}$ is the output state after performing the weak measurement (Eq. III.2), $\mathcal{K}_0$ and $\mathcal{K}_1$ are the Kraus operators:

$$\mathcal{K}_0 = \begin{pmatrix} 1 & 0 \\ 0 & \sqrt{1-\mathbf{p}} \end{pmatrix} \quad ; \quad \mathcal{K}_1 = \begin{pmatrix} 0 & \sqrt{\mathbf{p}} \\ 0 & 0 \end{pmatrix}, \tag{III.13}$$

$\mathcal{K}_0$ and $\mathcal{K}_1$ satisfy the completeness relation:

$$\sum_{\nu=0}^{1}\mathcal{K}_{\nu}\mathcal{K}_{\nu}^{\dagger} = \hat{I}_{2\times 2} \tag{III.14}$$

By applying the reversal measurements, the shared state between the users may be written in the computational basis $\{|00\rangle, |01\rangle, |10\rangle, |11\rangle\}$ as:

$$\hat{\varrho}_{AB}^{W-AD-R} = \frac{1}{N'}\begin{pmatrix} \mathcal{A} & 0 & 0 & \mathcal{D} \\ 0 & \mathcal{B} & 0 & 0 \\ 0 & 0 & \mathcal{B} & 0 \\ \mathcal{D} & 0 & 0 & \mathcal{C} \end{pmatrix}, \tag{III.15}$$

where:

$$\begin{aligned}\mathcal{A} &= (1-p_r)^2(1+\mathbf{p}^2+(1-p_w)^2) \quad ; \quad \mathcal{B} = \mathbf{p}(1-\mathbf{p})(1-p_w)^2(1-p_r)\\ \mathcal{C} &= ((1-\mathbf{p})(1-p_w))^2 \quad ; \quad \mathcal{D} = (1-\mathbf{p})(1-p_w)(1-p_r).\end{aligned}$$

The normalisation factor N' is given as:

$$N' = (1-p_r)^2 + (1-p_w)^2(1-\mathbf{p})^2 + 2\mathbf{p}(1-\mathbf{p})(1-p_r)(1-p_w)^2 + \mathbf{p}^2(1-p_w)^2(1-p_r)^2. \tag{III.16}$$

The negativity of this state is written:

$$\mathcal{N'}_{Ad}^{PT} = \frac{-2}{N'}\Big[\mathbf{p}(1-\mathbf{p})(1-p_r)(1-p_w)^2 - (1-\mathbf{p})(1-p_w)(1-p_r)\Big]. \tag{III.17}$$

It is worth mentioning that in the case where only one qubit (let suppose it to be the qubit "B") passes through the noisy channel, Bob will apply the weak measurement with strength p_w. The output state after

Bob's weak measurement is shown as follows:

$$|\psi^{+}_{AB}\rangle^{W} = \frac{1}{\sqrt{2-p_w}}(|000\rangle + \sqrt{1-p_w}|110\rangle)_{ABE_W}. \tag{III.18}$$

Now, Bob performs the reversal measurement on his qubit, then the final state between Alice and Bob becomes:

$$\hat{\varrho}^{W-AD'-R}_{AB} = \begin{pmatrix} 1-p_r & 0 & 0 & \sqrt{(1-\mathbf{p})(1-p_r)(1-p_w)} \\ 0 & 0 & 0 & 0 \\ 0 & 0 & \mathbf{p}(1-p_w)(1-p_r) & 0 \\ \sqrt{(1-\mathbf{p})(1-p_r)(1-p_w)} & 0 & 0 & (1-\mathbf{p})(1-p_w), \end{pmatrix}, \tag{III.19}$$

N is the normalization factor of the state Eq.(III.19), where:

$$N = 1 - p_r + (1-\mathbf{p})(1-p_w) + (1-p_w)\mathbf{p}(1-p_r). \tag{III.20}$$

The amount of the entanglement by means of the negativity is given as:

$$\mathcal{N}^{PT}_{Ad} = -\frac{1}{N}\left[\mathbf{p}(1-p_w)(1-p_r) - \sqrt{\mathbf{p}^2(1-p_w)^2(1-p_r)^2 + 4(1-p_r)(1-\mathbf{p})(1-p_w)}\right]. \tag{III.21}$$

The behavior of the negativity, as a measure of the entanglement, is displayed in the Fig. (III.4.a). It is shown that the negativity is maximal at $\mathbf{p} = 0$, namely when the initial state is maximally entangled. Obviously, the negativity decreases as the strength of the damping channel $\mathbf{p}$ increases. However, the decreasing rate depends on whether one or both qubits are affected by the amplitude damping channel. It is clear that, if both qubits are forced to pass through the amplitude damping channel (solid-red curve), the entanglement is much smaller than that depicted when only one qubit passes through this noisy channel (dashed-black). Moreover, the entanglement decreases linearly when one qubit is affected by the amplitude damping noisy channel.

The effect of the weak and reversed measurements on the degree of the entanglement of the states (III.19) and (III.15) is displayed in Fig. (III.4.b), Fig. (III.4.c) and Fig. (III.4.d). In general, the behavior of the entanglement is similar to that displayed in Fig. (III.4.a), in other words, the entanglement decays as the strength of the noise channel increases. The effect of the weak and the reversed measurements is displayed clearly on the negativity, where it increases as one increases the strength of both measurements, p_w and p_r. Moreover, the entanglement decreases slowly and gradually only if one qubit is forced to pass through the amplitude damping channel followed by the local weak and reversed measurements. Generally, the local weak and reversed measurements can improve and can recover the losses of the entanglement if the quantum channel of BQT is distributed through an amplitude damping channel.

III.2 Bidirectional teleportation via ADC

The purpose of this section is to investigate the effect of weak and reversed measurements on information bidirectional teleportation. Let us clarify this idea by considering that the users Alice and Bob want to teleport unknown states bidirectionally between them. We assume that the users share a noisy state, where both qubits are affected by the amplitude damping with strengths p_1 and p_2, respectively. To simplify the

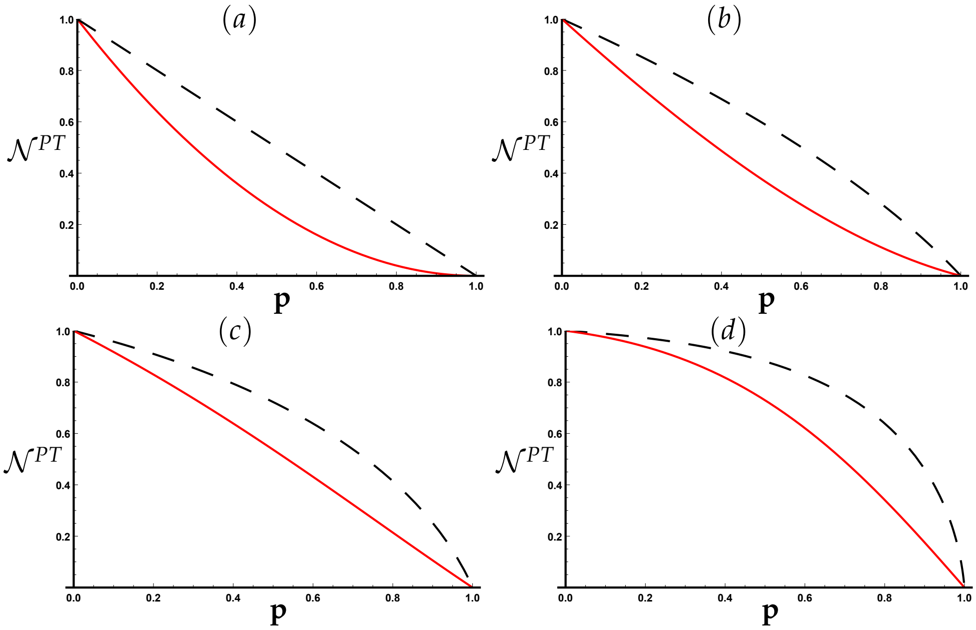

FIGURE III.4: $\mathcal{N}^{PT}$ vs $(\mathbf{p})$ the ADC strength with the weak-reversed measurements, when only Bob's qubit suffers ADC (Red solid), and both qubits suffered ADC (Black dashed), at (a) $p_w = 0$ and $p_r = 0$. (b) $p_w = 0,2$ and $p_r = 0,4$. (c) $p_w = 0,3$ and $p_r = 0,7$. (d) $p_w = 0,6$ and $p_r = 0,9$.

calculation, we suppose that the amplitude damping channel strengths are equal, namely $p_1 = p_2 = \mathbf{p}$.

$$\tilde{\varrho}_{AB}^{ADC} = \frac{1}{2}\begin{pmatrix} 1+\mathbf{p}^2 & 0 & 0 & 1-\mathbf{p} \\ 0 & \mathbf{p}(1-\mathbf{p}) & 0 & 0 \\ 0 & 0 & \mathbf{p}(1-\mathbf{p}) & 0 \\ 1-\mathbf{p} & 0 & 0 & (1-\mathbf{p})^2 \end{pmatrix}. \tag{III.22}$$

Alice and Bob are given the qubits $|Q_A\rangle$ and $|Q_B\rangle$ to be teleported between them

$$|Q_A\rangle = \cos\left(\frac{\theta_A}{2}\right)|0_A\rangle + e^{i\phi_A}\sin\left(\frac{\theta_A}{2}\right)|1_A\rangle, \quad |Q_B\rangle = \cos\left(\frac{\theta_B}{2}\right)|0_B\rangle + e^{i\phi_B}\sin\left(\frac{\theta_B}{2}\right)|1_B\rangle. \tag{III.23}$$

Moreover, each user has been supplied by a trigger qubit defined as:

$$|T_A\rangle = \cos\left(\frac{\tilde{\theta}_A}{2}\right)|0_A\rangle + \sin\left(\frac{\tilde{\theta}_A}{2}\right)|1_A\rangle\,, \quad |T_B\rangle = \cos\left(\frac{\tilde{\theta}_B}{2}\right)|0_B\rangle + \sin\left(\frac{\tilde{\theta}_B}{2}\right)|1_B\rangle\,. \tag{III.24}$$

Now, Alice and Bob have all the ingredients to perform the bidirectional teleportation scheme (as shown in Fig II.2). The whole BQT process may be summarized in four steps, where the details are described extensively in Ref. [233].

III.2.1 Implementation of BQT circuit

By performing the quantum circuit of the bidirectional quantum teleportation, the final output state depends on the triggers' states. However, we assume that the noise acts on both Bell qubits. In other words, the noise acts on qubit "i" with factor p_i, for $i = A, B$. We have the following possibilities:

1. *Both triggers are prepared in the state* $\varrho_{T_A} = \frac{1}{2}(\hat{I} + \hat{\sigma}_z^{(A)})$, *and* $\varrho_{T_B} = \frac{1}{2}(\hat{I} + \hat{\sigma}_z^{(B)})$ *:*

   In this case, no measurement has been done, i.e, $(\hat{\sigma_x}, \hat{\sigma_z})$ gates are not triggered. Therefore, the collapsed states at Alice's and Bob's hands can be written as:

$$\varrho_{(0A)}^{(Tel)} = \frac{1}{2}\begin{pmatrix} 1+\mathbf{p} & 0 \\ 0 & 1-\mathbf{p} \end{pmatrix}, \qquad \varrho_{(0B)}^{(Tel)} = \frac{1}{2}\begin{pmatrix} 1+\mathbf{p} & 0 \\ 0 & 1-\mathbf{p} \end{pmatrix} \tag{III.25}$$

2. *Alice's trigger qubit is prepared in* $\varrho_{T_A} = \frac{1}{2}(\hat{I} - \hat{\sigma}_z^{(A)})$, *and Bob's trigger qubit is prepared in* $\varrho_{T_B} = \frac{1}{2}(\hat{I} + \hat{\sigma}_z^{(B)})$:

   Then, only Bob has the ability to reconstruct the state that is sent by Alice. Therefore, the final state at Bob's side is given as:

$$\varrho_{(1B)}^{(Tel)} = \begin{pmatrix} (1-\mathbf{p})^2\cos\left(\frac{\theta_A}{2}\right)^2 + \mathbf{p}(1-\mathbf{p})\sin\left(\frac{\theta_A}{2}\right)^2 & (1-\mathbf{p})\cos\left(\frac{\theta_A}{2}\right)\sin\left(\frac{\theta_A}{2}\right)e^{i\phi_A} \\ (1-\mathbf{p})\cos\left(\frac{\theta_A}{2}\right)\sin\left(\frac{\theta_A}{2}\right)e^{-i\phi_A} & \mathbf{p}(1-\mathbf{p})\cos\left(\frac{\theta_A}{2}\right)^2 + (1+\mathbf{p}^2)\sin\left(\frac{\theta_A}{2}\right)^2 \end{pmatrix}, \tag{III.26}$$

   whereas, θ_A, θ_B and ϕ_A, ϕ_B are the weights and the phases of the initial qubits Eq.(III.23), and $\tilde{\theta}_A, \tilde{\theta}_B$ are the trigger's weights of Alice and Bob, respectively.

   In her side, Alice receives the mixed state:

$$\varrho_{(0A)}^{(Tel)} = \frac{1}{2}\begin{pmatrix} 1+\mathbf{p} & 0 \\ 0 & 1-\mathbf{p} \end{pmatrix} \tag{III.27}$$

3. *If Alice's trigger qubit is prepared in* $\varrho_{T_A} = \frac{1}{2}(\hat{I} + \hat{\sigma}_z^{(A)})$, *and Bob's trigger qubit is prepared in* $\varrho_{T_B} = \frac{1}{2}(\hat{I} - \hat{\sigma}_z^{(B)})$:

   Then, the teleported state at Alice's hand $\varrho_A^{(Tel)}$ is the same as that obtained by Bob in Eq. (III.26), but we just replace θ_A by θ_B and ϕ_A by ϕ_B. However, the state at Bob's hand is $\varrho_{(0B)}^{(Tel)} = \frac{(1+\mathbf{p})}{2}|0\rangle\langle 0| + \frac{(1-\mathbf{p})}{2}|1\rangle\langle 1|$.

In general, depending on the probabilities, in which the users Alice and Bob perform projective measurements that are given as [233]:

$$\begin{aligned} \mathcal{P}_i &= \frac{1}{2}\Big(1 + \cos(\tilde{\theta}_i)\cos(\theta_i) + \sin(\tilde{\theta}_i)\sin(\theta_i)\cos(\phi_i)\Big) \\ \textit{where} \quad \bar{\mathcal{P}}_i &= 1 - \mathcal{P}_i, \quad \textit{and} \quad i = A, B. \end{aligned} \tag{III.28}$$

The users will end up their protocol by two states [193, 233]. One of them at Alice's side:

$$\varrho_A^{(Tel)} = \mathcal{P}_B\bar{\mathcal{P}}_A\varrho_{(1A)}^{(Tel)} + (1 - \mathcal{P}_B\bar{\mathcal{P}}_A)\varrho_{(0A)}^{(Tel)}, \;\; \bar{\mathcal{P}}_A = 1 - \mathcal{P}_A, \tag{III.29}$$

and the other in Bob's side,

$$\varrho_B^{(Tel)} = \mathcal{P}_A\bar{\mathcal{P}}_B\varrho_{(1B)}^{(Tel)} + (1-\mathcal{P}_A\bar{\mathcal{P}}_B)\varrho_{(0B)}^{(Tel)},\ \ \bar{\mathcal{P}}_B = 1-\mathcal{P}_B. \tag{III.30}$$

Whereas: $\varrho_{0i} = \frac{(1+\mathbf{p})}{2}|0\rangle\langle 0| + \frac{(1-\mathbf{p})}{2}|1\rangle\langle 1|$. Finally, the final teleported states by using the noise channel $\tilde{\varrho}_{AB}^{ADC}$ (III.22) are given as:

$$\varrho_A^{ADC} = \frac{1}{2}\Big(1+\sum_{i=1}^{x,y,z} a_i^{(ADC)}\hat{\sigma}_i\Big), \quad \varrho_B^{ADC} = \frac{1}{2}\Big(1+\sum_{i=1}^{x,y,z} b_i^{(ADC)}\hat{\tau}_i\Big) \tag{III.31}$$

where,

$$\begin{aligned}
a_x^{(ADC)} &= \mathcal{P}_A\bar{\mathcal{P}}_B(\mathcal{N}_{Ad}^{(PT)} - (\mathbf{p}^2-\mathbf{p}))\cos\phi_A\sin\Big(\theta_A\Big), \\
a_y^{(ADC)} &= -\mathcal{P}_A\bar{\mathcal{P}}_B(\mathcal{N}_{Ad}^{(PT)} - (\mathbf{p}^2-\mathbf{p}))\sin\phi_A\sin\Big(\theta_A\Big), \\
a_z^{(ADC)} &= \mathcal{P}_A\bar{\mathcal{P}}_B(1-\mathbf{p})\cos(\theta_A)^2 + \mathbf{p}(1-\mathcal{P}_A\bar{\mathcal{P}}_B).
\end{aligned} \tag{III.32}$$

Whereas, for Bob:

$$\begin{aligned}
b_x^{(ADC)} &= \mathcal{P}_B\bar{\mathcal{P}}_A(\mathcal{N}_{Ad}^{(PT)} - (\mathbf{p}^2-\mathbf{p}))\cos\phi_B\sin\Big(\theta_B\Big), \\
b_y^{(ADC)} &= -\mathcal{P}_B\bar{\mathcal{P}}_A(\mathcal{N}_{Ad}^{(PT)} - (\mathbf{p}^2-\mathbf{p}))\sin\phi_B\sin\Big(\theta_B\Big), \\
b_z^{(ADC)} &= \mathcal{P}_B\bar{\mathcal{P}}_A(1-\mathbf{p})\cos(\theta_B)^2 + \mathbf{p}(1-\mathcal{P}_B\bar{\mathcal{P}}_A).
\end{aligned} \tag{III.33}$$

III.2.2 Teleportation quantifiers

To show clearly the effect of the ADC on the bidirectional teleportation of information, we evaluate the averaged fidelities of teleportation and the quantum Fisher information. The expression of the fidelity of telepotation is given as:

$$f^{in\to out} = \langle Q^i|\varrho(tel)_{out}|Q^i\rangle, \quad i = A, B, \tag{III.34}$$

where $|Q^i\rangle$ and $\rho_{out}^{(tel)}$ are the input and the output states, respectively. The different expression of fidelities of teleportation are given as follows:

$$\begin{aligned}
f_{Ad}^{A\to B} &= \mathcal{P}_A\bar{\mathcal{P}}_B\big(\chi\sin(\theta_A)^2 + \frac{\mathcal{N}^{PT}}{2}(1+\cos(\theta_A)^2) + 2\mathbf{p}\sin\Big(\frac{\theta_A}{2}\Big)^4\big) + \frac{1-\mathcal{P}_A\bar{\mathcal{P}}_B}{2}(1+\mathbf{p}\cos(\theta_A)) \\
f_{Ad}^{B\to A} &= \mathcal{P}_B\bar{\mathcal{P}}_A\big(\chi\sin(\theta_B)^2 + \frac{\mathcal{N}^{PT}}{2}(1+\cos(\theta_B)^2) + 2\mathbf{p}\sin\Big(\frac{\theta_B}{2}\Big)^4\big) + \frac{1-\mathcal{P}_B\bar{\mathcal{P}}_A}{2}(1+\mathbf{p}\cos(\theta_B))
\end{aligned} \tag{III.35}$$

With:

$$\chi = \mathcal{N}_{Ad}^{(PT)} - (2\mathbf{p}^2 - 2\mathbf{p}). \tag{III.36}$$

To evaluate the expression of QFI of the parameter θ_A, namely $\mathcal{J}_{\theta_A}$, with "A" stands for Alice, respectively. We use the formula (Eq. II.21):

$$\mathcal{J}_{\theta_A} = |\partial_\theta \overrightarrow{a}|^2 + \frac{(\overrightarrow{a}.\partial_\theta \overrightarrow{a})^2}{1-|\overrightarrow{a}|^2}, \tag{III.37}$$

whereas, $\partial_\theta = \frac{\partial}{\partial_{\theta_i}}$. The norm $|\overrightarrow{a}|$ of the Bloch vectors of the teleported state from Alice to Bob which are given in equation (III.32) is:

$$|\overrightarrow{a}| = \sqrt{(\mathcal{P}_A\bar{\mathcal{P}}_B(\mathcal{N}^{PT} - (\mathbf{p}^2 - \mathbf{p}))^2 \sin(\theta_A)^2 + (\mathcal{P}_A\bar{\mathcal{P}}_B(1-\mathbf{p})\cos(\theta_A)^2 + \mathbf{p}(1 - \mathcal{P}_A\bar{\mathcal{P}}_B)^2}, \tag{III.38}$$

with

$$\partial_\theta \overrightarrow{a} = \begin{cases} \bar{\mathcal{P}}_B(\mathcal{N}^{PT}_{Ad} - (\mathbf{p}^2 - \mathbf{p}))\cos(\phi_A)(\partial_\theta\mathcal{P}_A \sin(\theta_A) + \mathcal{P}_A\cos(\theta_A)) \\ -\bar{\mathcal{P}}_B(\mathcal{N}^{PT}_{Ad} - (\mathbf{p}^2 - \mathbf{p}))(\partial_\theta\mathcal{P}_A \sin(\theta_A) + \mathcal{P}_A\cos(\theta_A)) \\ \bar{\mathcal{P}}_B(1-\mathbf{p})(\partial_\theta\mathcal{P}_A\cos(\theta_A)^2 - 2\mathcal{P}_A\cos(\theta_A)\sin(\theta_A)) - \mathbf{p}\bar{\mathcal{P}}_B\partial_\theta\mathcal{P}_A. \end{cases} \tag{III.39}$$

Similarly, QFI of the parameter θ_B could be easily evaluated using the same method, QFI of θ_B is written as:

$$\mathcal{J}_{\theta_B} = ((|\partial_{\theta_B}\overrightarrow{b}|^2 + \frac{(\overrightarrow{b}\partial_{\theta_B}\overrightarrow{b})^2}{1 - |\overrightarrow{b}|^2}. \tag{III.40}$$

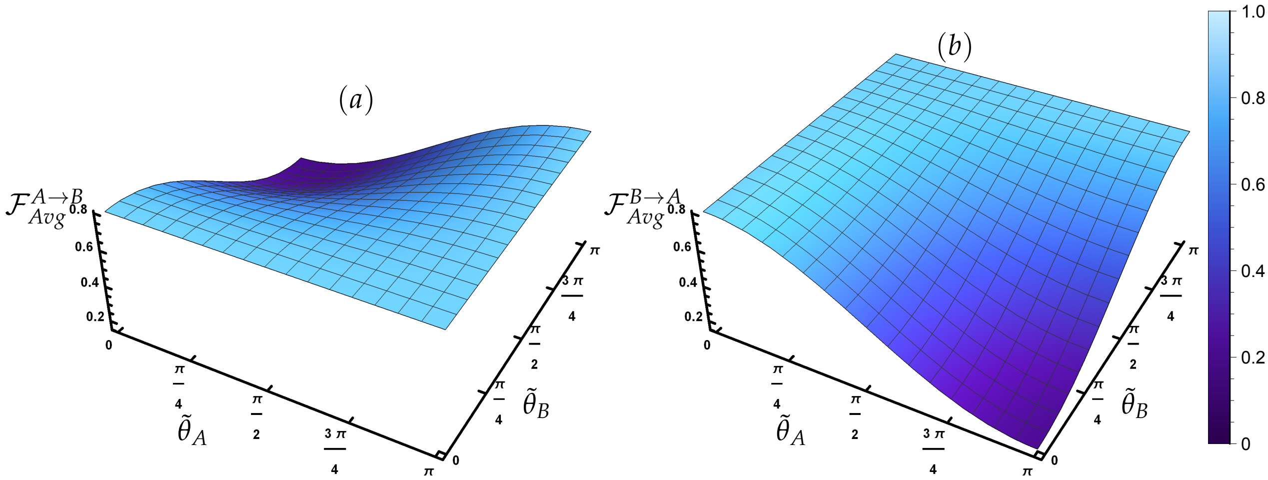

FIGURE III.5: $\mathcal{F}_{Avg}$; $p = 0.6$ the ADC strength with the weak-reversed measurements, when both qubits suffer ADC.

It is clear that the average fidelities depend on the initial teleported state and the trigger states. In the absence of the noise, Fig. (II.3), the fidelity $\mathcal{F}^{in\to out}_{Avg}$ increases as $\tilde{\theta}_{in}$ increases and $\tilde{\theta}_{out}$ decreases. The maximum value is depicted at $\tilde{\theta}_{in} = \pi$ and $\tilde{\theta}_{out} = 0$. At these points, Alice's and Bob's triggers have different states $|1\rangle$ and $|0\rangle$, respectively; while the teleported state is $|Q_B\rangle = |0\rangle$, wich contains only classical information. The minimum averaged fidelity that the sender "A" or "B" can obtain from the receiver's side is $\mathcal{F}^{in\to out}_{Avg} = 0.5$. Besides, in Fig. (III.5), we quantify the averaged fidelity of the teleported state from Alice to Bob, namely $\mathcal{F}^{A\to B}_{Avg}$, and from Bob to Alice, $\mathcal{F}^{B\to A}_{Avg}$, under a noisy amplitude damping channel of strength $\mathbf{p} = 0.6$. The effect of the amplitude noisy channels is predicted in Figs. (III.5.a) and (III.5.b), where we assume that both qubits pass through two identical amplitude damping channels, namely $p_1 = p_2 = \mathbf{p} = 0.6$. As it is displayed in Fig. (III.5.a), the behavior of $\mathcal{F}^{A\to B}_{Avg}$ is changed dramatically (compared to the behavior in Fig. II.3), where at $\tilde{\theta}_A = \pi$ and $\tilde{\theta}_B = 0$, $\mathcal{F}^{B\to A}_{Avg} = \frac{1}{2}(1-\mathbf{p})$. On the other hand, the maximum fidelity is depicted at $\tilde{\theta}_A = 0$ and $\tilde{\theta}_B = \pi$, namely $\mathcal{F}^{B\to A}_{Avg} = \frac{1}{2}(1+\mathbf{p})$. However, the fidelity decreases gradually as the weight angle of Alice's trigger (Bob's trigger) increases (decreases), respectively.

The fidelity of the teleported state from Bob to Alice, $\mathcal{F}_{Avg}^{B\to A}$ is displayed in Fig.(III.5.b), where we use the same initial state settings as in Fig.(III.5.a). As it is displayed in Fig.(III.5.b), the fidelity increases gradually as the weight angle of Bob's trigger state increases, while Alice's trigger state decreases. The maximum value of $\mathcal{F}_{Avg}^{B\to A} = \frac{(1+\mathbf{p})}{2}$ is predicted at $\tilde{\theta}_A = 0$ and $\tilde{\theta}_B = \pi$, while the minimum value $\mathcal{F}_{Avg}^{B\to A} = \frac{(1-\mathbf{p})}{2}$ is displayed at different initial state settings of the users' triggers.

So, the effect of the amplitude damping channel on the behavior of the average fidelities, $\mathcal{F}_{Avg}^{A\to B}$ and $\mathcal{F}_{Avg}^{B\to A}$, is displayed in Fig.(III.5). The maximum/minimum values of the average fidelities are shown at different initial state settings. However, as it is displayed in Fig.(III.5), the fidelity $\mathcal{F}_{Avg}^{B\to A}$ ($\mathcal{F}_{Avg}^{A\to B}$) is maximum when Alice's and Bob's triggers are prepared with $\tilde{\theta}_A = \pi$, and $\tilde{\theta}_B = 0$ ($\tilde{\theta}_A = 0$, and $\tilde{\theta}_B = \pi$), respectively.

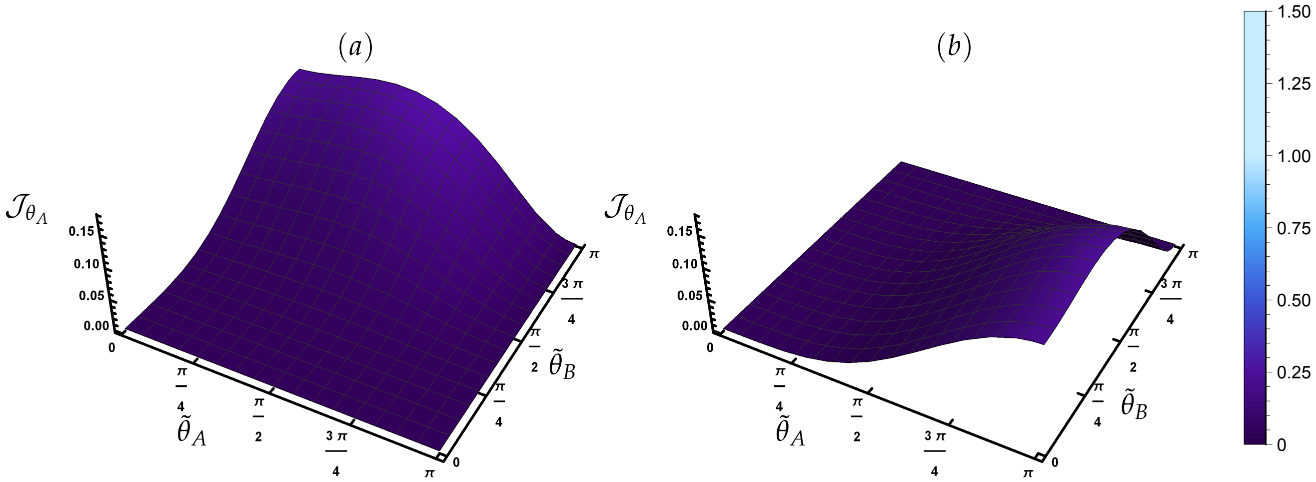

FIGURE III.6: $\mathcal{J}_\theta$; $p = 0.6$ the ADC strength when both qubits suffer ADC.

Now, we display the behavior of the quantum Fisher information with respect to the weight parameters θ_A and θ_B. The effect of amplitude noise on the quantum Fisher information for θ_A and θ_B, namely $\mathcal{J}_{\theta_A}$, $\mathcal{J}_{\theta_B}$, is shown in Fig.(III.6). As has been shown in this figure, the noise dramatically decreases the quantum Fisher information with respect to the weight parameters θ_A and θ_B. However, the maximum bound of $\mathcal{J}_{\theta_A} = \frac{\mathcal{J}_{p=0}}{2} - p(\mathcal{J}_{\theta_B})$; where $\mathcal{J}_{p=0}$ is the maximum value of QFI without noise, is predicted at $\theta_A = 0$ and $\theta_B = \pi$ ($\theta_A = \pi$ and $\theta_B = 0$), respectively. Next, we investigate the effect of the weak and reversed measurements on the BQT of information.

III.3 WR measurements effect of BQT

Some quantum phenomena are frequently enhanced by using weak and reversal measurements. In the following, we investigate the possibility of improving the fidelities of the bidirectional teleportation of information discussed previously. If the partners (Alice and Bob) apply the weak and reversal measurements on the noisy channel shared between them, they will end-up the protocol with the state in Alice's hand:

$$\varrho_A^{(Tel)} = \begin{pmatrix} \varrho_{11}^A & \varrho_{12}^A \\ \varrho_{21}^A & \varrho_{22}^A \end{pmatrix}, \tag{III.41}$$

with,

$$
\begin{aligned}
\varrho_{11}^{A} &= \mathcal{P}_B\bar{\mathcal{P}}_A\Big(|\beta|^2\cos\Big(\frac{\theta_B}{2}\Big)^2+|\eta|^2\sin\Big(\frac{\theta_B}{2}\Big)^2\Big)+\frac{(1-\mathcal{P}_B\bar{\mathcal{P}}_A)}{\lambda}\Big(|\alpha|^2+(1-p_w)^2\mathbf{p}(1-p_r)(1-\mathbf{p}p_r\Big),\\
\varrho_{12}^{A} &= \mathcal{P}_B\bar{\mathcal{P}}_A\beta\alpha\cos\frac{\theta_B}{2}\sin\frac{\theta_B}{2}e^{i\phi_B},\\
\varrho_{21}^{A} &= \varrho_{12}^{A*},\\
\varrho_{22}^{A} &= \mathcal{P}_B\bar{\mathcal{P}}_A\Big(|\zeta|^2\cos\Big(\frac{\theta_B}{2}\Big)^2+(|\alpha|^2+|\delta|^2)\sin\Big(\frac{\theta_B}{2}\Big)^2\Big)+\frac{(1-\mathcal{P}_B\bar{\mathcal{P}}_A)}{\lambda}\Big((1-p_w)^2(1-\mathbf{p})(1-\mathbf{p}p_r)\Big),
\end{aligned}
$$

$$
\begin{aligned}
&\alpha=1-p_r \quad;\quad \beta=(1-p_w)(1-\mathbf{p}) \quad;\quad \eta=(1-p_w)\sqrt{\mathbf{p}(1-\mathbf{p})p_r} \quad;\quad \delta=(1-p_w)\mathbf{p}(1-p_r)\\
&\zeta=(1-p_w)\sqrt{\mathbf{p}(1-\mathbf{p})(1-p_r)} \quad;\quad \lambda=|\alpha|^2+|\beta|^2+|\eta|^2+|\zeta|^2+|\delta|^2
\end{aligned}
\tag{III.42}
$$

p_r, p_w are the strength of the reversed, weak measurements, respectively. $\mathbf{p}p$ is *ADC* strength. However, the teleported state to Bob is given as:

$$
\varrho_B^{(Tel)}=\begin{pmatrix}\varrho_{11}^{B} & \varrho_{12}^{B}\\ \varrho_{21}^{B} & \varrho_{22}^{B}\end{pmatrix},
\tag{III.43}
$$

with

$$
\begin{aligned}
\varrho_{11}^{B} &= \mathcal{P}_A\bar{\mathcal{P}}_B\Big(|\beta|^2\cos\Big(\frac{\theta_A}{2}\Big)^2+|\zeta|^2\sin\Big(\frac{\theta_A}{2}\Big)^2\Big)+\frac{(1-\mathcal{P}_A\bar{\mathcal{P}}_B)}{\lambda}\Big(|\alpha|^2+(1-p_w)^2\mathbf{p}(1-p_r)(1-\mathbf{p}p_r\Big)\\
\varrho_{12}^{B} &= \mathcal{P}_A\bar{\mathcal{P}}_B\beta\alpha\cos\frac{\theta_A}{2}\sin\frac{\theta_A}{2}e^{i\phi_A};\qquad \varrho_{21}^{B}=\varrho_{12}^{B*},\\
\varrho_{22}^{B} &= \mathcal{P}_A\bar{\mathcal{P}}_B\Big((|\delta|+|\alpha|^2)\sin\Big(\frac{\theta_A}{2}\Big)^2+|\eta|^2\cos\Big(\frac{\theta_A}{2}\Big)^2\Big)+\frac{(1-\mathcal{P}_A\bar{\mathcal{P}}_B)}{\lambda}\Big((1-p_w)^2(1-\mathbf{p})(1-\mathbf{p}p_r)\Big).
\end{aligned}
$$

The fidelity of the teleported states from both users is given as:

$$
f^{B\rightarrow A}=\mathcal{P}_B\bar{\mathcal{P}}_A\kappa+\frac{1}{\lambda}(1-\mathcal{P}_B\bar{\mathcal{P}}_A)\chi,\quad f^{A\rightarrow B}=\mathcal{P}_A\bar{\mathcal{P}}_B\kappa^{'}+\frac{1}{\lambda}(1-\mathcal{P}_A\bar{\mathcal{P}}_B)\chi^{'};
\tag{III.44}
$$

where,

$$
\begin{aligned}
\kappa &= (\beta\cos\Big(\frac{\theta_B}{2}\Big)^2+\alpha\sin\Big(\frac{\theta_B}{2}\Big)^2)^2+\frac{\sin(\theta_B)^2}{4}(\eta^2+\zeta^2)+\delta^2\sin\Big(\frac{\theta_B}{2}\Big)^4,\\
\chi &= \alpha^2\cos\Big(\frac{\theta_B}{2}\Big)^2+(1-p_w)^2(1-\mathbf{p}p_r)(\mathbf{p}\cos(\theta_B)-p_r\mathbf{p}\cos\Big(\frac{\theta_B}{2}\Big)^2+\sin\Big(\frac{\theta_B}{2}\Big)^2)\\
\kappa^{'} &= (\beta\cos\Big(\frac{\theta_A}{2}\Big)^2+\alpha\sin\Big(\frac{\theta_A}{2}\Big)^2)^2+\frac{\sin(\theta_A)^2}{4}(\eta^2+\zeta^2)+\delta^2\sin\Big(\frac{\theta_A}{2}\Big)^4,\\
\chi^{'} &= \alpha^2\cos\Big(\frac{\theta_A}{2}\Big)^2+(1-p_w)^2(1-\mathbf{p}p_r)(\mathbf{p}\cos(\theta_A)-p_r\mathbf{p}\cos\Big(\frac{\theta_A}{2}\Big)^2+\sin\Big(\frac{\theta_A}{2}\Big)^2)
\end{aligned}
$$

The effect of the weak and the reversal measurements is displayed in Fig. (III.7) and Fig. (III.8), where we

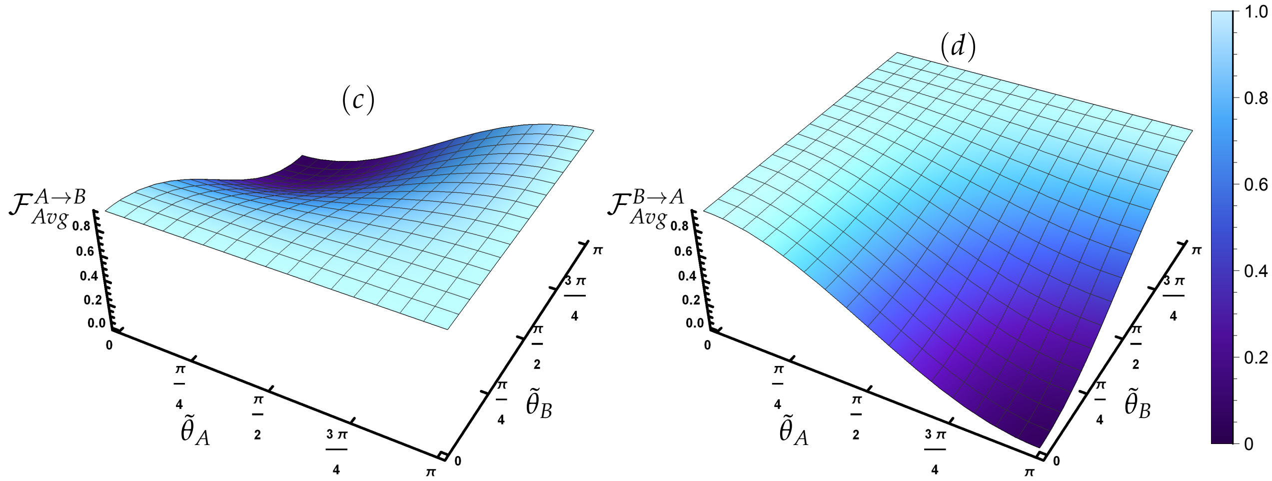

FIGURE III.7: $\mathcal{F}_{Avg}$; $p = 0.6$ the ADC strength with the weak-reversed measurements, when both qubits suffer ADC , at (b) $p_w = 0,7$ and $p_r = 0,4$.

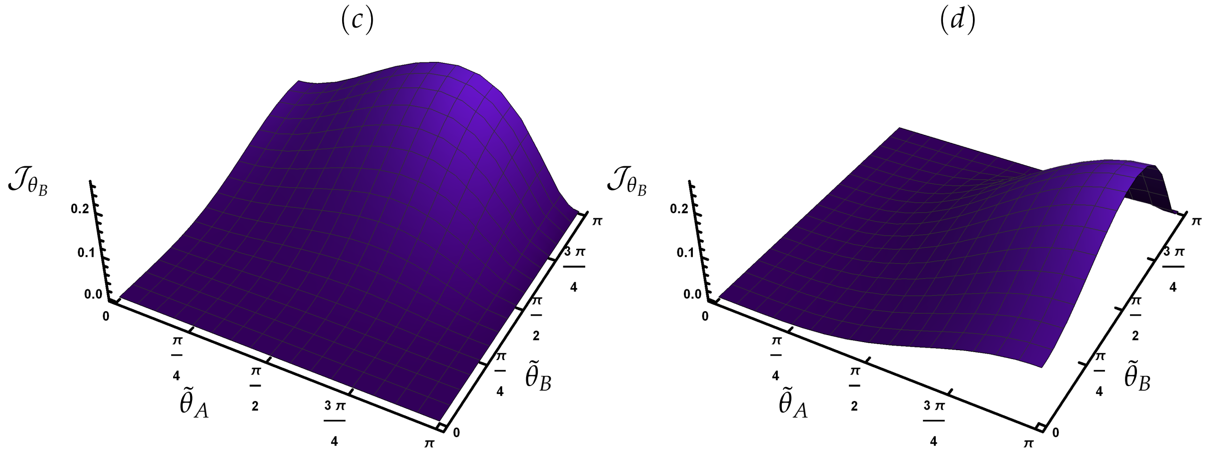

FIGURE III.8: $\mathcal{J}_{\theta}$; $p = 0.6$ the ADC strength with the weak-reversed measurements, when both qubits suffer ADC , at (b) $p_w = 0,7$ and $p_r = 0,4$.

assume that, the teleported states from both sides are prepared as $\theta_A = \theta_B = 0$. The general behavior shows that, the maximum values of the fidelities $\mathcal{F}^{B\to A}_{Avg}$ ($\mathcal{F}^{A\to B}_{Avg}$) and $\mathcal{J}_{\theta_A}$ ($\mathcal{J}_{\theta_B}$) increase as soon as the weak and reversal measurements are applied. These results can be seen by comparing the Fig. (III.7) with Fig. (III.5) for $\mathcal{F}^{B\to A}_{Avg}$, and $\mathcal{F}^{A\to B}_{Avg}$ and Fig. (III.8) with Fig. (III.6) for $\mathcal{J}_{\theta_A}$ and $\mathcal{J}_{\theta_B}$. When the trigger and teleported states are prepared in the same polarisation, the efficiency of the weak and reversed measurements increases. However, if any triggers are prepared in a polarisation that is different from the teleported state polarisation, then the weak and reversed measurements decrease the fidelities further.

The Fig. (III.9) shows the behavior of the fidelities averaged at different trigger weights, namely at $\tilde{\theta}_A = \tilde{\theta}_B = \tilde{\theta}_t$, with ($\tilde{\theta}_t = 0, \frac{\pi}{2}$ and $\frac{3\pi}{4}$). As it is displayed in Fig. (III.9.a), the averaged fidelities are maximal if the state and the trigger are polarized in the same direction. However, Fig. (III.9.b) when the users applied the weak and the reversed measurements, the averaged fidelities $\mathcal{F}_{Avg}$ decrease for all the initial teleported states, except for the state with an initial value greater than 0.5. This shows that the weak and reversed measurements cannot improve the fidelity of all the teleported states. Furthermore, based on the quantum purification [169], one cannot increase the fidelity of the teleported states by using local operation and quantum communication if the initial fidelity is smaller than $\frac{1}{2}$. Yet, the weak and the

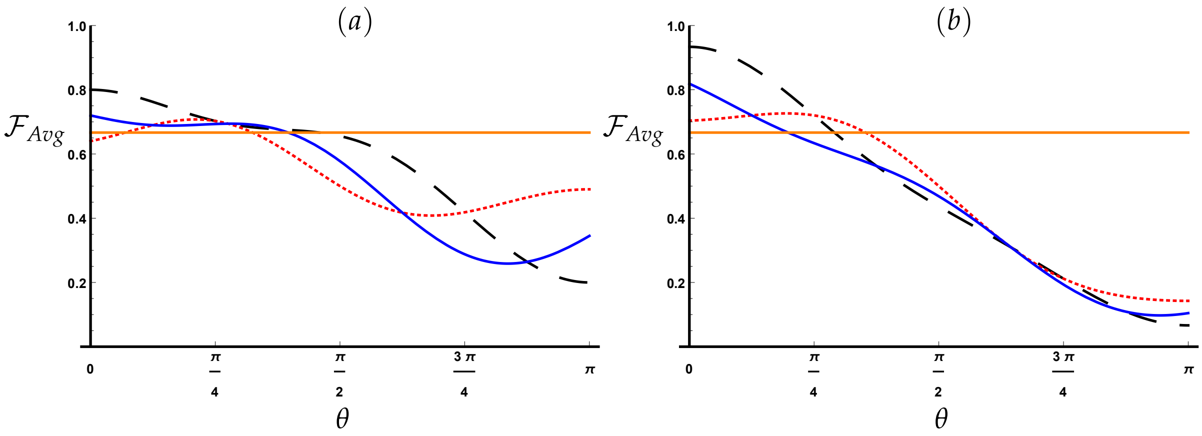

FIGURE III.9: $\mathcal{F}_{Avg}$; $p = 0.6$ the ADC strength with the weak-reversed measurements, when both qubits suffer ADC, at (b) $p_w = 0{,}7$ and $p_r = 0{,}4$. $\theta_A = \theta_B = \theta$; Black: $\tilde{\theta}_t = 0$; Red: $\tilde{\theta}_t = \frac{\pi}{2}$; Blue: $\tilde{\theta}_t = \frac{3\pi}{4}$. The orange line: $\mathcal{F}_{Avg}^{Classic} = \frac{2}{3}$

reversed measurements cannot overtake the fidelity limit attainable using only classical means and local operations which is $\frac{2}{3}$ described by the orange curve in Fig. (III.9).
Similarly, Fig.(III.10) depicts the behavior of fidelities averaged at various trigger weights, namely $\tilde{\theta}_A$ and $\tilde{\theta}$. The quantum Fisher information, $\mathcal{J}_{\theta_i}$, is maximized if the state and the trigger are polarized in the same direction, as shown in Fig.(III.10.a). However, as shown in Fig.(III.10.b) , when users use the weak and reversal measurements, the quantum Fisher information $\mathcal{J}_{\theta_i}$ increases for all initial teleported states except the state with a null initial value, namely $\mathcal{J}_{\theta_i} = 0$ $(i = A, B)$.

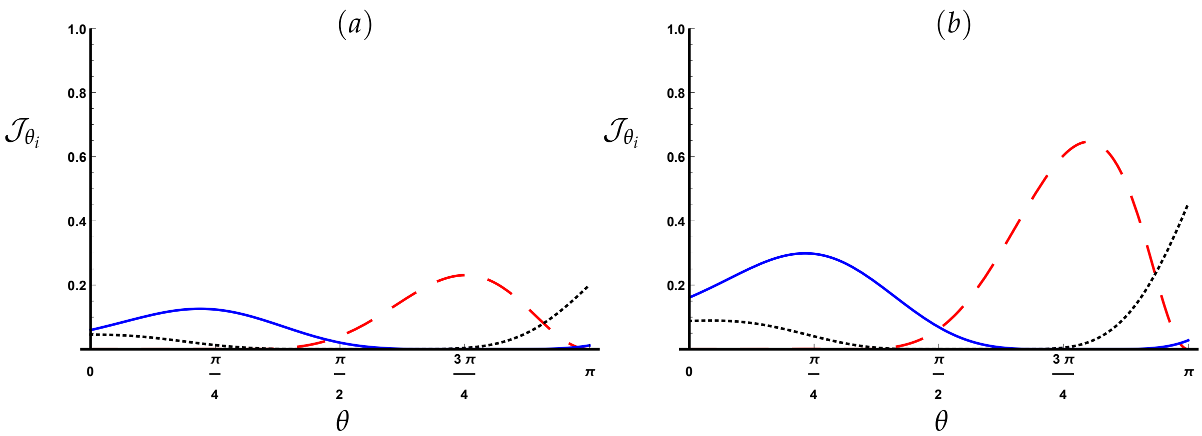

FIGURE III.10: $\mathcal{J}_{\theta_i}$; $p = 0.6$ the ADC strength with the weak-reversed measurements, when both qubits suffer ADC, at (b) $p_w = 0{,}7$ and $p_r = 0{,}4$. $\theta_A = \theta_B = \theta$; Black: $\tilde{\theta}_t = 0$; Red: $\tilde{\theta}_t = \frac{\pi}{2}$; Blue: $\tilde{\theta}_t = \frac{3\pi}{4}$.

The Fig. (III.11) shows the impact of the weak and reversed measurements on the quantum Fisher information, $\mathcal{J}_{\theta_i}$. It is clear that as soon as the weak and the reversed measurements increase the quantum Fisher information also increases. However, if the initial value of the quantum Fisher information is null, $\mathcal{J}_{\theta_i} = 0$, the weak and revised measurements cannot increase it.

We have already discussed the possibility of improving the entanglement, the average fidelities of the bidirectionally teleported states and the quantum Fisher information, where the shared channel between

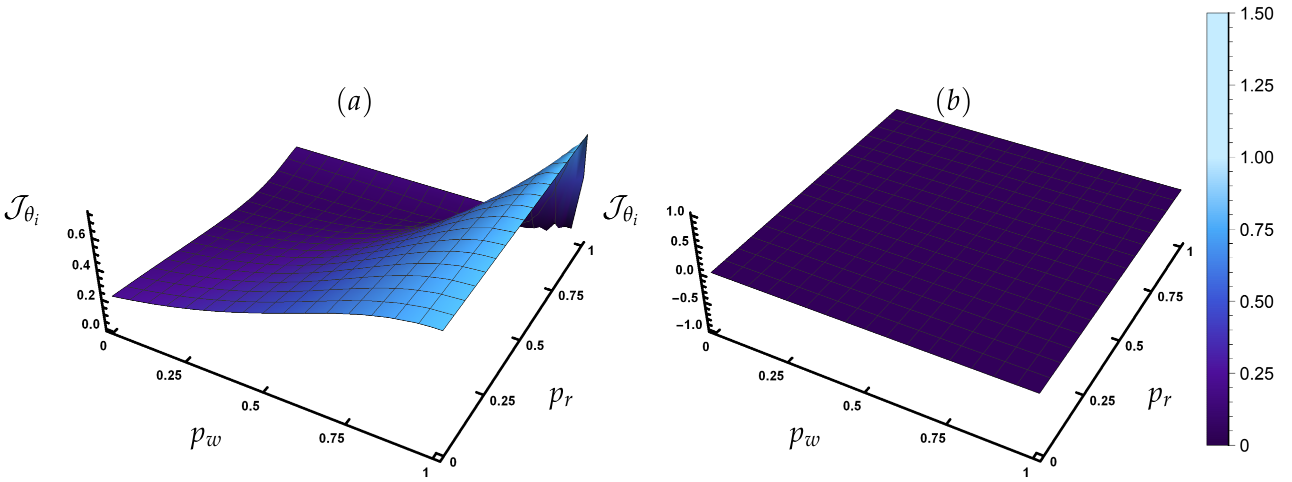

FIGURE III.11: $\mathcal{J}_{\theta_i}$ Vs the weak and the reversed measurements strengths. (a): The initial QFI $\mathcal{J}_{\theta_i} = 0.2$. (b): $\mathcal{J}_{\theta_i} = 0$.

the users is affected by different noisy channels. Based on the bidirectional teleportation protocol, the fidelity of the teleported state from each side depends on the initial teleported state and the trigger's states of both users. Since, the shared channel between the users is noisy, the efficiency of the bidirectional teleportation protocol decreases; though it is known that this channel plays the central role in the teleportation process. We discussed the entanglement behavior of this channel under different typical noisy channels such as, dephazing, bit-flip, phase-flip, depolarizing and amplitude damping channels; where we use the negativity of the partial transpose of the density operator as a measure of entanglement. It is shown that the entanglement decays as the channel's strength increases. However, the weak and reversed measurements cannot overcome the effect of all the previously mentioned noise, except the amplitude damping channel. Furthermore, the teleported states' average fidelities and the quantum Fisher information from both sides decrease when the protocol is performed using the noisy channel. However, the channel strength and the initial states of the triggers control the possibility of maximizing/ minimizing the fidelity of the teleported states and the quantum Fisher information. If the initial state of the teleported state and its corresponding trigger are prepared in a different polarization from the trigger on the other side, both quantities are minimized. This phenomenon is changed dramatically when the noise is applied to the shared channel between the users. However, in the presence of the noise, the maximum and minimum values are predicted at different states of the triggers. The upper bounds of both quantities are improved when the users apply the local weak and reversed measurements. However, these measurements do not change the maximum/minimum positions. Moreover, as it is predicted from the numerical calculations, the minimum values of the fidelities within the WR measurements are smaller than those predicted without the WR measurements. However, the bidirectional teleportation can be improved by using the WR measurements if the initial fidelities of the states are larger than (0.5) and the quantum Fisher information is not null. These results lead us to ask the question: Can we overcome the effects of the other types of noise? In the following, we will discuss the effect of the noise channels' correlations on the BQT.

III.4 BQT under correlated noise

Now our main mission is to discuss the robustness of the bidirectional protocol in the presence of different types of noises, where these noises may be correlated or non-correlated. Generally, a correlated noisy channel ϵ is a channel with correlated actions on a sequence of qubits. In contrast, a non-correlated channel is a channel with independent actions. Moreover, for the two-qubit input state ρ_i, the output state $\varrho(t)_f$ will be given as [228, 234]:

$$\hat{\varrho}(t)_f = \epsilon(\hat{\varrho}) = (1-\nu)\sum_{n,m=0}^{3} \mathcal{K}^u_{nm}\hat{\varrho}_i\mathcal{K}^{u\dagger}_{nm} + \nu\sum_{k=0}^{3}\mathcal{K}^c_{kk}\hat{\varrho}_i\mathcal{K}^{c\dagger}_{kk}. \tag{III.45}$$

Where the operators $\mathcal{K}$ are the Kraus operators which describe the actions of ϵ. The superscripts u and c denote uncorrelated and correlated, respectively. The parameter ν represents the strength of the successive actions of ϵ on qubits. It is noted that, if the channel is uncorrelated $(\nu = 0)$, the expression of $\mathcal{K}^u_{nm}$ is given by:

$$\mathcal{K}^u_{nm} = \sqrt{p_n}\hat{\sigma}_n \otimes \sqrt{p_m}\hat{\sigma}_m. \tag{III.46}$$

However, if the channel is totally correlated $(\nu = 1)$, the expression of Kraus operator is given as:

$$\mathcal{K}^c_{kk} = \sqrt{p_k}\hat{\sigma}_k\hat{\sigma}_k, \tag{III.47}$$

p_i is the probability with which the noise is applied to the channel's qubits.

We will proceed to investigate the effect of noise correlations on the amount of entanglement in the quantum channel. Subsequently, we will display the effect of noise correlations on the fidelities of teleportation and on quantum Fisher information.

III.4.1 Bit-flip

Let the qubits of the state (Eq. II.3) be prepared in the Laboratory (by a third part, let's call it "Charlie") and distributed to Alice and Bob under a bit-flip noise. With probability p_1, the bit-flip noise flips the state from $|0\rangle$ to $|1\rangle$ or vice versa. It commonly appears in quantum error correction [235]. The Kraus operators describing the actions of the correlated bit-flip channel are represented as follows:

$$\begin{aligned}\mathcal{K}^u_{00} &= p_0\hat{\mathcal{I}}\otimes\hat{\mathcal{I}};\quad \mathcal{K}^u_{01} = \sqrt{p_0p_1}\hat{\mathcal{I}}\otimes\hat{\sigma}_x;\quad \mathcal{K}^u_{10} = \sqrt{p_1p_0}\hat{\sigma}_x\otimes\hat{\mathcal{I}};\\ \mathcal{K}^u_{11} &= p_1\hat{\sigma}_x\otimes\hat{\sigma}_x;\quad \mathcal{K}^c_{00} = \sqrt{p_0}\hat{\mathcal{I}}\otimes\hat{\mathcal{I}};\quad \mathcal{K}^c_{11} = \sqrt{p_1}\hat{\sigma}_x\otimes\hat{\sigma}_x.\end{aligned} \tag{III.48}$$

whereas, $p_0 = 1-\mathbf{p}$, $p_1 = \mathbf{p}$. $0 \le \mathbf{p} \le 1$ is the decoherence factor, and $\hat{\mathcal{I}}, \hat{\sigma_x}$ are the unitary and the $\hat{\sigma_x}$ Pauli-operators, respectively.

By straightly substituting, the Kraus operators from Eq.(III.48) in the channel Eq.(III.45), the quantum channel of the BQT could be obtained as:

$$\hat{\varrho}^{bf}_{AB} = \frac{1}{2}\begin{pmatrix} 1-2(1-\nu)(\mathbf{p}-\mathbf{p}^2) & 0 & 0 & 1-2(1-\nu)(\mathbf{p}-\mathbf{p}^2) \\ 0 & 2(1-\nu)(\mathbf{p}-\mathbf{p}^2) & 2(1-\nu)(\mathbf{p}-\mathbf{p}^2) & 0 \\ 0 & 2(1-\nu)(\mathbf{p}-\mathbf{p}^2) & 2(1-\nu)(\mathbf{p}-\mathbf{p}^2) & 0 \\ 1-2(1-\nu)(\mathbf{p}-\mathbf{p}^2) & 0 & 0 & 1-2(1-\nu)(\mathbf{p}-\mathbf{p}^2) \end{pmatrix} \tag{III.49}$$

The amount of entanglement in the state Eq.(III.49) is given by:

$$\mathcal{N}^{(PT)}_{bf} = 1-4(1-\nu)(\mathbf{p}-\mathbf{p}^2). \tag{III.50}$$

Now, the users will implement the bidirectional protocol by using the channel $\hat{\varrho}_{AB}^{bf}$. Then, the received state at Bob's hand is given as:

$$\hat{\varrho}_{A}^{bf} = \frac{1}{2}(\hat{I} + \sum_i a_i^{bf}\hat{\sigma}_i), \tag{III.51}$$

where a_i^{bf} are the Bloch vectors given by,

$$a_x^{(bf)} = \mathcal{P}_A\bar{\mathcal{P}}_B\cos(\phi_A)\sin(\theta_A), \quad a_y^{(bf)} = -\mathcal{P}_A\bar{\mathcal{P}}_B\sin(\phi_A)\sin(\theta_A), \quad a_z^{(bf)} = \mathcal{P}_A\bar{\mathcal{P}}_B\mathcal{N}_{bf}^{PT}\cos(\theta_A). \tag{III.52}$$

However, the received state at Alice's hand is given as:

$$\hat{\varrho}_{B}^{bf} = \frac{1}{2}\left(\hat{I} + \sum_i b_i^{bf}\hat{\tau}_i\right), \tag{III.53}$$

where

$$b_x^{(bf)} = \mathcal{P}_B\bar{\mathcal{P}}_A\cos(\phi_B)\sin(\theta_B), \quad b_y^{(bf)} = -\mathcal{P}_B\bar{\mathcal{P}}_A\sin(\phi_B)\sin(\theta_B), \quad a_z^{(bf)} = \mathcal{P}_B\bar{\mathcal{P}}_A\mathcal{N}_{bf}^{PT}\cos(\theta_B). \tag{III.54}$$

By Substituting Eq. (III.52) and Eq. (III.54) into the expression of the quantum Fisher information that is given in Eq. (II.21), one could easily get the expression of the QFI with respect to the parameter θ_A, and θ_B, respectively.

Furthermore, the expressions of the teleportation Fidelities are given as follows:

$$\begin{aligned} f_{bf}^{A\to B} &= \mathcal{P}_A\bar{\mathcal{P}}_B\big(1 + \frac{\cos(\theta_A)^2}{2}(\mathcal{N}_{bf}^{PT} - 1)\big) + \frac{1 - \mathcal{P}_A\bar{\mathcal{P}}_B}{2} \\ f_{bf}^{B\to A} &= \mathcal{P}_B\bar{\mathcal{P}}_A\big(1 + \frac{\cos(\theta_B)^2}{2}(\mathcal{N}_{bf}^{PT} - 1))\big) + \frac{1 - \mathcal{P}_B\bar{\mathcal{P}}_A}{2}. \end{aligned} \tag{III.55}$$

III.4.2 Phase-flip

The phase flip operation describes the loss of information in a quantum state without energy loss [236]. The Kraus operators describing this process are given as follows:

$$\begin{aligned} \mathcal{K}_{00}^u &= p_0\hat{\mathcal{I}}\otimes\hat{\mathcal{I}}; \quad \mathcal{K}_{01}^u = \sqrt{p_0p_1}\hat{\mathcal{I}}\otimes\hat{\sigma}_z; \quad \mathcal{K}_{10}^u = \sqrt{p_1p_0}\hat{\sigma}_z\otimes\hat{\mathcal{I}} \\ \mathcal{K}_{11}^u &= p_1\hat{\sigma}_z\otimes\hat{\sigma}_z \quad \mathcal{K}_{00}^c = \sqrt{p_0}\hat{\mathcal{I}}\otimes\hat{\mathcal{I}}; \quad \mathcal{K}_{11}^c = \sqrt{p_1}\hat{\sigma}_z\otimes\hat{\sigma}_z, \end{aligned} \tag{III.56}$$

whereas, $p_0 = 1 - \mathbf{p}$, $p_1 = \mathbf{p}$, $\mathbf{p}$ is the decoherence factor, $0 \le \mathbf{p} \le 1$. Now, if the initial state passes through this noise channel. Then, By replacing the Kraus operators Eq. (III.56) in the channel Eq. (III.45), the quantum channel of the BQT under correlated phase flip noise could be obtained as:

$$\hat{\varrho}_{AB}^{pf} = \frac{1}{2}\begin{pmatrix} 1 & 0 & 0 & 1 - 4(1-\nu)(\mathbf{p} - \mathbf{p}^2) \\ 0 & 0 & 0 & 0 \\ 0 & 0 & 0 & 0 \\ 1 - 4(1-\nu)(\mathbf{p} - \mathbf{p}^2) & 0 & 0 & 1 \end{pmatrix} \tag{III.57}$$

The amount of the survival quantum correlation is measured by the negativity where,

$$\mathcal{N}_{pf}^{(PT)} = 1 - 4(1-\nu)(\mathbf{p} - \mathbf{p}^2). \tag{III.58}$$

After the bidirectional teleportation process using Eq.(III.57), Alice and Bob can reconstruct the quantum state:

$$\hat{\varrho}_A^{pf} = \frac{1}{2}\Big(\hat{I} + \sum_{i=1}^{x,y,z} a_i^{(pf)}\hat{\sigma}_i\Big),\ \hat{\varrho}_B^{pf} = \frac{1}{2}\Big(\hat{I} + \sum_{i=1}^{x,y,z} b_i^{(pf)}\hat{\tau}_i\Big) \tag{III.59}$$

where

$$\begin{gathered}
a_x^{(pf)} = \mathcal{P}_A\bar{\mathcal{P}}_B\sqrt{\mathcal{N}_{pf}^{PT}}\cos(\phi_A)\sin(\theta_A), \qquad a_y^{(pf)} = -\mathcal{P}_A\bar{\mathcal{P}}_B\sqrt{\mathcal{N}_{pf}^{PT}}\sin(\phi_A)\sin(\theta_A),\\
a_z^{(pf)} = \mathcal{P}_A\bar{\mathcal{P}}_B\cos(\theta_A).\\
b_x^{(pf)} = \mathcal{P}_B\bar{\mathcal{P}}_A\sqrt{\mathcal{N}_{pf}^{PT}}\cos(\phi_B)\sin(\theta_B), \qquad b_y^{(pf)} = -\mathcal{P}_B\bar{\mathcal{P}}_A\sqrt{\mathcal{N}_{pf}^{PT}}\cos(\phi_B)\sin(\theta_B),\\
b_z^{(pf)} = \mathcal{P}_B\bar{\mathcal{P}}_A\cos(\theta_B).
\end{gathered} \tag{III.60}$$

The Fidelities of teleported states are given by:

$$\begin{aligned}
f^{A\rightarrow B} &= \frac{\mathcal{P}_A\bar{\mathcal{P}}_B}{2}((1+\sqrt{\mathcal{N}_{pf}^{PT}}) + (1-\sqrt{\mathcal{N}_{pf}^{PT}})\cos(\theta_A)^2) + \frac{1-\mathcal{P}_A\bar{\mathcal{P}}_B}{2},\\
f^{B\rightarrow A} &= \frac{\mathcal{P}_B\bar{\mathcal{P}}_A}{2}((1+\sqrt{\mathcal{N}_{pf}^{PT}}) + (1-\sqrt{\mathcal{N}_{pf}^{PT}})\cos(\theta_B)^2) + \frac{1-\mathcal{P}_B\bar{\mathcal{P}}_A}{2}.
\end{aligned} \tag{III.61}$$

III.4.3 Depolarizing channel

This type of noise brings any density matrix to the completely depolarized state with probability p_i ($i = 1,2,3$), i.e, replaces it with a completely mixed state $\frac{1}{2}\hat{I}$. However, with the probability p_0, it is left untouched [77]. The noise is uncorrelated and specified by the Kraus operators:

$$\begin{aligned}
\mathcal{K}_{00}^u &= p_0\hat{\mathcal{I}}\otimes\hat{\mathcal{I}}; \quad \mathcal{K}_{01}^u = \sqrt{p_0p_1}\hat{\mathcal{I}}\otimes\sigma_x; \quad \mathcal{K}_{02}^u = \sqrt{p_0p_2}\hat{\mathcal{I}}\otimes\sigma_y; \quad \mathcal{K}_{03}^u = \sqrt{p_0p_3}\hat{\mathcal{I}}\otimes\sigma_z;\\
\mathcal{K}_{10}^u &= \sqrt{p_0p_1}\sigma_x\otimes\hat{\mathcal{I}}; \quad \mathcal{K}_{11}^u = p_1\sigma_x\otimes\sigma_x; \quad E_{12}^u = \sqrt{p_1p_2}\sigma_x\otimes\sigma_y; \quad \mathcal{K}_{13}^u = \sqrt{p_1p_3}\sigma_x\otimes\sigma_z;\\
\mathcal{K}_{20}^u &= \sqrt{p_0p_2}\sigma_y\otimes\hat{\mathcal{I}}; \quad \mathcal{K}_{21}^u = \sqrt{p_1p_2}\sigma_y\otimes\sigma_x; \quad \mathcal{K}_{22}^u = p_2\sigma_y\otimes\sigma_y; \quad E_{23}^u = \sqrt{p_2p_3}\sigma_y\otimes\sigma_z;\\
\mathcal{K}_{30}^u &= \sqrt{p_0p_3}\sigma_z\otimes\hat{\mathcal{I}}; \quad \mathcal{K}_{31}^u = \sqrt{p_1p_3}\sigma_z\otimes\sigma_x; \quad E_{32}^u = \sqrt{p_2p_3}\sigma_z\otimes\sigma_y; \quad \mathcal{K}_{33}^u = p_3\sigma_z\otimes\sigma_z;
\end{aligned}$$

$$\mathcal{K}_{00}^c = \sqrt{p_0}\hat{\mathcal{I}}\otimes\hat{\mathcal{I}}; \quad \mathcal{K}_{11}^c = \sqrt{p_1}\sigma_x\otimes\sigma_x; \quad \mathcal{K}_{22}^c = \sqrt{p_2}\sigma_y\otimes\sigma_y; \quad \mathcal{K}_{33}^c = \sqrt{p_3}\sigma_z\otimes\sigma_z, \tag{III.62}$$

with $p_0 = 1-\mathbf{p}$, $p_i = \frac{\mathbf{p}}{3}$ ($i = 1,2,3$) and $\mathbf{p}\in[0,1]$ is the decoherence factor. Then, By replacing the Kraus operators given in the above equations, and the state Eq. (III.62) in the channel Eq. (III.45), the quantum channel of the BQT under correlated depolarizing noise could be obtained as:

$$\hat{\varrho}_{AB}^{Dep} = \frac{1}{4}\begin{pmatrix} 2-\eta & 0 & 0 & 2-2\eta\\ 0 & \eta & 0 & 0\\ 0 & 0 & \eta & 0\\ 2-2\eta & 0 & 0 & 2-\eta \end{pmatrix}, \tag{III.63}$$

where: $\eta = \frac{8(1-\nu)(3\mathbf{p}-2\mathbf{p}^2)}{9}$. The amount of entanglement is given as,

$$\mathcal{N}_{Dep}^{(PT)} = 1 - \frac{4}{3}(1-\nu)(3\mathbf{p} - 2\mathbf{p}^2). \tag{III.64}$$

Similarly, after applying the bidirectional teleportation protocol, the users will get the states,

$$\hat{\varrho}_A^{Dep} = \frac{1}{2}\Big(\hat{I} + \sum_{i=1}^{x,y,z} a_i^{(Dep)}\hat{\sigma}_i\Big), \quad \hat{\varrho}_B^{Dep} = \frac{1}{2}\Big(\hat{I} + \sum_{i=1}^{x,y,z} b_i^{(Dep)}\hat{\tau}_i\Big) \tag{III.65}$$

where,

$$\begin{aligned}
a_x^{(Dep)} &= \mathcal{P}_A\bar{\mathcal{P}}_B\cos(\phi_A)\sin(\theta_A)\Big(1 - \frac{1-\mathcal{N}_{Dep}^{PT}}{3}\Big), \quad a_z^{(Dep)} = \mathcal{P}_A\bar{\mathcal{P}}_B\cos(\theta_A)\Big(1 - \frac{1-\mathcal{N}_{Dep}^{PT}}{3}\Big);\\
a_y^{(Dep)} &= -\mathcal{P}_A\bar{\mathcal{P}}_B\sin(\phi_A)\sin(\theta_A)\Big(1 - \frac{1-\mathcal{N}_{Dep}^{PT}}{3}\Big),\\
b_x^{(Dep)} &= \mathcal{P}_B\bar{\mathcal{P}}_A\cos(\phi_B)\sin(\theta_B)\Big(1 - \frac{1-\mathcal{N}_{Dep}^{PT}}{3}\Big), \quad b_z^{(Dep)} = \mathcal{P}_B\bar{\mathcal{P}}_A\cos(\theta_B)\Big(1 - \frac{1-\mathcal{N}_{Dep}^{PT}}{3}\Big).\\
b_y^{(Dep)} &= -\mathcal{P}_B\bar{\mathcal{P}}_A\cos(\phi_B)\sin(\theta_B)\Big(1 - \frac{1-\mathcal{N}_{Dep}^{PT}}{3}\Big).
\end{aligned} \tag{III.66}$$

The expressions of the teleportation fidelities are given as follows:

$$\begin{aligned}
f^{A\to B} &= \frac{\mathcal{P}_A\bar{\mathcal{P}}_B}{3}(2 + \mathcal{N}_{Dep}^{PT}) + \frac{1-\mathcal{P}_A\bar{\mathcal{P}}_B}{2};\\
f^{B\to A} &= \frac{\mathcal{P}_B\bar{\mathcal{P}}_A}{3}(2 + \mathcal{N}_{Dep}^{PT}) + \frac{1-\mathcal{P}_B\bar{\mathcal{P}}_A}{2}.
\end{aligned} \tag{III.67}$$

III.4.4 Amplitude damping channel

The amplitude damping channel (ADC) describes a general energy dissipation process between qubit system and environment [77]. ADC is a widely discussed model for various realistic physical evolution. From the Kraus operators, we can represent the correlated amplitude damping channel [234] is given as:

$$\mathcal{K}_{00}^{Ad} = |00\rangle\langle 00| + |01\rangle\langle 01| + |10\rangle\langle 10| + \sqrt{1-\mathbf{p}}\,|11\rangle\langle 11|, \quad \mathcal{K}_{11}^{Ad} = \sqrt{\mathbf{p}}\,|00\rangle\langle 11| \tag{III.68}$$

Then, By replacing the Kraus operators Eq. (III.68) in the channel Eq. (III.45), the quantum channel of the BQT under correlated Amplitude damping noise could be obtained as:

$$\hat{\varrho}_{AB}^{ADC} = \frac{1}{2}\begin{pmatrix} (1+\mathbf{p}^2)(1-\nu) + \nu(1+\mathbf{p}) & 0 & 0 & \frac{C}{\mathbf{p}} + \nu\sqrt{1-\mathbf{p}} \\ 0 & C & 0 & 0 \\ 0 & 0 & C & 0 \\ \frac{C}{\mathbf{p}} + \nu\sqrt{1-\mathbf{p}} & 0 & 0 & (1-\nu)(1-\mathbf{p})^2 + \nu(1-\mathbf{p}), \end{pmatrix} \tag{III.69}$$

with: $C = \mathbf{p}(1-\mathbf{p})(1-\nu)$. Similarly, the amount of entanglement of the output state $\hat{\varrho}_{AB}^{ADC}$, is given by:

$$\mathcal{N}_{ADC}^{(PT)} = (1-\mathbf{p})^2(1-\nu) + \nu\sqrt{1-\mathbf{p}}. \tag{III.70}$$

Finally, the final teleported states by using the noise channel $\hat{\varrho}_{AB}^{ADC}$ are given by:

$$\hat{\varrho}_A^{ADC} = \frac{1}{2}\Big(1 + \sum_{i=1}^{x,y,z} a_i^{(ADC)}\sigma_i\Big), \quad \hat{\varrho}_B^{ADC} = \frac{1}{2}\Big(1 + \sum_{i=1}^{x,y,z} b_i^{(ADC)}\tau_i\Big), \tag{III.71}$$

where different coefficients,

$$\begin{aligned}
a_x^{(ADC)} &= \mathcal{P}_A\bar{\mathcal{P}}_B(\mathcal{N}_{ADC}^{PT} - (1-\nu)(\mathbf{p}^2-\mathbf{p}))\cos\phi_A \sin\Big(\theta_A\Big),\\
a_y^{(ADC)} &= -\mathcal{P}_A\bar{\mathcal{P}}_B(\mathcal{N}_{ADC}^{PT} - (1-\nu)(\mathbf{p}^2-\mathbf{p}))\sin\phi_A \sin\Big(\theta_A\Big),\\
a_z^{(ADC)} &= \mathcal{P}_A\bar{\mathcal{P}}_B\Big((\mathbf{D}-\mathbf{B})\cos\Big(\frac{\theta_A}{2}\Big)^2 + (\mathbf{B}-\mathbf{A})\sin\Big(\frac{\theta_A}{2}\Big)^2\Big) + \mathbf{p}(1-\mathcal{P}_A\bar{\mathcal{P}}_B);\\
b_x^{(ADC)} &= \mathcal{P}_B\bar{\mathcal{P}}_A(\mathcal{N}_{ADC}^{PT} - (1-\nu)(\mathbf{p}^2-\mathbf{p}))\cos\phi_B \sin\Big(\theta_B\Big),\\
b_y^{(ADC)} &= -\mathcal{P}_B\bar{\mathcal{P}}_A(\mathcal{N}_{ADC}^{PT} - (1-\nu)(\mathbf{p}^2-\mathbf{p}))\sin\phi_B \sin\Big(\theta_B\Big);\\
b_z^{(ADC)} &= \mathcal{P}_B\bar{\mathcal{P}}_A\Big((\mathbf{D}-\mathbf{B})\cos\Big(\frac{\theta_B}{2}\Big)^2 + (\mathbf{B}-\mathbf{A})\sin\Big(\frac{\theta_B}{2}\Big)^2\Big) + \mathbf{p}(1-\mathcal{P}_B\bar{\mathcal{P}}_A),
\end{aligned} \tag{III.72}$$

and

$$\begin{aligned}
\mathbf{A} &= (1+\mathbf{p}^2)(1-\nu) + \nu(1+\mathbf{p}); \qquad \mathbf{B} = \mathbf{p}(1-\mathbf{p})(1-\nu);\\
\mathbf{D} &= (1-\nu)(1-\mathbf{p})^2 + \nu(1-\mathbf{p}); \qquad \mathbf{T} = (1-\mathbf{p})(1-\nu) + \nu\sqrt{1-\mathbf{p}}.
\end{aligned} \tag{III.73}$$

The expression of the teleportation Fidelities of are given as follows:

$$\begin{aligned}
f^{A\to B} &= \mathcal{P}_A\bar{\mathcal{P}}_B\big(\chi\sin(\theta_A)^2 + \delta\cos\Big(\frac{\theta_A}{2}\Big)^4 + \eta\sin\Big(\frac{\theta_A}{2}\Big)^4\big) + \frac{1-\mathcal{P}_A\bar{\mathcal{P}}_B}{2}(1+\mathbf{p}\cos(\theta_A));\\
f^{B\to A} &= \mathcal{P}_B\bar{\mathcal{P}}_A\big(\chi\sin(\theta_B)^2 + \delta\cos\Big(\frac{\theta_B}{2}\Big)^4 + \eta\sin\Big(\frac{\theta_B}{2}\Big)^4\big) + \frac{1-\mathcal{P}_B\bar{\mathcal{P}}_A}{2}(1+\mathbf{p}\cos(\theta_B)),
\end{aligned} \tag{III.74}$$

with different elements are presented as

$$\begin{aligned}
\chi = \mathcal{N}_{ADC}^{PT} - (1-\nu)(2\mathbf{p}^2 - 2\mathbf{p}); \qquad \delta = \mathcal{N}_{ADC}^{PT} + \nu(1-\mathbf{p}-\sqrt{1-\mathbf{p}});\\
\eta = \mathcal{N}_{ADC}^{PT} + (\nu + 2\mathbf{p} - \nu\sqrt{1-\mathbf{p}}).
\end{aligned} \tag{III.75}$$

III.4.5 The correlated noise effect on Entanglement

In this section, we display the negativity of the partially transposed density operator in order to show the amount of entanglement remaining in the quantum channel of the BQT. Also, the effect of the different noise correlations on this amount of entanglement.

Fig. (III.12) shows the behavior of the negativity $\mathcal{N}^{(PT)}$ of the bidirectional teleported states in the presence of correlated and non-correlated noise. As shown in Fig. (III.12a), the noisy channels are assumed to be uncorrelated, the entanglement is greatest at $\mathbf{p} = 0$. However, due to the decoherence caused by the noisy channels, the quantum channel of BQT loses its entanglement, where the negativity $\mathcal{N}^{(PT)}$ decreases as the channels' noise strengths increase. The decreasing rate depends on the type of the noisy channel, where the sudden decay of the entanglement is predicted for the depolarizing channel, while the gradual decay is displayed for the amplitude damping channel. Moreover, for the bit-flip channel and the phase-flip channels, the minimum value of the entanglement ($\mathcal{N}^{(PT)} = 0$) is depicted at $\mathbf{p} = 0.5$. As one increases the channel strength, the entanglement increases gradually to reach its maximum value at $\mathbf{p} = 1$. In this

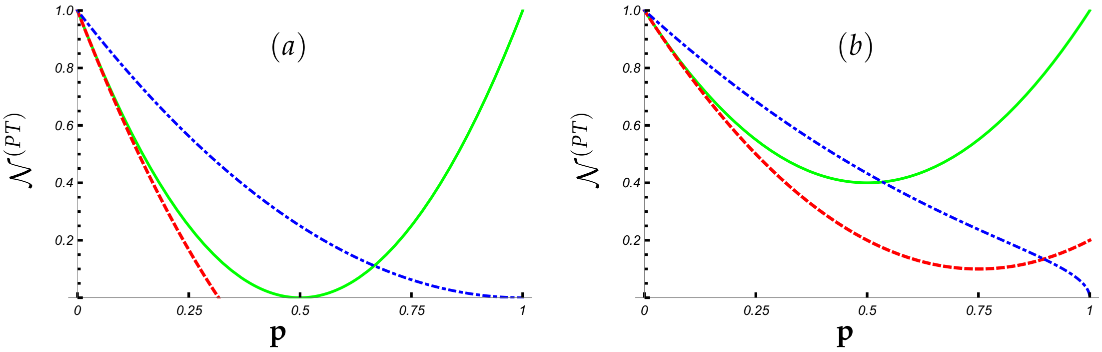

FIGURE III.12: Behavior of entanglement $\mathcal{N}^{(PT)}(p)$ in the presence of different noisy channels. The solid green, dashed red, and dot-dashed blue lines, correspond to, bit-flip and phase flip channels, depolarizing channels, and amplitude damping channel, respectively. For (a): uncorrelated channels ($\nu = 0$). (b): ($\nu = 0.4$)

context, it is worth mentioning that the vanishing entanglement is displayed at different strengths of the used channels, where the phase-flip and bit-flip channels are more robust than the other channels. The effect of the correlated noisy channels is depicted in Fig. (III.12b), where we set the channel parameter $\nu = 0.4$ to a non-zero value. The behavior of the entanglement is similar, where $\mathcal{N}^{(PT)}$ decreases as the channel strength increases. Moreover, the phenomena of the sudden decay disappear, where the entanglement survives at any value of the channel strength, only the amplitude damping channel vanishes at $\mathbf{p} = 1$. This result shows that the correlated noise channels improve the entanglement of the quantum channel of BQT, where the minus values of the negativity are always larger than those shown in Fig. (III.12a).

III.4.6 Bidirectional teleportation quantifiers

Let us now investigate the BQT of the quantum states. When the quantum channel of the BQT protocol is subjected to different correlated noisy channels, we use the expressions of the teleportation fidelities from Alice to Bob and from Bob to Alice to evaluate the average fidelities.

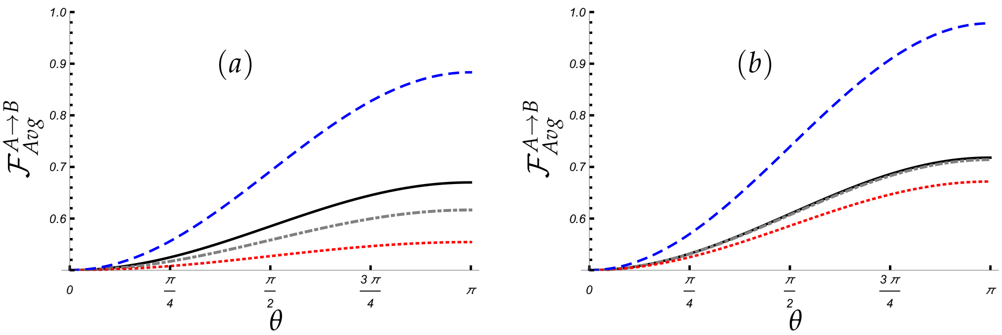

FIGURE III.13: The θ dependency of $\mathcal{F}^{A\to B}_{Avg}$ for the different types on noise. The solid Black, Dot-dashed Gray, dashed Blue, and dotted red lines, correspond to Bit flip, Phase flip, depolarizing, and amplitude damping channels, respectively. we set for, $p = 0.4$, and (a): $\nu = 0$, (b): $\nu = 0.6$.

From Fig. (III.13) and Fig. (III.14), we show the behavior of the average fidelities of teleportation from Alice to Bob and from Bob to Alice, namely $\mathcal{F}^{A\to B}_{Avg}$ and $\mathcal{F}^{B\to A}_{Avg}$, respectively. In this figures, we assume that Alice's trigger qubit is prepared in the state with weight $\tilde{\theta}_A = \pi$ and Bob's trigger qubit with weight $\tilde{\theta}_B = 0$. We can see that as shown in Fig. (III.13.a), the averaged fidelity $\mathcal{F}^{A\to B}_{Avg}$ could reach its maximum when Alice's trigger qubit and the initial state are prepared in the same polarization. However, it is clear from the Fig. (III.13.b) that $\mathcal{F}^{A\to B}_{Avg}$ increases if the correlation strength of channels increases. On the

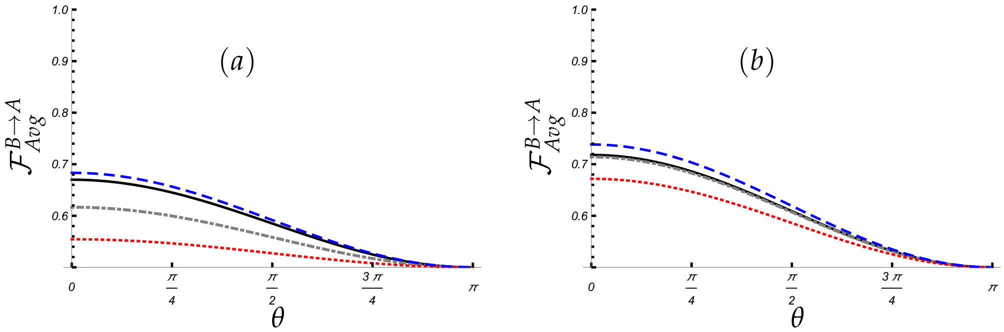

FIGURE III.14: The θ dependence of $\mathcal{F}_{Avg}^{B\to A}$ for the different types on noise. The solid Black, Dot-dashed Gray, dashed Blue, and dotted red lines, correspond to Bit flip, Phase flip, depolarizing, and amplitude damping channels, respectively. we set for, $p = 0.4$, and (a): $\nu = 0$ (b): $\nu = 0.6$.

other hand, Fig. (III.14) displays the behavior of the averaged fidelity of teleportation from Bob to Alice, namely$\mathcal{F}_{Avg}^{B\to A}$, where we assume that Bob's trigger is prepared with weight angle $\tilde{\theta}_B = 0$ and Alice's trigger with $\tilde{\theta}_A = \pi$. Clearly, from this plot, one can note that the average fidelity is minimum if Bob's trigger qubit and the initial state are prepared in totally different weight angles, namely, $\tilde{\theta}_B = 0$ and $\theta = \pi$. Besides, the averaged fidelity reach the maximum value when Bob's trigger qubit and the initial state are prepared in the same polarization direction, namely $\tilde{\theta}_B = 0$ and $\theta = 0$. However, we note that the averaged fidelity increases if the correlation strength of the noisy channels, bit-flip, phase-flip, depolarizing, and amplitude damping channel, increase.

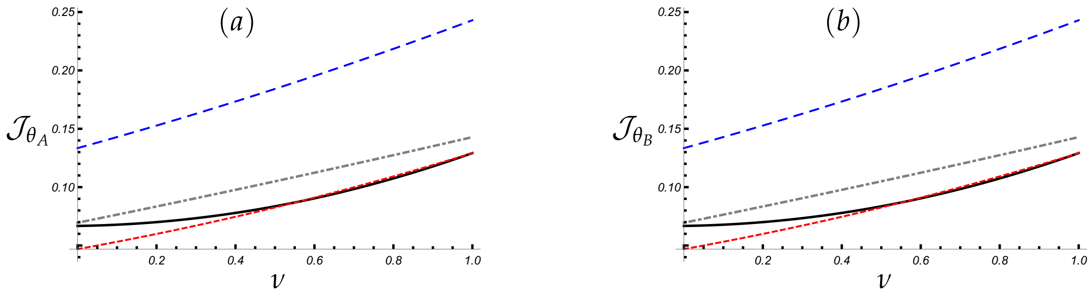

FIGURE III.15: The ν dependency of $\mathcal{J}_\theta$ for different noisy channel with $p = 0.3$. The solid Black, dashed green, dot-dashed blue, and dashed red lines, correspond to bit and phase flip channel, amplitude damping channel, and depolarizing channel, respectively. where we assume that, $\theta_A = \theta_B = \frac{\pi}{2}$ and $\phi_A = \phi_B = 0$ and $\tilde{\theta}_A = \pi$ and $\tilde{\theta}_B = 0$.

The behavior of the quantum Fisher information with respect to the weight parameters θ_A and θ_B, namely $\mathcal{J}_{\theta_A}$ and $\mathcal{J}_{\theta_B}$, versus the correlation strength of the noisy channels is depicted in Fig. (III.15); where we assume that Alice's trigger is prepared at $\tilde{\theta}_A = \pi$ and Bob's trigger qubit is prepared at $\tilde{\theta}_B = 0$. One can note that by increasing the correlation strength between successive actions of noisy channels, such as: bit-flip, phase-flip, depolarizing, and amplitude damping channels, the quantum Fisher information with respect to the weight parameter could notably be enhanced.

In Fig. (III.16), we display the behavior of the quantum Fisher information of the weight parameter, $\mathcal{J}_{\theta_i}$; where the sender's weight trigger is set to $\tilde{\theta}_i = \pi$ and the receiver's weight trigger is set to 0. Moreover, we assume that the initial states are prepared with $\theta_A = \theta_B = \theta$ and $\phi_A = \phi_B = 0$. As displayed in Fig. (III.16.a) and Fig. (III.16.b), the existence of correlations in the noisy channels enhances the estimation of the teleported weight parameter.

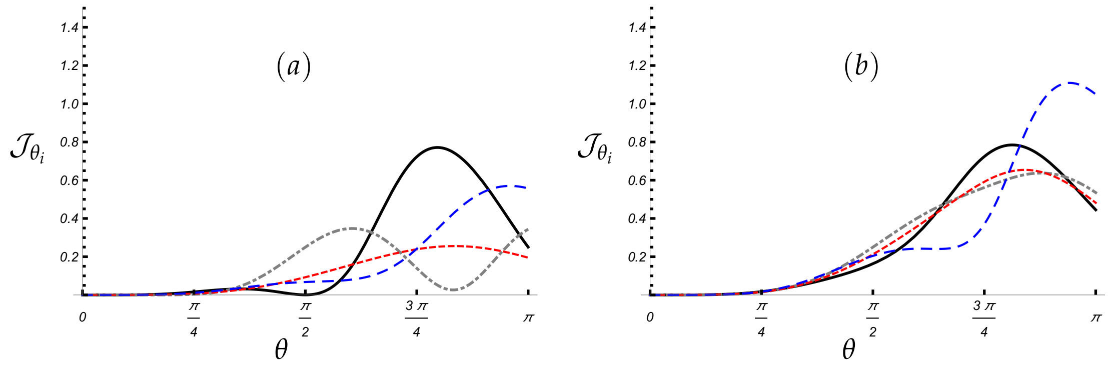

FIGURE III.16: Behavior of Fisher information with respect to the weight θ_i, namely $\mathcal{J}_\theta(\theta)$ (with i= Alice or Bob), in the presence of different noisy channels. The solid Black, Dot-dashed Gray, Dotted red, and Dashed Blue lines, correspond to, bit-flip and phase flip channels, depolarizing channels, and amplitude damping channel, respectively. For (a): uncorrelated channels ($\nu = 0$). (b): ($\nu = 0.8$)

In this section, we are interested in the effects of the noise correlations on the bidirectional teleportation of the quantum states between two legitimate partners, Alice and Bob. We have discussed the entanglement of the quantum channel of the bidirectional teleportation protocol through the negative partially transposed $\mathcal{N}^{PT}$ measure, under different noisy channels, such as the bit flip, phase flip, depolarizing, and amplitude damping channels. The $\mathcal{N}^{PT}$ depends on the noise factors and the correlation strengths between the successive actions of noise channels. However, it is shown that $\mathcal{N}^{PT}$ is increased when we take into account the correlations between noise actions for the bit-flip,phase-flip, depolarizing, and amplitude damping channels. Also, we have investigated the average fidelity of bidirectional teleportation and the quantum Fisher information with respect to the weight parameters. Analytical forms of the teleportation fidelities from one side to the other one, $f^{in\rightarrow out}$, and Fisher information $\mathcal{J}_{\theta_i}$ are obtained for the correlated bit-flip, phase-flip, depolarizing, and amplitude damping channels. Furthermore, the expressions of the averaged teleportation fidelities, and the quantum Fisher information depend on the noise factor, the correlation strength of the noise channel, and also on the trigger qubits and the initial state settings. It is shown that the maximum/minimum teleportation of information and the estimation of the weight parameter depend on the initial states of the triggers; where the maximization is achieved if the sender's trigger qubit and the initial qubits are initially prepared in the same direction. However, the effect of the noise that decreases both quantities dramatically could be tackled in a small range of time by exploiting the correlation between successive actions of the noise channel. In the following, we will investigate the effects of non-Markovianity on the BQT and the combined effect of the non-Markovianity and the correlated channel on the BQT.

III.5 BQT and non-Markovianity

Now, we investigate the effects of the combined memory types on the bidirectional quantum teleportation, where the quantum channel of the BQT is distributed by typical correlated decoherence channels, namely a dephasing channel and an amplitude damping channel. We show that the entanglement of the quantum channel of the BQT, the teleportation fidelities and quantum Fisher information could be enhanced further by taking into account the classical correlations between successive actions of the decoherence channels in a non-Markovian regime, compared with the classical correlations in the markovian regime of these decoherence channels.

III.5.1 Non-Markovian models

Now, to explore the **p** dependence on time, *Daffer et al.* [237] presented a colored dephasing model, where $\mathbf{p}_D$ could explicitly depend on time. This model describes the time evolution of a single qubit through the Hamiltonian $\hat{H}(t) = \alpha\hbar\beta(t)\hat{\sigma}_z$, where α is a coin-flip random variable with possible values ± 1. The random variable $\beta(t)$ has a Poisson distribution with a mean equal to $\frac{t}{2\tau}$. The decoherence factor can be given as[237]:

$$\mathbf{p}(t)_D = \frac{1-\gamma(t)}{2}, \tag{III.76}$$

where

$$\gamma(t) = e^{-\nu}\Big(\cosh(Ur) + \frac{1}{U}\sinh(Ur)\Big), \tag{III.77}$$

with $U = \sqrt{1-16\tau^2}$, and $r = \frac{t}{2\tau}$ is a dimensionless time. The parameter τ controls the degree of the non-Markovianity of the dephasing process, where $\tau < 0.25$ corresponds to the Markovian regime. However, $\tau > 0.25$ corresponds to the non-Markovian regime.

A well studied model that describes the interaction of two qubits, each one interacting only and independently with its local environment formed by the quantized modes of a high-Q cavity. The Hamiltonian describing the system is given as [238]:

$$\hat{H} = \omega_0\sigma_+\sigma_- + \sum_k \omega_k r_k^\dagger r_k + (\sigma_+ B + \sigma_- B^\dagger), \tag{III.78}$$

with $B = \sum_k g_k r_k$, where ω_0 is the transition frequency of the two-level qubit and $\sigma_\pm$ are the lowering and raising operators and k stands for the field modes of the reservoir with frequencies ω_k. $r_k, r_k^\dagger$ are the creation and annihilation mode operators, and g_k are the coupling constants. Indeed, two coupling regime can be distinguished; namely weak and strong regimes. In the case of a weak regime, the relaxation time is greater than the reservoir correlation time $\gamma < \Gamma/2$, $\tau_R > 2\tau_B$. The decoherence factor is given as follows [1],

$$\mathbf{p}(t)_A = e^{-\Gamma t}\Big(\cosh\Big(\frac{dt}{2}\Big) + \frac{\Gamma}{d}\sinh\Big(\frac{dt}{2}\Big)\Big)^2 \tag{III.79}$$

whereas, $d = i\sqrt{2\gamma\Gamma - \Gamma^2}$. Γ depends on the reservoir correlation time $\tau_r \approx \Gamma^{-1}$ and γ is the coupling strength related to qubit relaxation time $\tau_q \approx \gamma^{-1}$.

Besides, in the strong coupling regime, for $\gamma > \Gamma/2$, $\tau_R < 2\tau_B$, the large reservoir correlation time is greater or of the same order of the relaxation time. Consequently, the non-Markovian effects become important. The decoherence factor in the strong coupling regime can be obtained by substituting the hyperbolic functions with the corresponding harmonic ones and $d = \sqrt{2\gamma\Gamma - \Gamma^2}$ in Eq.(III.79).

III.5.2 BQT under dephasing noise

Supposing that the bidirectional teleportation quantum channel is distributed through a dephasing channel. Then, by replacing the decoherence factor **p** in the expression of the negativity of the partial transpose (in Eq. III.58), and in the fidelity averaged (in Eq. III.61) and the quantum Fisher information, we display the behavior of these three quantities in the following figures.

Fig. (III.17) depicts the negativity, fidelity averaged from the sender (denoted by "*in*") to the receiver (denoted by "*out*"), and quantum Fisher information of the parameter "θ_i", where "$i = A$" or "B", namely $\mathcal{N}_D^{(PT)}$, $\mathcal{F}_{Avg}^{in\to out}$ and $\mathcal{J}_{\theta_i}$ versus time in the Markovian regime. In this case, we consider $\tau = 0.1$, with U equal to $1-\tau$, where $U \approx 1-\tau$. The three quantities are decreasing monotonically with the flow of time

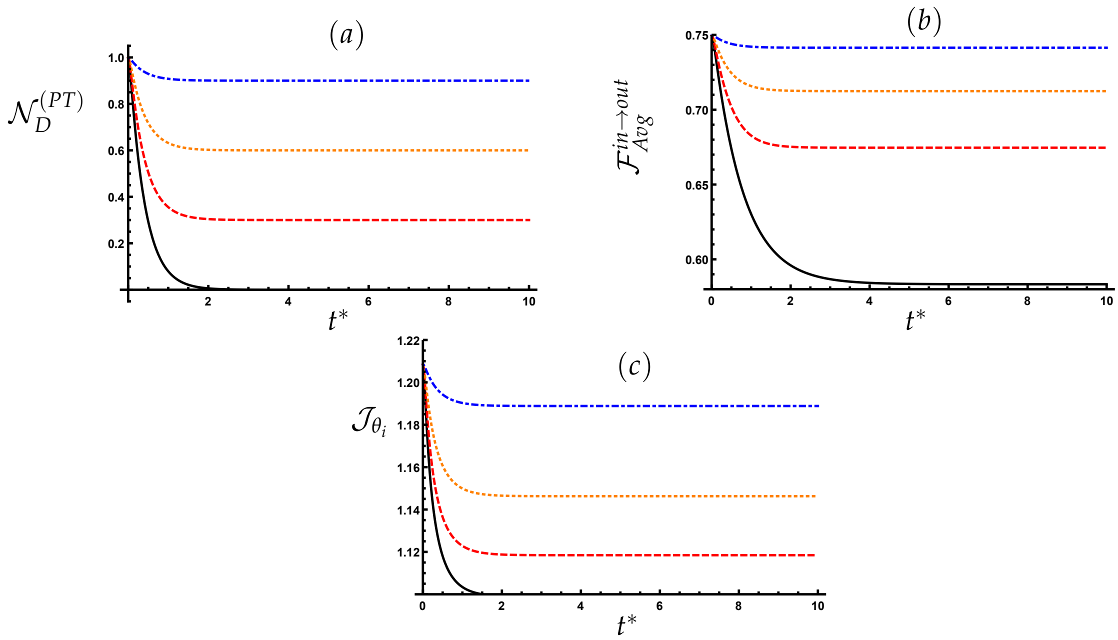

FIGURE III.17: $\mathcal{N}_D^{(PT)}$, $\mathcal{F}_{Avg}^{in\to out}$ and $\mathcal{J}_{\theta_i}$ for $i = A, B$, versus the re-scaled time $t^* = \frac{t}{\pi}$ for the phase flip channel in Markovian regime with $\tau = 0.1$. The solid black, Red dashed, Orange dotted and blue dashdotted correspond to $\nu = 0, 0.3, 0.6,$ and 0.9, respectively.

t. By increasing the correlation factor ν, the three quantities could be increased and reach their asymptotic values, $\mathcal{N}_D^{(PT)} \approx \nu$, $\mathcal{F}_{Avg}^{in\to out} \approx \frac{\nu}{n} + 0.5$ where $n = 1, 2, 3, 4.$ and $\mathcal{J}_{\theta_A} = 0.8 + \nu$.

In Fig. III.18, we present the behavior of the negativity, fidelity averaged and the quantum Fisher information of the parameter θ, namely $\mathcal{N}_D^{(PT)}$, $\mathcal{F}_{Avg}^{in\to out}$ and $\mathcal{J}_{\theta_i}$, with $i = A, B$ versus time in the non-Markovian regime of the colored dephasing channel, where we set $\tau > 0.25$. It is clear from these figures that the behavior of the three quantities show damped oscillations. If $\tau > 0.25$, then we get $|U| \approx 4\tau$, and $\mathbf{p}(t)_D = (1 - e^{-\frac{t}{2\tau}} \cos(2t))/2$. it is clear from the figure that $T = 0.5\pi$ is the oscillations period. At the instants $t = n(T)$ with $n \in \mathbb{N}$ the negativity, the averaged fidelity and QFI reach their maximum values. These maximum values decrease with time. However, at instants $t = m\frac{T}{2}$ where $m \in \mathbb{N}^*$, the three quantities, namely $\mathcal{N}_D^{(PT)}$, $\mathcal{F}_{Avg}^{in\to out}$ and $\mathcal{J}_{\theta_i}$ decrease to their minimum values, u, $\frac{\nu}{n} + 0.5$, $0.8 + \nu$, respectively. Hence, the exploitation of the combined effects of memory: the classical correlations between successive action of the dephasing channel and the non-Markovianity could enhance further the amount of entanglement remaining in qubits of the quantum channel which is distributed by a dephazing channel, and the teleportation of information bidirectionally.

III.5.3 BQT under amplitude damping

Fig. (III.19) depicts the behavior of the negativity, average fidelities and quantum Fisher information for the parameter θ, namely $\mathcal{N}_{ADC}^{(PT)}$, $\mathcal{F}_{Avg}^{in\to out}$ and $\mathcal{J}_{\theta_i}$, in the Markovian regime of the amplitude damping channel, with $\gamma < \Gamma/2$, and $d = -\Gamma$. As shown in these figures, the three quantities are decreasing monotonically with time and frozen at values of $0, 0.34$ and 0, respectively. However, by exploiting the correlation between the channel's actions, one can slightly increase the three quantities, where the three quantities, $\mathcal{N}_{ADC}^{(PT)}$, $\mathcal{F}_{Avg}^{in\to out}$ and $\mathcal{J}_{\theta_i}$ are frozen with values $0, 0.3 + \frac{\nu}{2n}$ and 0, respectively, where $i = 1, 2, 3, 4$.

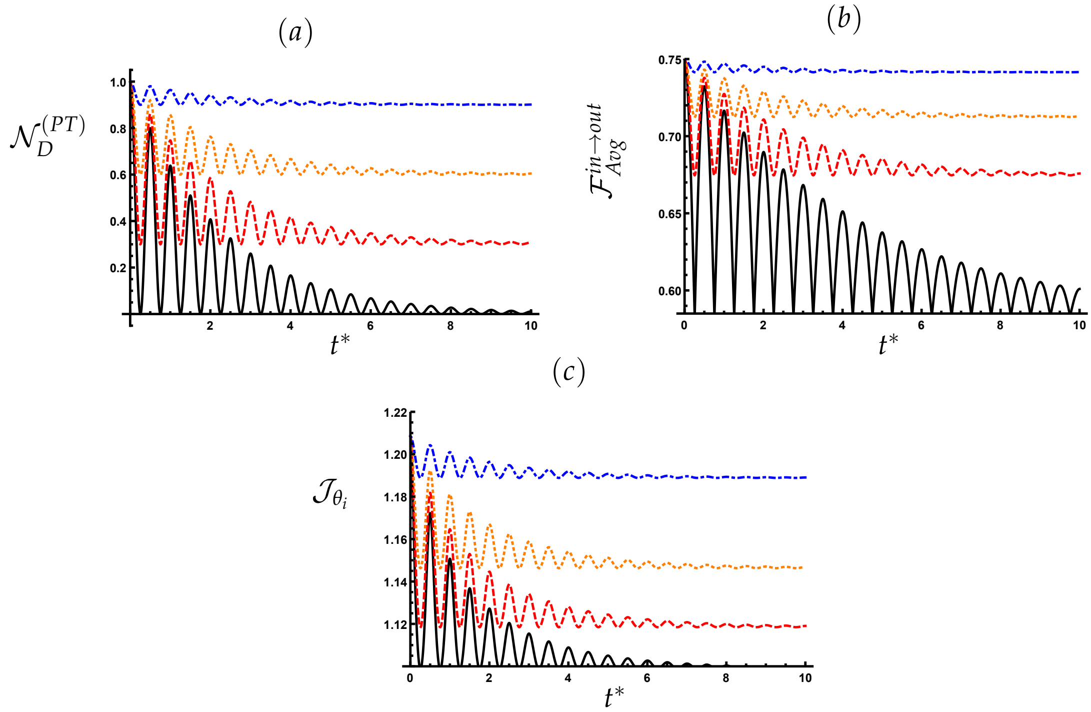

FIGURE III.18: Same as in Figure 2, but in the non-Markovian regime with $\tau = 7$.

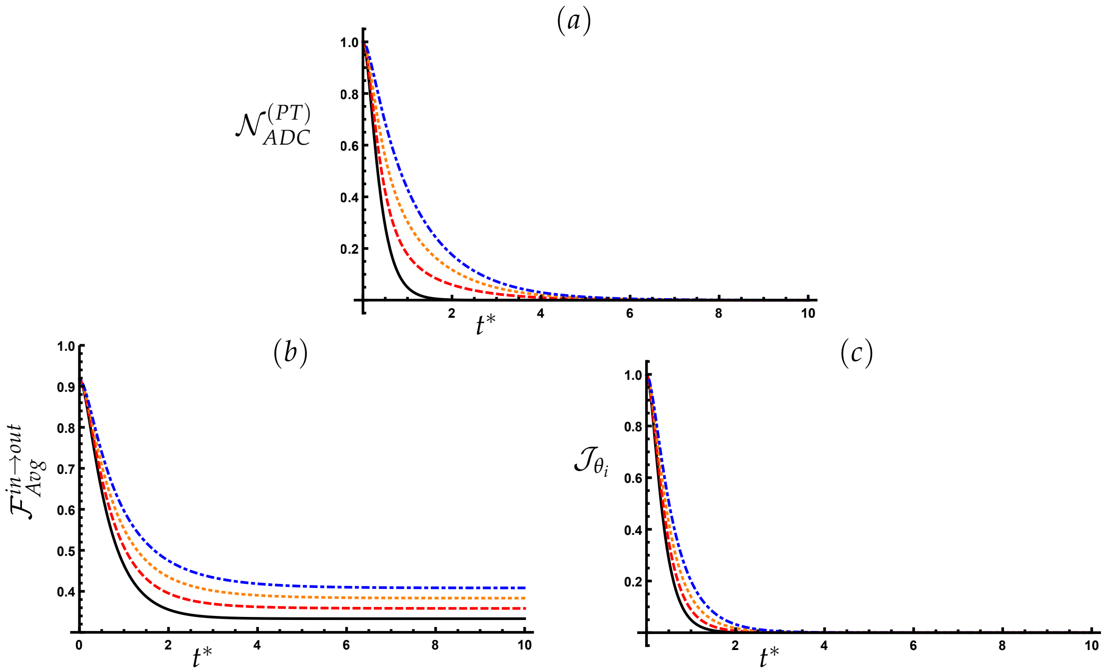

FIGURE III.19: Negativity, Fidelity averaged, and quantum Fisher information under Amplitude damping channel versus the re-scaled time in the Markovian regime ($\Gamma = 5\gamma$). The solid black, red dashed, orange dotted and bue dotdashed correspond to $\nu = 0, 0.3, 0.6$, and 0.9, respectively. We set here $\theta_A = \theta_B = 0$ and $\tilde{\theta}_A = 0, \tilde{\theta}_B = \pi$.

In Fig III.20 depicts the behavior of the negativity, fidelity averaged and the quantum Fisher information for the parameter θ, namely $\mathcal{N}_{ADC}^{(PT)}$, $\mathcal{F}_{Avg}^{in\to out}$ and $\mathcal{J}_{\theta_i}$ in the non-Markovian regime of the colored amplitude damping channel; when $\gamma > \Gamma/2$ and $d = \sqrt{2\gamma\Gamma}$, we have $\mathbf{p}(t)_A = e^{-\Gamma t}\cos(dt/2)^2$. Indeed,

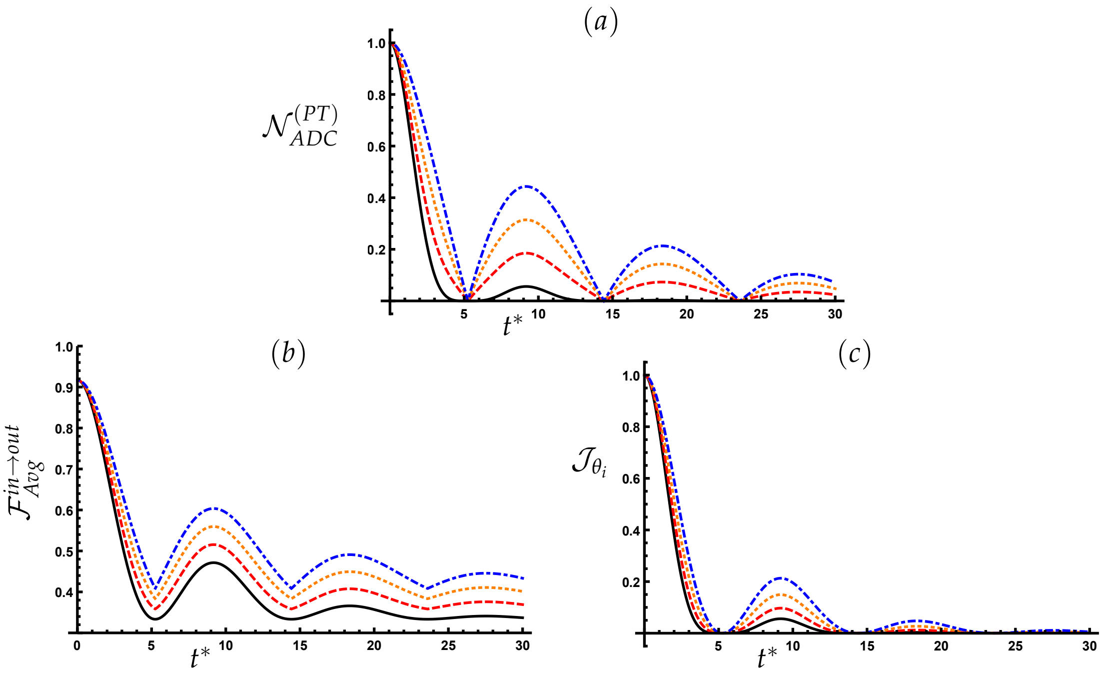

FIGURE III.20: Negativity, Fidelity averaged, and quantum Fisher information versus the re-scaled time in non-Markovian regime with $\Gamma = 0.1\gamma$. The solid black, red dashed, orange dotted and blue dotdashed correspond to $\nu = 0, 0.3, 0.6$, and 0.9, respectively. We set here $\theta_A = \theta_B = 0$ and $\tilde{\theta}_A = 0$, $\tilde{\theta}_B = \pi$.

the damped oscillations have a period $T = 9\pi$ of their evolution against time t. It is clear that the three quantities have maximum peaks at the instants of time $t = nT$ with $n \in \mathbb{N}$; these peaks decrease with time flow. Besides, at the instant time $t = n\frac{T}{2}$with $n \in \mathbb{N}^*$ the three quantities decrease to their minimum values $0, 0.3 + \frac{\nu}{2n}, 0$, respectively.

In general, we are interested in the combined memory effects, the channel correlation and the non-Markovianity of the channel, on the bidirectional quantum teleportation of single-qubit states between two parts, namely Alice and Bob. Firstly, we have investigated the entanglement of the quantum channel of the bidirectional teleportation protocol using the negative partially transposed measure $\mathcal{N}^{(PT)}$. We have derived $\mathcal{N}^{(PT)}$ of the quantum channel that is distributed through typical decoherence channels such as dephasing and amplitude damping channels. $\mathcal{N}^{(PT)}$ depends on the decoherence factor and the correlation strength of the channels. It is demonstrated that when the correlations between channel actions are considered, the value of $\mathcal{N}^{(PT)}$ increases. However, $\mathcal{N}^{(PT)}$ could be further enhanced by considering the correlations of the channel in the non-Markovian regime.

Also, we have investigated the average fidelities of the bidirectional teleportation and the Fisher information with respect to the weight parameters, θ_A and θ_B. The explicit forms of the fidelities of teleportation $f^{in\to out}$, and quantum Fisher information $\mathcal{J}_{\theta_i}$ (for $i = A, B$) are obtained for colored dephasing and amplitude damping channels. Furthermore, the expression of the teleportation fidelities and the quantum Fisher information depends on the amount of the survival entanglement of the quantum channel of the BQT and on the decoherence factor, correlation strength of the noise channel, and also on the trigger qubits and the initial state settings. It is shown that both quantities $\mathcal{F}_{Avg}^{in\to out}$ and $\mathcal{J}_{\theta_i}$ are decreasing monotonically in the course of the time evolution in the Markovian regime. However, by exploiting the correlation between the successive actions of the decoherence channel, one could slightly increase these quantities. We further discussed the effects of the channel correlations in the non-Markovian regime on the teleportation fidelities, and the quantum Fisher information. The result shows that, while they decrease monotonically with time in the Markovian regime, their strengths can be further enhanced due to the non-Markovian memory effect in a wide time range.

III.6 Conclusion

In this chapter, we are interested in the effect of the weak and reversed measurements on the quantum channel of the BQT. We assume for a realistic implementation that the quantum channel should be noisy, which we consider typical noise to model the noise channels that are frequently faced in real cases. We showed that the weak and reversed measurements could not mitigate the effect of the bit-flip, phase-flip, bit-phase flip and the depolarizing channel. However, the weak and the reversed measurements could only recover the entanglement if and only if the quantum channel is distributed over an amplitude damping channel. Furthermore, we evaluated the averaged fidelities and the quantum Fisher information to quantify the bidirectional quantum teleportation of information. We showed that the weak and the reversed measurements could improve the teleportation of the states and the parameters if the initial fidelities of this state are greater than 0.5, and the initial quantum Fisher information is non-null.

In addition, we investigated the effect of the noise correlation on the BQT. The exploitation of the noise correlations could protect the entanglement of the quantum channel. Moreover, the average fidelities and the quantum Fisher information with respect to the weight parameters could be noticeably enhanced by exploiting the noise correlations; by increasing the strength of the correlations of the noise channel and the partial transpose, the average fidelities of teleportation and the quantum Fisher information could be noticeably enhanced for a small range of time.

Nevertheless, by considering the interaction of the qubits and their environment in a non-Markovian fashion, the three quantities could be enhanced further for a long time range.

In the next chapter, we will extend the BQT protocol, we will suggest a new bidirectional teleportation protocol that allows the transmission of quantum information between three users.

Chapter IV

Bidirectional teleportation protocols

The reliable transfer of quantum information between multiple quantum devices is a focal step in the implementation of large scale quantum computing, communication processes, and the creation of quantum internet [239]. Therefore, the extension of the bidirectional teleportation process is an open challenge. Beside teleporting completely unknown states, it is possible to teleport entangled states and quantum operations. Although these results open up new possibilities for the transmission and the processing of qubits, but it is also useful for the realization of quantum repeaters [39].

In this chapter, we suggest a new three-party bidirectional quantum teleportation protocol which allows three legitimate partners to exchange their quantum states using a GHZ state as a quantum channel. We generalize this protocol to make the bidirectional quantum teleportation of states possible through a quantum network composed of N partners. Furthermore, we present a bidirectional non-local implementation of the $CNOT$ gate. The $CNOT$ gate is a universal quantum gate [77] frequently used in quantum processing protocols such as the quantum teleportation and quantum algorithm. Based on the latter scheme, we suggest a new scheme for the bidirectional quantum teleportation of generalized two-qubit, three-qubit and n-qubit states.

IV.1 Three-party bidirectional teleportation

We start by addressing the issue about the possibility to add a third direction of teleportation, by adding a third part called "*Charlie*" as a partner in the teleportation process discussed in Chapter II, by using a GHZ state as a quantum channel, three trigger qubits and classical communication channels (please see Fig. IV.1). Effectively, bidirectional teleportation can be assured between every two partners with the assistance of the third part. In the suggested teleportation scheme, the third part not only supervises the whole process but also could teleport and receive quantum states.

In this framework, let's assume that the users (Alice, Bob, and Charlie) share the GHZ state given as:

$$|GHZ_{A,B,C}\rangle = \frac{1}{\sqrt{2}}(|0_A 0_B 0_C\rangle + |1_A 1_B 1_C\rangle), \tag{IV.1}$$

where "A", "B" and "C" refer to Alice, Bob, and Charlie respectively. It is assumed that the users Alice, Bob and Charlie are given three different states, $|Q_A\rangle$, $|Q_B\rangle$ and $|Q_C\rangle$ to be teleported, where:

$$|Q_A\rangle \;=\; \cos\left(\frac{\theta_A}{2}\right)|0_A\rangle + e^{i\phi_A}\sin\left(\frac{\theta_A}{2}\right)|1_A\rangle\,, \quad |Q_B\rangle = \cos\left(\frac{\theta_B}{2}\right)|0_B\rangle + e^{i\phi_B}\sin\left(\frac{\theta_B}{2}\right)|1_B\rangle\,,$$

$$|Q_C\rangle \;=\; \cos\left(\frac{\theta_C}{2}\right)|0_C\rangle + e^{i\phi_C}\sin\left(\frac{\theta_C}{2}\right)|1_C\rangle\,. \tag{IV.2}$$

In the Bloch representation, the states Eqs. (IV.2) may be written as:

$$\hat{\varrho}_Q^{(A)} = \frac{1}{2}\Big(\hat{I} + \sum_{i=x,y,z} a_i \hat{\sigma}_i{}^{(A)}\Big),\ \hat{\varrho}_Q^{(B)} = \frac{1}{2}\Big(\hat{I} + \sum_{i=x,y,z} b_i \hat{\tau}_i{}^{(B)}\Big),\ \hat{\varrho}_Q^{(C)} = \frac{1}{2}\Big(\hat{I} + \sum_{i=x,y,z} c_i \hat{\gamma}_i{}^{(C)}\Big) \tag{IV.3}$$

where a_i, b_i and c_i (for $i = x, y, z$) are the Bloch vectors of Alice's, Bob's and Charlie's qubits, respectively. $\hat{\sigma}_i{}^A$, $\hat{\tau}_i{}^B$ and $\hat{\gamma}_i{}^C$ (for $i = x, y, z$), represent the Pauli operators of Alice's, Bob's and Charlie's qubits, respectively.

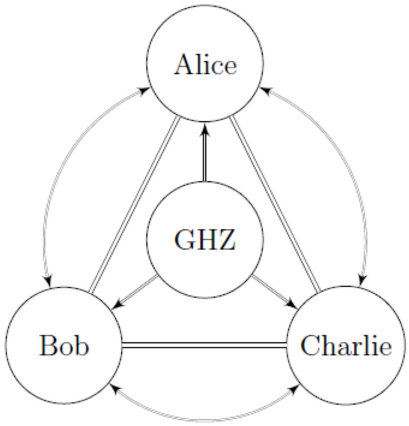

FIGURE IV.1: Alice − Bob and Charlie could exchange their states bilaterally by using a GHZ state together with local operations and classical communications *LOCC* (double line). Where the teleported state cannot be reconstructed by the receiver without the contribution of the other partners.

Furthermore, each user has three trigger qubits which they are defined initially as,

$$|T_A\rangle = \cos\Big(\frac{\tilde{\theta}_A}{2}\Big)|0_A\rangle + \sin\Big(\frac{\tilde{\theta}_A}{2}\Big)|1_A\rangle, \quad |T_B\rangle = \cos\Big(\frac{\tilde{\theta}_B}{2}\Big)|0_B\rangle + \sin\Big(\frac{\tilde{\theta}_B}{2}\Big)|1_B\rangle,$$

$$|T_C\rangle = \cos\Big(\frac{\tilde{\theta}_C}{2}\Big)|0_C\rangle + \sin\Big(\frac{\tilde{\theta}_C}{2}\Big)|1_C\rangle, \tag{IV.4}$$

Similarly, the triggers can be represented by their Bloch vectors as:

$$\hat{\varrho}_{T_A} = \frac{1}{2}\Big(\hat{I} + \sum_{i=x,y,z} t_i^{(A)} \hat{\sigma}_i{}^{(A)}\Big), \quad \hat{\varrho}_{T_B} = \frac{1}{2}\Big(\hat{I} + \sum_{i=x,y,z} t_i^{(B)} \hat{\tau}_i{}^{(B)}\Big), \quad \hat{\varrho}_{T_C} = \frac{1}{2}\Big(\hat{I} + \sum_{i=x,y,z} t_i^{(C)} \hat{\gamma}_i{}^{(C)}\Big) \tag{IV.5}$$

whereas $t_i^{(A)}$ $(t_i^{(B)})$ and $(t_i^{(C)})$ are the Bloch vectors of Alice's, Bob's and Charlie's trigger, respectively. Additionally, Alice is supplied by two storage qubits, $\left|S_A^{(1)}\right\rangle$ and $\left|S_A^{(2)}\right\rangle$. The same thing for Bob and Charlie, they are supplied by four storage qubits, two for Bob $(\left|S_B^{(1)}\right\rangle, \left|S_B^{(2)}\right\rangle)$ and two for Charlie $(\left|S_C^{(1)}\right\rangle, \left|S_C^{(2)}\right\rangle)$. It is assumed that, these qubits are initially prepared in a vacuum state, i.e., $\left|S_j^{(i)}\right\rangle = |0\rangle, i = 1, 2$ and $j = A, B, C$. These types of qubits are used as a storage of the projective measurement outcomes. All these types of qubits are described clearly in the circuit (please see Fig. (IV.2)). Indeed, the partners perform two types of quantum gates; the *CNOT* gate and the Toffoli gate $(CCNOT)$[169]. The

Toffoli gate flips the target qubit if, and only if, the two control qubits are in the state $|1\rangle$. In a generic form, one can write its effect as $CCNOT\,|abc\rangle = |ab, c \oplus a.b\rangle$. Where $\oplus$ is the addition modulo 2.

IV.1.1 Performing the protocol

To achieve the suggested three-party bidirectional teleportation protocol, the users perform the following quantum circuit step by step as described below:

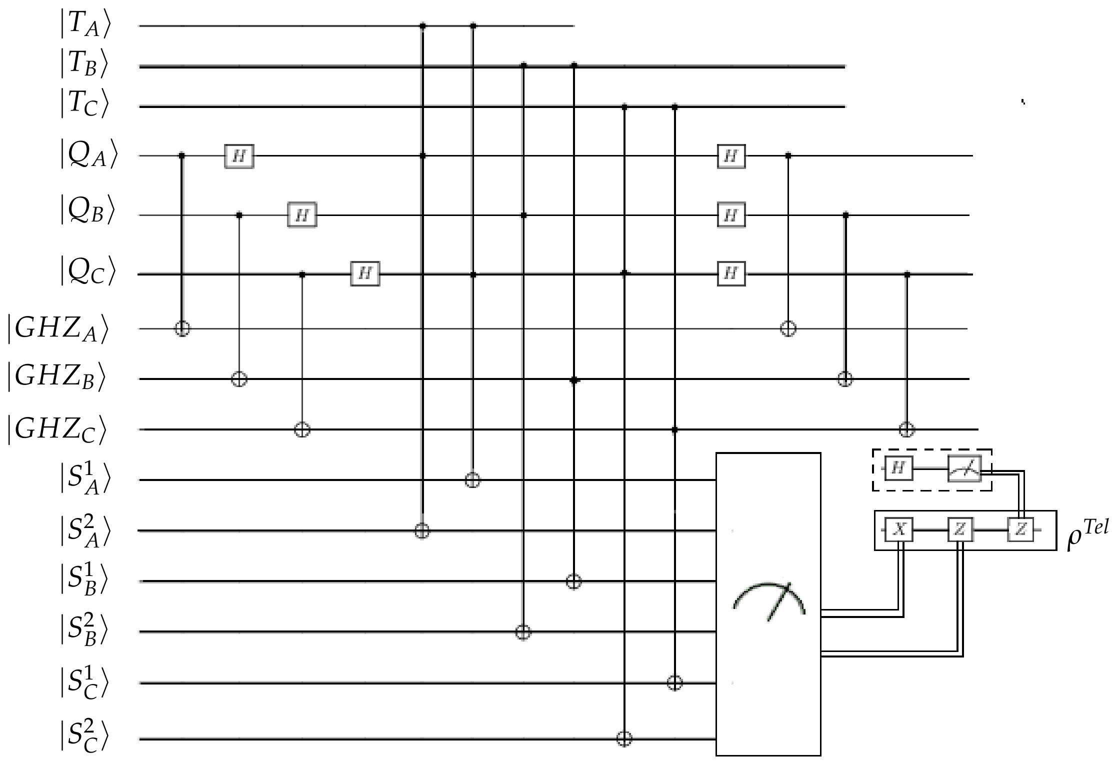

FIGURE IV.2: Quantum circuit of the three-party bidirectional teleportation between Alice, Bob, and Charlie using a single GHZ_3 state and three trigger qubits $|T_A\rangle$, $|T_B\rangle$ as well as $|T_C\rangle$. The gates X, Z, and H denote the Pauli and Hadamard gates respectively. • and $\oplus$ indicate the control and target qubits of $CNOT$ and $Toffoli$ gates respectively. All measurement outcomes (0 or 1) are transmitted via classical channels represented by double lines into gates X and Z. The dashed-line block stands for the contribution of the mediator. The receiver is concerned with the gates enclosed in the box with a solid-line.

- *From Alice to Bob through Charlie*

  1. **Step one:**

     The users prepare their initial state, which consists of 15 qubits, by using the states Eqs. (IV.1-II.7). This state may be written as:

$$|\psi_s\rangle = |GHZ_{A,B,C}\rangle \left|Q_A S_A^{(1)} S_A^{(2)} T_A\right\rangle \left|Q_B S_B^{(1)} S_B^{(2)} T_B\right\rangle \left|Q_C S_C^{(1)} S_C^{(2)} T_C\right\rangle. \tag{IV.6}$$

  2. **Step two:**

The users apply the $CNOT$ gate between the teleported state $|Q_{A,B,C}\rangle$ as control qubits and the GHZ qubits $|GHZ_{A,B,C}\rangle$ as target qubits. The state becomes:

$$|\psi_s\rangle' = CNOT_3\Big(|GHZ_{A,B,C}\rangle \left|Q_A S_A^{(1)} S_A^{(2)} T_A\right\rangle \left|Q_B S_B^{(1)} S_B^{(2)} T_B\right\rangle \left|Q_C S_C^{(1)} S_C^{(2)} T_C\right\rangle \Big) \tag{IV.7}$$

Then, the users apply Hadamard gates on the teleported qubits $|Q_{A,B,C}\rangle$ of the previous output results, which gives:

$$|\psi_s\rangle'' = H_3\Big(CNOT_3(|GHZ_{A,B,C}\rangle \left|Q_A S_A^{(1)} S_A^{(2)} T_A\right\rangle \left|Q_B S_B^{(1)} S_B^{(2)} T_B\right\rangle \left|Q_C S_C^{(1)} S_C^{(2)} T_C\right\rangle)\Big) \tag{IV.8}$$

3. **Step three:**

   The three users perform two Toffoli gates; where for the first one, the triggers $|T_{A,B,C}\rangle$ and $|Q_{A,B,C}\rangle$ represent the control qubits and $\left|S_{A,B,C}^{(2)}\right\rangle$ act as target qubits. While in the second Toffoli gate, the triggers $|T_{A,B,C}\rangle$ and the GHZ pairs; $|GHZ_{A,B,C}\rangle$, act as control qubits and $\left|S_{A,B,C}^{(1)}\right\rangle$ act as the target qubits. These operations are defined by:

$$CCNOT_3\Big(H_3\Big(CNOT_3(|GHZ_{A,B,C}\rangle \left|Q_A S_A^{(1)} S_A^{(2)} T_A\right\rangle \left|Q_B S_B^{(1)} S_B^{(2)} T_B\right\rangle \left|Q_C S_C^{(1)} S_C^{(2)} T_C\right\rangle)\Big)\Big) \tag{IV.9}$$

4. **Step four:**

   The outcome states after performing the $Toffoli$ gates are stored in the qubits $\left|S_A^{(1)}\right\rangle$ and $\left|S_A^{(2)}\right\rangle$. The results of the measurements in the computational basis$\{|0\rangle, |1\rangle\}$ are sent by classical channel to Bob. Based on Alice's measurements, Bob performs the adequate local operations $(\hat{X}, \hat{Z})$, on his GHZ_B qubit. Furthermore, Charlie performs a Hadamard gate followed by a projective measurement on the basis $\{|0\rangle, |1\rangle\}$. This result is also sent by a classical channel to Bob in order to recover the state $|Q_A\rangle$.

- *From Bob to Alice through Charlie:*
  Bob performs the same operation that Alice has done, and Charlie should always perform a Hadamard gate and a projective measurement to finally teleport the state $|Q_B\rangle$ to Alice.

The teleportation between any two random partners of the scheme may always be done with contribution of the third partner. Conventionally, we assume that the sender is "S", the receiver is "R" and the mediator is "M". the teleportation could be done in two sense $S \to M \to R$ and vice versa $R \to M \to S$ by performing the protocol steps described above. The proof of the suggested BQT scheme is clearly described in (Appendix. C).

IV.1.2 Implementation of the Circuit

The final output of the circuit depends on the initial state of the triggers. However, we have the following possibilities [233]:

1. The initial state of the three triggers are initially prepared in the states, $\hat{\varrho}_{T_S} = \frac{1}{2}\left(1 + \hat{\sigma_z}^{(S)}\right)$, $\hat{\varrho}_{T_M} = \frac{1}{2}\left(1 + \hat{\tau_z}^{(M)}\right)$ and $\hat{\varrho}_{T_R} = \frac{1}{2}\left(1 + \hat{\gamma_z}^{(R)}\right)$. In this case, each partner obtains the completely mixed state, i.e., $\hat{\varrho}_Q^{(S)} = \rho_Q^{(R)} = \hat{\varrho}_0 = \frac{1}{2}(|0\rangle\langle 0| + |1\rangle\langle 1|)$, and $\hat{\varrho}_Q^{(M)} = |0\rangle\langle 0|$ or $|1\rangle\langle 1|$.

2. The sender's, the mediator's, and the receiver's triggers are prepared in the states $\hat{\varrho}_{T_S} = \frac{1}{2}\Big(1 - \hat{\sigma_z}^{(S)}\Big)$, $\hat{\varrho}_{T_M} = \frac{1}{2}\Big(1 - \hat{\tau_z}^{(M)}\Big)$, and $\hat{\varrho}_{T_R} = \frac{1}{2}\Big(1 - \hat{\gamma_z}^{(R)}\Big)$. In this case, all the partners perform a perfect projective measurement with the probability:

$$\mathcal{P}_i = \mathrm{Tr}\Big\{\rho_{T_S}\hat{\varrho}_Q^{(S)}\Big\} = \mathrm{Tr}\Big\{\hat{\varrho}_{T_M}\rho_Q^{(M)}\Big\} = \mathrm{Tr}\Big\{\hat{\varrho}_{T_R}\hat{\varrho}_Q^{(R)}\Big\} = \sin^2(\theta_i/2), \qquad i = S, M, R. \tag{IV.10}$$

The process will end up by the state bellow,

$$\rho_{tel}^{(R)} = \mathcal{P}_S\bar{\mathcal{P}}_R\bar{\mathcal{P}}_M\hat{\varrho}_Q^{(S)} + (1 - \mathcal{P}_S\bar{\mathcal{P}}_R\bar{\mathcal{P}}_M)\hat{\varrho}_0, \;\; \bar{\mathcal{P}}_i = 1 - \mathcal{P}_i \quad\; i = S, M, R. \tag{IV.11}$$

3. If the sender's trigger qubit is prepared in the state $\hat{\varrho}_{T_S} = \frac{1}{2}\Big(\hat{I} - \hat{\sigma_z}^{(S)}\Big)$, the mediator's trigger qubit is prepared in the state $\hat{\varrho}_{T_M} = \frac{1}{2}\Big(\hat{I} + \hat{\tau_z}^{(M)}\Big)$, receiver's trigger qubit is prepared in the state $\hat{\varrho}_{T_R} = \frac{1}{2}\Big(\hat{I} + \hat{\gamma_z}^{(R)}\Big)$, and if the mediator performs on his/her GHZ qubit a Hadamard gate followed by a projective measurement on the basis $\{|0\rangle, |1\rangle\}$, only the sender has the ability to teleport his/her qubit to the receiver. Accordingly, when the sender gets the completely mixed state, i.e., the final state at the sender's hand is $\hat{\varrho}_{tel}^{(S)} = \hat{\varrho}_0$, the final state at the receiver's hand is $\hat{\varrho}_{tel}^{(R)} = \hat{\varrho}_Q^{(S)}$.

IV.1.3 The fidelity of teleported states

The fidelity that measures the overlap between the input state $|Q\rangle_{in}$ and the final teleported state $\hat{\varrho}_{out}$ is given by:

$$f^{in\rightarrow out} = \; {}_{in}\langle Q|\,\hat{\varrho}_{out}\,|Q\rangle_{in}, \tag{IV.12}$$

we can easily get:

$$f^{S\rightarrow R} = \; {}_S\langle\psi|\,\hat{\varrho}^R\,|\psi\rangle_S = \frac{1 + \mathcal{P}_S\bar{\mathcal{P}}_R\bar{\mathcal{P}}_M}{2}, \tag{IV.13}$$

where the probabilities may be written as:

$$\begin{aligned}
\mathcal{P}_S &= \frac{1}{2}\Big(1 + \cos(\tilde{\theta}_S)\cos(\theta_S) + \sin(\tilde{\theta}_S)\sin(\theta_S)\cos\phi_S\Big),\\
\bar{\mathcal{P}}_M &= \frac{1}{2}\Big(1 + \cos(\tilde{\theta}_M)\cos(\theta_M) + \sin(\tilde{\theta}_M)\sin(\theta_M)\cos\phi_M\Big),\\
\bar{\mathcal{P}}_R &= \frac{1}{2}\Big(1 + \cos(\tilde{\theta}_R)\cos(\theta_R) + \sin(\tilde{\theta}_R)\sin(\theta_R)\cos\phi_R\Big)
\end{aligned} \tag{IV.14}$$

where $\bar{\mathcal{P}}_i = 1 - \mathcal{P}_i$, and $\tilde{\theta}_i$, θ_i, ϕ_i (for $i = S, M, R$) stand for initial state weight, trigger weight and initial state phase, respectively.

However, the averaged fidelity over all the input states may be described by the fidelity average:

$$\mathcal{F}_{avg}^{S\rightarrow R} = \frac{1}{4\pi}\int_0^{\pi} d\theta_i \int_0^{2\pi} f^{S\rightarrow R}(\theta_i, \phi_i)\sin\theta_i d\phi_i \tag{IV.15}$$

where, 4π is the solid angle.

- **Teleportation from Alice to Bob through Charlie**

Let us clarify this protocol by discussing the possibility of teleporting a state from Alice to Bob with Charlie's assistance. The aim of Alice is sending the state $\hat{\varrho}_Q^A$ to Bob, the trigger states of the users, Alice, Charlie and Bob are prepared in the states $\hat{\varrho}_{T_A} = \frac{1}{2}\left(\hat{I} - \hat{\sigma_z}^{(A)}\right)$, $\hat{\varrho}_{T_C} = \frac{1}{2}\left(\hat{I} + \hat{\tau_z}^{(C)}\right)$, and $\hat{\varrho}_{T_B} = \frac{1}{2}\left(\hat{I} + \hat{\gamma_z}^{(B)}\right)$ respectively. Under these assumptions, Alice has the ability to teleport her qubit to Bob by the help of Charlie, where Charlie performs a Hadamard gate followed by a projective measurement in the basis $\{|0\rangle, |1\rangle\}$ in order to allow Alice to transfer her state to Bob. Otherwise, the teleportation fails. Due to this process, Alice's state reduces into a mixed state i.e., $\hat{\varrho}_{tel}^{(A)} = \hat{\varrho}_0$, while Bob gets the teleported state, $\hat{\varrho}_{tel}^{(B)} = \hat{\varrho}_Q^{(A)}$. However, if Alice's trigger is prepared in the state $\hat{\varrho}_{T_A} = \frac{1}{2}\left(\hat{I} + \hat{\sigma_z}^{(A)}\right)$, the teleportation process will not be completed.

Fig. (IV.3) shows the average teleportation fidelity from Alice as a sender to a receiver (Bob) through a mediator (Charlie), namely $\mathcal{F}_{avg}^{A\rightarrow B}$. It is assumed that the initial and the trigger states of the receiver and the mediator are the same, i.e. $\theta_C = \tilde{\theta}_C = \theta_B = \tilde{\theta}_B = \theta$, and $\phi_B = \phi_C = \phi$. In the numerical computations, we set $\theta_A = \tilde{\theta}_A = 0$ and ϕ_A is arbitrary, namely the teleported state codes classical information i,e. $\hat{\varrho}_Q^A = |0\rangle\langle 0|$. It is clear that the fidelity average increases gradually as the weight angle θ and the phase angle ϕ increase. The maximum value of the teleported state from Alice to Bob is predicted when the states of Bob and Charlie and their triggers are initially prepared with $\theta_B = \tilde{\theta}_B = \theta_C = \tilde{\theta}_C = \frac{\pi}{2}$ and $\phi_B = \tilde{\phi}_B = \phi_C = \tilde{\phi}_C = \pi$. This means that to maximize the average fidelity of the teleported classical information, the receiver and the mediator prepare their initial states as: $|Q_B\rangle = |Q_C\rangle = \frac{1}{\sqrt{2}}(|0\rangle - |1\rangle)$.

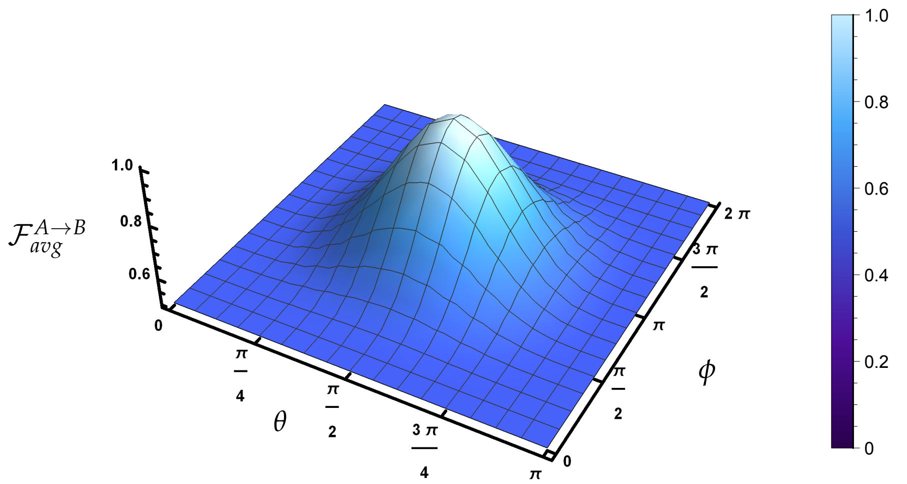

FIGURE IV.3: The teleportation fidelity $|Q_A\rangle = |0\rangle, \phi_A$ is arbitrary, namely $\theta_A = 0$ from Alice to Bob, where the initial states of Charlie and Bob are prepared with $\theta_B = \theta_C = \tilde{\theta}_C = \tilde{\theta}_B = \theta$ and $\phi_B = \phi_C = \phi$.

In Fig. (IV.4), we describe the behavior of the fidelity $\mathcal{F}_{avg}^{A\rightarrow B}$ at different teleportation states; where we set $\theta_A = \frac{\pi}{2}$. Therefore, the teleported state at Alice may be written as: $|Q_A\rangle = \frac{1}{\sqrt{2}}(|0\rangle + e^{i\phi_A}|1\rangle)$. The effect of the phase angle ϕ_A on the behavior of the fidelity is displayed at different values of ϕ_A. However, the behavior of $\mathcal{F}_{avg}^{A\rightarrow B}$ at $\phi = 0$ is the same as it is displayed in Fig. (IV.3), because ϕ_A is arbitrary. On the other hand, at $\phi = \frac{\pi}{4}$, the fidelity behavior of the teleported state $|Q_A\rangle = \frac{1}{\sqrt{2}}|0\rangle + \frac{1}{2}(1+i)|1\rangle$, as it is displayed in Fig. (IV.4.a) is similar to that in Fig. (IV.3), but the maximum values are smaller. Moreover, the maximum values of the fidelity are predicted at the same values of the weight and phase angles of the receiver and the mediator. Fig. (IV.4.b) describes the behavior of $\mathcal{F}_{avg}^{A\to B}$, at $\phi_A = \frac{\pi}{2}$, i.e. $|Q_A\rangle = \frac{1}{\sqrt{2}}(|0\rangle - i\,|1\rangle)$. It is clear that, the fidelity is smaller than that displayed in Fig. (IV.4.a), which means that the structure of the teleported state plays an important role to maximize the fidelity average. Furthermore, the behavior of the fidelity $\mathcal{F}_{avg}^{A\to B}$ at different initial state settings, where we set $|Q_A\rangle = \frac{1}{\sqrt{2}}(|0\rangle - |1\rangle)$ and $\phi_A = \pi$, is displayed in Fig. (IV.4.c). In this case, the fidelity has a different behavior; where it is independent of the receiver and the mediator states.

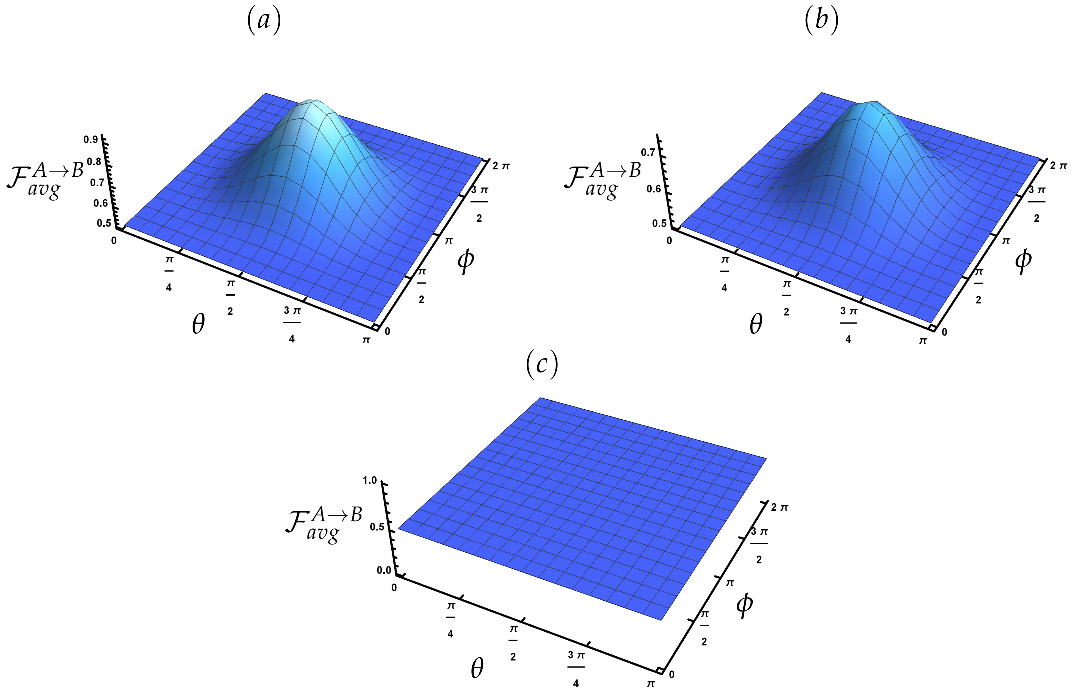

FIGURE IV.4: Fidelity of teleportation from Alice to Bob, where $\theta_A = \tilde{\theta}_A = \frac{\pi}{2}$, and (a): $\phi_A = \frac{\pi}{4}$, (b): $\phi_A = \frac{\pi}{2}$, and (c): $\phi_A = \pi$.

In Fig. (IV.5), we assume that Alice's qubit is prepared in different state settings, namely $(\theta_A = \frac{\pi}{3}; \frac{\pi}{4})$, while the phase angle is $\phi_A = \frac{\pi}{4}$. Explicitly, Fig. (IV.5a) describes the behavior of the fidelity average of the state $|Q_A\rangle = \frac{\sqrt{3}}{2}\,|0\rangle + \frac{\sqrt{2}(1+i)}{4}\,|1\rangle$. It is clear that the behavior is similar to that shown in Fig. (IV.3) and Fig. (IV.4). However, the maximum bounds of the fidelity average are predicted at the same values that maximize the fidelity of the teleported state at $\theta_A = 0$ (see Fig. (IV.3)) and at $\theta_A = \frac{\pi}{2}$ (please see Fig. (IV.4)). The maximum values of the fidelity $\mathcal{F}_{avg}^{A\to B}$ that are displayed in Fig. (IV.5a) are larger than those displayed in Fig.(IV.4b). Fig. (IV.5b) shows the behavior of the teleported state fidelity at Bob's hand, where Alice's state is prepared in the state $|Q_A\rangle = 0.9238\,|0\rangle + 0.382(1+i)\,|1\rangle$. The behavior is similar to that shown in Fig. (IV.3) and Fig. (IV.4), but the maximum bounds of the fidelity are larger.

From the previous numerical behavior of the fidelities, one may conclude that, the initial state settings of the teleported states play an important role to maximize/ minimize the average teleportation fidelity at the receiver's hand. The phase angles of the receiver and the mediator could be used as a control parameter to maximize/minimize the teleported state fidelity.

- **Teleportation from Bob to Alice through Charlie:**

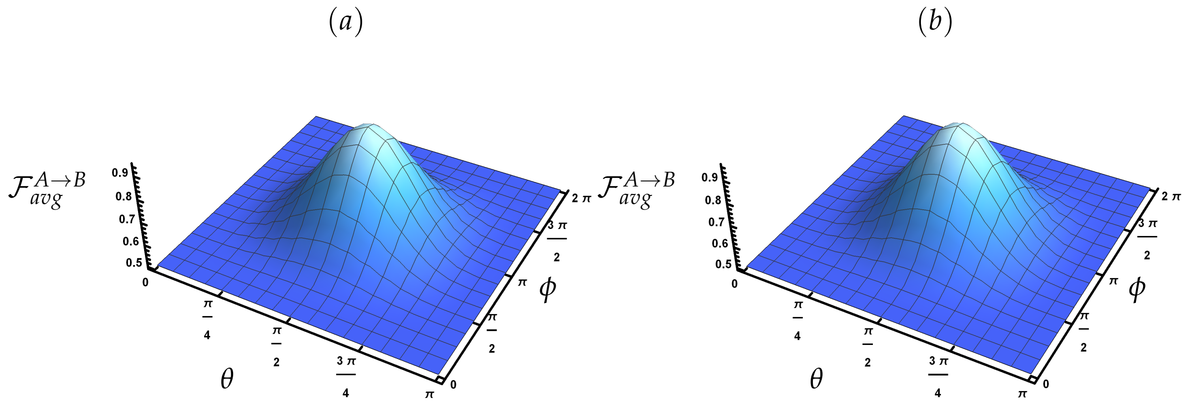

FIGURE IV.5: The fidelity of the teleported state at $\phi_A = \pi/4$, where (a): $\theta_A = \tilde{\theta}_A = \frac{\pi}{3}$ and (b): $\theta_A = \tilde{\theta}_A = \pi/4$.

Now, let us discuss the fidelity average of the teleported state from Bob to Alice by the help of Charlie. Due to the symmetry of the initial states of all the users, we expect that the behavior of the fidelity is similar to that displayed when Alice teleports her state to Bob. However, Fig. (IV.6) describes the behavior of $\mathcal{F}_{avg}^{B\to A}$, where it is assumed that Bob prepared the teleported state with $\theta_B = \frac{\pi}{2}$ and different values of the phase angle. The maximum values of the fidelities are the same as those shown in Fig. (IV.4).

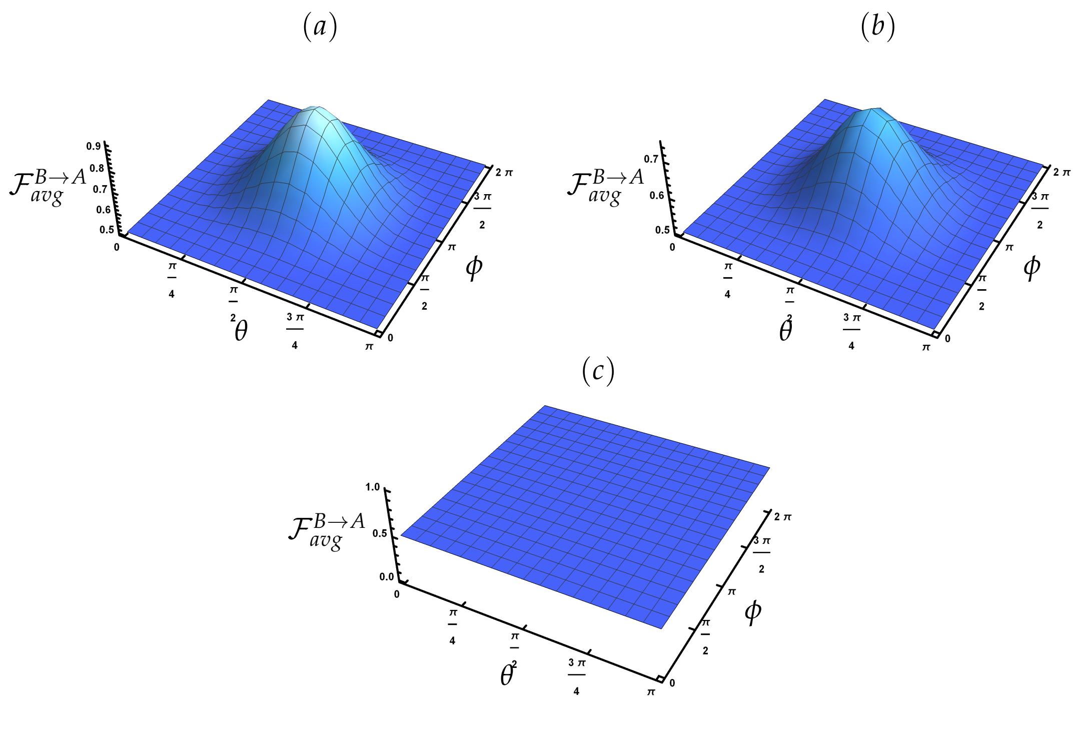

FIGURE IV.6: Fidelity of teleportation from Bob to Alice through Charlie, where $\theta_B = \tilde{\theta}_B = \frac{\pi}{2}$. (a): $\phi_B = \frac{\pi}{4}$; (b): $\phi_B = \frac{\pi}{2}$; (c): $\phi_B = \pi$.

- **Fidelity in the presence of different triggers:**

In this context, it is important to discuss the behavior of the fidelity average when the triggers are initially prepared in different states. Fig. (IV.7) describes the behavior of $\mathcal{F}_{avg}^{B\to A}$, where the states of the users are prepared similarly, while different states of the triggers are considered. As it is displayed in Fig. (IV.7), the fidelity behavior depends on the trigger states.

Fig. (IV.7a) displays the fidelity $\mathcal{F}_{avg}^{B\rightarrow A}$ $(\tilde{\theta}_B = \frac{\pi}{3}, \tilde{\theta}_A, \tilde{\theta}_C)$, where it is assumed that the teleported state $|Q_B\rangle = |0\rangle$ and the state of the sender's trigger is prepared in the states $|T_B\rangle = \frac{\sqrt{3}}{2}|0\rangle + \frac{1}{2}|1\rangle$. At $\tilde{\theta}_A = \tilde{\theta}_C = 0$, namely the receiver and the mediator prepared their triggers in the states $|T_A\rangle = |T_C\rangle = |0\rangle$, the fidelity is minimum, namely $\mathcal{F}_{avg}^{B\rightarrow A} = 0.5$. However, as the trigger's weight angle of the receiver and of the mediator increases, where they are represented as a super position between $|0\rangle$ and $|1\rangle$, the fidelity average increases gradually. As an example, if we examine the behavior of the fidelity average at $\tilde{\theta}_A = \tilde{\theta}_C = \frac{\pi}{2}$, namely, Alice and Charlie's triggers are prepared in the state $|T_A\rangle = |T_C\rangle = \frac{1}{\sqrt{2}}(|0\rangle + |1\rangle)$, the fidelity average increases. If the trigger's states of the receiver and of the mediator are different, the fidelity average will be small. Therefore, the state of the receiver's trigger is another factor that plays a central role on maximizing/minimizing the teleportation fidelity. This result can be depicted clearly if the receiver prepares his/her trigger on the state $|T_A\rangle = |0\rangle$ and the mediator's trigger is prepared at any weight angle $\tilde{\theta}_C \in [0, \pi]$. In this case, the fidelity is small. Nevertheless, as one increases $\tilde{\theta}_A$, the fidelity increases as $\tilde{\theta}_C$ increases.

In Fig. (IV.7b), it is assumed that the sender "Bob" prepares his trigger with a weight angle $\tilde{\theta}_B = \frac{\pi}{4}$, namely $|T_B\rangle = \cos\left(\frac{\pi}{8}\right)|0\rangle + \sin\left(\frac{\pi}{8}\right)|1\rangle$. The behavior is similar to that displayed in Fig. (IV.7a), where the upper bounds of the fidelity is larger. The largest value of the fidelity is displayed at $\tilde{\theta}_A = \tilde{\theta}_C = \pi$, where, in this case, the triggers of the receiver and mediator are given by the state $|1\rangle$.

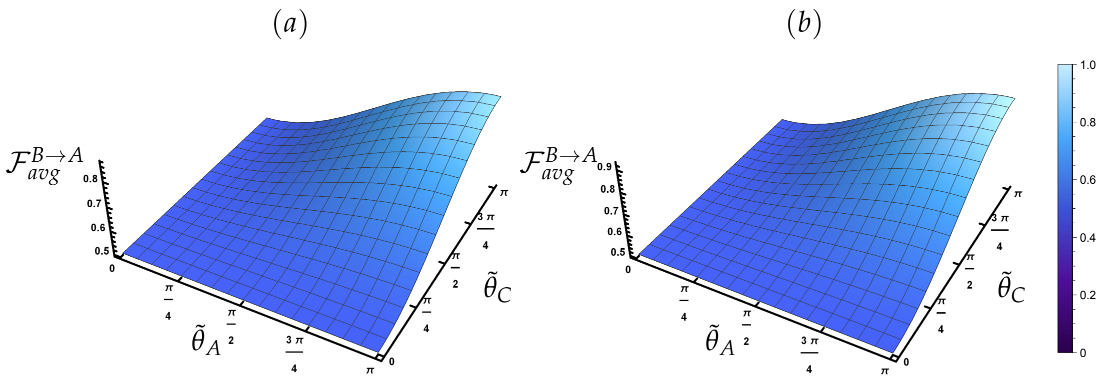

FIGURE IV.7: Fidelity of teleportation from Bob to Alice, where $\theta_A = \theta_B = \theta_C = \theta = 0.$ and $\phi_A = \phi_B = \phi_C = 0$. (a) $\tilde{\theta}_B = \frac{\pi}{3}$; (b) $\tilde{\theta}_B = \frac{\pi}{4}$.

- **Average fidelity of different states:**

In Fig. (IV.8) it is assumed that the receiver (R) and the mediator (M) prepared their triggers in the same state; while the sender (S) prepared his trigger in a different state. The displayed behavior of the fidelity shows that the upper bounds depend on the states of receiver and the mediator's triggers. However, at $\theta_S = 0$, namely $|Q_S\rangle = |0\rangle$ and the trigger states of the receiver and mediator are also prepared in the states $|T_j\rangle = |0\rangle$, (for $j = R, M$), the fidelity average $\mathcal{F}_{avg}^{B\rightarrow A} = 0.5$. However, as one increases the weight angle θ_i, $i = S, R, M$, the fidelity average increases, where the maximum value is reached at $\theta = \frac{3\pi}{4}$, namely, $|Q_S\rangle = 0.3826\,|0\rangle + 0.9238\,|1\rangle$. If the initial states of the three triggers are initially prepared with the same weight angle $\tilde{\theta}_i = \frac{\pi}{2}$, $i = S, R, M$, i.e., $|T_i\rangle = \frac{1}{\sqrt{2}}(|0\rangle + |1\rangle)$ and the sender has classical information, the fidelity average is larger,

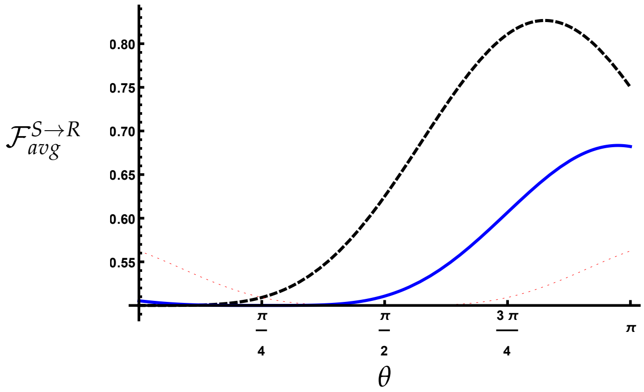

FIGURE IV.8: Fidelity of teleportation from Bob to Alice through Charlie, where $\theta_A = \theta_B = \theta_C = \theta$, $\tilde{\theta}_B = \pi/2$ and $\phi = 0$. The solid, dash and dot curves are evaluated at $\tilde{\theta}_A = \tilde{\theta}_C = 0$; $\tilde{\theta}_A = \tilde{\theta}_C = \frac{\pi}{2}$; and $\tilde{\theta}_A = \tilde{\theta}_C = \frac{\pi}{4}$.

i.e., $\mathcal{F}_{avg}^{S\to R} = 0.56$. As θ_i increases more the fidelity average decreases gradually to reach its minimum values. This means that sending classical information over quantum channels is much better than sending quantum information. If the receiver and the mediator prepared their triggers in the state $\left|T_{R(M)}\right\rangle = \cos(\frac{\pi}{8})\,|0\rangle + \sin(\frac{\pi}{8})\,|1\rangle$, and the sender's trigger is prepared in the state $|T_S\rangle = \frac{1}{\sqrt{2}}(|0\rangle + |1\rangle)$, the fidelity average of the teleported state is almost the initial value. However, at $\theta_i = \frac{\pi}{2}, for:\ (S, R, M)$, namely the state of Bob's trigger and its state is prepared with a weight angle $\frac{\pi}{2}$, the fidelity increases to reach it maximum value at $\theta = \pi$, namely the sender teleport classical information.

IV.2 Comparison

In the suggested three-party bidirectional quantum teleportation protocol, Alice, Bob and Charlie can exchange their states by using the GHZ state as a quantum channel. This protocol is based on $CNOT$, $Toffoli$, Hadamard operations, and single-qubit measurements. This scheme could be generalized to N partners.
In Refs [215, 216, 217, 218, 219], the process of teleportation needs five entangled qubits at least to teleport one qubit and nine entangled qubits to teleport two qubits. Nevertheless, our protocol needs a single GHZ state to teleport a single-qubit state. So, the proposed protocol requires less quantum resources. Additionally, In Refs [215, 216, 217, 221], the partners apply two-qubit measurements which are less efficient than single-qubit measurements [240]. In Table(1), we introduce details of comparison between our proposed protocol and previous ones.

IV.3 Multi-party bidirectional teleportation

The scheme in section IV.1 may be extended to teleport quantum states through a quantum network (QN). The extension of the teleportation scheme presented previously require an extension of the quantum channel. In other words, for N nodes of QN, one needs an $n-$ qubit GHZ state to be shared between all the partners. Mathematically, it is assumed that the $N-$ partners of the QN share the following $n-$qubit GHZ state:

$$|GHZ\rangle_N = \frac{1}{2}(|0\rangle^{\otimes n} + |1\rangle^{\otimes n})_{ABCD...}, \tag{IV.16}$$

Where N is the number of QN's partners and n is the number of nodes. From Eq.(IV.16), qubit A belongs to node "A" and qubit B belongs to node "B" and so on, as it is displayed in Fig.(IV.9). Using the same

Reference	Partners	Teleported qubits	Quantum channel	Auxiliary qubits
[215]	2	1	5-qubit	0
[216]	2	2	9-qubits	0
[217]	2	1	6-qubits	0
[218]	2	$(2)EPR$	$(6qubits)GHZ_6$	0
[219]	2	$(3)GHZ$	$(8qubits)GHZ_8$	0
[193]	2	1	Bell state	2
The suggested scheme	3	1	GHZ	3

TABLE IV.1: Comparison between this work and previous works.

suggested protocol in Sec.2.1, the bidirectional teleportation from a random sender to a random receiver on the QN could be completed successfully, using an $n-$qubit GHZ state as a quantum channel. In this scheme, only the sender $''S''$ needs to perform a projective measurement and informs the receiver of measurement's outcome. All the other partners in the QN should perform a *Hadamard* gate on their GHZ qubits followed by a measurement on the basis $\{|0\rangle, |1\rangle\}$. Based on this, the receiver $''R''$ could reconstruct the teleported state.

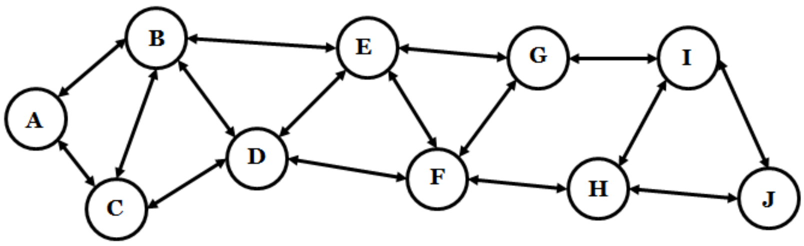

FIGURE IV.9: The suggested generalized quantum network, where the nodes (members) are sharing initially $n-$qubit GHZ state.

IV.4 BQT of CNOT gate

The CNOT gate is a two-qubit unitary gate [77], in which the upper qubit is called the control qubit and the lower one is the target qubit (Fig. I.5). If the control qubit is $|0\rangle$, nothing happens to the target qubit. Otherwise, if the control qubit is $|1\rangle$, the target qubit is flipped. The non-local implementation of the $CNOT$ gate is essential for the construction of large scale quantum network in which each node from the quantum network can act as a sender or as a receiver. It is also primordial for the distributed computation processes, wherein each node of the quantum network deals with a small part of the whole computational operation.

In fact, the unidirectional non-local implementation of $CNOT$ gate has been considered previously by *Eisert et al*. [241], where it is proven that one classical bit in each direction and one shared Bell state is necessary and sufficient for the non-local implementation of the $CNOT$ gate. However, in what follows, we present a scheme to perform a bidirectional non-local $CNOT$ gate between two qubits, one of them is at Alice's hand and the other one is at Bob's hand as it is described in Fig. (IV.10).

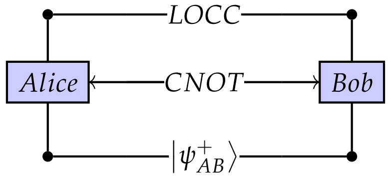

FIGURE IV.10: Scheme for the Bidirectional non-local implementation of the CNOT gate using a Bell state $|\psi^+_{AB}\rangle$ and classical communication.

The initial state at the partners' sides are necessarily arbitrary. Namely, Alice has the state:

$$|\Phi_A\rangle = (\alpha|0\rangle + \beta|1\rangle)_A \tag{IV.17}$$

Where: α and β are complex coefficients with : $|\alpha|^2 + |\beta|^2 = 1$.

Similarly, Bob has the state:

$$|\Phi_B\rangle = (\gamma|0\rangle + \delta|1\rangle)_B \tag{IV.18}$$

Where: γ and δ are complex coefficients with : $|\gamma|^2 + |\delta|^2 = 1$.

The main aim of our scheme is to allow Alice to perform a non-local CNOT gate at Bob's side, where the qubit $|\Phi\rangle_A$ is the control qubit of the CNOT gate and $|\Phi\rangle_B$ is the target qubit of the CNOT gate. On the other hand, Bob could perform a non-local CNOT gate at Alice's side, where the qubit $|\Phi\rangle_B$ is the control qubit of the CNOT gate and $|\Phi\rangle_A$ is the target qubit of the $CNOT$ gate.

The $CNOT$ is performed between Alice and Bob, by following the steps shown in the quantum circuit bellow (Fig. IV.11):
Before performing the protocol, Alice and Bob share the state:

$$|\psi\rangle^+_{ab} = \frac{1}{\sqrt{2}}(|00\rangle + |11\rangle)_{ab} \tag{IV.19}$$

Where the qubit "a" belongs to Alice and the qubit "b" belongs to Bob.

The quantum circuit uses 7 qubits. The trigger qubit $|T\rangle$ is used in this scheme to select which qubit, $|\Phi_A\rangle$ or $|\Phi_B\rangle$, will play the role of the control qubit or the target qubit. If $|T\rangle = |1\rangle$, $|\Phi_A\rangle$ is the control qubit and $|\Phi_B\rangle$ is the target qubit. Otherwise, if $|T\rangle = |0\rangle$, $|\Phi_B\rangle$ is the control qubit and $|\Phi_A\rangle$ is the target qubit. Furthermore, the qubits $|S_A\rangle$ and $|S_B\rangle$ are two storage qubits prepared initially in the state $|0\rangle$. The storage qubits $|S_i\rangle$ $(i = A, B)$ are used to store the measurement results of the $toffoli$ gate.

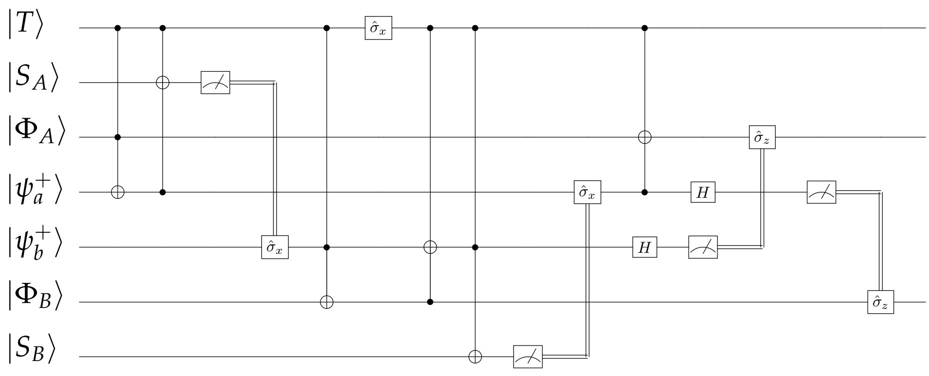

FIGURE IV.11: The circuit for implementation of Bidirectional non-local CNOT gate using Bell state. • and ⊕ denote the control and target qubits respectively of local *CNOT* and *CCNOT* gates. *X*, *Z*, and *H* stand for Pauli's and Hadamard gates respectively. the doube-line indicates the classical channels.

IV.4.1 Performing the protocol

Our main aim is that Alice performs the CNOT gate at Bob's side, where $|\Phi\rangle_A$ is the control qubit and $|\Phi\rangle_B$ is the target qubit. In this case, the trigger qubit is considered at the state $|1\rangle$, namely $(|T\rangle = |1\rangle)$.

The initial state of the whole system is written as:

$$|\Delta\rangle = |\Phi_A S_A\rangle \otimes |\Phi_B S_B\rangle \otimes |T\rangle \otimes |\psi\rangle^+_{ab} \tag{IV.20}$$

1. **Step One:**

   Alice performs a $Toffoli$ gate with the control qubits $|T\rangle$ and $|\Phi_A\rangle$ and the target qubit $|\psi\rangle^+_a$. It is worthy to mention that the $Toffoli$ gate acts exactly as a $CNOT$ gate if the control qubit is set to the state $|1\rangle$ [241]. After performing the $toffoli$ gate, the state of the system becomes:

$$|\Delta\rangle' = CNOT|\Phi_A S_A\rangle \otimes |\Phi_B S_B\rangle \otimes |T\rangle \otimes |\psi\rangle^+_{ab} \tag{IV.21}$$

   Explicitly, we can write:

$$|\Delta\rangle' = \alpha\gamma|00\rangle|\psi\rangle^+_{ab} + \alpha\delta|01\rangle|\psi\rangle^+_{ab} + \beta\gamma|10\rangle|\psi\rangle^-_{ab} + \beta\delta|11\rangle|\psi\rangle^-_{ab} \tag{IV.22}$$

   Where:

$$|\psi\rangle^-_{ab} = \frac{1}{\sqrt{2}}(|10\rangle + |01\rangle)_{ab} \tag{IV.23}$$

2. **Step Two:**

   Alice performs a projective measurement on the state $|\Phi_A\rangle$ in the basis $\{|0\rangle, |1\rangle\}$. Actually, if the measurement outcome is $|1\rangle_A$, the Pauli gate $\hat{\sigma}_x$ is applied on the qubit $|\psi\rangle^+_b$. Otherwise, if the measurement outcome is $|0\rangle_a$, the Pauli gate is not triggered. Hence, the state is collapsed to the state:

$$|\Delta\rangle'' = \frac{1}{\sqrt{2}}(\alpha\gamma|00\rangle_{AB}|0\rangle_b + \alpha\delta|01\rangle_{AB}|0\rangle_b + \beta\gamma|10\rangle_{AB}|1\rangle_b + \beta\delta|11\rangle_{AB}|1\rangle_b) \tag{IV.24}$$

3. **Step Three:**

A Toffoli gate is applied with the control qubits $|T\rangle$ and $|\psi\rangle_b^+$ and $|\Phi_B\rangle$ is the target qubit. By considering the trigger qubit $|T\rangle = |1\rangle$, the state becomes:

$$|\Delta\rangle''' = \frac{1}{\sqrt{2}}(\alpha\gamma|00\rangle_{AB}|0\rangle_b + \alpha\delta|01\rangle_{AB}|0\rangle_b + \beta\gamma|11\rangle_{AB}|1\rangle_b + \beta\delta|10\rangle_{AB}|1\rangle_b) \tag{IV.25}$$

4. **Step four:**

Here, we need to get rid of the qubit $|\psi\rangle_b^+$. So, we apply a Hadamard gate followed by a quantum measurement in the computational basis $\{|0\rangle, |1\rangle\}$. Depending on the measurement outcome ($|0\rangle$ or $|1\rangle$), a Pauli gate $\hat{\sigma}_z$ is applied on on the qubit $|\Phi_A\rangle$.

By applying the Hadamard gate on the qubit $|\Phi_B\rangle$, the state is written as:

$$H|\Delta\rangle''' = \frac{1}{\sqrt{2}}(\alpha\gamma|00\rangle_{AB}|+\rangle_b + \alpha\delta|01\rangle_{AB}|+\rangle_b + \beta\gamma|11\rangle_{AB}|-\rangle_b + \beta\delta|10\rangle_{AB}|-\rangle_b) \tag{IV.26}$$

Whereas:

$$|+\rangle_b = \frac{1}{\sqrt{2}}(|0\rangle + |1\rangle)_b \qquad ; \qquad |-\rangle_b = \frac{1}{\sqrt{2}}(|0\rangle - |1\rangle)_b \tag{IV.27}$$

Now, we perform a projective measurement of the state $|\psi\rangle_b^+$ in the computational basis $\{|0\rangle, |1\rangle\}$.

If the measurement result is the state $|0\rangle_b$, the Pauli gate $\hat{\sigma}_z$ is not triggred. Otherwise, if the measurement result is : $|1\rangle_b$, the Pauli gate $\hat{\sigma}_z$ is applied on the state $|\Phi_A\rangle$. However, the resulting state is:

$$\alpha\gamma|00\rangle_{AB} + \alpha\delta|01\rangle_{AB} + \beta\gamma|11\rangle_{AB} + \beta\delta|10\rangle_{AB} \tag{IV.28}$$

Thus, the non-local CNOT gate is applied where the control qubit $|\Phi_A\rangle$ is at Aice's side, and the target qubit $|\Phi_B\rangle$ is at Bob's side. However, one could set the trigger state at $|0\rangle$ and follow the same steps to perform the *CNOT* gate between $|\Phi\rangle_B$ and $|\Phi\rangle_A$, where $|\Phi\rangle_B$ is the control qubit and $|\Phi\rangle_A$ is the target qubit.

Overall, the suggested scheme allows the bidirectional teleportation of *CNOT* gate, where the control qubit is on the one side and the target qubit is on the other side of the teleportation scheme. The trigger state controls which qubit is the control and which one is the target of the *CNOT* operation. Namely, if $|T\rangle = |1\rangle$, the qubit on Alice's side is the control qubit of the CNOT gate and Bob has the target qubit. However, if $|T\rangle = |0\rangle$, the qubit on Bob's side is the control qubit of the CNOT gate and Alice has the target qubit.

IV.5 Bidirectional teleportation of n-qubit state

In this section, we present a bidirectional teleportation protocol, where Alice and Bob exchange n-qubit states bilaterally, by using the previously proposed scheme of the bidirectional non-local *CNOT* implementation (described in IV.4).

IV.5.1 Bidirectional teleportation of 2-qubit states

Let us start by the case of 2-qubits states . We assume that Alice has the state to be teleported:

$$|Q\rangle_A = x_0 |00\rangle + x_1 |01\rangle + x_2 |10\rangle + x_3 |11\rangle \tag{IV.29}$$

and Bob has the state to be teleported:

$$|Q\rangle_B = y_0 |00\rangle + y_1 |01\rangle + y_2 |10\rangle + y_3 |11\rangle \tag{IV.30}$$

x_i and y_i are complex coefficients. Where:

$$|x_0|^2 + |x_1|^2 + |x_2|^2 + |x_3|^2 = 1; \quad and \quad |y_0|^2 + |y_1|^2 + |y_2|^2 + |y_3|^2 = 1 \tag{IV.31}$$

The main goal of this scheme is to allow the two legitimate partners, Alice and Bob, to exchange their states (Eq. IV.29 and Eq. IV.30). The quantum channel of the teleportation scheme is a composite GHZ_3 state, given as follows:

$$|\mathcal{G}\rangle_{a_1a_2a_3b_1b_2b_3} = |GHZ\rangle_{a_1a_2a_3} \otimes |GHZ\rangle_{b_1b_2b_3} = \frac{1}{2}(|000000\rangle + |000111\rangle + |111000\rangle + |1111111\rangle)_{a_1a_2a_3b_1b_2b_3} \tag{IV.32}$$

where a_1 a_2 and a_3 belong to Alice. While, b_1 b_2 and b_3 belong to Bob.

Now, the partners have all the details to perform the bidirectional quantum teleportation.

IV.5.2 Performing BQT protocol

By using the states in Eqs. (IV.29, IV.30, and IV.32), the state of the whole system is given as:

$$|\psi\rangle_S = |Q\rangle_A \otimes |Q\rangle_B \otimes |\mathcal{G}\rangle_{a_1a_2a_3b_1b_2b_3} \tag{IV.33}$$

$$\begin{aligned} |\psi\rangle_S = (x_0 |00\rangle + x_1 |01\rangle + x_2 |10\rangle + x_3 |11\rangle)_{A_1A_2} \otimes (y_0 |00\rangle + y_1 |01\rangle + y_2 |10\rangle + y_3 |11\rangle)_{B_1B_2} \\ \otimes \frac{1}{2}(|0000\rangle + |0011\rangle + |1100\rangle + |1111\rangle)_{a_1a_2a_3b_1b_2b_3} \end{aligned} \tag{IV.34}$$

1. **Step one:**

   Two Non-Local CNOT gates ($CNOT^{NL}$) are applied between qubits A_1 (A_2) as control qubits and ($|GHZ\rangle_{b1}$ ($|GHZ\rangle_{b2}$) as target qubits, respectively. Moreover, the ($CNOT^{NL}$) gate is applied between the qubits B_1 (B_2) are control qubits and ($|GHZ\rangle_{a1}$ ($|GHZ\rangle_{a2}$) are target qubits, respectively.

$$|\psi\rangle_S^{'} = CNOT_2^{NL} |\psi\rangle_S \tag{IV.35}$$

namely,

$$
\begin{aligned}
|\psi\rangle_S^{'} = &\frac{x_0y_0}{2}|0000\rangle_{A_1A_2B_1B_2} \otimes (|000000\rangle + |000111\rangle + |111000\rangle + |110011\rangle)_{a_1a_2a_3b_1b_2b_3} + \\
&\frac{x_0y_1}{2}|0001\rangle_{A_1A_2B_1B_2} \otimes (|010000\rangle + |010111\rangle + |101000\rangle + |100011\rangle)_{a_1a_2a_3b_1b_2b_3} + \\
&\frac{x_0y_2}{2}|0010\rangle_{A_1A_2B_1B_2} \otimes (|100000\rangle + |100111\rangle + |011000\rangle + |010011\rangle)_{a_1a_2a_3b_1b_2b_3} + \\
&\frac{x_0y_3}{2}|0011\rangle_{A_1A_2B_1B_2} \otimes (|110000\rangle + |110111\rangle + |001000\rangle + |000011\rangle)_{a_1a_2a_3b_1b_2b_3} + \\
&\frac{x_1y_0}{2}|0100\rangle_{A_1A_2B_1B_2} \otimes (|000010\rangle + |000101\rangle + |111010\rangle + |110001\rangle)_{a_1a_2a_3b_1b_2b_3} + \\
&\frac{x_1y_1}{2}|0101\rangle_{A_1A_2B_1B_2} \otimes (|010010\rangle + |010101\rangle + |111010\rangle + |100001\rangle)_{a_1a_2a_3b_1b_2b_3} + \\
&\frac{x_1y_2}{2}|0110\rangle_{A_1A_2B_1B_2} \otimes (|100010\rangle + |100101\rangle + |011010\rangle + |010001\rangle)_{a_1a_2a_3b_1b_2b_3} + \\
&\frac{x_1y_3}{2}|0111\rangle_{A_1A_2B_1B_2} \otimes (|110010\rangle + |110101\rangle + |001010\rangle + |000001\rangle)_{a_1a_2a_3b_1b_2b_3} + \\
&\frac{x_2y_0}{2}|1000\rangle_{A_1A_2B_1B_2} \otimes (|000100\rangle + |000011\rangle + |111100\rangle + |110111\rangle)_{a_1a_2a_3b_1b_2b_3} + \\
&\frac{x_2y_1}{2}|1001\rangle_{A_1A_2B_1B_2} \otimes (|010100\rangle + |010011\rangle + |101100\rangle + |100111\rangle)_{a_1a_2a_3b_1b_2b_3} + \\
&\frac{x_2y_2}{2}|1010\rangle_{A_1A_2B_1B_2} \otimes (|100100\rangle + |100011\rangle + |011100\rangle + |010111\rangle)_{a_1a_2a_3b_1b_2b_3} + \\
&\frac{x_2y_3}{2}|1011\rangle_{A_1A_2B_1B_2} \otimes (|110100\rangle + |110011\rangle + |001100\rangle + |000111\rangle)_{a_1a_2a_3b_1b_2b_3} + \\
&\frac{x_3y_0}{2}|1100\rangle_{A_1A_2B_1B_2} \otimes (|000110\rangle + |000001\rangle + |111110\rangle + |110101\rangle)_{a_1a_2a_3b_1b_2b_3} + \\
&\frac{x_3y_1}{2}|1101\rangle_{A_1A_2B_1B_2} \otimes (|100110\rangle + |100001\rangle + |011110\rangle + |010101\rangle)_{a_1a_2a_3b_1b_2b_3} + \\
&\frac{x_3y_2}{2}|1110\rangle_{A_1A_2B_1B_2} \otimes (|100110\rangle + |100001\rangle + |011110\rangle + |0100101\rangle)_{a_1a_2a_3b_1b_2b_3} + \\
&\frac{x_3y_3}{2}|1111\rangle_{A_1A_2B_1B_2} \otimes (|110110\rangle + |110001\rangle + |001110\rangle + |000101\rangle)_{a_1a_2a_3b_1b_2b_3}
\end{aligned}
\tag{IV.36}
$$

2. **Step Two:**

   We perform a projective measurement of the qubits a_3 and b_3 on the computational basis: $(\{|00\rangle, |01\rangle, |10\rangle, |11\rangle\})$. After the projective measurement, we get 16 possibilities depending on the measurement outcome. The collapsed state is explicitly given in the table (IV.2).

3. **Step three:**

   Alice and Bob make measurement on their qubits A_1 and B_1 in the Basis: $\{|++\rangle, |+-\rangle, |-+\rangle, |--\rangle\}$. Furthermore, they make measurements on their qubits A_2 and B_2 in the Basis: $\{|++\rangle, |+-\rangle, |-+\rangle, |--\rangle\}$.

   Similarly, the collapsed state is given in the Tables given in the Appendix A.

4. **Step Four:**

$\lvert a_3b_3\rangle$	Collapsed state
$\lvert 0_30_3\rangle$	$x_0y_0\lvert 0000\rangle_{A_1A_2B_1B_2}\lvert 0000\rangle_{a_1a_2b_1b_2} + x_0y_1\lvert 0001\rangle_{A_1A_2B_1B_2}\lvert 0100\rangle_{a_1a_2b_1b_2} +$ $x_0y_2\lvert 0010\rangle_{A_1A_2B_1B_2}\lvert 1000\rangle_{a_1a_2b_1b_2} + x_0y_3\lvert 0011\rangle_{A_1A_2B_1B_2}\lvert 1100\rangle_{a_1a_2b_1b_2} +$ $x_1y_0\lvert 0100\rangle_{A_1A_2B_1B_2}\lvert 0010\rangle_{a_1a_2b_1b_2} + x_1y_1\lvert 0101\rangle_{A_1A_2B_1B_2}\lvert 0101\rangle_{a_1a_2b_1b_2} +$ $x_1y_2\lvert 0110\rangle_{A_1A_2B_1B_2}\lvert 1001\rangle_{a_1a_2b_1b_2} + x_1y_3\lvert 0111\rangle_{A_1A_2B_1B_2}\lvert 1101\rangle_{a_1a_2b_1b_2} +$ $x_2y_0\lvert 1000\rangle_{A_1A_2B_1B_2}\lvert 0010\rangle_{a_1a_2b_1b_2} + x_2y_1\lvert 1001\rangle_{A_1A_2B_1B_2}\lvert 0110\rangle_{a_1a_2b_1b_2} +$ $x_2y_2\lvert 1010\rangle_{A_1A_2B_1B_2}\lvert 1010\rangle_{a_1a_2b_1b_2} + x_2y_3\lvert 1011\rangle_{A_1A_2B_1B_2}\lvert 1110\rangle_{a_1a_2b_1b_2} +$ $x_3y_0\lvert 1100\rangle_{A_1A_2B_1B_2}\lvert 0011\rangle_{a_1a_2b_1b_2} + x_3y_1\lvert 1101\rangle_{A_1A_2B_1B_2}\lvert 0111\rangle_{a_1a_2b_1b_2} +$ $x_3y_2\lvert 1110\rangle_{A_1A_2B_1B_2}\lvert 1011\rangle_{a_1a_2b_1b_2} + x_3y_3\lvert 1111\rangle_{A_1A_2B_1B_2}\lvert 1111\rangle_{a_1a_2b_1b_2}$
$\lvert 0_31_3\rangle$	$x_0y_0\lvert 0000\rangle_{A_1A_2B_1B_2}\lvert 0011\rangle_{a_1a_2b_1b_2} + x_0y_1\lvert 0001\rangle_{A_1A_2B_1B_2}\lvert 0111\rangle_{a_1a_2b_1b_2} +$ $x_0y_2\lvert 0010\rangle_{A_1A_2B_1B_2}\lvert 1011\rangle_{a_1a_2b_1b_2} + x_0y_3\lvert 0011\rangle_{A_1A_2B_1B_2}\lvert 1111\rangle_{a_1a_2b_1b_2} +$ $x_1y_0\lvert 0100\rangle_{A_1A_2B_1B_2}\lvert 0010\rangle_{a_1a_2b_1b_2} + x_1y_1\lvert 0101\rangle_{A_1A_2B_1B_2}\lvert 0110\rangle_{a_1a_2b_1b_2} +$ $x_1y_2\lvert 0110\rangle_{A_1A_2B_1B_2}\lvert 1010\rangle_{a_1a_2b_1b_2} + x_1y_3\lvert 0111\rangle_{A_1A_2B_1B_2}\lvert 1110\rangle_{a_1a_2b_1b_2} +$ $x_2y_0\lvert 1000\rangle_{A_1A_2B_1B_2}\lvert 0001\rangle_{a_1a_2b_1b_2} + x_2y_1\lvert 1001\rangle_{A_1A_2B_1B_2}\lvert 0101\rangle_{a_1a_2b_1b_2} +$ $x_2y_2\lvert 1010\rangle_{A_1A_2B_1B_2}\lvert 1001\rangle_{a_1a_2b_1b_2} + x_2y_3\lvert 1011\rangle_{A_1A_2B_1B_2}\lvert 1101\rangle_{a_1a_2b_1b_2} +$ $x_3y_0\lvert 1100\rangle_{A_1A_2B_1B_2}\lvert 0000\rangle_{a_1a_2b_1b_2} + x_3y_1\lvert 1101\rangle_{A_1A_2B_1B_2}\lvert 0100\rangle_{a_1a_2b_1b_2} +$ $x_3y_2\lvert 1110\rangle_{A_1A_2B_1B_2}\lvert 1000\rangle_{a_1a_2b_1b_2} + x_3y_3\lvert 1111\rangle_{A_1A_2B_1B_2}\lvert 1100\rangle_{a_1a_2b_1b_2}$
$\lvert 1_30_3\rangle$	$x_0y_0\lvert 0000\rangle_{A_1A_2B_1B_2}\lvert 1100\rangle_{a_1a_2b_1b_2} + x_0y_1\lvert 0001\rangle_{A_1A_2B_1B_2}\lvert 1000\rangle_{a_1a_2b_1b_2} +$ $x_0y_2\lvert 0010\rangle_{A_1A_2B_1B_2}\lvert 0100\rangle_{a_1a_2b_1b_2} + x_0y_3\lvert 0011\rangle_{A_1A_2B_1B_2}\lvert 0000\rangle_{a_1a_2b_1b_2} +$ $x_1y_0\lvert 0100\rangle_{A_1A_2B_1B_2}\lvert 1101\rangle_{a_1a_2b_1b_2} + x_1y_1\lvert 0101\rangle_{A_1A_2B_1B_2}\lvert 1001\rangle_{a_1a_2b_1b_2} +$ $x_1y_2\lvert 0110\rangle_{A_1A_2B_1B_2}\lvert 0101\rangle_{a_1a_2b_1b_2} + x_1y_3\lvert 0111\rangle_{A_1A_2B_1B_2}\lvert 0001\rangle_{a_1a_2b_1b_2} +$ $x_2y_0\lvert 1000\rangle_{A_1A_2B_1B_2}\lvert 1110\rangle_{a_1a_2b_1b_2} + x_2y_1\lvert 1001\rangle_{A_1A_2B_1B_2}\lvert 1010\rangle_{a_1a_2b_1b_2} +$ $x_2y_2\lvert 1010\rangle_{A_1A_2B_1B_2}\lvert 0110\rangle_{a_1a_2b_1b_2} + x_2y_3\lvert 1011\rangle_{A_1A_2B_1B_2}\lvert 0010\rangle_{a_1a_2b_1b_2} +$ $x_3y_0\lvert 1100\rangle_{A_1A_2B_1B_2}\lvert 1111\rangle_{a_1a_2b_1b_2} + x_3y_1\lvert 1101\rangle_{A_1A_2B_1B_2}\lvert 1011\rangle_{a_1a_2b_1b_2} +$ $x_3y_2\lvert 1110\rangle_{A_1A_2B_1B_2}\lvert 0111\rangle_{a_1a_2b_1b_2} + x_3y_3\lvert 1111\rangle_{A_1A_2B_1B_2}\lvert 0011\rangle_{a_1a_2b_1b_2}$
$\lvert 1_31_3\rangle$	$x_0y_0\lvert 0000\rangle_{A_1A_2B_1B_2}\lvert 1111\rangle_{a_1a_2b_1b_2} + x_0y_1\lvert 0001\rangle_{A_1A_2B_1B_2}\lvert 1011\rangle_{a_1a_2b_1b_2} +$ $x_0y_2\lvert 0010\rangle_{A_1A_2B_1B_2}\lvert 0111\rangle_{a_1a_2b_1b_2} + x_0y_3\lvert 0011\rangle_{A_1A_2B_1B_2}\lvert 0011\rangle_{a_1a_2b_1b_2} +$ $x_1y_0\lvert 0100\rangle_{A_1A_2B_1B_2}\lvert 1110\rangle_{a_1a_2b_1b_2} + x_1y_1\lvert 0101\rangle_{A_1A_2B_1B_2}\lvert 1010\rangle_{a_1a_2b_1b_2} +$ $x_1y_2\lvert 0110\rangle_{A_1A_2B_1B_2}\lvert 0110\rangle_{a_1a_2b_1b_2} + x_1y_3\lvert 0111\rangle_{A_1A_2B_1B_2}\lvert 0010\rangle_{a_1a_2b_1b_2} +$ $x_2y_0\lvert 1000\rangle_{A_1A_2B_1B_2}\lvert 1101\rangle_{a_1a_2b_1b_2} + x_2y_1\lvert 1001\rangle_{A_1A_2B_1B_2}\lvert 1001\rangle_{a_1a_2b_1b_2} +$ $x_2y_2\lvert 1010\rangle_{A_1A_2B_1B_2}\lvert 0101\rangle_{a_1a_2b_1b_2} + x_2y_3\lvert 1011\rangle_{A_1A_2B_1B_2}\lvert 0001\rangle_{a_1a_2b_1b_2} +$ $x_3y_0\lvert 1100\rangle_{A_1A_2B_1B_2}\lvert 1100\rangle_{a_1a_2b_1b_2} + x_3y_1\lvert 1101\rangle_{A_1A_2B_1B_2}\lvert 1000\rangle_{a_1a_2b_1b_2} +$ $x_3y_2\lvert 1110\rangle_{A_1A_2B_1B_2}\lvert 0100\rangle_{a_1a_2b_1b_2} + x_3y_3\lvert 1111\rangle_{A_1A_2B_1B_2}\lvert 0000\rangle_{a_1a_2b_1b_2}$

TABLE IV.2: The collapsed state after performing the projective measurement on the states $\lvert a_3b_3\rangle$.

Depending on the measurement outcome of the qubits $\lvert A_iB_i\rangle$ for $i = 1, 2$, Alice and Bob perform the Pauli gate $\hat{\sigma}_z$ or $\hat{I}$ on the corresponding qubits as displayed in the table (IV.3).

$\lvert AB\rangle_{jk}$	$\lvert ++\rangle_{jk}$	$\lvert +-\rangle_{jk}$	$\lvert -+\rangle_{jk}$	$\lvert --\rangle_{jk}$
$\hat{U}$	$\hat{I}_j \otimes \hat{I}_k$	$\hat{\sigma}_{zk} \otimes \hat{I}_j$	$\hat{I}_k \otimes \hat{\sigma}_{zj}$	$\hat{\sigma}_{zj} \otimes \hat{\sigma}_{zk}$

TABLE IV.3: The corresponding Pauli operator to the result of measurement of qubits $\lvert AB\rangle_{jk}$ where, $i, j = 1, 2$.

For the sake of simplicity, we assume that the result of measurement is: $|00\rangle_{a_3b_3}$ and $|{+}{+}\rangle_{A_1B_1}, |{+}{+}\rangle_{A_2B_2}$.

After all these measurements, the final state collapse to:

$$\begin{aligned}|\psi\rangle_{a_1a_2b_1b_2} &= (x_0y_0\,|0000\rangle + x_0y_1\,|0100\rangle + x_0y_2\,|1000\rangle + x_0y_3\,|1100\rangle + x_1y_0\,|0001\rangle \\ &+x_1y_1\,|0101\rangle + x_1y_2\,|1001\rangle + x_1y_3\,|1101\rangle + x_2y_0\,|0010\rangle + x_2y_1\,|0110\rangle + x_2y_2\,|1010\rangle \\ &+x_2y_3\,|1110\rangle + x_3y_0\,|0011\rangle + x_3y_1\,|0111\rangle + x_3y_2\,|1011\rangle + x_3y_3\,|1111\rangle)_{a_1a_2b_1b_2} \\ &= (y_0\,|00\rangle + y_1\,|01\rangle + y_2\,|10\rangle + y_3\,|11\rangle)_{a_1a_2} \otimes (x_0\,|00\rangle + x_1\,|01\rangle + x_2\,|10\rangle + x_3\,|11\rangle)_{b_1b_2}\end{aligned} \tag{IV.37}$$

It is clear from the Eq. (IV.37) that the quantum information about the state $|Q\rangle_A$ is reconstructed in qubits b_1b_2, and the state $|Q\rangle_B$ is reconstructed in qubits a_1a_2. Indeed, depending on the measurement of the qubits $|A_1B_1\rangle$ and $|A_2B_2\rangle$, the users should apply Pauli gates $\hat{I}, \hat{\sigma}_x, \hat{\sigma}_y$, as displayed in table IV.3. On the other hand, it is important to note that the proposed protocol allows the bidirectional quantum teleportation of 2-qubit states. To achieve the BQT of the bipartite entangled state, we just set the corresponding coefficient $x_i = 0$ and $y_i = 0$ in the Eqs. (IV.29 and IV.30), e.g if we set $x_1 = 0$, $x_3 = 0$ and $y_1 = 0$, $y_3 = 0$, one could bidirectionally teleport the bipartite entangled states $|\psi^-\rangle_A = x_1|01\rangle + x_1|10\rangle$ and $|\psi^-\rangle_B = y_1|01\rangle + y_1|10\rangle$.

IV.5.3 Bidirectional teleportation of 3-qubit states

We consider a three qubit state following GSD forms [242], which is the most general pure tripartite states written in the Generalized Schmidt Decomposition (GSD) form:

$$|\psi^{GSD}\rangle = \alpha_i|000\rangle + \beta_i|001\rangle + \delta_i|010\rangle + \epsilon_i|100\rangle + \omega_i|111\rangle \tag{IV.38}$$

Where $|\alpha_i|^2 + |\beta_i|^2 + |\delta_i|^2 + |\epsilon_i|^2 + |\omega_i|^2 = 1$.

Depending on the coefficient α_i, β_i, δ_i, ϵ_i and ω_i. One can get GHZ_3 (β_i= δ_i=ϵ_i =0) or a W_3 state ($\alpha_i = \omega_i = 0$).

Now, let Alice and Bob have the following states to be teleportatd bilaterally:

$$|Q\rangle_A = \alpha_1|000\rangle + \beta_1|001\rangle + \delta_1|010\rangle + \epsilon_1|100\rangle + \omega_1|111\rangle \tag{IV.39}$$

and

$$|Q\rangle_B = \alpha_2|000\rangle + \beta_2|001\rangle + \delta_2|010\rangle + \epsilon_2|100\rangle + \omega_2|111\rangle \tag{IV.40}$$

The quantum channel is given as follows:

$$\begin{aligned}|\mathcal{Y}\rangle &= |GHZ\rangle_{a_1a_2a_3a_4} \otimes |GHZ\rangle_{b_1b_2b_3b_4} \\ &= \frac{1}{2}(|00000000\rangle + |00001111\rangle + |11110000\rangle + |111111111\rangle)_{a_1a_2a_3a_4b_1b_2b_3b_4}\end{aligned} \tag{IV.41}$$

Where : a_1 a_2 a_3 a_4 belong to Alice and b_1 b_2 b_3 b_4 belong to Bob.

The whole state of the system is given as:

$$|\psi_t\rangle = |Q\rangle_A \otimes |Q\rangle_B \otimes |GHZ\rangle_{a_1a_2a_3a_4} \otimes |GHZ\rangle_{b_1b_2b_3b_4} \tag{IV.42}$$

Now, by following the previous protocol step by step, one could bidirectionally teleport the three-qubit states.

Firstly, three non-local CNOT gates ($CNOT^{NL}$) are applied between qubits A_i ($i = 1, 2, 3$) as control qubits and ($|GHZ\rangle_{b_i}$ as target qubits, respectively. Moreover, ($CNOT^{NL}$) gate is applied between qubits B_i ($i = 1, 2, 3$) as control qubits and ($|GHZ\rangle_{a_i}$ as target qubits, respectively.

$$|\psi\rangle_t' = CNOT_3^{NL}\,|\psi\rangle_t \tag{IV.43}$$

$$\begin{aligned}
&= \alpha_1\alpha_2|000000\rangle \otimes |\mathcal{Y}\rangle + \alpha_1\beta_2|000001\rangle \otimes |\mathcal{A}\rangle + \alpha_1\delta_2|000010\rangle \otimes |\mathcal{B}\rangle + \alpha_1\epsilon_2|000100\rangle \otimes |\mathcal{D}\rangle \\
&+\alpha_1\omega_2|000111\rangle \otimes |\mathcal{E}\rangle + \beta_1\alpha_2|001000\rangle \otimes |\mathcal{F}\rangle + \beta_1\beta_2|001001\rangle \otimes |\mathcal{J}\rangle + \beta_1\delta_2|001010\rangle \otimes |\mathcal{L}\rangle \\
&+\beta_1\epsilon_2|001100\rangle \otimes |\mathcal{M}\rangle + \beta_1\omega_2|001111\rangle \otimes |\mathcal{N}\rangle + \delta_1\alpha_2|010000\rangle \otimes |\mathcal{O}\rangle + \delta_1\beta_2|010001\rangle \otimes |\mathcal{P}\rangle \\
&+\delta_1\delta_2|010010\rangle \otimes |\mathcal{Q}\rangle + \delta_1\epsilon_2|010100\rangle \otimes |\mathcal{R}\rangle + \delta_1\omega_2|010111\rangle \otimes |\mathcal{S}\rangle + \epsilon_1\alpha_2|100000\rangle \otimes |\mathcal{U}\rangle \\
&+\epsilon_1\beta_2|100001\rangle \otimes |\mathcal{V}\rangle + \epsilon_1\delta_2|100010\rangle \otimes |\mathcal{W}\rangle + \epsilon_1\epsilon_2|100100\rangle \otimes |\mathcal{X}\rangle + \epsilon_1\omega_2|100111\rangle \otimes |\mathcal{Z}\rangle \\
&+\omega_1\alpha_2|111000\rangle \otimes |v\rangle + \omega_1\beta_2|111001\rangle \otimes |\mathcal{W}'\rangle + \omega_1\delta_2|111010\rangle \otimes |\mathcal{X}'\rangle + \omega_1\epsilon_2|111100\rangle \otimes |\mathcal{Y}'\rangle \\
&+\omega_1\omega_2|111111\rangle \otimes |\mathcal{Z}'\rangle
\end{aligned} \tag{IV.44}$$

Where:

$$\begin{aligned}
|\mathcal{A}\rangle &= \frac{1}{2}(|00100000\rangle + |00101111\rangle + |11010000\rangle + |110111111\rangle)_{a_1a_2a_3a_4b_1b_2b_3b_4} \\
|\mathcal{B}\rangle &= \frac{1}{2}(|01000000\rangle + |01001111\rangle + |10110000\rangle + |101111111\rangle)_{a_1a_2a_3a_4b_1b_2b_3b_4} \\
|\mathcal{D}\rangle &= \frac{1}{2}(|10000000\rangle + |10001111\rangle + |01110000\rangle + |011111111\rangle)_{a_1a_2a_3a_4b_1b_2b_3b_4} \\
|\mathcal{E}\rangle &= \frac{1}{2}(|11100000\rangle + |11101111\rangle + |00010000\rangle + |000111111\rangle)_{a_1a_2a_3a_4b_1b_2b_3b_4} \\
|\mathcal{N}\rangle &= \frac{1}{2}(|11100010\rangle + |11101101\rangle + |00010010\rangle + |000111101\rangle)_{a_1a_2a_3a_4b_1b_2b_3b_4} \\
|\mathcal{F}\rangle &= \frac{1}{2}(|00000010\rangle + |00001101\rangle + |11110010\rangle + |111111101\rangle)_{a_1a_2a_3a_4b_1b_2b_3b_4} \\
|\mathcal{J}\rangle &= \frac{1}{2}(|00100010\rangle + |00101101\rangle + |11010010\rangle + |110111101\rangle)_{a_1a_2a_3a_4b_1b_2b_3b_4} \\
|\mathcal{L}\rangle &= \frac{1}{2}(|01000010\rangle + |01001101\rangle + |10110010\rangle + |101111101\rangle)_{a_1a_2a_3a_4b_1b_2b_3b_4} \\
|\mathcal{M}\rangle &= \frac{1}{2}(|10000010\rangle + |10001101\rangle + |01110010\rangle + |011111101\rangle)_{a_1a_2a_3a_4b_1b_2b_3b_4} \\
|\mathcal{N}\rangle &= \frac{1}{2}(|00000000\rangle + |00001111\rangle + |11110000\rangle + |111111111\rangle)_{a_1a_2a_3a_4b_1b_2b_3b_4}
\end{aligned}$$

$$
\begin{aligned}
|\mathcal{O}\rangle &= \frac{1}{2}(|00000100\rangle + |00001011\rangle + |11110100\rangle + |111111011\rangle)_{a_1a_2a_3a_4b_1b_2b_3b_4} \\
|\mathcal{P}\rangle &= \frac{1}{2}(|00100100\rangle + |00101011\rangle + |11010100\rangle + |110111011\rangle)_{a_1a_2a_3a_4b_1b_2b_3b_4} \\
|\mathcal{Q}\rangle &= \frac{1}{2}(|01000100\rangle + |01001011\rangle + |10110100\rangle + |101111011\rangle)_{a_1a_2a_3a_4b_1b_2b_3b_4} \\
|\mathcal{R}\rangle &= \frac{1}{2}(|10000100\rangle + |10001011\rangle + |01110100\rangle + |011111011\rangle)_{a_1a_2a_3a_4b_1b_2b_3b_4} \\
|\mathcal{S}\rangle &= \frac{1}{2}(|11101000\rangle + |11101011\rangle + |00010100\rangle + |000110111\rangle)_{a_1a_2a_3a_4b_1b_2b_3b_4} \\
|\mathcal{U}\rangle &= \frac{1}{2}(|10000000\rangle + |10001111\rangle + |01110000\rangle + |011111111\rangle)_{a_1a_2a_3a_4b_1b_2b_3b_4} \\
|\mathcal{V}\rangle &= \frac{1}{2}(|00101000\rangle + |00100111\rangle + |11011000\rangle + |11010111\rangle)_{a_1a_2a_3a_4b_1b_2b_3b_4} \\
|\mathcal{W}\rangle &= \frac{1}{2}(|01001000\rangle + |01000111\rangle + |10111000\rangle + |101110111\rangle)_{a_1a_2a_3a_4b_1b_2b_3b_4} \\
|\mathcal{X}\rangle &= \frac{1}{2}(|10001000\rangle + |10000111\rangle + |01111000\rangle + |01110111\rangle)_{a_1a_2a_3a_4b_1b_2b_3b_4} \\
|\mathcal{Z}\rangle &= \frac{1}{2}(|11101000\rangle + |11100111\rangle + |00011000\rangle + |00010111\rangle)_{a_1a_2a_3a_4b_1b_2b_3b_4} \\
|v\rangle &= \frac{1}{2}(|00001110\rangle + |00000001\rangle + |11111110\rangle + |111110001\rangle)_{a_1a_2a_3a_4b_1b_2b_3b_4} \\
|\mathcal{W}'\rangle &= \frac{1}{2}(|00101110\rangle + |00100001\rangle + |11011110\rangle + |110110001\rangle)_{a_1a_2a_3a_4b_1b_2b_3b_4} \\
|\mathcal{X}'\rangle &= \frac{1}{2}(|01001110\rangle + |01000001\rangle + |10111110\rangle + |101110001\rangle)_{a_1a_2a_3a_4b_1b_2b_3b_4} \\
|\mathcal{Y}'\rangle &= \frac{1}{2}(|10001110\rangle + |10000001\rangle + |01111110\rangle + |01110001\rangle)_{a_1a_2a_3a_4b_1b_2b_3b_4} \\
|\mathcal{Z}'\rangle &= \frac{1}{2}(|11101110\rangle + |11100001\rangle + |00011110\rangle + |00010001\rangle)_{a_1a_2a_3a_4b_1b_2b_3b_4}
\end{aligned} \tag{IV.45}
$$

Then, the users perform measurements on the qubits $|a_4b_4\rangle$ on the computational basis: $\{|00\rangle, |01\rangle, |10\rangle, |11\rangle\}$.

Later on, they perform a measurement on the qubits $|A_i, B_i\rangle$ (for $i = 1, 2, 3$). For the sake of simplicity, let us assume that the measurement outcomes of the states $|a_4b_4\rangle$ is $|0_40_4\rangle$ and the states $|A_i\rangle$ (for $i = 1, 2, 3$) are $|+_i +_i\rangle$ respectively. The outcome state is given as follows:

$$
\begin{aligned}
&|\psi\rangle_{a_1a_2a_3b_1b_2b_3} = \\
&(\alpha_1\alpha_2\,|000000\rangle + \alpha_1\beta_2\,|001000\rangle + \alpha_1\delta_2\,|010000\rangle + \alpha_1\epsilon_2\,|100000\rangle + \alpha_1\omega_2\,|111000\rangle \\
&+\beta_1\alpha_0\,|000001\rangle + \beta_1\beta_2\,|001001\rangle + \beta_1\delta_2\,|010001\rangle + \beta_1\epsilon\,|100001\rangle + \beta_1\omega\,|111001\rangle \\
&+\delta_1\alpha_2|000010\rangle + \delta_1\beta_2\,|001010\rangle + \delta_1\delta_2\,|010010\rangle + \delta_1\epsilon_2\,|100010\rangle + \delta_1\omega_2\,|111010\rangle \\
&+\epsilon_1\alpha_2|000100\rangle + \epsilon_1\beta_2\,|001100\rangle + \epsilon_1\delta_2\,|010100\rangle + \epsilon_1\epsilon_2\,|100100\rangle + \epsilon_1\omega_2\,|111100\rangle \\
&+\omega_1\alpha_2|000111\rangle + \omega_1\beta_2\,|001111\rangle + \omega_1\delta_2\,|010111\rangle + \omega_1\epsilon_2\,|100111\rangle + \omega_1\omega_2\,|111111\rangle)_{a_1a_2a_3b_1b_2b_3}
\end{aligned}
$$

$$
\begin{aligned}
|\psi\rangle_{a_1a_2a_3b_1b_2b_3} = &(\alpha_2|000\rangle + \beta_2|001\rangle + \delta_2|010\rangle + \epsilon_2|100\rangle + \omega_2|111\rangle)_{a_1a_2a_3} \\
&\otimes(\alpha_1|000\rangle + \beta_1|001\rangle + \delta_1|010\rangle + \epsilon_1|100\rangle + \omega_1|111\rangle)_{b_1b_2b_3}
\end{aligned}
\tag{IV.46}
$$

From the equation (IV.46), the information in the qubit $|Q\rangle_A$ is now contained in the state $|Q\rangle_B$. Similarly, the information of the state $|Q\rangle_B$ is now contained in the state $|Q\rangle_A$.

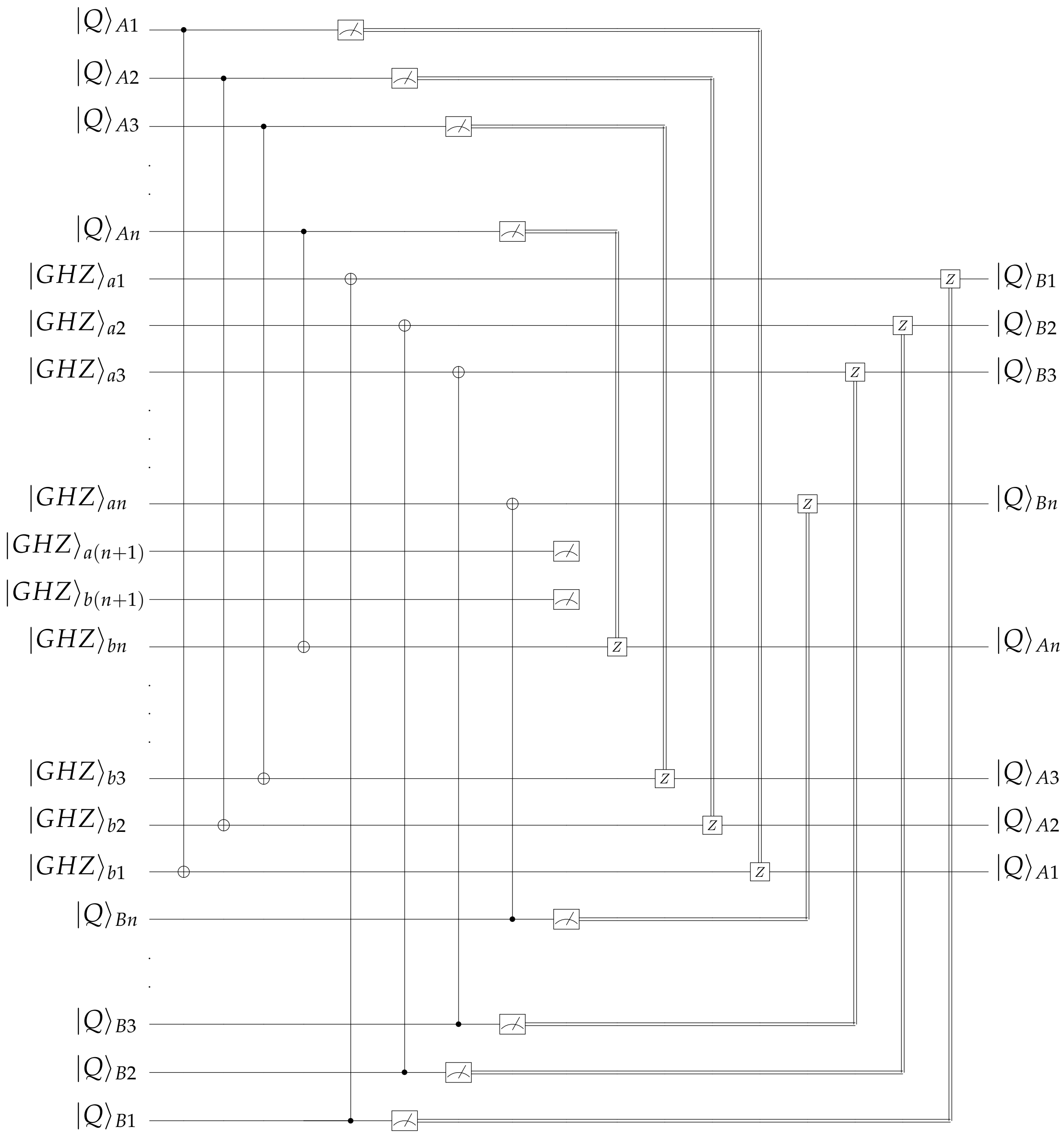

FIGURE IV.12: Quantum circuit of the n-qubit states bidirectional teleportation protocol between Alice and Bob, by means of two composite $GHZ_{(n+1)}$ state and classical communication described by double lines. The controlled Z gate denotes the Z-Pauli gate. $\bullet$ and $\oplus$ indicate the control and the target qubits of $CNOT$ gates. All the measurement outcomes (0 or 1) are transmitted via classical channels represented by double lines into gates Z.

IV.5.4 Bidirectional teleportation of n-qubit states

In fact, the suggested protocol could be extended to allow the simultaneous bidirectional teleportation of n-qubit $(n > 3)$ states, by means of an $(n+1)$ GHZ state and n trigger qubits.

We assume that Alice has the state to be teleported:

$$|Q\rangle_A = \sum_{m=1}^{2^n-1} \mathbf{A}_m |a_m\rangle \tag{IV.47}$$

Where $\mathbf{A}_m$ are complex coefficients ensuring the normalization condition:
$\sum_{m=1}^{n} |\mathbf{A}_m|^2 = 1$. In addition, a_m is a decimal value $(a_1, ..., a_n)_2$. a_m are mutually orthogonal to each other, i.e, $\langle a_j|a_k\rangle = \delta_{jk}$.

Similarly, Bob has the state:

$$|Q\rangle_B = \sum_{o=1}^{2^n-1} \mathbf{B}_o |b_o\rangle \tag{IV.48}$$

Where $\mathbf{B}_m$ are complex coefficients ensuring the normalization condition:
$\sum_{m=1}^{n} |\mathbf{B}_m|^2 = 1$. In addition, $b_m$is a decimal value $(b_1, ..., b_n)_2$. b_m are mutually orthogonal to each other, i.e, $\langle b_j|b_k\rangle = \delta_{jk}$.

The quantum channel of the proposed protocol is given as:

$$\begin{aligned}|\mathcal{G}\rangle_{a_1...a_{n+1},b_1...b_{n+1}} &= |GHZ\rangle^{\otimes(n+1)} \otimes |GHZ\rangle^{\otimes(n+1)} \\ &= \frac{1}{2}(|0\rangle^{\otimes(n+1)} + |1\rangle^{\otimes(n+1)}) \otimes (|0\rangle^{\otimes(n+1)} + |1\rangle^{\otimes(n+1)})\end{aligned} \tag{IV.49}$$

In order to allow the simultaneous bidirectional teleportation of the n-qubit stats between Alice and Bob, the same steps that are described previously for the *BQT* of 2-qubit states are required here. Alice and Bob should perform the quantum circuit given in Fig. (IV.12):

The whole state is described as follows:

$$|\psi_w\rangle = |Q\rangle_A \otimes |Q\rangle_B \otimes |\mathcal{G}\rangle_{a_1...a_{n+1},b_1...b_{n+1}} \tag{IV.50}$$

The first step is to perform non-local CNOT gates between the qubits described by the state IV.47 and the target qubits which are described by the state $|\mathcal{G}\rangle_{b_1...b_{(n+1)}}$. Moreover, non-local *CNOT* gates are applied between the qubits described by the state IV.48 and the target qubits which are described by the state $|\mathcal{G}\rangle_{a_1...a_{(n+1)}}$. Hence, we write the whole state of the system:

$$|\psi_w\rangle' = CNOT^{NL}|\psi_w\rangle \tag{IV.51}$$

Now, Alice and Bob should perform projective measurements in the qubits $|a_{n+1}, b_{n+1}\rangle$ in the computational basis $\{|00\rangle, |01\rangle, |10\rangle, |11\rangle\}$. Furthermore, Alice and Bob perform measurements on the qubits $|Q\rangle_A$ and $|Q\rangle_B$ in the X-basis, $\{|++\rangle, |+-\rangle, |-+\rangle, |--\rangle\}$.

Finally, depending on the measurements results, Alice and Bob apply the appropriate Pauli gate $\hat{\sigma}_z$ to recover the teleported states.

IV.5.5 Efficiency

The efficiency $\mathcal{E}$ provides a tool to judge the feasibility of the bidirectional quantum teleportation. Actually, the efficiency expression [243].

$$\mathcal{E} = \frac{N_t}{N_q + N_c + N_{Ax}} \tag{IV.52}$$

Where: N_t: indicates the number of qubits to be teleported.
N_q: is the number of the qubits used as the quantum channel.
N_c: represents the number of qubits used as the classical channel.
N_{Ax}: is the number of the auxiliary qubits used in the protocol.

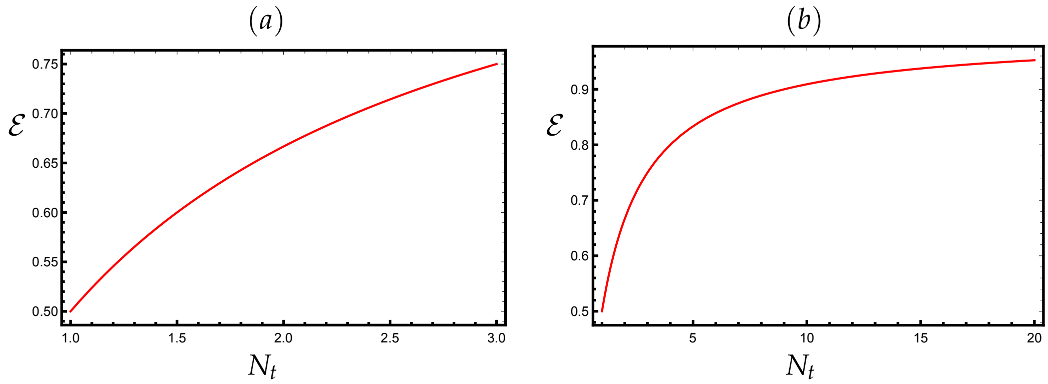

FIGURE IV.13: Efficiency of the suggested protocol versus the number of teleported qubits N_t.

The suggested protocol allows the teleportation of n-qubit, $N_t = n$, by means of $N_q = n + 1$ entangled state GHZ state. In addition, classical communication channels is essential to accomplish the bidirectional teleportation process. In fact, the efficiency of the bidirectional teleportation is rather about the ratio of the number of the teleported qubits on the number of the qubits that serves as the quantum teleportation of the BQT. Hence, the expression of the BQT efficiency is given as:

$$\mathcal{E} = \frac{n}{n+1} \tag{IV.53}$$

The efficiency of the teleportation protocol is shown in Figs. (IV.13) as a function of the number of the teleported qubits N_t. By inspection of the Figs. (IV.13.a and IV.13.b), it is apparent that the BQT efficiency gradually increases by increasing the number of the teleported qubits n.

IV.6 Conclusion

In this chapter, we suggested a new three-party bidirectional teleportation scheme, where Alice, Bob and Charlie could exchange their quantum states using a GHZ_3 state as a quantum channel and three trigger qubits. The teleportation fidelity average could be maximized by setting the trigger qubit and the initial state in the same polarization. Actually, in this suggested scheme, the receiver cannot reconstruct the teleported scheme without the contribution of the other partner, which plays the role of a mediator in the teleportation process. In addition, we extended the three-party bidirectional scheme to cover a quantum network composed by N partners. In this quantum network, an n-qubit GHZ state is considered as the quantum channel of the bidirectional quantum teleportation through this quantum network.

Furthermore, we suggested a scheme for the bidirectional non-local implementation of the $CNOT$ gate, where Alice could perform the CNOT gate on Bob's side, and reversely, Bob could perform the $CNOT$ gate on Alice's side. Based on the latter scheme, we suggested a scheme for the simultaneous bidirectional teleportation of two and three qubit states. We have shown, in particular, that by using this scheme, one could simultaneously teleport bipartite and tripartite entangled states. Also, we discussed the possibility to generalize this scheme to bidirectionally teleportation n-qubit states (with $n > 3$).

Summary and Outlook

The aim of our work was to investigate the bidirectional quantum teleportation (BQT) and to explore the new possibilities and challenges related to it. We focused on how to mitigate the effect of noise, which is a major obstacle to achieve the BQT of information with high efficiency. Furthermore, we suggested a new bidirectional teleportation scheme for quantum operation and multiparticle states. We generalized the bidirectional teleportation to cover a quantum network. The main motivation of this thesis is that the BQT is essential for quantum communication [244, 245], quantum blind computing [246] and it is crucial for the development of the quantum repeaters [39] and the quantum internet [37].

This thesis proceeds with a simplified and a focused review of some quantum information processing notions and concepts. We have investigated the BQT in perfect conditions, in which the quantum channel of the teleportation process is noiseless. We have considered the average fidelities of teleportation and the quantum Fisher information as a figure of merit to assess the bidirectional teleportation protocol. We have gone over the relationship between average fidelities and quantum Fisher information in greater detail. Indeed, the maximum values of the average fidelities and the quantum Fisher information are predicted when the quantum states to be teleported and their triggers are polarized in the same direction. However, both quantities are minimum if the initial qubits and their corresponding triggers have different polarization or non-zero phases. In the frame of the parameter estimation, we have noted that simultaneous estimation of parameters is more precise than the individual estimation form.

On the one hand, we have investigated the BQT in a more realistic situation, where the environmental noise affects the quantum channel of the BQT. The environmental noise has been modeled by typical quantum channels, which are generally used in the quantum information theory, such as the bit-flip, the phase-flip, the depolarizing and the amplitude damping channel. Moreover, we have used two techniques to suppress the effect of noise on the BQT, which are the weak and the reversed measurements (WRM), and the non-Markovian memory effects. Our objective in this part of our study was to know if these methods were efficient for all the considered types of noise. Finally, the findings of this study were that the WRM could just mitigate the amplitude damping noise if, and only if, the average fidelities of the teleported states were greater than 0.5 and the quantum Fisher information were not null. Besides, in the non-Markovian regime, the exploitation of the classical correlations of the noisy channels could enhance, to some extent, the bidirectional teleportation of information. Whilst, by taking into account the memory effects due to the temporal correlations, the drastic effect of all the considered types of noise on the bidirectional teleportation of information could notably be mitigated for a large range of time.

In addition, we have extended the BQT protocol in order to allow three legitimate partners to exchange bilaterally their quantum states using a three qubit GHZ state as a quantum channel of the teleportation. We have generalized the suggested three-party bidirectional scheme to a quantum network composed of N partners. In the suggested scheme the teleportation task cannot be completed successfully without the contribution of all the partners. In another context, so as no to restrict the BQT to the teleportation of unknown quantum states only, we have suggested a new scheme for the bidirectional implementation of the $CNOT$ gate, which is an important quantum gate for almost all quantum information and quantum computation protocols. Based on the latter scheme, we have designed a BQT protocol for the teleportation of two-qubit and three-qubit states. We have discussed the possibility to generalize this protocol to n-qubit states. To further our work, we are currently concentrating on the investigation of different topics based on the findings and the achievements of this thesis. Firstly, to further our research, we intend to generalize the bidirectional non-local implementation scheme of the $CNOT$ gate, which is suggested in this work, to other quantum gates such as the $Toffoli$ gate and other controlled gates. Secondly, we plan to investigate all the possible situations in which noise could affect the bidirectional teleportation circuit.

Generally, the findings of the current study are consistent with research that is concerned with teleportation through noisy channels, and the improvement of the teleportation efficiency. We believe that this work is a contribution to the understanding of the bidirectional teleportation and the most frequently used techniques to overcome the problem of decoherence.

Based on the different findings of this work, several and interesting issues emerge to open new future perspectives. Above all, our investigation here is limited to discrete variables (qubits) and it can be extend to opto-mechanical systems [248] and collective spins of atomic ensembles [249]. Future aspects of bidirectional quantum teleportation might focus on quantum teleportation of the energy [250]. Furthermore, our investigation of the BQT is specifically concentrated on the types of noise that are commonly used and the most probably faced in realistic situations. This work does not cover all the types of noise that exist. We may take our study further to other types of noise in future works. On the other hand, we are focused on the case in which the noise affects the BQT during the distribution process of the entangled pairs between the partners. Actually, the noise could affect the teleportation process at several points, during the measurement or the preparation of the quantum states, for example.

The future realization of scalable quantum network, where bidirectional quantum teleportation is a cornerstone, relies on the development of quantum memories [251]. This would not only allow us to distribute and receive quantum states but also guarantees the storage and the coherent processing of information. Moreover, quantum memories will allow us to use quantum repeaters for extending quantum communication well, beyond direct transmission by way of quantum error correcting codes. It will be a real future challenge to study the bidirectional quantum teleportation integrated with quantum memories since this could ultimately transform the network into a world-wide distributed quantum computer and it is a promising idea for the future quantum internet.

Overall, bidirectional teleportation is a topical subject that will undoubtly be experimentally realised soon. We are confident that our results will serve as a theoretical study that proceed the experimental realization of the bidirectional quantum teleportation.

Appendix A

The collapsed states after measurements

In the suggested bidirectional teleportation protocol for 2-qubit state, Alice and Bob make a projective measurements on the qubits $|a_3b_3\rangle$ in the computational basis $\{|00\rangle, |01\rangle, |10\rangle, |11\rangle\}$. Then, Alice and Bob make measurement on their qubits A_1 (A_2) and B_1 (B_2), respectively. In the Basis:
$\{|++\rangle, |+-\rangle, |-+\rangle, |--\rangle\}_{A_iB_j}$, for $(i, j = 1, 2)$. The results of these measurements is given in the tables bellow:

$\lvert 0_3 0_3\rangle$	$\lvert ++\rangle_{A1B1}$	$\lvert +-\rangle_{A1B1}$	$\lvert -+\rangle_{A1B1}$	$\lvert --\rangle_{A1B1}$
$\lvert ++\rangle_{A2B2}$	$x_0y_0\lvert 0000\rangle_{a_1a_2b_1b_2} +$ $x_0y_1\lvert 0100\rangle_{a_1a_2b_1b_2} +$ $x_0y_2\lvert 1000\rangle_{a_1a_2b_1b_2} +$ $x_0y_3\lvert 1100\rangle_{a_1a_2b_1b_2} +$ $x_1y_0\lvert 0010\rangle_{a_1a_2b_1b_2} +$ $x_1y_1\lvert 0101\rangle_{a_1a_2b_1b_2} +$ $x_1y_2\lvert 1001\rangle_{a_1a_2b_1b_2} +$ $x_1y_3\lvert 1101\rangle_{a_1a_2b_1b_2} +$ $x_2y_0\lvert 0010\rangle_{a_1a_2b_1b_2} +$ $x_2y_1\lvert 0110\rangle_{a_1a_2b_1b_2} +$ $x_2y_2\lvert 1010\rangle_{a_1a_2b_1b_2} +$ $x_2y_3\lvert 1110\rangle_{a_1a_2b_1b_2} +$ $x_3y_0\lvert 0011\rangle_{a_1a_2b_1b_2} +$ $x_3y_1\lvert 0111\rangle_{a_1a_2b_1b_2} +$ $x_3y_2\lvert 1011\rangle_{a_1a_2b_1b_2} +$ $x_3y_3\lvert 1111\rangle_{a_1a_2b_1b_2}$	$x_0y_0\lvert 0000\rangle_{a_1a_2b_1b_2} +$ $x_0y_1\lvert 0100\rangle_{a_1a_2b_1b_2} -$ $x_0y_2\lvert 1000\rangle_{a_1a_2b_1b_2} -$ $x_0y_3\lvert 1100\rangle_{a_1a_2b_1b_2} +$ $x_1y_0\lvert 0010\rangle_{a_1a_2b_1b_2} +$ $x_1y_1\lvert 0101\rangle_{a_1a_2b_1b_2} -$ $x_1y_2\lvert 1001\rangle_{a_1a_2b_1b_2} -$ $x_1y_3\lvert 1101\rangle_{a_1a_2b_1b_2} +$ $x_2y_0\lvert 0010\rangle_{a_1a_2b_1b_2} +$ $x_2y_1\lvert 0110\rangle_{a_1a_2b_1b_2} -$ $x_2y_2\lvert 1010\rangle_{a_1a_2b_1b_2} -$ $x_2y_3\lvert 1110\rangle_{a_1a_2b_1b_2} +$ $x_3y_0\lvert 0011\rangle_{a_1a_2b_1b_2} +$ $x_3y_1\lvert 0111\rangle_{a_1a_2b_1b_2} -$ $x_3y_2\lvert 1011\rangle_{a_1a_2b_1b_2} -$ $x_3y_3\lvert 1111\rangle_{a_1a_2b_1b_2}$	$x_0y_0\lvert 0000\rangle_{a_1a_2b_1b_2} +$ $x_0y_1\lvert 0100\rangle_{a_1a_2b_1b_2} +$ $x_0y_2\lvert 1000\rangle_{a_1a_2b_1b_2} +$ $x_0y_3\lvert 1100\rangle_{a_1a_2b_1b_2} +$ $x_1y_0\lvert 0010\rangle_{a_1a_2b_1b_2} +$ $x_1y_1\lvert 0101\rangle_{a_1a_2b_1b_2} +$ $x_1y_2\lvert 1001\rangle_{a_1a_2b_1b_2} +$ $x_1y_3\lvert 1101\rangle_{a_1a_2b_1b_2} -$ $x_2y_0\lvert 0010\rangle_{a_1a_2b_1b_2} -$ $x_2y_1\lvert 0110\rangle_{a_1a_2b_1b_2} -$ $x_2y_2\lvert 1010\rangle_{a_1a_2b_1b_2} -$ $x_2y_3\lvert 1110\rangle_{a_1a_2b_1b_2} -$ $x_3y_0\lvert 0011\rangle_{a_1a_2b_1b_2} -$ $x_3y_1\lvert 0111\rangle_{a_1a_2b_1b_2} -$ $x_3y_2\lvert 1011\rangle_{a_1a_2b_1b_2} -$ $x_3y_3\lvert 1111\rangle_{a_1a_2b_1b_2}$	$x_0y_0\lvert 0000\rangle_{a_1a_2b_1b_2} +$ $x_0y_1\lvert 0100\rangle_{a_1a_2b_1b_2} -$ $x_0y_2\lvert 1000\rangle_{a_1a_2b_1b_2} -$ $x_0y_3\lvert 1100\rangle_{a_1a_2b_1b_2} +$ $x_1y_0\lvert 0010\rangle_{a_1a_2b_1b_2} +$ $x_1y_1\lvert 0101\rangle_{a_1a_2b_1b_2} -$ $x_1y_2\lvert 1001\rangle_{a_1a_2b_1b_2} -$ $x_1y_3\lvert 1101\rangle_{a_1a_2b_1b_2} -$ $x_2y_0\lvert 0010\rangle_{a_1a_2b_1b_2} -$ $x_2y_1\lvert 0110\rangle_{a_1a_2b_1b_2} +$ $x_2y_2\lvert 1010\rangle_{a_1a_2b_1b_2} +$ $x_2y_3\lvert 1110\rangle_{a_1a_2b_1b_2} -$ $x_3y_0\lvert 0011\rangle_{a_1a_2b_1b_2} -$ $x_3y_1\lvert 0111\rangle_{a_1a_2b_1b_2} +$ $x_3y_2\lvert 1011\rangle_{a_1a_2b_1b_2} +$ $x_3y_3\lvert 1111\rangle_{a_1a_2b_1b_2}$
$\lvert +-\rangle_{A2B2}$	$x_0y_0\lvert 0000\rangle_{a_1a_2b_1b_2} -$ $x_0y_1\lvert 0100\rangle_{a_1a_2b_1b_2} +$ $x_0y_2\lvert 1000\rangle_{a_1a_2b_1b_2} -$ $x_0y_3\lvert 1100\rangle_{a_1a_2b_1b_2} +$ $x_1y_0\lvert 0010\rangle_{a_1a_2b_1b_2} -$ $x_1y_1\lvert 0101\rangle_{a_1a_2b_1b_2} +$ $x_1y_2\lvert 1001\rangle_{a_1a_2b_1b_2} -$ $x_1y_3\lvert 1101\rangle_{a_1a_2b_1b_2} +$ $x_2y_0\lvert 0010\rangle_{a_1a_2b_1b_2} -$ $x_2y_1\lvert 0110\rangle_{a_1a_2b_1b_2} +$ $x_2y_2\lvert 1010\rangle_{a_1a_2b_1b_2} -$ $x_2y_3\lvert 1110\rangle_{a_1a_2b_1b_2} +$ $x_3y_0\lvert 0011\rangle_{a_1a_2b_1b_2} -$ $x_3y_1\lvert 0111\rangle_{a_1a_2b_1b_2} +$ $x_3y_2\lvert 1011\rangle_{a_1a_2b_1b_2} -$ $x_3y_3\lvert 1111\rangle_{a_1a_2b_1b_2}$	$x_0y_0\lvert 0000\rangle_{a_1a_2b_1b_2} -$ $x_0y_1\lvert 0100\rangle_{a_1a_2b_1b_2} -$ $x_0y_2\lvert 1000\rangle_{a_1a_2b_1b_2} +$ $x_0y_3\lvert 1100\rangle_{a_1a_2b_1b_2} +$ $x_1y_0\lvert 0010\rangle_{a_1a_2b_1b_2} -$ $x_1y_1\lvert 0101\rangle_{a_1a_2b_1b_2} -$ $x_1y_2\lvert 1001\rangle_{a_1a_2b_1b_2} +$ $x_1y_3\lvert 1101\rangle_{a_1a_2b_1b_2} +$ $x_2y_0\lvert 0010\rangle_{a_1a_2b_1b_2} -$ $x_2y_1\lvert 0110\rangle_{a_1a_2b_1b_2} -$ $x_2y_2\lvert 1010\rangle_{a_1a_2b_1b_2} +$ $x_2y_3\lvert 1110\rangle_{a_1a_2b_1b_2} +$ $x_3y_0\lvert 0011\rangle_{a_1a_2b_1b_2} -$ $x_3y_1\lvert 0111\rangle_{a_1a_2b_1b_2} -$ $x_3y_2\lvert 1011\rangle_{a_1a_2b_1b_2} +$ $x_3y_3\lvert 1111\rangle_{a_1a_2b_1b_2}$	$x_0y_0\lvert 0000\rangle_{a_1a_2b_1b_2} -$ $x_0y_1\lvert 0100\rangle_{a_1a_2b_1b_2} -$ $x_0y_2\lvert 1000\rangle_{a_1a_2b_1b_2} -$ $x_0y_3\lvert 1100\rangle_{a_1a_2b_1b_2} +$ $x_1y_0\lvert 0010\rangle_{a_1a_2b_1b_2} -$ $x_1y_1\lvert 0101\rangle_{a_1a_2b_1b_2} +$ $x_1y_2\lvert 1001\rangle_{a_1a_2b_1b_2} -$ $x_1y_3\lvert 1101\rangle_{a_1a_2b_1b_2} -$ $x_2y_0\lvert 0010\rangle_{a_1a_2b_1b_2} +$ $x_2y_1\lvert 0110\rangle_{a_1a_2b_1b_2} -$ $x_2y_2\lvert 1010\rangle_{a_1a_2b_1b_2} +$ $x_2y_3\lvert 1110\rangle_{a_1a_2b_1b_2} -$ $x_3y_0\lvert 0011\rangle_{a_1a_2b_1b_2} +$ $x_3y_1\lvert 0111\rangle_{a_1a_2b_1b_2} -$ $x_3y_2\lvert 1011\rangle_{a_1a_2b_1b_2} +$ $x_3y_3\lvert 1111\rangle_{a_1a_2b_1b_2}$	$x_0y_0\lvert 0000\rangle_{a_1a_2b_1b_2} -$ $x_0y_1\lvert 0100\rangle_{a_1a_2b_1b_2} -$ $x_0y_2\lvert 1000\rangle_{a_1a_2b_1b_2} +$ $x_0y_3\lvert 1100\rangle_{a_1a_2b_1b_2} +$ $x_1y_0\lvert 0010\rangle_{a_1a_2b_1b_2} -$ $x_1y_1\lvert 0101\rangle_{a_1a_2b_1b_2} -$ $x_1y_2\lvert 1001\rangle_{a_1a_2b_1b_2} +$ $x_1y_3\lvert 1101\rangle_{a_1a_2b_1b_2} -$ $x_2y_0\lvert 0010\rangle_{a_1a_2b_1b_2} +$ $x_2y_1\lvert 0110\rangle_{a_1a_2b_1b_2} +$ $x_2y_2\lvert 1010\rangle_{a_1a_2b_1b_2} -$ $x_2y_3\lvert 1110\rangle_{a_1a_2b_1b_2} -$ $x_3y_0\lvert 0011\rangle_{a_1a_2b_1b_2} +$ $x_3y_1\lvert 0111\rangle_{a_1a_2b_1b_2} +$ $x_3y_2\lvert 1011\rangle_{a_1a_2b_1b_2} -$ $x_3y_3\lvert 1111\rangle_{a_1a_2b_1b_2}$
$\lvert -+\rangle_{A2B2}$	$x_0y_0\lvert 0000\rangle_{a_1a_2b_1b_2} -$ $x_0y_1\lvert 0100\rangle_{a_1a_2b_1b_2} +$ $x_0y_2\lvert 1000\rangle_{a_1a_2b_1b_2} +$ $x_0y_3\lvert 1100\rangle_{a_1a_2b_1b_2} -$ $x_1y_0\lvert 0010\rangle_{a_1a_2b_1b_2} -$ $x_1y_1\lvert 0101\rangle_{a_1a_2b_1b_2} -$ $x_1y_2\lvert 1001\rangle_{a_1a_2b_1b_2} -$ $x_1y_3\lvert 1101\rangle_{a_1a_2b_1b_2} +$ $x_2y_0\lvert 0010\rangle_{a_1a_2b_1b_2} +$ $x_2y_1\lvert 0110\rangle_{a_1a_2b_1b_2} +$ $x_2y_2\lvert 1010\rangle_{a_1a_2b_1b_2} +$ $x_2y_3\lvert 1110\rangle_{a_1a_2b_1b_2} -$ $x_3y_0\lvert 0011\rangle_{a_1a_2b_1b_2} -$ $x_3y_1\lvert 0111\rangle_{a_1a_2b_1b_2} -$ $x_3y_2\lvert 1011\rangle_{a_1a_2b_1b_2} -$ $x_3y_3\lvert 1111\rangle_{a_1a_2b_1b_2}$	$x_0y_0\lvert 0000\rangle_{a_1a_2b_1b_2} +$ $x_0y_1\lvert 0100\rangle_{a_1a_2b_1b_2} -$ $x_0y_2\lvert 1000\rangle_{a_1a_2b_1b_2} -$ $x_0y_3\lvert 1100\rangle_{a_1a_2b_1b_2} -$ $x_1y_0\lvert 0010\rangle_{a_1a_2b_1b_2} -$ $x_1y_1\lvert 0101\rangle_{a_1a_2b_1b_2} +$ $x_1y_2\lvert 1001\rangle_{a_1a_2b_1b_2} +$ $x_1y_3\lvert 1101\rangle_{a_1a_2b_1b_2} +$ $x_2y_0\lvert 0010\rangle_{a_1a_2b_1b_2} +$ $x_2y_1\lvert 0110\rangle_{a_1a_2b_1b_2} -$ $x_2y_2\lvert 1010\rangle_{a_1a_2b_1b_2} -$ $x_2y_3\lvert 1110\rangle_{a_1a_2b_1b_2} -$ $x_3y_0\lvert 0011\rangle_{a_1a_2b_1b_2} +$ $x_3y_1\lvert 0111\rangle_{a_1a_2b_1b_2} +$ $x_3y_2\lvert 1011\rangle_{a_1a_2b_1b_2} +$ $x_3y_3\lvert 1111\rangle_{a_1a_2b_1b_2}$	$x_0y_0\lvert 0000\rangle_{a_1a_2b_1b_2} +$ $x_0y_1\lvert 0100\rangle_{a_1a_2b_1b_2} +$ $x_0y_2\lvert 1000\rangle_{a_1a_2b_1b_2} +$ $x_0y_3\lvert 1100\rangle_{a_1a_2b_1b_2} -$ $x_1y_0\lvert 0010\rangle_{a_1a_2b_1b_2} -$ $x_1y_1\lvert 0101\rangle_{a_1a_2b_1b_2} -$ $x_1y_2\lvert 1001\rangle_{a_1a_2b_1b_2} -$ $x_1y_3\lvert 1101\rangle_{a_1a_2b_1b_2} -$ $x_2y_0\lvert 0010\rangle_{a_1a_2b_1b_2} -$ $x_2y_1\lvert 0110\rangle_{a_1a_2b_1b_2} -$ $x_2y_2\lvert 1010\rangle_{a_1a_2b_1b_2} -$ $x_2y_3\lvert 1110\rangle_{a_1a_2b_1b_2} +$ $x_3y_0\lvert 0011\rangle_{a_1a_2b_1b_2} +$ $x_3y_1\lvert 0111\rangle_{a_1a_2b_1b_2} +$ $x_3y_2\lvert 1011\rangle_{a_1a_2b_1b_2} +$ $x_3y_3\lvert 1111\rangle_{a_1a_2b_1b_2}$	$x_0y_0\lvert 0000\rangle_{a_1a_2b_1b_2} +$ $x_0y_1\lvert 0100\rangle_{a_1a_2b_1b_2} -$ $x_0y_2\lvert 1000\rangle_{a_1a_2b_1b_2} -$ $x_0y_3\lvert 1100\rangle_{a_1a_2b_1b_2} -$ $x_1y_0\lvert 0010\rangle_{a_1a_2b_1b_2} -$ $x_1y_1\lvert 0101\rangle_{a_1a_2b_1b_2} +$ $x_1y_2\lvert 1001\rangle_{a_1a_2b_1b_2} +$ $x_1y_3\lvert 1101\rangle_{a_1a_2b_1b_2} -$ $x_2y_0\lvert 0010\rangle_{a_1a_2b_1b_2} -$ $x_2y_1\lvert 0110\rangle_{a_1a_2b_1b_2} +$ $x_2y_2\lvert 1010\rangle_{a_1a_2b_1b_2} +$ $x_2y_3\lvert 1110\rangle_{a_1a_2b_1b_2} +$ $x_3y_0\lvert 0011\rangle_{a_1a_2b_1b_2} +$ $x_3y_1\lvert 0111\rangle_{a_1a_2b_1b_2} -$ $x_3y_2\lvert 1011\rangle_{a_1a_2b_1b_2} -$ $x_3y_3\lvert 1111\rangle_{a_1a_2b_1b_2}$
$\lvert --\rangle_{A2B2}$	$x_0y_0\lvert 0000\rangle_{a_1a_2b_1b_2} -$ $x_0y_1\lvert 0100\rangle_{a_1a_2b_1b_2} +$ $x_0y_2\lvert 1000\rangle_{a_1a_2b_1b_2} -$ $x_0y_3\lvert 1100\rangle_{a_1a_2b_1b_2} -$ $x_1y_0\lvert 0010\rangle_{a_1a_2b_1b_2} +$ $x_1y_1\lvert 0101\rangle_{a_1a_2b_1b_2} -$ $x_1y_2\lvert 1001\rangle_{a_1a_2b_1b_2} +$ $x_1y_3\lvert 1101\rangle_{a_1a_2b_1b_2} +$ $x_2y_0\lvert 0010\rangle_{a_1a_2b_1b_2} -$ $x_2y_1\lvert 0110\rangle_{a_1a_2b_1b_2} +$ $x_2y_2\lvert 1010\rangle_{a_1a_2b_1b_2} -$ $x_2y_3\lvert 1110\rangle_{a_1a_2b_1b_2} -$ $x_3y_0\lvert 0011\rangle_{a_1a_2b_1b_2} +$ $x_3y_1\lvert 0111\rangle_{a_1a_2b_1b_2} -$ $x_3y_2\lvert 1011\rangle_{a_1a_2b_1b_2} +$ $x_3y_3\lvert 1111\rangle_{a_1a_2b_1b_2}$	$x_0y_0\lvert 0000\rangle_{a_1a_2b_1b_2} -$ $x_0y_1\lvert 0100\rangle_{a_1a_2b_1b_2} -$ $x_0y_2\lvert 1000\rangle_{a_1a_2b_1b_2} +$ $x_0y_3\lvert 1100\rangle_{a_1a_2b_1b_2} -$ $x_1y_0\lvert 0010\rangle_{a_1a_2b_1b_2} +$ $x_1y_1\lvert 0101\rangle_{a_1a_2b_1b_2} +$ $x_1y_2\lvert 1001\rangle_{a_1a_2b_1b_2} -$ $x_1y_3\lvert 1101\rangle_{a_1a_2b_1b_2} +$ $x_2y_0\lvert 0010\rangle_{a_1a_2b_1b_2} -$ $x_2y_1\lvert 0110\rangle_{a_1a_2b_1b_2} -$ $x_2y_2\lvert 1010\rangle_{a_1a_2b_1b_2} +$ $x_2y_3\lvert 1110\rangle_{a_1a_2b_1b_2} -$ $x_3y_0\lvert 0011\rangle_{a_1a_2b_1b_2} +$ $x_3y_1\lvert 0111\rangle_{a_1a_2b_1b_2} +$ $x_3y_2\lvert 1011\rangle_{a_1a_2b_1b_2} -$ $x_3y_3\lvert 1111\rangle_{a_1a_2b_1b_2}$	$x_0y_0\lvert 0000\rangle_{a_1a_2b_1b_2} -$ $x_0y_1\lvert 0100\rangle_{a_1a_2b_1b_2} +$ $x_0y_2\lvert 1000\rangle_{a_1a_2b_1b_2} -$ $x_0y_3\lvert 1100\rangle_{a_1a_2b_1b_2} -$ $x_1y_0\lvert 0010\rangle_{a_1a_2b_1b_2} +$ $x_1y_1\lvert 0101\rangle_{a_1a_2b_1b_2} -$ $x_1y_2\lvert 1001\rangle_{a_1a_2b_1b_2} +$ $x_1y_3\lvert 1101\rangle_{a_1a_2b_1b_2} -$ $x_2y_0\lvert 0010\rangle_{a_1a_2b_1b_2} +$ $x_2y_1\lvert 0110\rangle_{a_1a_2b_1b_2} -$ $x_2y_2\lvert 1010\rangle_{a_1a_2b_1b_2} +$ $x_2y_3\lvert 1110\rangle_{a_1a_2b_1b_2} +$ $x_3y_0\lvert 0011\rangle_{a_1a_2b_1b_2} -$ $x_3y_1\lvert 0111\rangle_{a_1a_2b_1b_2} +$ $x_3y_2\lvert 1011\rangle_{a_1a_2b_1b_2} -$ $x_3y_3\lvert 1111\rangle_{a_1a_2b_1b_2}$	$x_0y_0\lvert 0000\rangle_{a_1a_2b_1b_2} -$ $x_0y_1\lvert 0100\rangle_{a_1a_2b_1b_2} -$ $x_0y_2\lvert 1000\rangle_{a_1a_2b_1b_2} +$ $x_0y_3\lvert 1100\rangle_{a_1a_2b_1b_2} -$ $x_1y_0\lvert 0010\rangle_{a_1a_2b_1b_2} +$ $x_1y_1\lvert 0101\rangle_{a_1a_2b_1b_2} +$ $x_1y_2\lvert 1001\rangle_{a_1a_2b_1b_2} -$ $x_1y_3\lvert 1101\rangle_{a_1a_2b_1b_2} -$ $x_2y_0\lvert 0010\rangle_{a_1a_2b_1b_2} +$ $x_2y_1\lvert 0110\rangle_{a_1a_2b_1b_2} +$ $x_2y_2\lvert 1010\rangle_{a_1a_2b_1b_2} -$ $x_2y_3\lvert 1110\rangle_{a_1a_2b_1b_2} +$ $x_3y_0\lvert 0011\rangle_{a_1a_2b_1b_2} -$ $x_3y_1\lvert 0111\rangle_{a_1a_2b_1b_2} -$ $x_3y_2\lvert 1011\rangle_{a_1a_2b_1b_2} +$ $x_3y_3\lvert 1111\rangle_{a_1a_2b_1b_2}$

TABLE A.1: The collapsed state after measurement on the states $\lvert A_iB_j\rangle$, with $\lvert 00\rangle_{a_3b_3}$.

$\|0_3 1_3\rangle$	$\|{++}\rangle_{A1B1}$	$\|{+-}\rangle_{A1B1}$	$\|{-+}\rangle_{A1B1}$	$\|{--}\rangle_{A1B1}$
$\|++\rangle_{A2B2}$	$x_0y_0\|0011\rangle_{a_1a_2b_1b_2} +$ $x_0y_1\|0111\rangle_{a_1a_2b_1b_2} +$ $x_0y_2\|1011\rangle_{a_1a_2b_1b_2} +$ $x_0y_3\|1111\rangle_{a_1a_2b_1b_2} +$ $x_1y_0\|0010\rangle_{a_1a_2b_1b_2} +$ $x_1y_1\|0110\rangle_{a_1a_2b_1b_2} +$ $x_1y_2\|1010\rangle_{a_1a_2b_1b_2} +$ $x_1y_3\|1110\rangle_{a_1a_2b_1b_2} +$ $x_2y_0\|0001\rangle_{a_1a_2b_1b_2} +$ $x_2y_1\|0101\rangle_{a_1a_2b_1b_2} +$ $x_2y_2\|1001\rangle_{a_1a_2b_1b_2} +$ $x_2y_3\|1101\rangle_{a_1a_2b_1b_2} +$ $x_3y_0\|0000\rangle_{a_1a_2b_1b_2} +$ $x_3y_1\|0100\rangle_{a_1a_2b_1b_2} +$ $x_3y_2\|1000\rangle_{a_1a_2b_1b_2} +$ $x_3y_3\|1100\rangle_{a_1a_2b_1b_2}$	$x_0y_0\|0011\rangle_{a_1a_2b_1b_2} +$ $x_0y_1\|0111\rangle_{a_1a_2b_1b_2} -$ $x_0y_2\|1011\rangle_{a_1a_2b_1b_2} -$ $x_0y_3\|1111\rangle_{a_1a_2b_1b_2} +$ $x_1y_0\|0010\rangle_{a_1a_2b_1b_2} +$ $x_1y_1\|0110\rangle_{a_1a_2b_1b_2} -$ $x_1y_2\|1010\rangle_{a_1a_2b_1b_2} -$ $x_1y_3\|1110\rangle_{a_1a_2b_1b_2} +$ $x_2y_0\|0001\rangle_{a_1a_2b_1b_2} +$ $x_2y_1\|0101\rangle_{a_1a_2b_1b_2} -$ $x_2y_2\|1001\rangle_{a_1a_2b_1b_2} -$ $x_2y_3\|1101\rangle_{a_1a_2b_1b_2} +$ $x_3y_0\|0000\rangle_{a_1a_2b_1b_2} +$ $x_3y_1\|0100\rangle_{a_1a_2b_1b_2} -$ $x_3y_2\|1000\rangle_{a_1a_2b_1b_2} -$ $x_3y_3\|1100\rangle_{a_1a_2b_1b_2}$	$x_0y_0\|0011\rangle_{a_1a_2b_1b_2} +$ $x_0y_1\|0111\rangle_{a_1a_2b_1b_2} +$ $x_0y_2\|1011\rangle_{a_1a_2b_1b_2} +$ $x_0y_3\|1111\rangle_{a_1a_2b_1b_2} +$ $x_1y_0\|0010\rangle_{a_1a_2b_1b_2} +$ $x_1y_1\|0110\rangle_{a_1a_2b_1b_2} +$ $x_1y_2\|1010\rangle_{a_1a_2b_1b_2} +$ $x_1y_3\|1110\rangle_{a_1a_2b_1b_2} -$ $x_2y_0\|0001\rangle_{a_1a_2b_1b_2} -$ $x_2y_1\|0101\rangle_{a_1a_2b_1b_2} -$ $x_2y_2\|1001\rangle_{a_1a_2b_1b_2} -$ $x_2y_3\|1101\rangle_{a_1a_2b_1b_2} -$ $x_3y_0\|0000\rangle_{a_1a_2b_1b_2} -$ $x_3y_1\|0100\rangle_{a_1a_2b_1b_2} -$ $x_3y_2\|1000\rangle_{a_1a_2b_1b_2} -$ $x_3y_3\|1100\rangle_{a_1a_2b_1b_2}$	$x_0y_0\|0011\rangle_{a_1a_2b_1b_2} +$ $x_0y_1\|0111\rangle_{a_1a_2b_1b_2} -$ $x_0y_2\|1011\rangle_{a_1a_2b_1b_2} -$ $x_0y_3\|1111\rangle_{a_1a_2b_1b_2} +$ $x_1y_0\|0010\rangle_{a_1a_2b_1b_2} +$ $x_1y_1\|0110\rangle_{a_1a_2b_1b_2} -$ $x_1y_2\|1010\rangle_{a_1a_2b_1b_2} -$ $x_1y_3\|1110\rangle_{a_1a_2b_1b_2} -$ $x_2y_0\|0001\rangle_{a_1a_2b_1b_2} -$ $x_2y_1\|0101\rangle_{a_1a_2b_1b_2} +$ $x_2y_2\|1001\rangle_{a_1a_2b_1b_2} +$ $x_2y_3\|1101\rangle_{a_1a_2b_1b_2} -$ $x_3y_0\|0000\rangle_{a_1a_2b_1b_2} -$ $x_3y_1\|0100\rangle_{a_1a_2b_1b_2} +$ $x_3y_2\|1000\rangle_{a_1a_2b_1b_2} -$ $x_3y_3\|1100\rangle_{a_1a_2b_1b_2}$
$\|+-\rangle_{A2B2}$	$x_0y_0\|0011\rangle_{a_1a_2b_1b_2} -$ $x_0y_1\|0111\rangle_{a_1a_2b_1b_2} +$ $x_0y_2\|1011\rangle_{a_1a_2b_1b_2} -$ $x_0y_3\|1111\rangle_{a_1a_2b_1b_2} +$ $x_1y_0\|0010\rangle_{a_1a_2b_1b_2} -$ $x_1y_1\|0110\rangle_{a_1a_2b_1b_2} +$ $x_1y_2\|1010\rangle_{a_1a_2b_1b_2} -$ $x_1y_3\|1110\rangle_{a_1a_2b_1b_2} +$ $x_2y_0\|0001\rangle_{a_1a_2b_1b_2} -$ $x_2y_1\|0101\rangle_{a_1a_2b_1b_2} +$ $x_2y_2\|1001\rangle_{a_1a_2b_1b_2} -$ $x_2y_3\|1101\rangle_{a_1a_2b_1b_2} +$ $x_3y_0\|0000\rangle_{a_1a_2b_1b_2} -$ $x_3y_1\|0100\rangle_{a_1a_2b_1b_2} +$ $x_3y_2\|1000\rangle_{a_1a_2b_1b_2} -$ $x_3y_3\|1100\rangle_{a_1a_2b_1b_2}$	$x_0y_0\|0011\rangle_{a_1a_2b_1b_2} -$ $x_0y_1\|0111\rangle_{a_1a_2b_1b_2} -$ $x_0y_2\|1011\rangle_{a_1a_2b_1b_2} +$ $x_0y_3\|1111\rangle_{a_1a_2b_1b_2} +$ $x_1y_0\|0010\rangle_{a_1a_2b_1b_2} -$ $x_1y_1\|0110\rangle_{a_1a_2b_1b_2} -$ $x_1y_2\|1010\rangle_{a_1a_2b_1b_2} +$ $x_1y_3\|1110\rangle_{a_1a_2b_1b_2} +$ $x_2y_0\|0001\rangle_{a_1a_2b_1b_2} -$ $x_2y_1\|0101\rangle_{a_1a_2b_1b_2} -$ $x_2y_2\|1001\rangle_{a_1a_2b_1b_2} +$ $x_2y_3\|1101\rangle_{a_1a_2b_1b_2} +$ $x_3y_0\|0000\rangle_{a_1a_2b_1b_2} -$ $x_3y_1\|0100\rangle_{a_1a_2b_1b_2} -$ $x_3y_2\|1000\rangle_{a_1a_2b_1b_2} +$ $x_3y_3\|1100\rangle_{a_1a_2b_1b_2}$	$x_0y_0\|0011\rangle_{a_1a_2b_1b_2} -$ $x_0y_1\|0111\rangle_{a_1a_2b_1b_2} +$ $x_0y_2\|1011\rangle_{a_1a_2b_1b_2} -$ $x_0y_3\|1111\rangle_{a_1a_2b_1b_2} +$ $x_1y_0\|0010\rangle_{a_1a_2b_1b_2} -$ $x_1y_1\|0110\rangle_{a_1a_2b_1b_2} +$ $x_1y_2\|1010\rangle_{a_1a_2b_1b_2} -$ $x_1y_3\|1110\rangle_{a_1a_2b_1b_2} -$ $x_2y_0\|0001\rangle_{a_1a_2b_1b_2} +$ $x_2y_1\|0101\rangle_{a_1a_2b_1b_2} -$ $x_2y_2\|1001\rangle_{a_1a_2b_1b_2} +$ $x_2y_3\|1101\rangle_{a_1a_2b_1b_2} -$ $x_3y_0\|0000\rangle_{a_1a_2b_1b_2} +$ $x_3y_1\|0100\rangle_{a_1a_2b_1b_2} -$ $x_3y_2\|1000\rangle_{a_1a_2b_1b_2} +$ $x_3y_3\|1100\rangle_{a_1a_2b_1b_2}$	$x_0y_0\|0011\rangle_{a_1a_2b_1b_2} -$ $x_0y_1\|0111\rangle_{a_1a_2b_1b_2} -$ $x_0y_2\|1011\rangle_{a_1a_2b_1b_2} +$ $x_0y_3\|1111\rangle_{a_1a_2b_1b_2} +$ $x_1y_0\|0010\rangle_{a_1a_2b_1b_2} -$ $x_1y_1\|0110\rangle_{a_1a_2b_1b_2} -$ $x_1y_2\|1010\rangle_{a_1a_2b_1b_2} +$ $x_1y_3\|1110\rangle_{a_1a_2b_1b_2} -$ $x_2y_0\|0001\rangle_{a_1a_2b_1b_2} +$ $x_2y_1\|0101\rangle_{a_1a_2b_1b_2} +$ $x_2y_2\|1001\rangle_{a_1a_2b_1b_2} -$ $x_2y_3\|1101\rangle_{a_1a_2b_1b_2} -$ $x_3y_0\|0000\rangle_{a_1a_2b_1b_2} +$ $x_3y_1\|0100\rangle_{a_1a_2b_1b_2} +$ $x_3y_2\|1000\rangle_{a_1a_2b_1b_2} -$ $x_3y_3\|1100\rangle_{a_1a_2b_1b_2}$
$\|-+\rangle_{A2B2}$	$x_0y_0\|0011\rangle_{a_1a_2b_1b_2} +$ $x_0y_1\|0111\rangle_{a_1a_2b_1b_2} +$ $x_0y_2\|1011\rangle_{a_1a_2b_1b_2} +$ $x_0y_3\|1111\rangle_{a_1a_2b_1b_2} -$ $x_1y_0\|0010\rangle_{a_1a_2b_1b_2} -$ $x_1y_1\|0110\rangle_{a_1a_2b_1b_2} -$ $x_1y_2\|1010\rangle_{a_1a_2b_1b_2} -$ $x_1y_3\|1110\rangle_{a_1a_2b_1b_2} +$ $x_2y_0\|0001\rangle_{a_1a_2b_1b_2} +$ $x_2y_1\|0101\rangle_{a_1a_2b_1b_2} +$ $x_2y_2\|1001\rangle_{a_1a_2b_1b_2} +$ $x_2y_3\|1101\rangle_{a_1a_2b_1b_2} -$ $x_3y_0\|0000\rangle_{a_1a_2b_1b_2} -$ $x_3y_1\|0100\rangle_{a_1a_2b_1b_2} -$ $x_3y_2\|1000\rangle_{a_1a_2b_1b_2} -$ $x_3y_3\|1100\rangle_{a_1a_2b_1b_2}$	$x_0y_0\|0011\rangle_{a_1a_2b_1b_2} +$ $x_0y_1\|0111\rangle_{a_1a_2b_1b_2} -$ $x_0y_2\|1011\rangle_{a_1a_2b_1b_2} -$ $x_0y_3\|1111\rangle_{a_1a_2b_1b_2} -$ $x_1y_0\|0010\rangle_{a_1a_2b_1b_2} -$ $x_1y_1\|0110\rangle_{a_1a_2b_1b_2} +$ $x_1y_2\|1010\rangle_{a_1a_2b_1b_2} +$ $x_1y_3\|1110\rangle_{a_1a_2b_1b_2} +$ $x_2y_0\|0001\rangle_{a_1a_2b_1b_2} +$ $x_2y_1\|0101\rangle_{a_1a_2b_1b_2} -$ $x_2y_2\|1001\rangle_{a_1a_2b_1b_2} -$ $x_2y_3\|1101\rangle_{a_1a_2b_1b_2} -$ $x_3y_0\|0000\rangle_{a_1a_2b_1b_2} -$ $x_3y_1\|0100\rangle_{a_1a_2b_1b_2} +$ $x_3y_2\|1000\rangle_{a_1a_2b_1b_2} +$ $x_3y_3\|1100\rangle_{a_1a_2b_1b_2}$	$x_0y_0\|0011\rangle_{a_1a_2b_1b_2} +$ $x_0y_1\|0111\rangle_{a_1a_2b_1b_2} +$ $x_0y_2\|1011\rangle_{a_1a_2b_1b_2} +$ $x_0y_3\|1111\rangle_{a_1a_2b_1b_2} -$ $x_1y_0\|0010\rangle_{a_1a_2b_1b_2} -$ $x_1y_1\|0110\rangle_{a_1a_2b_1b_2} -$ $x_1y_2\|1010\rangle_{a_1a_2b_1b_2} -$ $x_1y_3\|1110\rangle_{a_1a_2b_1b_2} -$ $x_2y_0\|0001\rangle_{a_1a_2b_1b_2} -$ $x_2y_1\|0101\rangle_{a_1a_2b_1b_2} -$ $x_2y_2\|1001\rangle_{a_1a_2b_1b_2} -$ $x_2y_3\|1101\rangle_{a_1a_2b_1b_2} +$ $x_3y_0\|0000\rangle_{a_1a_2b_1b_2} +$ $x_3y_1\|0100\rangle_{a_1a_2b_1b_2} +$ $x_3y_2\|1000\rangle_{a_1a_2b_1b_2} +$ $x_3y_3\|1100\rangle_{a_1a_2b_1b_2}$	$x_0y_0\|0011\rangle_{a_1a_2b_1b_2} +$ $x_0y_1\|0111\rangle_{a_1a_2b_1b_2} -$ $x_0y_2\|1011\rangle_{a_1a_2b_1b_2} -$ $x_0y_3\|1111\rangle_{a_1a_2b_1b_2} -$ $x_1y_0\|0010\rangle_{a_1a_2b_1b_2} -$ $x_1y_1\|0110\rangle_{a_1a_2b_1b_2} +$ $x_1y_2\|1010\rangle_{a_1a_2b_1b_2} +$ $x_1y_3\|1110\rangle_{a_1a_2b_1b_2} -$ $x_2y_0\|0001\rangle_{a_1a_2b_1b_2} -$ $x_2y_1\|0101\rangle_{a_1a_2b_1b_2} +$ $x_2y_2\|1001\rangle_{a_1a_2b_1b_2} +$ $x_2y_3\|1101\rangle_{a_1a_2b_1b_2} +$ $x_3y_0\|0000\rangle_{a_1a_2b_1b_2} +$ $x_3y_1\|0100\rangle_{a_1a_2b_1b_2} -$ $x_3y_2\|1000\rangle_{a_1a_2b_1b_2} -$ $x_3y_3\|1100\rangle_{a_1a_2b_1b_2}$
$\|--\rangle_{A2B2}$	$x_0y_0\|0011\rangle_{a_1a_2b_1b_2} -$ $x_0y_1\|0111\rangle_{a_1a_2b_1b_2} +$ $x_0y_2\|1011\rangle_{a_1a_2b_1b_2} -$ $x_0y_3\|1111\rangle_{a_1a_2b_1b_2} -$ $x_1y_0\|0010\rangle_{a_1a_2b_1b_2} +$ $x_1y_1\|0110\rangle_{a_1a_2b_1b_2} -$ $x_1y_2\|1010\rangle_{a_1a_2b_1b_2} +$ $x_1y_3\|1110\rangle_{a_1a_2b_1b_2} +$ $x_2y_0\|0001\rangle_{a_1a_2b_1b_2} -$ $x_2y_1\|0101\rangle_{a_1a_2b_1b_2} +$ $x_2y_2\|1001\rangle_{a_1a_2b_1b_2} -$ $x_2y_3\|1101\rangle_{a_1a_2b_1b_2} -$ $x_3y_0\|0000\rangle_{a_1a_2b_1b_2} +$ $x_3y_1\|0100\rangle_{a_1a_2b_1b_2} +$ $x_3y_2\|1000\rangle_{a_1a_2b_1b_2} -$ $x_3y_3\|1100\rangle_{a_1a_2b_1b_2}$	$x_0y_0\|0011\rangle_{a_1a_2b_1b_2} -$ $x_0y_1\|0111\rangle_{a_1a_2b_1b_2} -$ $x_0y_2\|1011\rangle_{a_1a_2b_1b_2} +$ $x_0y_3\|1111\rangle_{a_1a_2b_1b_2} -$ $x_1y_0\|0010\rangle_{a_1a_2b_1b_2} +$ $x_1y_1\|0110\rangle_{a_1a_2b_1b_2} +$ $x_1y_2\|1010\rangle_{a_1a_2b_1b_2} -$ $x_1y_3\|1110\rangle_{a_1a_2b_1b_2} +$ $x_2y_0\|0001\rangle_{a_1a_2b_1b_2} -$ $x_2y_1\|0101\rangle_{a_1a_2b_1b_2} -$ $x_2y_2\|1001\rangle_{a_1a_2b_1b_2} +$ $x_2y_3\|1101\rangle_{a_1a_2b_1b_2} -$ $x_3y_0\|0000\rangle_{a_1a_2b_1b_2} +$ $x_3y_1\|0100\rangle_{a_1a_2b_1b_2} +$ $x_3y_2\|1000\rangle_{a_1a_2b_1b_2} +$ $x_3y_3\|1100\rangle_{a_1a_2b_1b_2}$	$x_0y_0\|0011\rangle_{a_1a_2b_1b_2} -$ $x_0y_1\|0111\rangle_{a_1a_2b_1b_2} +$ $x_0y_2\|1011\rangle_{a_1a_2b_1b_2} -$ $x_0y_3\|1111\rangle_{a_1a_2b_1b_2} -$ $x_1y_0\|0010\rangle_{a_1a_2b_1b_2} +$ $x_1y_1\|0110\rangle_{a_1a_2b_1b_2} -$ $x_1y_2\|1010\rangle_{a_1a_2b_1b_2} +$ $x_1y_3\|1110\rangle_{a_1a_2b_1b_2} -$ $x_2y_0\|0001\rangle_{a_1a_2b_1b_2} +$ $x_2y_1\|0101\rangle_{a_1a_2b_1b_2} -$ $x_2y_2\|1001\rangle_{a_1a_2b_1b_2} +$ $x_2y_3\|1101\rangle_{a_1a_2b_1b_2} +$ $x_3y_0\|0000\rangle_{a_1a_2b_1b_2} -$ $x_3y_1\|0100\rangle_{a_1a_2b_1b_2} -$ $x_3y_2\|1000\rangle_{a_1a_2b_1b_2} +$ $x_3y_3\|1100\rangle_{a_1a_2b_1b_2}$	$x_0y_0\|0011\rangle_{a_1a_2b_1b_2} -$ $x_0y_1\|0111\rangle_{a_1a_2b_1b_2} -$ $x_0y_2\|1011\rangle_{a_1a_2b_1b_2} -$ $x_0y_3\|1111\rangle_{a_1a_2b_1b_2} -$ $x_1y_0\|0010\rangle_{a_1a_2b_1b_2} +$ $x_1y_1\|0110\rangle_{a_1a_2b_1b_2} +$ $x_1y_2\|1010\rangle_{a_1a_2b_1b_2} -$ $x_1y_3\|1110\rangle_{a_1a_2b_1b_2} -$ $x_2y_0\|0001\rangle_{a_1a_2b_1b_2} +$ $x_2y_1\|0101\rangle_{a_1a_2b_1b_2} +$ $x_2y_2\|1001\rangle_{a_1a_2b_1b_2} -$ $x_2y_3\|1101\rangle_{a_1a_2b_1b_2} -$ $x_3y_0\|0000\rangle_{a_1a_2b_1b_2} -$ $x_3y_1\|0100\rangle_{a_1a_2b_1b_2} -$ $x_3y_2\|1000\rangle_{a_1a_2b_1b_2} -$ $x_3y_3\|1100\rangle_{a_1a_2b_1b_2}$

TABLE A.2: The collapsed state after performing the measurement on the states $|A_iB_j\rangle$, with $|01\rangle_{a_3b_3}$

$\vert 1_3 0_3\rangle$	$\vert ++\rangle_{A1B1}$	$\vert +-\rangle_{A1B1}$	$\vert -+\rangle_{A1B1}$	$\vert --\rangle_{A1B1}$
$\vert ++\rangle_{A2B2}$	$x_0y_0\vert 1100\rangle_{a_1a_2b_1b_2} +$ $x_0y_1\vert 1000\rangle_{a_1a_2b_1b_2} +$ $x_0y_2\vert 0100\rangle_{a_1a_2b_1b_2} +$ $x_0y_3\vert 0000\rangle_{a_1a_2b_1b_2} +$ $x_1y_0\vert 1101\rangle_{a_1a_2b_1b_2} +$ $x_1y_1\vert 1001\rangle_{a_1a_2b_1b_2} +$ $x_1y_2\vert 0101\rangle_{a_1a_2b_1b_2} +$ $x_1y_3\vert 0001\rangle_{a_1a_2b_1b_2} +$ $x_2y_0\vert 1110\rangle_{a_1a_2b_1b_2} +$ $x_2y_1\vert 1010\rangle_{a_1a_2b_1b_2} +$ $x_2y_2\vert 0110\rangle_{a_1a_2b_1b_2} +$ $x_2y_3\vert 0010\rangle_{a_1a_2b_1b_2} +$ $x_3y_0\vert 1111\rangle_{a_1a_2b_1b_2} +$ $x_3y_1\vert 1011\rangle_{a_1a_2b_1b_2} +$ $x_3y_2\vert 0111\rangle_{a_1a_2b_1b_2} +$ $x_3y_3\vert 0011\rangle_{a_1a_2b_1b_2}$	$x_0y_0\vert 1100\rangle_{a_1a_2b_1b_2} -$ $x_0y_1\vert 1000\rangle_{a_1a_2b_1b_2} +$ $x_0y_2\vert 0100\rangle_{a_1a_2b_1b_2} -$ $x_0y_3\vert 0000\rangle_{a_1a_2b_1b_2} +$ $x_1y_0\vert 1101\rangle_{a_1a_2b_1b_2} +$ $x_1y_1\vert 1001\rangle_{a_1a_2b_1b_2} -$ $x_1y_2\vert 0101\rangle_{a_1a_2b_1b_2} -$ $x_1y_3\vert 0001\rangle_{a_1a_2b_1b_2} +$ $x_2y_0\vert 1110\rangle_{a_1a_2b_1b_2} +$ $x_2y_1\vert 1010\rangle_{a_1a_2b_1b_2} -$ $x_2y_2\vert 0110\rangle_{a_1a_2b_1b_2} -$ $x_2y_3\vert 0010\rangle_{a_1a_2b_1b_2} +$ $x_3y_0\vert 1111\rangle_{a_1a_2b_1b_2} +$ $x_3y_1\vert 1011\rangle_{a_1a_2b_1b_2} -$ $x_3y_2\vert 0111\rangle_{a_1a_2b_1b_2} -$ $x_3y_3\vert 0011\rangle_{a_1a_2b_1b_2}$	$x_0y_0\vert 1100\rangle_{a_1a_2b_1b_2} +$ $x_0y_1\vert 1000\rangle_{a_1a_2b_1b_2} +$ $x_0y_2\vert 0100\rangle_{a_1a_2b_1b_2} +$ $x_0y_3\vert 0000\rangle_{a_1a_2b_1b_2} +$ $x_1y_0\vert 1101\rangle_{a_1a_2b_1b_2} +$ $x_1y_1\vert 1001\rangle_{a_1a_2b_1b_2} +$ $x_1y_2\vert 0101\rangle_{a_1a_2b_1b_2} +$ $x_1y_3\vert 0001\rangle_{a_1a_2b_1b_2} -$ $x_2y_0\vert 1110\rangle_{a_1a_2b_1b_2} -$ $x_2y_1\vert 1010\rangle_{a_1a_2b_1b_2} -$ $x_2y_2\vert 0110\rangle_{a_1a_2b_1b_2} -$ $x_2y_3\vert 0010\rangle_{a_1a_2b_1b_2} -$ $x_3y_0\vert 1111\rangle_{a_1a_2b_1b_2} -$ $x_3y_1\vert 1011\rangle_{a_1a_2b_1b_2} -$ $x_3y_2\vert 0111\rangle_{a_1a_2b_1b_2} -$ $x_3y_3\vert 0011\rangle_{a_1a_2b_1b_2}$	$x_0y_0\vert 1100\rangle_{a_1a_2b_1b_2} -$ $x_0y_1\vert 1000\rangle_{a_1a_2b_1b_2} +$ $x_0y_2\vert 0100\rangle_{a_1a_2b_1b_2} -$ $x_0y_3\vert 0000\rangle_{a_1a_2b_1b_2} +$ $x_1y_0\vert 1101\rangle_{a_1a_2b_1b_2} +$ $x_1y_1\vert 1001\rangle_{a_1a_2b_1b_2} -$ $x_1y_2\vert 0101\rangle_{a_1a_2b_1b_2} -$ $x_1y_3\vert 0001\rangle_{a_1a_2b_1b_2} -$ $x_2y_0\vert 1110\rangle_{a_1a_2b_1b_2} -$ $x_2y_1\vert 1010\rangle_{a_1a_2b_1b_2} +$ $x_2y_2\vert 0110\rangle_{a_1a_2b_1b_2} +$ $x_2y_3\vert 0010\rangle_{a_1a_2b_1b_2} -$ $x_3y_0\vert 1111\rangle_{a_1a_2b_1b_2} -$ $x_3y_1\vert 1011\rangle_{a_1a_2b_1b_2} +$ $x_3y_2\vert 0111\rangle_{a_1a_2b_1b_2} +$ $x_3y_3\vert 0011\rangle_{a_1a_2b_1b_2}$
$\vert +-\rangle_{A2B2}$	$x_0y_0\vert 1100\rangle_{a_1a_2b_1b_2} -$ $x_0y_1\vert 1000\rangle_{a_1a_2b_1b_2} +$ $x_0y_2\vert 0100\rangle_{a_1a_2b_1b_2} -$ $x_0y_3\vert 0000\rangle_{a_1a_2b_1b_2} +$ $x_1y_0\vert 1101\rangle_{a_1a_2b_1b_2} -$ $x_1y_1\vert 1001\rangle_{a_1a_2b_1b_2} +$ $x_1y_2\vert 0101\rangle_{a_1a_2b_1b_2} -$ $x_1y_3\vert 0001\rangle_{a_1a_2b_1b_2} +$ $x_2y_0\vert 1110\rangle_{a_1a_2b_1b_2} -$ $x_2y_1\vert 1010\rangle_{a_1a_2b_1b_2} +$ $x_2y_2\vert 0110\rangle_{a_1a_2b_1b_2} -$ $x_2y_3\vert 0010\rangle_{a_1a_2b_1b_2} +$ $x_3y_0\vert 1111\rangle_{a_1a_2b_1b_2} -$ $x_3y_1\vert 1011\rangle_{a_1a_2b_1b_2} +$ $x_3y_2\vert 0111\rangle_{a_1a_2b_1b_2} -$ $x_3y_3\vert 0011\rangle_{a_1a_2b_1b_2}$	$x_0y_0\vert 1100\rangle_{a_1a_2b_1b_2} -$ $x_0y_1\vert 1000\rangle_{a_1a_2b_1b_2} -$ $x_0y_2\vert 0100\rangle_{a_1a_2b_1b_2} +$ $x_0y_3\vert 0000\rangle_{a_1a_2b_1b_2} +$ $x_1y_0\vert 1101\rangle_{a_1a_2b_1b_2} -$ $x_1y_1\vert 1001\rangle_{a_1a_2b_1b_2} -$ $x_1y_2\vert 0101\rangle_{a_1a_2b_1b_2} +$ $x_1y_3\vert 0001\rangle_{a_1a_2b_1b_2} +$ $x_2y_0\vert 1110\rangle_{a_1a_2b_1b_2} -$ $x_2y_1\vert 1010\rangle_{a_1a_2b_1b_2} -$ $x_2y_2\vert 0110\rangle_{a_1a_2b_1b_2} +$ $x_2y_3\vert 0010\rangle_{a_1a_2b_1b_2} +$ $x_3y_0\vert 1111\rangle_{a_1a_2b_1b_2} -$ $x_3y_1\vert 1011\rangle_{a_1a_2b_1b_2} -$ $x_3y_2\vert 0111\rangle_{a_1a_2b_1b_2} +$ $x_3y_3\vert 0011\rangle_{a_1a_2b_1b_2}$	$x_0y_0\vert 1100\rangle_{a_1a_2b_1b_2} -$ $x_0y_1\vert 1000\rangle_{a_1a_2b_1b_2} -$ $x_0y_2\vert 0100\rangle_{a_1a_2b_1b_2} +$ $x_0y_3\vert 0000\rangle_{a_1a_2b_1b_2} +$ $x_1y_0\vert 1101\rangle_{a_1a_2b_1b_2} -$ $x_1y_1\vert 1001\rangle_{a_1a_2b_1b_2} -$ $x_1y_2\vert 0101\rangle_{a_1a_2b_1b_2} +$ $x_1y_3\vert 0001\rangle_{a_1a_2b_1b_2} -$ $x_2y_0\vert 1110\rangle_{a_1a_2b_1b_2} +$ $x_2y_1\vert 1010\rangle_{a_1a_2b_1b_2} +$ $x_2y_2\vert 0110\rangle_{a_1a_2b_1b_2} -$ $x_2y_3\vert 0010\rangle_{a_1a_2b_1b_2} -$ $x_3y_0\vert 1111\rangle_{a_1a_2b_1b_2} +$ $x_3y_1\vert 1011\rangle_{a_1a_2b_1b_2} +$ $x_3y_2\vert 0111\rangle_{a_1a_2b_1b_2} -$ $x_3y_3\vert 0011\rangle_{a_1a_2b_1b_2}$	$x_0y_0\vert 1100\rangle_{a_1a_2b_1b_2} -$ $x_0y_1\vert 1000\rangle_{a_1a_2b_1b_2} -$ $x_0y_2\vert 0100\rangle_{a_1a_2b_1b_2} +$ $x_0y_3\vert 0000\rangle_{a_1a_2b_1b_2} +$ $x_1y_0\vert 1101\rangle_{a_1a_2b_1b_2} -$ $x_1y_1\vert 1001\rangle_{a_1a_2b_1b_2} -$ $x_1y_2\vert 0101\rangle_{a_1a_2b_1b_2} +$ $x_1y_3\vert 0001\rangle_{a_1a_2b_1b_2} -$ $x_2y_0\vert 1110\rangle_{a_1a_2b_1b_2} +$ $x_2y_1\vert 1010\rangle_{a_1a_2b_1b_2} +$ $x_2y_2\vert 0110\rangle_{a_1a_2b_1b_2} -$ $x_2y_3\vert 0010\rangle_{a_1a_2b_1b_2} -$ $x_3y_0\vert 1111\rangle_{a_1a_2b_1b_2} +$ $x_3y_1\vert 1011\rangle_{a_1a_2b_1b_2} +$ $x_3y_2\vert 0111\rangle_{a_1a_2b_1b_2} -$ $x_3y_3\vert 0011\rangle_{a_1a_2b_1b_2}$
$\vert -+\rangle_{A2B2}$	$x_0y_0\vert 1100\rangle_{a_1a_2b_1b_2} -$ $x_0y_1\vert 1000\rangle_{a_1a_2b_1b_2} +$ $x_0y_2\vert 0100\rangle_{a_1a_2b_1b_2} +$ $x_0y_3\vert 0000\rangle_{a_1a_2b_1b_2} -$ $x_1y_0\vert 1101\rangle_{a_1a_2b_1b_2} -$ $x_1y_1\vert 1001\rangle_{a_1a_2b_1b_2} -$ $x_1y_2\vert 0101\rangle_{a_1a_2b_1b_2} -$ $x_1y_3\vert 0001\rangle_{a_1a_2b_1b_2} +$ $x_2y_0\vert 1110\rangle_{a_1a_2b_1b_2} +$ $x_2y_1\vert 1010\rangle_{a_1a_2b_1b_2} +$ $x_2y_2\vert 0110\rangle_{a_1a_2b_1b_2} +$ $x_2y_3\vert 0010\rangle_{a_1a_2b_1b_2} -$ $x_3y_0\vert 1111\rangle_{a_1a_2b_1b_2} -$ $x_3y_1\vert 1011\rangle_{a_1a_2b_1b_2} -$ $x_3y_2\vert 0111\rangle_{a_1a_2b_1b_2} -$ $x_3y_3\vert 0011\rangle_{a_1a_2b_1b_2}$	$x_0y_0\vert 1100\rangle_{a_1a_2b_1b_2} -$ $x_0y_1\vert 1000\rangle_{a_1a_2b_1b_2} -$ $x_0y_2\vert 0100\rangle_{a_1a_2b_1b_2} -$ $x_0y_3\vert 0000\rangle_{a_1a_2b_1b_2} -$ $x_1y_0\vert 1101\rangle_{a_1a_2b_1b_2} -$ $x_1y_1\vert 1001\rangle_{a_1a_2b_1b_2} +$ $x_1y_2\vert 0101\rangle_{a_1a_2b_1b_2} +$ $x_1y_3\vert 0001\rangle_{a_1a_2b_1b_2} +$ $x_2y_0\vert 1110\rangle_{a_1a_2b_1b_2} +$ $x_2y_1\vert 1010\rangle_{a_1a_2b_1b_2} -$ $x_2y_2\vert 0110\rangle_{a_1a_2b_1b_2} -$ $x_2y_3\vert 0010\rangle_{a_1a_2b_1b_2} -$ $x_3y_0\vert 1111\rangle_{a_1a_2b_1b_2} -$ $x_3y_1\vert 1011\rangle_{a_1a_2b_1b_2} +$ $x_3y_2\vert 0111\rangle_{a_1a_2b_1b_2} +$ $x_3y_3\vert 0011\rangle_{a_1a_2b_1b_2}$	$x_0y_0\vert 1100\rangle_{a_1a_2b_1b_2} -$ $x_0y_1\vert 1000\rangle_{a_1a_2b_1b_2} +$ $x_0y_2\vert 0100\rangle_{a_1a_2b_1b_2} +$ $x_0y_3\vert 0000\rangle_{a_1a_2b_1b_2} -$ $x_1y_0\vert 1101\rangle_{a_1a_2b_1b_2} -$ $x_1y_1\vert 1001\rangle_{a_1a_2b_1b_2} -$ $x_1y_2\vert 0101\rangle_{a_1a_2b_1b_2} -$ $x_1y_3\vert 0001\rangle_{a_1a_2b_1b_2} -$ $x_2y_0\vert 1110\rangle_{a_1a_2b_1b_2} -$ $x_2y_1\vert 1010\rangle_{a_1a_2b_1b_2} -$ $x_2y_2\vert 0110\rangle_{a_1a_2b_1b_2} -$ $x_2y_3\vert 0010\rangle_{a_1a_2b_1b_2} +$ $x_3y_0\vert 1111\rangle_{a_1a_2b_1b_2} +$ $x_3y_1\vert 1011\rangle_{a_1a_2b_1b_2} +$ $x_3y_2\vert 0111\rangle_{a_1a_2b_1b_2} +$ $x_3y_3\vert 0011\rangle_{a_1a_2b_1b_2}$	$x_0y_0\vert 1100\rangle_{a_1a_2b_1b_2} -$ $x_0y_1\vert 1000\rangle_{a_1a_2b_1b_2} -$ $x_0y_2\vert 0100\rangle_{a_1a_2b_1b_2} -$ $x_0y_3\vert 0000\rangle_{a_1a_2b_1b_2} -$ $x_1y_0\vert 1101\rangle_{a_1a_2b_1b_2} -$ $x_1y_1\vert 1001\rangle_{a_1a_2b_1b_2} +$ $x_1y_2\vert 0101\rangle_{a_1a_2b_1b_2} +$ $x_1y_3\vert 0001\rangle_{a_1a_2b_1b_2} -$ $x_2y_0\vert 1110\rangle_{a_1a_2b_1b_2} -$ $x_2y_1\vert 1010\rangle_{a_1a_2b_1b_2} +$ $x_2y_2\vert 0110\rangle_{a_1a_2b_1b_2} +$ $x_2y_3\vert 0010\rangle_{a_1a_2b_1b_2} +$ $x_3y_0\vert 1111\rangle_{a_1a_2b_1b_2} +$ $x_3y_1\vert 1011\rangle_{a_1a_2b_1b_2} -$ $x_3y_2\vert 0111\rangle_{a_1a_2b_1b_2} -$ $x_3y_3\vert 0011\rangle_{a_1a_2b_1b_2}$
$\vert --\rangle_{A2B2}$	$x_0y_0\vert 1100\rangle_{a_1a_2b_1b_2} -$ $x_0y_1\vert 1000\rangle_{a_1a_2b_1b_2} +$ $x_0y_2\vert 0100\rangle_{a_1a_2b_1b_2} -$ $x_0y_3\vert 0000\rangle_{a_1a_2b_1b_2} -$ $x_1y_0\vert 1101\rangle_{a_1a_2b_1b_2} +$ $x_1y_1\vert 1001\rangle_{a_1a_2b_1b_2} -$ $x_1y_2\vert 0101\rangle_{a_1a_2b_1b_2} +$ $x_1y_3\vert 0001\rangle_{a_1a_2b_1b_2} +$ $x_2y_0\vert 1110\rangle_{a_1a_2b_1b_2} -$ $x_2y_1\vert 1010\rangle_{a_1a_2b_1b_2} +$ $x_2y_2\vert 0110\rangle_{a_1a_2b_1b_2} -$ $x_2y_3\vert 0010\rangle_{a_1a_2b_1b_2} -$ $x_3y_0\vert 1111\rangle_{a_1a_2b_1b_2} +$ $x_3y_1\vert 1011\rangle_{a_1a_2b_1b_2} -$ $x_3y_2\vert 0111\rangle_{a_1a_2b_1b_2} +$ $x_3y_3\vert 0011\rangle_{a_1a_2b_1b_2}$	$x_0y_0\vert 1100\rangle_{a_1a_2b_1b_2} -$ $x_0y_1\vert 1000\rangle_{a_1a_2b_1b_2} -$ $x_0y_2\vert 0100\rangle_{a_1a_2b_1b_2} +$ $x_0y_3\vert 0000\rangle_{a_1a_2b_1b_2} -$ $x_1y_0\vert 1101\rangle_{a_1a_2b_1b_2} +$ $x_1y_1\vert 1001\rangle_{a_1a_2b_1b_2} +$ $x_1y_2\vert 0101\rangle_{a_1a_2b_1b_2} -$ $x_1y_3\vert 0001\rangle_{a_1a_2b_1b_2} +$ $x_2y_0\vert 1110\rangle_{a_1a_2b_1b_2} -$ $x_2y_1\vert 1010\rangle_{a_1a_2b_1b_2} -$ $x_2y_2\vert 0110\rangle_{a_1a_2b_1b_2} +$ $x_2y_3\vert 0010\rangle_{a_1a_2b_1b_2} -$ $x_3y_0\vert 1111\rangle_{a_1a_2b_1b_2} +$ $x_3y_1\vert 1011\rangle_{a_1a_2b_1b_2} +$ $x_3y_2\vert 0111\rangle_{a_1a_2b_1b_2} -$ $x_3y_3\vert 0011\rangle_{a_1a_2b_1b_2}$	$x_0y_0\vert 1100\rangle_{a_1a_2b_1b_2} -$ $x_0y_1\vert 1000\rangle_{a_1a_2b_1b_2} +$ $x_0y_2\vert 0100\rangle_{a_1a_2b_1b_2} -$ $x_0y_3\vert 0000\rangle_{a_1a_2b_1b_2} -$ $x_1y_0\vert 1101\rangle_{a_1a_2b_1b_2} +$ $x_1y_1\vert 1001\rangle_{a_1a_2b_1b_2} -$ $x_1y_2\vert 0101\rangle_{a_1a_2b_1b_2} +$ $x_1y_3\vert 0001\rangle_{a_1a_2b_1b_2} -$ $x_2y_0\vert 1110\rangle_{a_1a_2b_1b_2} +$ $x_2y_1\vert 1010\rangle_{a_1a_2b_1b_2} -$ $x_2y_2\vert 0110\rangle_{a_1a_2b_1b_2} +$ $x_2y_3\vert 0010\rangle_{a_1a_2b_1b_2} +$ $x_3y_0\vert 1111\rangle_{a_1a_2b_1b_2} -$ $x_3y_1\vert 1011\rangle_{a_1a_2b_1b_2} +$ $x_3y_2\vert 0111\rangle_{a_1a_2b_1b_2} -$ $x_3y_3\vert 0011\rangle_{a_1a_2b_1b_2}$	$x_0y_0\vert 1100\rangle_{a_1a_2b_1b_2} -$ $x_0y_1\vert 1000\rangle_{a_1a_2b_1b_2} -$ $x_0y_2\vert 0100\rangle_{a_1a_2b_1b_2} +$ $x_0y_3\vert 0000\rangle_{a_1a_2b_1b_2} -$ $x_1y_0\vert 1101\rangle_{a_1a_2b_1b_2} +$ $x_1y_1\vert 1001\rangle_{a_1a_2b_1b_2} +$ $x_1y_2\vert 0101\rangle_{a_1a_2b_1b_2} -$ $x_1y_3\vert 0001\rangle_{a_1a_2b_1b_2} -$ $x_2y_0\vert 1110\rangle_{a_1a_2b_1b_2} +$ $x_2y_1\vert 1010\rangle_{a_1a_2b_1b_2} +$ $x_2y_2\vert 0110\rangle_{a_1a_2b_1b_2} -$ $x_2y_3\vert 0010\rangle_{a_1a_2b_1b_2} +$ $x_3y_0\vert 1111\rangle_{a_1a_2b_1b_2} -$ $x_3y_1\vert 1011\rangle_{a_1a_2b_1b_2} -$ $x_3y_2\vert 0111\rangle_{a_1a_2b_1b_2} +$ $x_3y_3\vert 0011\rangle_{a_1a_2b_1b_2}$

TABLE A.3: The collapsed state after performing the measurement on the states $\vert A_iB_j\rangle$, with $\vert 10\rangle_{a_3b_3}$

$\|1_31_3\rangle$	$\|{+}{+}\rangle_{A1B1}$	$\|{+}{-}\rangle_{A1B1}$	$\|{-}{+}\rangle_{A1B1}$	$\|{-}{-}\rangle_{A1B1}$
$\|{+}{+}\rangle_{A2B2}$	$x_0y_0\|1111\rangle_{a_1a_2b_1b_2}+$ $x_0y_1\|1011\rangle_{a_1a_2b_1b_2}+$ $x_0y_2\|0111\rangle_{a_1a_2b_1b_2}+$ $x_0y_3\|0011\rangle_{a_1a_2b_1b_2}+$ $x_1y_0\|1110\rangle_{a_1a_2b_1b_2}+$ $x_1y_1\|1010\rangle_{a_1a_2b_1b_2}+$ $x_1y_2\|0110\rangle_{a_1a_2b_1b_2}+$ $x_1y_3\|0010\rangle_{a_1a_2b_1b_2}+$ $x_2y_0\|1101\rangle_{a_1a_2b_1b_2}+$ $x_2y_1\|1001\rangle_{a_1a_2b_1b_2}+$ $x_2y_2\|0101\rangle_{a_1a_2b_1b_2}+$ $x_2y_3\|0001\rangle_{a_1a_2b_1b_2}+$ $x_3y_0\|1100\rangle_{a_1a_2b_1b_2}+$ $x_3y_1\|1000\rangle_{a_1a_2b_1b_2}+$ $x_3y_2\|0100\rangle_{a_1a_2b_1b_2}+$ $x_3y_3\|0000\rangle_{a_1a_2b_1b_2}$	$x_0y_0\|1111\rangle_{a_1a_2b_1b_2}+$ $x_0y_1\|1011\rangle_{a_1a_2b_1b_2}-$ $x_0y_2\|0111\rangle_{a_1a_2b_1b_2}-$ $x_0y_3\|0011\rangle_{a_1a_2b_1b_2}+$ $x_1y_0\|1110\rangle_{a_1a_2b_1b_2}+$ $x_1y_1\|1010\rangle_{a_1a_2b_1b_2}-$ $x_1y_2\|0110\rangle_{a_1a_2b_1b_2}-$ $x_1y_3\|0010\rangle_{a_1a_2b_1b_2}+$ $x_2y_0\|1101\rangle_{a_1a_2b_1b_2}+$ $x_2y_1\|1001\rangle_{a_1a_2b_1b_2}-$ $x_2y_2\|0101\rangle_{a_1a_2b_1b_2}-$ $x_2y_3\|0001\rangle_{a_1a_2b_1b_2}+$ $x_3y_0\|1100\rangle_{a_1a_2b_1b_2}+$ $x_3y_1\|1000\rangle_{a_1a_2b_1b_2}-$ $x_3y_2\|0100\rangle_{a_1a_2b_1b_2}-$ $x_3y_3\|0000\rangle_{a_1a_2b_1b_2}$	$x_0y_0\|1111\rangle_{a_1a_2b_1b_2}+$ $x_0y_1\|1011\rangle_{a_1a_2b_1b_2}+$ $x_0y_2\|0111\rangle_{a_1a_2b_1b_2}+$ $x_0y_3\|0011\rangle_{a_1a_2b_1b_2}+$ $x_1y_0\|1110\rangle_{a_1a_2b_1b_2}+$ $x_1y_1\|1010\rangle_{a_1a_2b_1b_2}+$ $x_1y_2\|0110\rangle_{a_1a_2b_1b_2}+$ $x_1y_3\|0010\rangle_{a_1a_2b_1b_2}-$ $x_2y_0\|1101\rangle_{a_1a_2b_1b_2}-$ $x_2y_1\|1001\rangle_{a_1a_2b_1b_2}-$ $x_2y_2\|0101\rangle_{a_1a_2b_1b_2}-$ $x_2y_3\|0001\rangle_{a_1a_2b_1b_2}-$ $x_3y_0\|1100\rangle_{a_1a_2b_1b_2}-$ $x_3y_1\|1000\rangle_{a_1a_2b_1b_2}-$ $x_3y_2\|0100\rangle_{a_1a_2b_1b_2}-$ $x_3y_3\|0000\rangle_{a_1a_2b_1b_2}$	$x_0y_0\|1111\rangle_{a_1a_2b_1b_2}+$ $x_0y_1\|1011\rangle_{a_1a_2b_1b_2}-$ $x_0y_2\|0111\rangle_{a_1a_2b_1b_2}-$ $x_0y_3\|0011\rangle_{a_1a_2b_1b_2}+$ $x_1y_0\|1110\rangle_{a_1a_2b_1b_2}+$ $x_1y_1\|1010\rangle_{a_1a_2b_1b_2}-$ $x_1y_2\|0110\rangle_{a_1a_2b_1b_2}-$ $x_1y_3\|0010\rangle_{a_1a_2b_1b_2}-$ $x_2y_0\|1101\rangle_{a_1a_2b_1b_2}-$ $x_2y_1\|1001\rangle_{a_1a_2b_1b_2}+$ $x_2y_2\|0101\rangle_{a_1a_2b_1b_2}+$ $x_2y_3\|0001\rangle_{a_1a_2b_1b_2}-$ $x_3y_0\|1100\rangle_{a_1a_2b_1b_2}-$ $x_3y_1\|1000\rangle_{a_1a_2b_1b_2}+$ $x_3y_2\|0100\rangle_{a_1a_2b_1b_2}+$ $x_3y_3\|0000\rangle_{a_1a_2b_1b_2}$
$\|{+}{-}\rangle_{A2B2}$	$x_0y_0\|1111\rangle_{a_1a_2b_1b_2}-$ $x_0y_1\|1011\rangle_{a_1a_2b_1b_2}+$ $x_0y_2\|0111\rangle_{a_1a_2b_1b_2}-$ $x_0y_3\|0011\rangle_{a_1a_2b_1b_2}+$ $x_1y_0\|1110\rangle_{a_1a_2b_1b_2}-$ $x_1y_1\|1010\rangle_{a_1a_2b_1b_2}+$ $x_1y_2\|0110\rangle_{a_1a_2b_1b_2}-$ $x_1y_3\|0010\rangle_{a_1a_2b_1b_2}+$ $x_2y_0\|1101\rangle_{a_1a_2b_1b_2}-$ $x_2y_1\|1001\rangle_{a_1a_2b_1b_2}+$ $x_2y_2\|0101\rangle_{a_1a_2b_1b_2}-$ $x_2y_3\|0001\rangle_{a_1a_2b_1b_2}+$ $x_3y_0\|1100\rangle_{a_1a_2b_1b_2}-$ $x_3y_1\|1000\rangle_{a_1a_2b_1b_2}+$ $x_3y_2\|0100\rangle_{a_1a_2b_1b_2}-$ $x_3y_3\|0000\rangle_{a_1a_2b_1b_2}$	$x_0y_0\|1111\rangle_{a_1a_2b_1b_2}-$ $x_0y_1\|1011\rangle_{a_1a_2b_1b_2}-$ $x_0y_2\|0111\rangle_{a_1a_2b_1b_2}+$ $x_0y_3\|0011\rangle_{a_1a_2b_1b_2}+$ $x_1y_0\|1110\rangle_{a_1a_2b_1b_2}-$ $x_1y_1\|1010\rangle_{a_1a_2b_1b_2}-$ $x_1y_2\|0110\rangle_{a_1a_2b_1b_2}+$ $x_1y_3\|0010\rangle_{a_1a_2b_1b_2}+$ $x_2y_0\|1101\rangle_{a_1a_2b_1b_2}-$ $x_2y_1\|1001\rangle_{a_1a_2b_1b_2}-$ $x_2y_2\|0101\rangle_{a_1a_2b_1b_2}+$ $x_2y_3\|0001\rangle_{a_1a_2b_1b_2}+$ $x_3y_0\|1100\rangle_{a_1a_2b_1b_2}-$ $x_3y_1\|1000\rangle_{a_1a_2b_1b_2}-$ $x_3y_2\|0100\rangle_{a_1a_2b_1b_2}+$ $x_3y_3\|0000\rangle_{a_1a_2b_1b_2}$	$x_0y_0\|1111\rangle_{a_1a_2b_1b_2}-$ $x_0y_1\|1011\rangle_{a_1a_2b_1b_2}+$ $x_0y_2\|0111\rangle_{a_1a_2b_1b_2}-$ $x_0y_3\|0011\rangle_{a_1a_2b_1b_2}+$ $x_1y_0\|1110\rangle_{a_1a_2b_1b_2}-$ $x_1y_1\|1010\rangle_{a_1a_2b_1b_2}+$ $x_1y_2\|0110\rangle_{a_1a_2b_1b_2}-$ $x_1y_3\|0010\rangle_{a_1a_2b_1b_2}-$ $x_2y_0\|1101\rangle_{a_1a_2b_1b_2}+$ $x_2y_1\|1001\rangle_{a_1a_2b_1b_2}-$ $x_2y_2\|0101\rangle_{a_1a_2b_1b_2}+$ $x_2y_3\|0001\rangle_{a_1a_2b_1b_2}-$ $x_3y_0\|1100\rangle_{a_1a_2b_1b_2}+$ $x_3y_1\|1000\rangle_{a_1a_2b_1b_2}-$ $x_3y_2\|0100\rangle_{a_1a_2b_1b_2}+$ $x_3y_3\|0000\rangle_{a_1a_2b_1b_2}$	$x_0y_0\|1111\rangle_{a_1a_2b_1b_2}-$ $x_0y_1\|1011\rangle_{a_1a_2b_1b_2}-$ $x_0y_2\|0111\rangle_{a_1a_2b_1b_2}+$ $x_0y_3\|0011\rangle_{a_1a_2b_1b_2}+$ $x_1y_0\|1110\rangle_{a_1a_2b_1b_2}-$ $x_1y_1\|1010\rangle_{a_1a_2b_1b_2}-$ $x_1y_2\|0110\rangle_{a_1a_2b_1b_2}+$ $x_1y_3\|0010\rangle_{a_1a_2b_1b_2}-$ $x_2y_0\|1101\rangle_{a_1a_2b_1b_2}+$ $x_2y_1\|1001\rangle_{a_1a_2b_1b_2}+$ $x_2y_2\|0101\rangle_{a_1a_2b_1b_2}-$ $x_2y_3\|0001\rangle_{a_1a_2b_1b_2}-$ $x_3y_0\|1100\rangle_{a_1a_2b_1b_2}+$ $x_3y_1\|1000\rangle_{a_1a_2b_1b_2}+$ $x_3y_2\|0100\rangle_{a_1a_2b_1b_2}-$ $x_3y_3\|0000\rangle_{a_1a_2b_1b_2}$
$\|{-}{+}\rangle_{A2B2}$	$x_0y_0\|1111\rangle_{a_1a_2b_1b_2}+$ $x_0y_1\|1011\rangle_{a_1a_2b_1b_2}+$ $x_0y_2\|0111\rangle_{a_1a_2b_1b_2}+$ $x_0y_3\|0011\rangle_{a_1a_2b_1b_2}-$ $x_1y_0\|1110\rangle_{a_1a_2b_1b_2}-$ $x_1y_1\|1010\rangle_{a_1a_2b_1b_2}-$ $x_1y_2\|0110\rangle_{a_1a_2b_1b_2}-$ $x_1y_3\|0010\rangle_{a_1a_2b_1b_2}+$ $x_2y_0\|1101\rangle_{a_1a_2b_1b_2}+$ $x_2y_1\|1001\rangle_{a_1a_2b_1b_2}+$ $x_2y_2\|0101\rangle_{a_1a_2b_1b_2}+$ $x_2y_3\|0001\rangle_{a_1a_2b_1b_2}-$ $x_3y_0\|1100\rangle_{a_1a_2b_1b_2}-$ $x_3y_1\|1000\rangle_{a_1a_2b_1b_2}-$ $x_3y_2\|0100\rangle_{a_1a_2b_1b_2}-$ $x_3y_3\|0000\rangle_{a_1a_2b_1b_2}$	$x_0y_0\|1111\rangle_{a_1a_2b_1b_2}+$ $x_0y_1\|1011\rangle_{a_1a_2b_1b_2}-$ $x_0y_2\|0111\rangle_{a_1a_2b_1b_2}-$ $x_0y_3\|0011\rangle_{a_1a_2b_1b_2}-$ $x_1y_0\|1110\rangle_{a_1a_2b_1b_2}-$ $x_1y_1\|1010\rangle_{a_1a_2b_1b_2}+$ $x_1y_2\|0110\rangle_{a_1a_2b_1b_2}+$ $x_1y_3\|0010\rangle_{a_1a_2b_1b_2}+$ $x_2y_0\|1101\rangle_{a_1a_2b_1b_2}+$ $x_2y_1\|1001\rangle_{a_1a_2b_1b_2}-$ $x_2y_2\|0101\rangle_{a_1a_2b_1b_2}-$ $x_2y_3\|0001\rangle_{a_1a_2b_1b_2}-$ $x_3y_0\|1100\rangle_{a_1a_2b_1b_2}-$ $x_3y_1\|1000\rangle_{a_1a_2b_1b_2}+$ $x_3y_2\|0100\rangle_{a_1a_2b_1b_2}+$ $x_3y_3\|0000\rangle_{a_1a_2b_1b_2}$	$x_0y_0\|1111\rangle_{a_1a_2b_1b_2}+$ $x_0y_1\|1011\rangle_{a_1a_2b_1b_2}+$ $x_0y_2\|0111\rangle_{a_1a_2b_1b_2}+$ $x_0y_3\|0011\rangle_{a_1a_2b_1b_2}-$ $x_1y_0\|1110\rangle_{a_1a_2b_1b_2}-$ $x_1y_1\|1010\rangle_{a_1a_2b_1b_2}-$ $x_1y_2\|0110\rangle_{a_1a_2b_1b_2}-$ $x_1y_3\|0010\rangle_{a_1a_2b_1b_2}-$ $x_2y_0\|1101\rangle_{a_1a_2b_1b_2}-$ $x_2y_1\|1001\rangle_{a_1a_2b_1b_2}-$ $x_2y_2\|0101\rangle_{a_1a_2b_1b_2}-$ $x_2y_3\|0001\rangle_{a_1a_2b_1b_2}+$ $x_3y_0\|1100\rangle_{a_1a_2b_1b_2}+$ $x_3y_1\|1000\rangle_{a_1a_2b_1b_2}+$ $x_3y_2\|0100\rangle_{a_1a_2b_1b_2}+$ $x_3y_3\|0000\rangle_{a_1a_2b_1b_2}$	$x_0y_0\|1111\rangle_{a_1a_2b_1b_2}+$ $x_0y_1\|1011\rangle_{a_1a_2b_1b_2}-$ $x_0y_2\|0111\rangle_{a_1a_2b_1b_2}-$ $x_0y_3\|0011\rangle_{a_1a_2b_1b_2}-$ $x_1y_0\|1110\rangle_{a_1a_2b_1b_2}-$ $x_1y_1\|1010\rangle_{a_1a_2b_1b_2}+$ $x_1y_2\|0110\rangle_{a_1a_2b_1b_2}+$ $x_1y_3\|0010\rangle_{a_1a_2b_1b_2}-$ $x_2y_0\|1101\rangle_{a_1a_2b_1b_2}-$ $x_2y_1\|1001\rangle_{a_1a_2b_1b_2}+$ $x_2y_2\|0101\rangle_{a_1a_2b_1b_2}+$ $x_2y_3\|0001\rangle_{a_1a_2b_1b_2}+$ $x_3y_0\|1100\rangle_{a_1a_2b_1b_2}+$ $x_3y_1\|1000\rangle_{a_1a_2b_1b_2}-$ $x_3y_2\|0100\rangle_{a_1a_2b_1b_2}-$ $x_3y_3\|0000\rangle_{a_1a_2b_1b_2}$
$\|{-}{-}\rangle_{A2B2}$	$x_0y_0\|1111\rangle_{a_1a_2b_1b_2}-$ $x_0y_1\|1011\rangle_{a_1a_2b_1b_2}+$ $x_0y_2\|0111\rangle_{a_1a_2b_1b_2}-$ $x_0y_3\|0011\rangle_{a_1a_2b_1b_2}-$ $x_1y_0\|1110\rangle_{a_1a_2b_1b_2}+$ $x_1y_1\|1010\rangle_{a_1a_2b_1b_2}-$ $x_1y_2\|0110\rangle_{a_1a_2b_1b_2}+$ $x_1y_3\|0010\rangle_{a_1a_2b_1b_2}+$ $x_2y_0\|1101\rangle_{a_1a_2b_1b_2}-$ $x_2y_1\|1001\rangle_{a_1a_2b_1b_2}+$ $x_2y_2\|0101\rangle_{a_1a_2b_1b_2}-$ $x_2y_3\|0001\rangle_{a_1a_2b_1b_2}-$ $x_3y_0\|1100\rangle_{a_1a_2b_1b_2}+$ $x_3y_1\|1000\rangle_{a_1a_2b_1b_2}-$ $x_3y_2\|0100\rangle_{a_1a_2b_1b_2}+$ $x_3y_3\|0000\rangle_{a_1a_2b_1b_2}$	$x_0y_0\|1111\rangle_{a_1a_2b_1b_2}-$ $x_0y_1\|1011\rangle_{a_1a_2b_1b_2}-$ $x_0y_2\|0111\rangle_{a_1a_2b_1b_2}+$ $x_0y_3\|0011\rangle_{a_1a_2b_1b_2}-$ $x_1y_0\|1110\rangle_{a_1a_2b_1b_2}+$ $x_1y_1\|1010\rangle_{a_1a_2b_1b_2}+$ $x_1y_2\|0110\rangle_{a_1a_2b_1b_2}-$ $x_1y_3\|0010\rangle_{a_1a_2b_1b_2}+$ $x_2y_0\|1101\rangle_{a_1a_2b_1b_2}-$ $x_2y_1\|1001\rangle_{a_1a_2b_1b_2}-$ $x_2y_2\|0101\rangle_{a_1a_2b_1b_2}+$ $x_2y_3\|0001\rangle_{a_1a_2b_1b_2}-$ $x_3y_0\|1100\rangle_{a_1a_2b_1b_2}+$ $x_3y_1\|1000\rangle_{a_1a_2b_1b_2}+$ $x_3y_2\|0100\rangle_{a_1a_2b_1b_2}-$ $x_3y_3\|0000\rangle_{a_1a_2b_1b_2}$	$x_0y_0\|1111\rangle_{a_1a_2b_1b_2}-$ $x_0y_1\|1011\rangle_{a_1a_2b_1b_2}+$ $x_0y_2\|0111\rangle_{a_1a_2b_1b_2}-$ $x_0y_3\|0011\rangle_{a_1a_2b_1b_2}-$ $x_1y_0\|1110\rangle_{a_1a_2b_1b_2}+$ $x_1y_1\|1010\rangle_{a_1a_2b_1b_2}-$ $x_1y_2\|0110\rangle_{a_1a_2b_1b_2}+$ $x_1y_3\|0010\rangle_{a_1a_2b_1b_2}-$ $x_2y_0\|1101\rangle_{a_1a_2b_1b_2}+$ $x_2y_1\|1001\rangle_{a_1a_2b_1b_2}-$ $x_2y_2\|0101\rangle_{a_1a_2b_1b_2}+$ $x_2y_3\|0001\rangle_{a_1a_2b_1b_2}+$ $x_3y_0\|1100\rangle_{a_1a_2b_1b_2}-$ $x_3y_1\|1000\rangle_{a_1a_2b_1b_2}+$ $x_3y_2\|0100\rangle_{a_1a_2b_1b_2}-$ $x_3y_3\|0000\rangle_{a_1a_2b_1b_2}$	$x_0y_0\|1111\rangle_{a_1a_2b_1b_2}-$ $x_0y_1\|1011\rangle_{a_1a_2b_1b_2}-$ $x_0y_2\|0111\rangle_{a_1a_2b_1b_2}+$ $x_0y_3\|0011\rangle_{a_1a_2b_1b_2}-$ $x_1y_0\|1110\rangle_{a_1a_2b_1b_2}+$ $x_1y_1\|1010\rangle_{a_1a_2b_1b_2}+$ $x_1y_2\|0110\rangle_{a_1a_2b_1b_2}-$ $x_1y_3\|0010\rangle_{a_1a_2b_1b_2}-$ $x_2y_0\|1101\rangle_{a_1a_2b_1b_2}+$ $x_2y_1\|1001\rangle_{a_1a_2b_1b_2}+$ $x_2y_2\|0101\rangle_{a_1a_2b_1b_2}-$ $x_2y_3\|0001\rangle_{a_1a_2b_1b_2}+$ $x_3y_0\|1100\rangle_{a_1a_2b_1b_2}-$ $x_3y_1\|1000\rangle_{a_1a_2b_1b_2}-$ $x_3y_2\|0100\rangle_{a_1a_2b_1b_2}+$ $x_3y_3\|0000\rangle_{a_1a_2b_1b_2}$

TABLE A.4: The collapsed state after performing the measurement on the states $|A_iB_j\rangle$, with $|11\rangle_{a_3b_3}$

Appendix B

QFI and QFIM formulas

To demonstrate the QFI and QFI we use the following expression matrix given in B.1:

$$\mathcal{J}_{\theta_i\theta_j} = Tr[(\partial_{\theta_i}\hat{\varrho})(\partial_{\theta_j}\hat{\varrho})] + \frac{1}{det\hat{\varrho}} Tr[(\partial_{\theta_i}\hat{\varrho} - \hat{\varrho}\partial_{\theta_i}\hat{\varrho})(\partial_{\theta_j}\hat{\varrho} - \hat{\varrho}\partial_{\theta_j}\hat{\varrho})]. \tag{B.1}$$

Since the operator $\hat{\varrho}$ represents a single qubit density operator. Hence, we can decompose it as follows: $\hat{\varrho} = \lambda_1|\lambda_1\rangle\langle\lambda_1| + \lambda_2|\lambda_2\rangle\langle\lambda_2|$. Hence the first term of Eq.(B.1) is written as:

$$Tr[(\partial_{\theta_i}\hat{\varrho})(\partial_{\theta_j}\hat{\varrho})] = \langle\lambda_1|\partial_{\theta_i}\hat{\varrho}|\lambda_1\rangle\langle\lambda_1|\partial_{\theta_j}\hat{\varrho}|\lambda_1\rangle + \langle\lambda_2|\partial_{\theta_i}\hat{\varrho}|\lambda_2\rangle\langle\lambda_2|\partial_{\theta_j}\hat{\varrho}|\lambda_2\rangle + 2\,\mathrm{Re}(\langle\lambda_1|\partial_{\theta_i}\hat{\varrho}|\lambda_2\rangle\langle\lambda_2|\partial_{\theta_j}\hat{\varrho}|\lambda_1\rangle). \tag{B.2}$$

Furthermore, the second term of Eq.(B.1) is:

$$\frac{1}{\det\hat{\varrho}} Tr[(\partial_{\theta_i}\hat{\varrho} - \hat{\varrho}\partial_{\theta_i}\hat{\varrho})(\partial_{\theta_j}\hat{\varrho} - \hat{\varrho}\partial_{\theta_j}\hat{\varrho})] = \frac{1}{\det\hat{\varrho}} Tr[(\partial_{\theta_i}\hat{\varrho})(\partial_{\theta_j}\hat{\varrho}) + \hat{\varrho}(\partial_{\theta_i}\hat{\varrho})\hat{\varrho}(\partial_{\theta_j}\hat{\varrho}) - \hat{\varrho}\{\partial_{\theta_i}\hat{\varrho}, \partial_{\theta_j}\hat{\varrho}\}]. \tag{B.3}$$

Thus,

$$\begin{aligned}
\frac{1}{\det\hat{\varrho}} Tr[\hat{\varrho}(\partial_{\theta_i}\hat{\varrho})\hat{\varrho}(\partial_{\theta_j}\hat{\varrho})] &= \frac{\lambda_1}{\lambda_2}\langle\lambda_1|\partial_{\theta_i}\hat{\varrho}|\lambda_1\rangle\langle\lambda_1|\partial_{\theta_j}\hat{\varrho}|\lambda_1\rangle + \frac{\lambda_2}{\lambda_1}\langle\lambda_2|\partial_{\theta_i}\hat{\varrho}|\lambda_2\rangle\langle\lambda_2|\partial_{\theta_j}\hat{\varrho}|\lambda_2\rangle \\
&+ 2\,\mathrm{Re}(\langle\lambda_1|\partial_{\theta_i}\hat{\varrho}|\lambda_2\rangle\langle\lambda_2|\partial_{\theta_j}\hat{\varrho}|\lambda_1\rangle) \\
-\frac{1}{\det\hat{\varrho}} Tr[\hat{\varrho}\{\partial_i\hat{\varrho}, \partial_{\theta_j}\hat{\varrho}\}] &= \frac{-2}{\lambda_2}\langle\lambda_1|\partial_{\theta_i}\hat{\varrho}|\lambda_1\rangle\langle\lambda_1|\partial_{\theta_j}\varrho|\lambda_1\rangle - \frac{2}{\lambda_1}\langle\lambda_2|\partial_{\theta_i}\hat{\varrho}|\lambda_2\rangle\langle\lambda_2|\partial_{\theta_j}\hat{\varrho}|\lambda_2\rangle \\
&- \frac{2}{\lambda_1\lambda_2}\mathrm{Re}(\langle\lambda_{\theta_i}|\partial_{\theta_i}\hat{\varrho}|\lambda_2\rangle\langle\lambda_2|\partial_{\theta_j}\hat{\varrho}|\lambda_1\rangle).
\end{aligned} \tag{B.4}$$

Therefore,

$$\begin{aligned}
&Tr[(\partial_{\theta_i}\hat{\varrho})(\partial_{\theta_j}\hat{\varrho})] + \frac{1}{\det\hat{\varrho}} Tr[(\partial_{\theta_i}\hat{\varrho} - \hat{\varrho}\partial_{\theta_i}\hat{\varrho})(\partial_{\theta_j}\hat{\varrho} - \hat{\varrho}\partial_{\theta_j}\hat{\varrho})] \\
&= \frac{1}{\lambda_1}\langle\lambda_1|\partial_{\theta_i}\hat{\varrho}|\lambda_1\rangle\langle\lambda_1|\partial_{\theta_j}\hat{\varrho}|\lambda_1\rangle + \frac{1}{\lambda_2}\langle\lambda_2|\partial_{\theta_i}\hat{\varrho}|\lambda_2\rangle\langle\lambda_2|\partial_{\theta_j}\hat{\varrho}|\lambda_2\rangle + 4\,\mathrm{Re}(\langle\lambda_1|\partial_{\theta_i}\hat{\varrho}|\lambda_2\rangle\langle\lambda_2|\partial_{\theta_j}\hat{\varrho}|\lambda_1\rangle),
\end{aligned} \tag{B.5}$$

It is well known that: $\langle\lambda_{1(2)}|\partial_{\theta_i}\hat{\varrho}|\lambda_{1(2)}\rangle$, while $\langle\lambda_1|\partial_{\theta_i}\hat{\varrho}|\lambda_2\rangle = \langle\partial_{\theta_i}\lambda_1|\lambda_2\rangle + \langle\lambda_1|\partial_{\theta_i}\lambda_2\rangle = 0$. Hence, one can obtain $Tr[(\partial_{\theta_i}\hat{\varrho})(\partial_{\theta_j}\hat{\varrho}) - \hat{\varrho}\{\partial_{\theta_i}\hat{\varrho}, \partial_{\theta_j}\hat{\varrho}\}] = (\partial_{\theta_i}\lambda_1)(\partial_{\theta_j}\lambda_1) - \lambda_1(\partial_{\theta_i}\lambda_1)(\partial_{\theta_j}\lambda_1) - \lambda_2(\partial_{\theta_i}\lambda_2)(\partial_{\theta_j}\lambda_2)$, which means that $Tr[(\partial_{\theta_i}\hat{\varrho})(\partial_{\theta_j}\hat{\varrho})] = Tr[\hat{\varrho}\{\partial_{\theta_i}\hat{\varrho}, \partial_{\theta_j}\hat{\varrho}\}]$. Finally, the Eq.(B.1) takes the following compact form:

$$\mathcal{J}_{\theta_i\theta_j} = Tr[(\partial_{\theta_i}\hat{\varrho})(\partial_{\theta_j}\hat{\varrho})] + \frac{1}{\det\varrho} Tr[\hat{\varrho}(\partial_{\theta_i}\hat{\varrho})\hat{\varrho}(\partial_{\theta_j}\hat{\varrho})], \tag{B.6}$$

Indeed, a single qubit state can be written by means of Bloch vector :

$$\hat{\varrho} = \frac{1}{2}(\hat{I} + \vec{h}.\vec{\sigma}), \tag{B.7}$$

where $\vec{h} = (h_x, h_y, h_z)^T$ and $\vec{\sigma} = (\sigma_x, \sigma_y, \sigma_z)$ denote the Bloch vector and Pauli matrices, respectively.

$$Tr[(\partial_{\theta_i}\hat{\varrho})(\partial_{\theta_j}\hat{\varrho})] = \frac{1}{4}Tr[(\partial_{\theta_i}\vec{h}.\vec{\sigma})(\partial_{\theta_j}\vec{h}.\vec{\sigma})] = \frac{1}{2}(\partial_{\theta_i}\vec{h}).(\partial_{\theta_j}\vec{h}), \tag{B.8}$$

By means of the relationship: $\det\hat{\varrho} = \frac{1}{4}(1 - |\vec{h}|^2)$, one can obtain

$$\frac{1}{\det\hat{\varrho}}Tr[\hat{\varrho}(\partial_{\theta_i}\hat{\varrho})\hat{\varrho}(\partial_{\theta_j}\hat{\varrho})] = \frac{1}{2}(\partial_{\theta_i}\vec{h}).(\partial_{\theta_j}\vec{h}) + \frac{(\vec{h}.\partial_{\theta_i}\vec{h})(\vec{h}.\partial_{\theta_j}\vec{h})}{1 - |\vec{h}|^2}. \tag{B.9}$$

Finally, one can obtain the formula of QFI matrix as:

$$\mathcal{J}_{\theta_i\theta_j} = (\partial_{\theta_i}\vec{h})(\partial_{\theta_j}\vec{h}) + \frac{(\vec{h}.\partial_{\theta_i}\vec{h})(\vec{h}.\partial_{\theta_j}\vec{h})}{1 - |\vec{h}|^2}. \tag{B.10}$$

The QFI is exactly the diagonal elements of the $QFIM$. Thus, the expression of QFI is given as follows:

$$\mathcal{J}_{\theta} = |\partial_{\theta}\vec{h}|^2 + \frac{(\vec{h}.\partial_{\theta}\vec{h})^2}{1 - |\vec{h}|^2}. \tag{B.11}$$

Appendix C

Performing the Three-party bidirectional teleportation

To perform the BQT from Alice to Bob through Charlie.

We assume that Alice, Bob and Charlie have the states:

$$|Q_A\rangle = \alpha|0\rangle + \beta|1\rangle; \qquad |Q_B\rangle = \gamma|0\rangle + \delta|1\rangle; \qquad |Q_C\rangle = \eta|0\rangle + \zeta|1\rangle \tag{C.1}$$

Where:

$$\alpha = \cos\left(\frac{\theta_A}{2}\right), \beta = e^{i\phi_A}\sin\left(\frac{\theta_A}{2}\right); \gamma = \cos\left(\frac{\theta_B}{2}\right), \delta = e^{i\phi_B}\sin\left(\frac{\theta_B}{2}\right); \eta = \cos\left(\frac{\theta_C}{2}\right), \zeta = e^{i\phi_C}\sin\left(\frac{\theta_C}{2}\right) \tag{C.2}$$

The input state is given as

$$|\psi_s\rangle \quad = \quad |Q_a\rangle \otimes |Q_b\rangle \otimes |Q_c\rangle \otimes |GHZ_{ABC}\rangle \tag{C.3}$$

- By performing $CNOT_3$ gate with $|Q_{a,b,c}\rangle$ as control qubits and $|GHZ_{ABC}\rangle$ as targets, the state is given as

$$\begin{aligned}
|\psi_s^1\rangle = \alpha\gamma\eta\,|000\rangle \otimes \frac{1}{\sqrt{2}}(|000\rangle + |111\rangle) + \alpha\gamma\zeta\,|001\rangle \otimes \frac{1}{\sqrt{2}}(|001\rangle + |110\rangle) \\
+\alpha\delta\eta\,|010\rangle \otimes \frac{1}{\sqrt{2}}(|010\rangle + |101\rangle) + \alpha\delta\zeta\,|011\rangle \otimes \frac{1}{\sqrt{2}}(|011\rangle + |100\rangle) \\
+\beta\gamma\eta\,|100\rangle \otimes \frac{1}{\sqrt{2}}(|100\rangle + |011\rangle) + \beta\gamma\zeta\,|101\rangle \otimes \frac{1}{\sqrt{2}}(|101\rangle + |010\rangle) \\
+\beta\delta\eta\,|110\rangle \otimes \frac{1}{\sqrt{2}}(|110\rangle + |001\rangle) + \beta\delta\zeta\,|111\rangle \otimes \frac{1}{\sqrt{2}}(|111\rangle + |000\rangle)
\end{aligned} \tag{C.4}$$

- Apply H_3 on $|Q_{a,b,c}\rangle$ we get the state

$$\begin{aligned}
|\psi_s^2\rangle &= \alpha\gamma\eta(\frac{|0\rangle+|1\rangle}{\sqrt{2}}\frac{|0\rangle+|1\rangle}{\sqrt{2}}\frac{|0\rangle+|1\rangle}{\sqrt{2}})_{abc}\otimes\frac{1}{\sqrt{2}}(|000\rangle+|111\rangle) \\
&+ \alpha\gamma\zeta(\frac{|0\rangle+|1\rangle}{\sqrt{2}}\frac{|0\rangle+|1\rangle}{\sqrt{2}}\frac{|0\rangle-|1\rangle}{\sqrt{2}})_{abc}\otimes\frac{1}{\sqrt{2}}(|001\rangle+|110\rangle) \\
&+ \alpha\delta\eta(\frac{|0\rangle+|1\rangle}{\sqrt{2}}\frac{|0\rangle-|1\rangle}{\sqrt{2}}\frac{|0\rangle+|1\rangle}{\sqrt{2}})_{abc}\otimes\frac{1}{\sqrt{2}}(|010\rangle+|101\rangle) \\
&+ \alpha\delta\zeta(\frac{|0\rangle+|1\rangle}{\sqrt{2}}\frac{|0\rangle-|1\rangle}{\sqrt{2}}\frac{|0\rangle-|1\rangle}{\sqrt{2}})_{abc}\otimes\frac{1}{\sqrt{2}}(|011\rangle+|100\rangle) \\
&+ \beta\gamma\eta(\frac{|0\rangle-|1\rangle}{\sqrt{2}}\frac{|0\rangle+|1\rangle}{\sqrt{2}}\frac{|0\rangle+|1\rangle}{\sqrt{2}})_{abc}\otimes\frac{1}{\sqrt{2}}(|100\rangle+|011\rangle) \\
&+ \beta\gamma\zeta(\frac{|0\rangle-|1\rangle}{\sqrt{2}}\frac{|0\rangle+|1\rangle}{\sqrt{2}}\frac{|0\rangle-|1\rangle}{\sqrt{2}})_{abc}\otimes\frac{1}{\sqrt{2}}(|101\rangle+|010\rangle) \\
&+ \beta\delta\eta(\frac{|0\rangle-|1\rangle}{\sqrt{2}}\frac{|0\rangle-|1\rangle}{\sqrt{2}}\frac{|0\rangle+|1\rangle}{\sqrt{2}})_{abc}\otimes\frac{1}{\sqrt{2}}(|110\rangle+|001\rangle) \\
&+ \beta\delta\zeta(\frac{|0\rangle-|1\rangle}{\sqrt{2}}\frac{|0\rangle-|1\rangle}{\sqrt{2}}\frac{|0\rangle-|1\rangle}{\sqrt{2}})_{abc}\otimes\frac{1}{\sqrt{2}}(|111\rangle+|000\rangle)
\end{aligned} \tag{C.5}$$

- Now, we apply double $CCNOT$ gate. We assume here that :$|T_A\rangle = |1\rangle$ $|Q_a\rangle = |1\rangle$, $|C_A\rangle = |1\rangle$ in this case the state $\left|S_A^{1,2}\right\rangle = |1\rangle$. Furthermore, we assume that : $|T_B\rangle = |0\rangle$ and $|T_C\rangle = |0\rangle$. in this case only Alice does a perfect projective measurement.

$$\begin{aligned}
|\psi_s^3\rangle &= \alpha\gamma\eta(\frac{|1\rangle}{\sqrt{2}}\frac{|0\rangle+|1\rangle}{\sqrt{2}}\frac{|0\rangle+|1\rangle}{\sqrt{2}})_{abc}\otimes\frac{1}{\sqrt{2}}(|111\rangle)+\alpha\gamma\zeta(\frac{|1\rangle}{\sqrt{2}}\frac{|0\rangle+|1\rangle}{\sqrt{2}}\frac{|0\rangle-|1\rangle}{\sqrt{2}})_{abc}\otimes\frac{1}{\sqrt{2}}(|110\rangle) \\
&+ \alpha\delta\eta(\frac{|1\rangle}{\sqrt{2}}\frac{|0\rangle-|1\rangle}{\sqrt{2}}\frac{|0\rangle+|1\rangle}{\sqrt{2}})_{abc}\otimes\frac{1}{\sqrt{2}}(|101\rangle)+\alpha\delta\zeta(\frac{|1\rangle}{\sqrt{2}}\frac{|0\rangle-|1\rangle}{\sqrt{2}}\frac{|0\rangle-|1\rangle}{\sqrt{2}})_{abc}\otimes\frac{1}{\sqrt{2}}(|100\rangle) \\
&+ \beta\gamma\eta(\frac{-|1\rangle}{\sqrt{2}}\frac{|0\rangle+|1\rangle}{\sqrt{2}}\frac{|0\rangle+|1\rangle}{\sqrt{2}})_{abc}\otimes\frac{1}{\sqrt{2}}(|100\rangle)+\beta\gamma\zeta(\frac{-|1\rangle}{\sqrt{2}}\frac{|0\rangle+|1\rangle}{\sqrt{2}}\frac{|0\rangle-|1\rangle}{\sqrt{2}})_{abc}\otimes\frac{1}{\sqrt{2}}(|101\rangle) \\
&+ \beta\delta\eta(\frac{-|1\rangle}{\sqrt{2}}\frac{|0\rangle-|1\rangle}{\sqrt{2}}\frac{|0\rangle+|1\rangle}{\sqrt{2}})_{abc}\otimes\frac{1}{\sqrt{2}}(|110\rangle)+\beta\delta\zeta(\frac{-|1\rangle}{\sqrt{2}}\frac{|0\rangle-|1\rangle}{\sqrt{2}}\frac{|0\rangle-|1\rangle}{\sqrt{2}})_{abc}\otimes\frac{1}{\sqrt{2}}(|111\rangle)
\end{aligned} \tag{C.6}$$

- Then, the partners apply a H_3 on $|Q_{a,b,c}\rangle$, followed by $CNOT_3$ gate on $|Q_{a,b,c}\rangle$ and $|GHZ\rangle$:

$$\begin{aligned}
\left|\psi_s^4\right\rangle &= \gamma\eta\frac{|0001\rangle_{abcA}}{\sqrt{2}}\otimes\frac{1}{\sqrt{2}}(\alpha\,|11\rangle-\beta\,|00\rangle)_{B,C}+\gamma\eta\frac{|1000\rangle_{abcA}}{\sqrt{2}}\otimes\frac{1}{\sqrt{2}}(-\alpha\,|11\rangle+\beta\,|00\rangle)_{B,C} \\
&+\gamma\zeta\frac{|0011\rangle_{abcA}}{\sqrt{2}}\otimes\frac{1}{\sqrt{2}}(\alpha\,|11\rangle-\beta\,|00\rangle)_{B,C}+\gamma\zeta\frac{|1010\rangle_{abcA}}{\sqrt{2}}\otimes\frac{1}{\sqrt{2}}(-\alpha\,|11\rangle+\beta\,|00\rangle)_{B,C} \\
&+\delta\eta\frac{|0101\rangle_{abcA}}{\sqrt{2}}\otimes\frac{1}{\sqrt{2}}(\alpha\,|11\rangle-\beta\,|00\rangle)_{B,C}+\delta\eta\frac{|1100\rangle_{abcA}}{\sqrt{2}}\otimes\frac{1}{\sqrt{2}}(-\alpha\,|11\rangle+\beta\,|00\rangle)_{B,C} \\
&+\delta\zeta\frac{|0111\rangle_{abcA}}{\sqrt{2}}\otimes\frac{1}{\sqrt{2}}(\alpha\,|11\rangle-\beta\,|00\rangle)_{B,C}+\delta\zeta\frac{|1110\rangle_{abcA}}{\sqrt{2}}\otimes\frac{1}{\sqrt{2}}(-\alpha\,|11\rangle+\beta\,|00\rangle)_{B,C}
\end{aligned} \tag{C.7}$$

- Bob Applies X and Z gates on his GHZ qubit

$$\begin{aligned}\hat{Z}.\hat{X}\left|\psi_s^4\right\rangle &= \gamma\eta\frac{|0001\rangle_{abcA}}{\sqrt{2}} \otimes \frac{1}{\sqrt{2}}(\alpha|01\rangle + \beta|10\rangle) + \gamma\eta\frac{|1000\rangle_{abcA}}{\sqrt{2}} \otimes \frac{1}{\sqrt{2}}(-\alpha|01\rangle - \beta|10\rangle) \\ &+\gamma\zeta\frac{|0011\rangle_{abcA}}{\sqrt{2}} \otimes \frac{1}{\sqrt{2}}(\alpha|01\rangle + \beta|10\rangle)_{B,C} + \gamma\zeta\frac{|1010\rangle_{abcA}}{\sqrt{2}} \otimes \frac{1}{\sqrt{2}}(-\alpha|01\rangle - \beta|10\rangle)_{B,C} \\ &+\delta\eta\frac{|0101\rangle_{abcA}}{\sqrt{2}} \otimes \frac{1}{\sqrt{2}}(\alpha|01\rangle - \beta|10\rangle)_{B,C} + \delta\eta\frac{|1100\rangle_{abcA}}{\sqrt{2}} \otimes \frac{1}{\sqrt{2}}(-\alpha|01\rangle - \beta|10\rangle)_{B,C} \\ &+\delta\zeta\frac{|0111\rangle_{abcA}}{\sqrt{2}} \otimes \frac{1}{\sqrt{2}}(\alpha|01\rangle + \beta|10\rangle)_{B,C} + \delta\zeta\frac{|1100\rangle_{abcA}}{\sqrt{2}} \otimes \frac{1}{\sqrt{2}}(-\alpha|01\rangle - \beta|10\rangle)_{B,C}\end{aligned} \tag{C.8}$$

- Charlie performs a Hadamard gate followed by a measurement on her qubit from GHZ qubit If the measurement outcome is : $|GHZ_C\rangle = |0\rangle$, then the output state is:

$$\begin{aligned}\left|\psi_s^5\right\rangle &= \gamma\eta\frac{|0001\rangle_{abcA}}{2\sqrt{2}} \otimes (\alpha|0\rangle + \beta|1\rangle)_B + \gamma\eta\frac{|1000\rangle_{abcA}}{2\sqrt{2}} \otimes (-\alpha|0\rangle - \beta|1\rangle)_B \\ &+\gamma\zeta\frac{|0011\rangle_{abcA}}{2\sqrt{2}} \otimes (\alpha|0\rangle + \beta|1\rangle)_B + \gamma\zeta\frac{|1010\rangle_{abcA}}{2\sqrt{2}} \otimes (-\alpha|0\rangle - \beta|1\rangle)_B \\ &+\delta\eta\frac{|0101\rangle_{abcA}}{2\sqrt{2}} \otimes (\alpha|0\rangle + \beta|1\rangle)_B + \delta\eta\frac{|1100\rangle_{abcA}}{2\sqrt{2}} \otimes (-\alpha|0\rangle - \beta|1\rangle)_B \\ &+\delta\zeta\frac{|0111\rangle_{abcA}}{2\sqrt{2}} \otimes (\alpha|0\rangle + \beta|1\rangle)_B + \delta\zeta\frac{|1110\rangle_{abcA}}{2\sqrt{2}} \otimes (-\alpha|0\rangle - \beta|1\rangle)_B\end{aligned} \tag{C.9}$$

As shown in the equation (9), The quantum information of $|Q_a\rangle$ is restored in GHZ_B.

However, if $|GHZ_C\rangle = |1\rangle$. Then, Bob should apply a Z gate on his GHZ qubit to restore the teleported state by Alice.

Bibliography

[1] H. P. Breuer, and F. Petruccione. *The theory of open quantum systems*. Oxford University Press on Demand, 2002.

[2] B. W. Shore. Examples of counter-intuitive physics. *Contemporary physics*, 36(1):15-28, 1995.

[3] B. D'Espagnat, and H. Zwirn. *The Quantum World*. The Frontiers Collection (Eds.), 2017.

[4] M. Schlosshauer, J. Kofler, and A. Zeilinger. A snapshot of foundational attitudes toward quantum mechanics. *Studies in History and Philosophy of Science Part B: Studies in History and Philosophy of Modern Physics*, 44(3):222–230, 2013.

[5] R. Landauer. Information is a physical entity. *Physica A: Statistical Mechanics and its applications*, 263(1-4):63-67, 1999.

[6] C. E. Shannon. A mathematical theory of communication. *The Bell system technical journal*, 27(3):379-423, 1948.

[7] C. Shannon. Communication in the Presence of Noise. *Proc. IRE*, 37(1):10-21, 1949.

[8] B. Schumacher. Quantum coding. *Phys. Rev. A*, 51(4):2738, 1995.

[9] W. Dür, and S. Heusler. What we can learn about quantum physics from a single qubit. *arXiv* : 1312.1463, 2013.

[10] L. Marton, J. A. Simpson, and J. A. Suddeth. An electron interferometer. *Review of Scientific Instruments*, 25(11):1099-1104, 1954.

[11] D. W. Keith, C. R. Ekstrom, Q. A. Turchette, and D. E. Pritchard. An interferometer for atoms. *Phys. Rev. lett.*, 66(21):2693, 1991.

[12] H. Rauch, W. Treimer, and U. Bonse. Test of a single crystal neutron interferometer. *Physics Letters A*, 47(5):369-371, 1974.

[13] J. W. Pan, Z. B. Chen, C. Y. Lu, H. Weinfurter, A. Zeilinger, and M. Żukowski. Multiphoton entanglement and interferometry. *Reviews of Modern Physics*, 84(2):777, 2012.

[14] C. Hughes, J. Isaacson, A. Perry , R.F. Sun, and J. Turner. What Is a Qubit? *Quantum Computing for the Quantum Curious*. Springer, Cham, 2021; D. Deutsch, It from qubit. na, 2003.

[15] R. Feynman. Simulating physics with computers. *Int. J. Theor. Phys.*, 21:467–488, 1982.

[16] A. Einstein, B. Podolsky, and N. Rosen. Can quantum-mechanical description of physical reality be considered complete? *Phys. Rev.* 47(10):777, 1935.

[17] J. S. Bell. On the einstein podolsky rosen paradox. *Physics Physique Fizika*, 1(3):195, 1964.

[18] F. J. Clauser, M. A.Horne, A. Shimony, and R. A. Holt. Proposed experiment to test local hidden-variable theories". *Phys. Rev. Lett.*, 23(15):880–884, 1969.

[19] W. Tittel, J. Brendel, H. Zbinden, and N.Gisin. Violation of Bell inequalities by photons more than 10 km apart. *Phys. Rev. lett.*, 81(17):3563, 1998.

[20] A. Aspect. Proposed experiment to test separable hidden-variable theories. *Physics Letters A*, 54(2):117–118, 1975.

[21] A. Aspect, P. Grangier, and G. Roger. Experimental tests of realistic local theories via Bell's theorem. *Phys. Rev. Lett.*, 47(7):460–463, 1981.

[22] R.F. Werner. Quantum states with Einstein-Podolsky-Rosen correlations admitting a hiddenvariable model. *Phys. Rev. A*, 40(8):4277, 1989.

[23] W. K. Wootters, Entanglement of formation and concurrence. *Quantum. Inf. Comput.*, 1(1):27-44, 2001.

[24] D. P. DiVincenzo, P. W. Shor, J. A. Smolin, B. M. Terhal, and A. V. Thapliyal. Evidence for bound entangled states with negative partial transpose. *Phys. Rev. A*, 61(6):062312, 2000.

[25] V. Coffman, J. Kundu, and W. K. Wootters. Distributed entanglement. *Phys. Rev. A* 61(5):052306, 2000.

[26] P. Kok, W. J. Munro,K. Nemoto, T. C. Ralph, J. P. Dowling, and G. J. Milburn. Linear optical quantum computing with photonic qubits. *Rev. Mod. Phys.* 79(1):135, 2007.

[27] J. Clarke and F. K. Wilhelm. Superconducting quantum bits. *Nature* 453(7198), 1031-1042, 2008.

[28] B. B. Blinov, D. L. Moehring, L.-M. Duan, and C. Monroe. Observation of entanglement between a single trapped atom and a single photon. *Nature*, 428(6979):153-157, 2004.

[29] B. Hensen, H. Bernien, A. E. Dréau, A. Reiserer, N. Kalb, M. S. Blok, R. Hanson. Loophole-free Bell inequality violation using electron spins separated by 1.3 kilometres. *Nature*, 526(7575):682–686, 2015.

[30] P. Zoller, T. Beth, D. Binosi, R. Blatt, H. Briegel, D. Bruss, and A. Zeilinger. Quantum information processing and communication. *The European Physical Journal D – Atomic, Molecular, Optical and Plasma Physics*, 36(2):203-228, 2005.

[31] A. Poppe, A. Fedrizzi, R. Ursin, H. R. Böhm, T. Lorünser, O. Maurhardt, and A. Zeilinger. Practical quantum key distribution with polarization entangled photons. *Optics Express*, 12(16):3865-3871, 2004.

[32] P. W. Shor. Polynomial-time algorithms for prime factorization and discrete logarithms on a quantum computer. *SIAM review*, 41(2):303-332, 1999.

[33] L. K. Grover. Quantum mechanics helps in searching for a needle in a haystack. *Phys. Rev. lett.*, 79(2):325, 1997.

[34] C. H. Bennett, G. Brassard, C. Crépeau, R. Jozsa, A. Peres, and W. K. Wootters. Teleporting an unknown quantum state via dual classical and Einstein-Podolsky-Rosen channels. *Phys. Rev. lett.*, 70(13):1895, 1993.

[35] W. K. Wootters, W. H. Zurek, A single quantum cannot be cloned. *Nature*, 299(5886):802-803, 1982.

[36] S. Amai. Theory of Measurement in Quantum Mechanics: Destruction of Interference. *Progress of Theoretical Physics*, 30(4):550-562, 1963.

[37] G. Fürnkranz. *The Quantum Internet. In The Quantum Internet*, (pp. 83-189). Springer, Cham 2020.

[38] H. J. Kimble. The quantum internet. *Nature* (London), 453(7198):1023, 2008.

[39] H. J. Briegel, W. Dur, J. I. Cirac, and P. Zoller. Quantum repeaters: The role of imperfect local operations in quantum communication. *Phys. Rev. Lett.* 81(26):5932, 1998.

[40] T. Morimae, and K. Fujii. Blind quantum computation protocol in which Alice only makes measurements. *Phys. Rev. A*, 87(5):050301, 2013.

[41] Y. Tian, H. Chen, S. Ji, Z. Han, H. Lian, and X. Wen. A broadcasting multiple blind signature scheme based on quantum teleportation. *Optical and Quantum Electronics*, 46(6):769-777, 2014.

[42] S. Lloyd, and J. Preskill. Unitarity of black hole evaporation in final-state projection models. *Journal of High Energy Physics*, 2014(8):1-30, 2014.

[43] S. Lloyd, L.Maccone, R. Garcia-Patron, V.Giovannetti, Y. Shikano, S. Pirandola, and A. M. Steinberg. Closed timelike curves via post-selection: theory and experimental demonstration. *Phys. Rev. Lett.* 106(4):040403, 2011.

[44] D. Bouwmeester, J.-W. Pan, K. Mattle, M. Eibl, H. Weinfurter, and A. Zeilinger. *Nature* (London) 390(6660):575, 1997.

[45] R. Ursin, T. Jennewein, M. Aspelmeyer, R. Kaltenbaek, M. Lindenthal, P. Walther, and A. Zeilinger. *Nature*, 430(7002):849-849, 2004.

[46] X.-S. Ma, T. Herbst, T. Scheidl, D. Wang, S. Kropatschek, W. Naylor, A. Mech, B. Wittmann, J. Kofler, E. Anisimova, V. Makarov, T. Jennewein, R. Ursin, and A. Zeilinger. *Nature* (London), 489:269, 2012.

[47] H. Krauter, D. Salart, C.A. Muschik, J.M. Petersen, H. Shen, T. Fernholz, and E.S. Polzik. *Nature Phys.* 9(7):400, 2013.

[48] J. F. Sherson, H. Krauter, R.K. Olsson, B. Julsgaard, K. Hammerer, I. Cirac, and E.S. Polzik. *Nature* (London) 443(7111):557, 2006.

[49] I. Marcikic, H. de Riedmatten, W. Tittel, H Zbinden, and N. Gisin. Long-distance teleportation of qubits at telecommunication wavelengths. *Nature* 421(6922):509, 2003.

[50] O. Landry, J. A. W. van Houwelingen, A. Beveratos, H.Zbinden, and N. Gisin. Quantum teleportation over the Swisscom telecommunication network. *J. Opt. Soc. Am. B*, 24(2):398-403, 2007.

[51] M.A. Nielsen, E. Knill, and R. Laamme. *Nature* (London), 396(6706):52, 1998.

[52] J. F. Sherson, H. Krauter, R. K. Olsson, B. Julsgaard, K. Hammerer, I. Cirac, and E. S. Polzik. Quantum teleportation between light and matter. *Nature*, 443(7111):557-560, 2006.

[53] G. I. Harris, and W. P. Bowen. Quantum teleportation from light to motion. *Nature Photonics*, 15(11):792-793, 2021.

[54] S. Pirandola, J. Eisert, C. Weedbrook, A. Furusawa, and S. L. Braunstein. Advances in quantum teleportation. *Nature photonics*, 9(10):641-652, 2015.

[55] X. S. Ma, T. Herbst, T. Scheidl, D. Wang, S. Kropatschek, W. Naylor, and A. Zeilinger. Quantum teleportation over 143 kilometres using active feed-forward. *Nature*, 489(7415):269-273, 2012.

[56] J. G. Ren, P.Xu, H. L. Yong, L. Zhang, S. K. Liao, J. Yin, J. W. Pan. Ground-to-satellite quantum teleportation. *Nature*, 549(7670):70-73, 2017.

[57] C. P. Yang, S. I Chu, and S. Han. Efficient many-party controlled teleportation of multiqubit quantum information via entanglement. *Phys. Rev. A*, 70(2):022329, 2004.

[58] D. Gottesman, and I. L. Chuang. Demonstrating the viability of universal quantum computation using teleportation and single qubit operations. *Nature* 402(6760):390-393, 1999.

[59] F. Wu, M. Q Bai, Y. C. Zhang, R. J. Liu, and Z. W. Mo. Cyclic and cyclic controlled quantum teleportation in a high-dimension system. *Int. J. Quant. Info.*, 18(04):2050012, 2020.

[60] S. L. Braunstein, and H. J. Kimble. Teleportation of continuous quantum variables. *Phys. Rev. Lett.*, 80(4):869, 1998.

[61] L. Vaidman. Teleportation of quantum states. *Phys. Rev. A*, 49(2):1473, 1994.

[62] E. Prugovecki. *Quantum mechanics in Hilbert space*. Academic Press, 1982.

[63] L. Vaidman, and N. Yoran. Methods for reliable teleportation. *Phys. Rev. A*, 59(1):116, 1999.

[64] S. F. Huelga, J. A. Vaccaro, A. Chees, and M. B. Plenio. Quantum remote control: teleportation of unitary operations, *Phys. Rev. A*, 63(4):042303, 2001.

[65] S. F. Huelga, M. B. Plenio, and J. A. Vaccaro. Remote control of restricted sets of operations: teleportation of angles, *Phys. Rev. A*, 65(4):042316, 2002.

[66] S. Hassanpour, and M. Houshmand. Bidirectional teleportation of a pure EPR state by using GHZ states, *Quan. Inf. Proc.*, 15(2):905-912, 2016.

[67] Y. H. Li, and L. P. Nie. Bidirectional controlled teleportation by using a five-qubit composite GHZ-Bell state, *Int. J. Theor. Phys.* 52(5):1630-1634, 2013.

[68] Y. Chen. Bidirectional quantum controlled teleportation by using a genuine six-qubit entangled state, *Int. J. Theor. Phys.* 54(1):269-272, 2015.

[69] B. S. Choudhury and A. Dhara. A bidirectional teleportation protocol for arbitrary two-qubit state under the supervision of a third party, *Int. J. Theor. Phys.* 55(4):2275-2285, 2016.

[70] W. H. Zurek. Decoherence, einselection, and the quantum origins of the classical. *Reviews of modern physics*, 75(3):715, 2003.

[71] H. D. Zeh. On the interpretation of measurement in quantum theory, *Found. Phys.* 1(1):69–76, 1970.

[72] J. M. Raimond, M. Brune, and S. Haroche. Manipulating quantum entanglement with atoms and photons in a cavity, *Rev. Mod. Phys.* 73(3):565–582, 2001.

[73] J. Ghosh, A. G. Fowler, and M. R. Geller. Surface code with decoherence: An analysis of three superconducting architectures. *Phys. Rev. A*, 86(6):062318, 2012; A. J. Leggett. Testing the limits of quantum mechanics: motivation, state of play, prospects. *J. Phys. Condens. Matter*, 14(15):R415–R451, 2002.

[74] D. Leibfried, R. Blatt, C. Monroe, and D. Wineland. Quantum dynamics of single trapped ions, *Rev. Mod. Phys.* 75(1):281–324, 2003.

[75] K. Modi, A. Brodutch, H. Cable, T. Paterek, and V. Vedral. The classical-quantum boundary for correlations: Discord and related measures. *Reviews of Modern Physics*, 84(4):1655, 2012.

[76] F. Caruso, V. Giovannetti, C. Lupo, and S. Mancini. Quantum channels and memory effects. *Reviews of Modern Physics*, 86(4):1203, 2014.

[77] M. A Nielsen, and I. L Chuang. *Quantum computation and quantum information*, Cambridge University Press, Cambridge, 2000.

[78] K. Kraus. States. Effects and Operations. *Springer*, Berlin, 1983.

[79] M. M. Wilde. *Quantum information theory*. Cambridge University Press, 2013.

[80] R. Fortes, and G. Rigolin. Fighting noise with noise in realistic quantum teleportation. *Phys. Rev. A*, 92(1):012338, 2015.

[81] M. Orszag, and M. Hernandez. Coherence and entanglement in a two-qubit system. *Advances in Optics and Photonics*, 2(2):229-286, 2010.

[82] X. Liu, Z. Tian, J. Wang, and J. Jing. Protecting quantum coherence of two-level atoms from vacuum fluctuations of electromagnetic field. *Annals of Physics*, 366:102-112, 2016.

[83] T. Yu, and J. H. Eberly. Sudden death of entanglement. *Science*, 323(5914):598-601, 2009.

[84] J. W. Pan, C. Simon, Č. Brukner, and A. Zeilinger. Entanglement purification for quantum communication. *Nature*, 410(6832):1067-1070, 2001.

[85] P. G. Kwiat, A. J. Berglund, J. B. Altepeter, and A. G. White. Experimental verification of decoherence-free subspaces. *Science*, 290(5491):498-501, 2000.

[86] B. Misra, and E. C. G. Te Sudarshan. Zeno's paradox in quantum theory. *J. Math. Phys. (NY)* 18(4):756–763, 1977; P. Facchi, S. Pascazio. Quantum Zeno dynamics: mathematical and physical aspects. *J. Phys. A: Math. Teor.* 41(49):493001 (2008).

[87] F. Ghasemi, and A. Shafiee. A new approach to study the Zeno effect for a macroscopic quantum system under frequent interactions with a harmonic environment. *Scientific reports*, 9(1):1-10, 2019.

[88] Y. Aharonov, D. Z. Albert, and L. Vaidman. How the result of a measurement of a component of the spin of a spin-1/2 particle can turn out to be 100. Physical review letters, 60(14):1351, 1988.

[89] Y. Aharonov, L. Vaidman. The Two-State Vector Formalism: An Updated Review. In: J.Muga,, R.S. Mayato,,Í. Egusquiza, (eds). Time in Quantum Mechanics. Lecture Notes in Physics, 734. Springer, Berlin, Heidelberg, 2008.

[90] Y. S. Kim, J. C. Lee, O. Kwon, and Y. H. Kim. Protecting entanglement from decoherence using weak measurement and quantum measurement reversal. *Nature Physics*, 8(2):117-120, 2012.

[91] M. Koashi, and M. Ueda. Reversing measurement and probabilistic quantum error correction. *Phys. Rev. lett.*, 82(12):2598, 1999.

[92] A. N. Korotkov , and K. Kyle. Decoherence suppression by quantum measurement reversal, *Phys. Rev. A* 81(4):040103, 2010.

[93] Z. X. Man, Y. J. Xia, and N. B. An. Manipulating entanglement of two qubits in a common environment by means of weak measurements and quantum measurement reversals. *Phys. Rev. A*, 86(1):012325, 2012.

[94] Z. X. Man, Y. J. Xia, and N. B. An. Enhancing entanglement of two qubits undergoing independent decoherences by local pre-and postmeasurements. *Phys. Rev. A*, 86(5):052322, 2012.

[95] X. Xiao, and Y. L. Li. Protecting qutrit-qutrit entanglement by weak measurement and reversal. *The European Physical Journal D*, 67(10):1-7, 2013.

[96] X. P. Liao, M. F.Fang, and J. S. Fang. Preserving entanglement and the fidelity of three-qubit quantum states undergoing decoherence using weak measurement, *Chinese Physics B*, 23(2):020304, 2013.

[97] T. Pramanik, and A. S. Majumdar. Improving the fidelity of teleportation through noisy channels using weak measurement, *Phys. Lett.*, 377(44):3209-3215, 2013.

[98] H.-P. Breuer, E.-M. Laine, and J. Piilo, *Phys. Rev. Lett.* 103(21):210401, 2009.

[99] J. Piilo, S. Maniscalco, K. Harkonen, and K.-A. Suominen, *Phys. Rev. Lett.*, 100(18), 180402, 2008.

[100] E.-M. Laine, J. Piilo, and H.-P. Breuer, *Phys. Rev. A* 81(6):062115, 2010.

[101] F. Caruso, V. Giovannetti, C. Lupo, and S. Mancini, *Rev. Mod. Phys.* 86(4):1203, 2014.

[102] S. B. Xue, R. B.Wu, W. M. Zhang, J. Zhang, C. W. Li, and T. J. Tarn. Decoherence suppression via non-Markovian coherent feedback control. *Phys. Rev. A*, 86(5):052304, 2012.

[103] A. Rivas, S. F. Huelga, and M. B. Plenio, *Rep. Prog. Phys.*, 77(9):094001, 2014.

[104] H. P. Breuer. Foundations and measures of quantum non-Markovianity. *Journal of Physics B: Atomic, Molecular and Optical Physics*, 45(15):154001, 2012.

[105] Á. Rivas, S. F. Huelga, M. B. Plenio, Quantum non-Markovianity: characterization, quantification and detection. *Reports on Progress in Physics*, 77(9):094001, 2014.

[106] H-P. Breuer, E-M. Laine, and J. Piilo. Measure for the degree of non-Markovian behavior of quantum processes in open systems. *Phys. Rev. Lett.* 103(21):210401, 2009.

[107] R. Vasile, S. Maniscalco, M. G. A., Paris, H.-P. Breuer, and J. Piilo. Quantifying non-Markovianity of continuousvariable Gaussian dynamical maps. *Phys. Rev. A* 84(5):052118, 2011.

[108] X.-M. Lu, X. Wang, and C.P. Sun. Quantum Fisher information flow and non-Markovian processes of open systems. *Phys. Rev. A* 82(4):042103, 2010.

[109] S. Luo, S. Fu, and H. Song. Quantifying non Markovianity via correlations. *Phys. Rev. A* 86(4):044101, 2012.

[110] C. Addis, G. Karpat, C. Macchiavello, and S. Maniscalco. Dynamical memory effects in correlated quantum channels. *Phys. Rev. A*, 94(3):032121, 2016.

[111] M. Hu, and W. Zhou. Enhancing two-qubit quantum coherence in a correlated dephasing channel. *Laser Physics Letters*, 16(4):045201, 2019.

[112] A. Uhlmann. The "transition probability" in the state space of a$\star-$algebra. *Reports on Mathematical Physics*, 9(2):273–279, 1976.

[113] P. M. Alberti. A note on the transition probability over C^*-algebras. *Lett. Math. Phys.*, 7(1):25-32, 1983.

[114] R. Jozsa. Fidelity for mixed quantum states. *J. Mod. Opt.*, 41(12):2315–2323, 1994.

[115] B. Schumacher. Quantum coding. *Phys. Rev. A*, 51(4):2738, 1995.

[116] D.Petz, and C. Ghinea. Introduction to quantum Fisher information. *In Quantum probability and related topics* (261-281), 2011.

[117] X. Xiao, Y. Yao, W. J. Zhong, Y. Li, and Y. Xie. Enhancing teleportation of quantum Fisher information by partial measurements. *Phys. Rev. A*, 93(1):012307, 2016.

[118] R. A. Fisher. On the mathematical foundations of theoretical statistics. *Phil. Trans. Roy. Soc. Lond.* 222:309–368, 1922.

[119] C. W. Helstrom. Quantum detection and estimation theory. *J. Stat. Phys.*, 1(2):231-252, 1969.

[120] H. Strobel, W. Muessel, D. Linnemann, T. Zibold, D. B. Hume, L. Pezzè, A. Smerzi, and M. K. Oberthaler. Fisher information and entanglement of non-gaussian spin states. *Science*, 345(6195):6195, 2014. schrödinger cat states. Science, 342, 6158, (2013).

[121] G. Tóth, and I. Apellaniz. Quantum metrology from a quantum information science perspective. *J. Phys. A: Math. Theo.*, 47(42):424006, 2014.

[122] M. G. Paris. Quantum estimation for quantum technology. *Int J. Qua. Inf.*, 7(supp01):125-137, 2009.

[123] A. S. Holevo. *Probabilistic and statistical aspects of quantum theory*, (Vol. 1). Springer Science Business Media, 2011.

[124] T. J. Proctor, P. A. Knott, and J. A. Dunningham. Multiparameter estimation in networked quantum sensors. *Phys. Rev. lett.*, 120(8):080501, 2018.

[125] J.Liu, H. Yuan, X. M. Lu, and X. Wang. Quantum Fisher information matrix and multiparameter estimation. *J. Phys. A: Math. Theor.*, 53(2):023001, 2019.

[126] V. Giovannetti, S. Lloyd, and L. Maccone. Advances in quantum metrology. *Nat. Photon.* 5(222), 2011.

[127] V. Giovannetti, S. Lloyd, and L. Maccone. Quantum metrology. *Phys. Rev. Lett.* 96(1):010401, 2006.

[128] C. L. Degen, F. Reinhard, and P. Cappellaro, Quantum sensing, *Rev. Mod. Phys.*, 89(3):035002, 2017.

[129] T. L. Wang, L. N. Wu, W. Yang, G. R. Jin, N. Lambert, and F. Nori. Quantum Fisher information as a signature of the superradiant quantum phase transition. *New Journal of Physics* 16(6):063039, 2014.

[130] U. Marzolino, and T. Prosen. Fisher information approach to nonequilibrium phase transitions in a quantum XXZ spin chain with boundary noise, *Phys. Rev. B* 96(10):104402, 2017.

[131] N. Li, and S. Luo. Entanglement detection via quantum Fisher information, *Phys. Rev. A* 88(1):014301, 2013.

[132] Z. Zakai. Error Bounds for Quantum Parameter Estimation. *Phys. Rev. Lett.*, 108(23):230401, 2012.

[133] N. Metwally. Fisher information of accelerated two-qubit systems. *Int. J. Mod. Phys. B*, 32(05):1850050, 2018.

[134] N. Metwally. Unruh acceleration effect on the precision of parameter estimation. *arXiv* : 1609.02092, 2016.

[135] S. P. Nolan, and S. A. Haine. Quantum Fisher information as a predictor of decoherence in the preparation of spin-cat states for quantum metrology. *Phys. Rev. A*, 95(4):043642, 2017.

[136] Q. Zhang, Y.Yao, and Y. Li. Optimal quantum channel estimation of two interacting qubits subject to decoherence. *Eur. phys. J. D*, 68(6):1-7, 2014.

[137] K. El Anouz, A. El Allati, N. Metwally, and T. Mourabit. Estimating the teleported initial parameters of a single-and two-qubit systems. *Applied Physics B*, 125(1):1-15, (2019).

[138] D. Safranek. Discontinuities of the quantum Fisher information and the Bures metric. *Phys. Rev. A*, 95(5):052320, (2017).

[139] M. Hubner, *Phys. Lett. A* 163(4): 239-242, 1992.

[140] H. J. Sommers and K. Zyczkowski, J. Phys. A: Math. Gen. ´ 36, 10083-10100 (2003)

[141] J. Liu, H. N. Xiong, F. Song, and X. Wang. Fidelity susceptibility and quantum Fisher information for density operators with arbitrary ranks. *Physica A: Statistical Mechanics and its Applications*, 410: 167-173, 2014.

[142] F. Özaydın, A. A. Altıntaş, C. Yeşilyurt, S. Buğu, and V. Erol. Quantum fisher information of bipartitions of W states, *Acta Physica Polonica A*, 127(4):1233-1235, 2015.

[143] S. Oh, S. Lee, and H. W. Lee. Fidelity of quantum teleportation through noisy channels. *Phys. Rev. A*, 66(2):022316, 2002.

[144] D. Wolfgang, and S. Heusler. What we can learn about quantum physics from a single qubit, *arXiv* : 1312.1463, 2013.

[145] R. Riebe, H. Häffner, C. F. Roos, W.Hänsel, J. Benhelm, G. P. T. Lancaster, R. Blatt, *Nature*, 429(6993):734, 2004.

[146] M. D. Barrett, J.Chiaverini, T. Schaetz, J. Britton, W. M. Itano, J. D. Jost, and D. J. Wineland, *Nature*, 429(6993):737, 2004.

[147] S. Olmschenk, D. N. Matsukevich, P. Maunz, D. Hayes, L. M. Duan, and C. Monroe, *Science* 323(5913):486, 2009.

[148] W. Pfaff, B. J. Hensen, H. Bernien, S. B.van Dam, M. S. Blok, T. H. Taminiau, R. Hanson, *Science* 345(6196):532, 2014.

[149] M. Jammer. *The philosophy of quantum mechanics: the interpretations of quantum mechanics in historical perspective*. Wiley, New York, 1974

[150] B. d'Espagnat. *Conceptual foundations of quantum mechanics*. Perseus Books, Reading, 1999.

[151] A. Peres. *Quantum theory: Concepts and methods*. Kluwer Academic Publishers, New York, 2002.

[152] M. Koashi, and M. Ueda. Reversing measurement and probabilistic quantum error correction. *Phys. Rev. lett.*, 82(12):2598, 1999.

[153] S. K. Berberian. *Notes on Spectral Theory*. D. Van Nostrand Company, Inc., Princeton, 1966.

[154] L. A. de Castro, O. P. D. S. Neto, and C. A. Brasil. An introduction to quantum measurements with a historical motivation. arXiv:1908.03949, 2019.

[155] Y. Aharonov, and L. Vaidman. The two-state vector formalism: an updated review. Time in quantum mechanics, 399-447, 2008.

[156] N. Katz, M.Neeley, M. Ansmann, R. C. Bialczak, M. Hofheinz, E. Lucero, and A. N. Korotkov. Reversal of the weak measurement of a quantum state in a superconducting phase qubit. *Phys. Rev. lett.*, 101(20):200401, 2008.

[157] A. N. Jordan, and A. N. Korotkov. Uncollapsing the wavefunction by undoing quantum measurements. *Contemporary Physics*, 51(2):125-147, 2010.

[158] Y. S. Kim, Y. W. Cho, Y. S. Ra, and Y. H. Kim. Reversing the weak quantum measurement for a photonic qubit. *Optics express*, 17(14):11978-11985, 2009.

[159] N. Katz, M. Neeley, M. Ansmann, R. C. Bialczak, M. Hofheinz, E. Lucero, and A. N. Korotkov. Reversal of the weak measurement of a quantum state in a superconducting phase qubit. *Phys. Rev. lett.*, 101(20):200401, 2008.

[160] A. N. Korotkov, and A. N. Jordan. Undoing a weak quantum measurement of a solid-state qubit. *Phys.* r*Rev. lett.*, 97(16):166805, 2006.

[161] N. Katz, M. Neeley, M. Ansmann, R. C. Bialczak, M. Hofheinz, E. Lucero, and A. N. Korotkov. Reversal of the weak measurement of a quantum state in a superconducting phase qubit. *Phys. Rev. lett.*, 101(20):200401, 2008.

[162] J. Preskill, $Lecture\ notes\ for\ /cs219 : Quantum\ information\ and\ computation$, 2001.

[163] J. A. Bergou, and M. Hillery. Introduction to the theory of quantum information processing. *Springer Science Business Media*, 2013.

[164] T. Toffoli. Reversible computing. In International colloquium on automata, languages, and programming (pp. 632-644). *Springer, Berlin, Heidelberg*, 1980.

[165] D. Aharonov. A simple proof that Toffoli and Hadamard are quantum universal. $arXiv$: 0301040, 2003.

[166] D. G. Cory, M. Price, W. Maas, Em. Knill, R. Laflamme, W. H Zurek, T. F Havel, and S. S. Somaroo. Experimental quantum error correction. *Phys. Rev. Lett.*, 81(10):2152, 1998.

[167] E. Dennis. Toward fault-tolerant quantum computation without concatenation. *Phys. Rev. A*, 63(5):052314, 2001.

[168] P. W. Shor. Scheme for reducing decoherence in quantum computer memory. *Phys. rRev. A*, 52(4):R2493, 1995.

[169] N. Metwally, and A. S. Obada. More efficient purifying scheme via controlled-controlled Not gate. *Phys. Lett. A*, 352(1-2):45-48, 2006.

[170] D. G.Cory, M. D. Price, W. Maas, E. Knill, R. Laflamme, W. H. Zurek, and S. S. Somaroo. Experimental quantum error correction. *Phys. Rev. Lett.*, 81:2152–2155, 1998.

[171] T. Aoki, G. Takahashi, T. Kajiya, J. I. Yoshikawa, S. L. Braunstein, P. Van Loock, and A. Furusawa. Quantum error correction beyond qubits. *Nat Phys*, 5:541–546, 2009.

[172] B. P. Lanyon, M. Barbieri, M. P. Almeida, T. Jennewein, T. C. Ralph, K. J. Resch, and A. G. White. Simplifying quantum logic using higher-dimensional hilbert spaces. *Nat. Phys.*, 5:134–140, 2009.

[173] T. Monz, K. Kim, W. Hänsel, M. Riebe, A. S. Villar, P. Schindler, and R. Blatt. Realization of the quantum Toffoli gate with trapped ions. *Phys. Rev. Lett.*, 102:040501, 2009.

[174] D. Deutsch. Quantum computational networks. *Proceedings of the Royal Soceity of London*, A(425):73, 1989.

[175] R. Vathsan. Introduction to quantum physics and information processing. *CRC Press*, 2015.

[176] F. Caruso, V. Giovannetti, C. Lupo, and S. Mancini. Quantum channels and memory effects. *Reviews of Modern Physics*, 86(4):1203, 2014.

[177] G. Bowen, and S. Bose. Teleportation as a depolarizing quantum channel, relative entropy, and classical capacity. *Phys. Rev. Lett.*, 87(26):267901, 2001.

[178] A. Furusawa, and P. van Loock. *Quantum Teleportation and Entanglement - A Hybrid Approach to Optical Quantum Information Processing*, Wiley-VCH, 2011.

[179] F. Caruso, V.Giovannetti, C. Lupo, S. Mancini. Quantum channels and memory effects. *Reviews of Modern Physics*, 86(4):1203, 2014.

[180] C. Macchiavello, and G. M.Palma. Entanglement-enhanced information transmission over a quantum channel with correlated noise. *Phys. Rev. A*, 65(5):050301, 2002.

[181] A. Salles, F. de Melo, M. P. Almeida, M. Hor Meyll, S. P. Walborn, P. S. Ribeiro, and L. Davidovich. Experimental investigation of the dynamics of entanglement: Sudden death, complementarity, and continuous monitoring of the environment. *Phys. Rev. A*, 78(2):022322, 2008.

[182] Y. Yeo, A. Skeen. Time-correlated quantum amplitude-damping channel. *Phys. Rev. A*, 67(6):064301, 2003.

[183] C. H. Bennett, and D. P. DiVincenzo. Quantum information and computation. *Nature*, 404 (6775):247-255, 2000.

[184] D. Spehner. Quantum correlations and distinguishability of quantum states. *Journal of Mathematical Physics*, 55,(7):075211, 2014.

[185] Z. W. Liu. *Quantum correlations, quantum resource theories and exclusion game*. Doctoral dissertation Massachusetts Institute of Technology, 2015.

[186] A. Peres. Separability criterion for density matrices. *Phys. Rev. Lett.*, 77:1413, 1996; M. Horodecki, P. Horodecki, R. Horodecki, *Phys. Lett. A*, 223(1), 1996.

[187] J. Lee, and M. S. Kim. Entanglement teleportation via Werner states. *Phy. Rev. lett.*, 84(18):4236, 2000; M. Paternostro, W. Son, M. S. Kim, G. Falci, G. M. Palma. Dynamical entanglement transfer for quantum-information networks. *Phys. Rev. A*, 70(2):022320, 2004.

[188] W. K. Wootters, and W. H. Zurek. A single quantum cannot be cloned. *Nature*, 299(5886):802-803, 1982.

[189] X.W. Zha, Z.C. Zou, and J. X. Qi. Bidirectional Quantum Controlled Teleportation via Five-Qubit Cluster State. *Int. J. Theor. Phys.*, 52(6):1740-1744, 2013.

[190] Y. Li, and L. Nie. Bidirectional Controlled Teleportation by Using a Five-Qubit Composite GHZ-Bell State. *Int. J. Theor. Phys.*, 52:1630, 2013.

[191] S. Zadeh, M. Sadegh, M. Houshmand, and H. Aghababa. Bidirectional teleportation of a two-qubit state by using eight-qubit entangled state as a quantum channel. *Int. J. Theor. Phys.*, 56(7):2101-2112, 2017.

[192] B. S. Choudhury, and S. Samanta. Bidirectional Teleportation of Three-Qubit Generalized W-States Using Multipartite Quantum Entanglement. *Phys. Part. Nucl. Lette.*, 16(6):206-215, 2019.

[193] E.O.Kiktenko, A. A. Popov, and A. K. Fedorov. Bidirectional imperfect quantum teleportation with a single Bell state. *Phys. Rev. A* 93(6):062305, 2016.

[194] A. El Allati, N. Metwally, and Y. Hassouni. Transfer information remotely via noise entangled coherent channels. *Opt. commu.*, 284(1):519-526, 2011.

[195] R. A. Fisher. *Proc. Cambridge Phil. Soc.*, 22:700, 1929 reprinted in Collected Papers of R. A. Fisher, edited by J. H. Bennett (Univ. of Adelaide Press, South Australia, 1972), pp. 15-40.

[196] D. R. Cox, and D. V. Hinkley. *Theoretical Statistics* (Chapman and Hall, London, 1974), Chapter 8.

[197] B. R. Frieden. *Science from Fisher information: a unification*. Cambridge University Press, 2004.

[198] H. L. Van Trees. Detection, Estimation, and Modulation Theory, *Part* I. *New York*: *Wiley*, 1968; T. A. Cover, J. M. Thomas. Elements of Information Theory. *New York*: *Wiley*, 1991.

[199] J. Dittmann. Explicit formulae for the Bures metric. *Journal of Physics A*: *Mathematical and General*, 32(14):2663, 1999.

[200] W. Zhong, Z. Sun, J. Ma, X. Wang, and F. Nori. Fisher information under decoherence in Bloch representation. *Phys. Rev. A*, 87(2):022337, 2013.

[201] J. Liu, X. Jing, and X. Wang. Phase-matching condition for enhancement of phase sensitivity in quantum metrology. *Phys. Rev. A*, 88:042316, 2013.

[202] J. Liu, H. Yuan, X. M. Lu, X. Wang. Quantum Fisher information matrix and multiparameter estimation. *Journal of Physics A*: *Mathematical and Theoretical*, 53(2):023001, 2019.

[203] D. Šafránek. Simple expression for the quantum Fisher information matrix. *Physical Review A*, 97(4):042322, 2018.

[204] J. A. Gyamfi. Fundamentals of quantum mechanics in Liouville space. *European Journal of Physics*, 41(6):063002, 2020.

[205] A. Gilchrist, D. R. Terno, and C. J. Wood. Vectorization of quantum operations and its use. *arXiv* : 0911.2539, 2009.

[206] C. J. Wood, J. D. Biamonteand, and D. G. Cory. Tensor Networks and Graphical Calculus for Open Quantum Systems. *Quant. Inf. Comp.*, 15:759, 2015.

[207] A. Furusawa, and P. van Loock. *Quantum Teleportation and Entanglement - A Hybrid Approach to Optical Quantum Information Processing*. Wiley-VCH, 2011.

[208] L. Vaidman. Teleportation of quantum states. *Phys. Rev. A* 49:1473, 1994; A. El Allati, Y. Hassouni, and N. Metwally. Communication via an entangled coherent quantum network. *Physica Scripta*, 83(6):065002, 2011.

[209] D. Bouwmeester, J. W. Pan, K. Mattle, M. Eibl, H. Weinfurter, and A. Zeilinger. Experimental quantum teleportation. *Nature*. 390:575-579, 1997; A. Furusawa, J. L. Sørensen, S. L. Braunstein, C. A. Fuchs, H. J. Kimble, and E. S. Polzik. Unconditional quantum teleportation. *Science*, 282(5389):706-709, 1998.

[210] L. Vaidman, and N. Yoran. Methods for reliable teleportation. *Phys. Rev. A*, 59(1):116, 1999.

[211] S. F. Huelga, J. A. Vaccaro, A. Chefles, and M. B. Plenio. Quantum remote control: teleportation of unitary operations. *Phys. Rev. A*, 63:042303, 2001; S. F. Huelga, M. B. Plenio, and J. A. Vaccaro. Remote control of restricted sets of operations: teleportation of angles. *Phys. Rev. A*, 65:042316, 2002.

[212] N. B. Zhao, A. M. Wang. Hybrid protocol of remote implementations of quantum operations. *Phys. Rev. A*, 76(6):062317, 2007.

[213] A. Yan, Bidirectional controlled teleportation via six qubit cluster state. *Inter Jour of Theor Phys*, 52(11):3870-3873, 2013; Y. Li, L. Nie, X. Li. Asymmetric Bidirectional Controlled Teleportation by Using Six qubit Cluster State. *Int J Theor Phys*, 55:3008-3016, 2016.

[214] Y. H. Li, L. P. Nie. Bidirectional controlled teleportation by using a five-qubit composite GHZ-Bell state. *International Journal of Theoretical Physics*, 52(5):1630-1634, 2013.

[215] Y. H. Li, X. L. Li, M. H. Sang, Y. Y. Nie, Z. S. Wang. Bidirectional controlled quantum teleportation and secure direct communication using five-qubit entangled state. *Quantum information processing*, 12(12):3835-3844, 2013.

[216] Y. H. Li, X. M. Jin. Bidirectional controlled teleportation by using nine-qubit entangled state in noisy environments. *Quantum Information Processing*, 15(2):929-945, 2016.

[217] X. M. Sun , X. W. Zha. A scheme of bidirectional quantum controlled teleportation via six-qubit maximally entangled state. *Acta Photonica Sinica*, 42(9):1052, 2013.

[218] S. Hassanpour, M. Houshmand. Bidirectional teleportation of a pure EPR state by using GHZ states. *Quantum Information Processing*, 15(2):905-912, 2016.

[219] G. Yang, B. W. Lian, M. Nie, J. Jin. Bidirectional multi-qubit quantum teleportation in noisy channel aided with weak measurement. *Chinese Physics B*, 26(4):040305, 2017.

[220] X. Xiao, Y. Yao, W-J. Zhong, Y. L. Li, Y. M. Xie. Enhancing teleportation of quantum Fisher information by partial measurements. *Phys. Rev. A*, 93(1):012307, 2016.

[221] N. Metwally, and A. A. Al –Amin. Maximum entangled states and quantum Teleportation via Single Cooper pair Box. *Physica E*, 41:718-722, 2009; N. Metwally. Teleportation of Accelerated Information. *J. Opt. Soc. Am. B*, 30(1):233-237, 2013.

[222] K. El Anouz, A. El Allati, N. Metwally, and T. Mourabit. Estimating the teleported initial parameters of a single and two-qubit systems. *Applied Physics B* 125:11, 2019; N. Metwally. Fisher information of accelerated two-qubit systems, *Inter. J. Mod. Phys. B*, 32(5):1850050, 2018.

[223] R. G. Zhou, R.Xu, H. Lan. Bidirectional quantum teleportation by using six-qubit cluster state. *IEEE Access*, 7:44269-44275, 2019.

[224] Z-Y. Chen, J-R. Xu, J. Yu, and K. Hou. Enhancing teleportation of a single-qubit state by the unitary transformation in arbitrary decoherence rate. *Phys. Scr.*, 96(3):035107, 2021.

[225] H. Nakazato, Y.Hida, K. Yuasa, B. Militello, A. Napoli, A. Messina. Solution of the Lindblad equation in the Kraus representation. *Phys. Rev. A*, 74(6):062113, 2006.

[226] D. A. Lidar, I. Chuang, K. B. Whaley. Decoherence free subspaces for quantum computation. *Phys. Rev. Lett.* 81:2594–2597, 1998; S. Maniscalco, F. Francica, R. L. Zaffino, N. Lo Gullo, and F. Plastina. Protecting entanglement via the quantum Zeno effect. *Phys. Rev. Lett.* 100:090503, 2008.

[227] C. Seida, A. El Allati, N. Metwally, and Y. Hassouni. Bidirectional teleportation under correlated noise. *Eur. Phys. J. D.*, 75:170, 2021.

[228] C. Macchiavello, and G. M. Palma. Entanglement-enhanced information transmission over a quantum channel with correlated noise. *Phys. Rev. A*, 65(5):050301, 2002.

[229] M. Koashi, and M. Ueda. Reversing measurement and probabilistic quantum error correction. *Phys. Rev. lett.*, 82(12):2598, 1999.

[230] N. Katz, M. Neeley, M. Ansmann, R. C. Bialczak, M. Hofheinz, E. Lucero, and A. N. Korotkov. Reversal of the weak measurement of a quantum state in a superconducting phase qubit. *Phys. Rev. Lett.* 101:200401, 2008.

[231] W. H. Zurek. Decoherence, einselection, and the quantum origins of the classical. *Rev. Mod. Phys.* 75:715–775, 2003.

[232] M. P. Almeida, F. de Melo, M. Hor-Meyll, A. Salles, S. P. Walborn, P. S. Ribeiro, L. Davidovich. Environment-induced sudden death of entanglement. *Science*, 316:579–582, 2007.

[233] C. Seida, A. El Allati, N. Metwally, and Y. Hassouni. Bidirectional teleportation using Fisher information. *Modern Physics Letters A*, 35(33):2050272, 2020.

[234] Y. Yeo, and A. Skeen. Time-correlated quantum amplitude-damping channel. *Phys. Rev. A*, 67(6):064301, 2003.

[235] A. El Allati, H. Amellal and A. Meslouhi, *Int. J. Quant. Inf.*, 17:1950044, 2019.

[236] J. Maziero, T. Werlang, F. F. Fanchini, L. C. Céleri, and R. M. Serra. System-reservoir dynamics of quantum and classical correlations. *Phys. Rev. A*, 81(2):022116, 2010.

[237] S. Daffer, K. Wodkiewicz, J. D. Cresser, and J. K. Mclver. Depolarizing channel as a completely positive map with memory. *Phys. Rev. A*, 70:010304, 2004.

[238] B. Bellomo, R. L. Franco, and G. Compagno. Non-Markovian effects on the dynamics of entanglement. *Phys. Rev. Lett.*, 99(16):160502, 2007.

[239] C. Simon. Towards a global quantum network. *Nature Photonics*, 11(11):678-680, 2017.

[240] F. G. Deng, X. H. Li, C. Y. Li, P. Zhou, and H. Y. Zhou. Quantum state sharing of an arbitrary two-qubit state with two-photon entanglements and Bell-state measurements. *Eur. Phys. J. D.*, 39:459, 2006.

[241] J. Eisert, K. Jacobs, P. Papadopoulos, and M. B. Plenio. Optimal local implementation of nonlocal quantum gates. *Phys. Rev. A*, 62(5):052317, 2000.

[242] N. Linden, S. Popescu, and W. K. Wootters. Almost every pure state of three qubits is completely determined by its two-particle reduced density matrices. *Phys. Rev. lett.*, 89(20):207901, 2002.

[243] R. G. Zhou, R. Xu, and H. Lan. Bidirectional quantum teleportation by using six-qubit cluster state. *IEEE Access*, 7:44269-44275, 2019.

[244] N. Gisin, and R. Thew. Quantum communication. *Nature photonics*, 1(3):165-171, 2007.

[245] X. M. Jin, J. G. Ren, B. Yang, Z. H. Yi, F. Zhou, X. F. Xu, and J. W. Pan. Experimental free-space quantum teleportation. *Nature photonics*, 4(6):376-381, 2010.

[246] D. Gottesman, and I. L. Chuang. Demonstrating the viability of universal quantum computation using teleportation and single-qubit operations. *Nature* 402(6760): 390-393, 1999.

[247] S. Barz, E. Kashefi, A. Broadbent, J. F. Fitzsimons, A. Zeilinger, and P. Walther. Demonstration of blind quantum computing. *Science*, 335(6066):303-308, 2012.

[248] S. Mancini, D. Vitali, P. Tombesi. Scheme for teleportation of quantum states onto a mechanical resonator. *Phys. Rev. lett.*, 90(13):137901, 2003.

[249] H. Krauter, D. Salart, C. A. Muschik, J. M. Petersen, H. Shen, T. Fernholz, and E. S. Polzik. Deterministic quantum teleportation between distant atomic objects. *Nature Physics*, 9(7):400-404, 2013.

[250] M. Hotta, J. Matsumoto and G. Yusa. Quantum energy teleportation without a limit of distance. *Phys. Rev. A*, 89(1):012311, 2014.

[251] A. I. Lvovsky, B. C. Sanders and W. Tittel. Optical quantum memory. *Nature Photonics* 3:706-714, 2009.

Résume (max 200 mots)

L'objectif principal de cette recherche théorique est d'étudier la téléportation quantique bidirectionnelle des états quantiques inconnus et de certains paramètres pertinents. Nous considérons que le canal quantique du protocole de téléportation bidirectionnelle est soumis au bruit ambiant, qui induit la décohérence quantique. Nous évaluons la négativité pour quantifier la quantité d'intrication dans le canal quantique du protocole de téléportation quantique bidirectionnel. En outre, nous considérons les fidélités moyennes de téléportation et l'information quantique de Fisher comme des figures de mérite pour évaluer le protocole de téléportation bidirectionnelle. Afin de surmonter l'effet de décohérence quantique et d'augmenter l'efficacité du protocole de téléportation, nous utilisons la méthode des mesures faibles et inversées. Nous montrons que ces mesures ne peuvent supprimer l'effet de l'amplitude damping que si, et seulement si, les fidélités moyennes des états téléportes sont supérieures a 0, 5 et que l'information quantique de Fisher n'est pas nulle. Néanmoins, l'utilisation de corrélations classiques et temporelles dans le régime non-markovien pourrait améliorer légèrement la téléportation bidirectionnelle. Dans une étape ultérieure, nous proposons trois schémas pour la téléportation bidirectionnelle de la porte CNOT et des états de n-qubits.

Mots-clefs (5) : téléportation bidirectionnelle, Décohérence, fidélité, information quantique de Fisher, intrication

Abstract (max 200 mots)

In this thesis, we address the issue of bidirectional quantum teleportation, which is one of the most interesting subjects in quantum information science. The prime objective of this research is to investigate the bidirectional quantum teleportation of unknown quantum states and some relevant parameters. We consider that the quantum channel of the bidirectional teleportation protocol is subjected to environmental noise, which induces decoherence. We evaluate the negativity to quantify the amount of entanglement in the quantum channel of the bidirectional quantum teleportation protocol. Furthermore, we consider the average fidelities of teleportation and the quantum Fisher information as figures of merit to assess the bidirectional teleportation protocol. In order to overcome the decoherence effect and increase the BQT efficiency, we use the weak and reversed measurements method. Nonetheless, using noise classical and temporal correlations in the non-Markovian regime we could slightly improve the BQT. We extend the BQT protocol to a three-party scheme. Then, we generalize the proposed scheme to a quantum network composed of N partners. We also suggest a new bidirectional scheme for the non-local implementation of CNOT operations. Based on the latter bidirectional scheme, we propose a bidirectional teleportation protocol for n-qubit.

Key Words (5) : Bidirectional teleportation, Decoherence, fidelity, quantum Fisher information, entanglement